

# Pennsylvania State University

## Annual Progress Report: 2009 Formula Grant

### Reporting Period

July 1, 2010 – June 30, 2011

### Formula Grant Overview

The Pennsylvania State University received \$8,412,824 in formula funds for the grant award period January 1, 2010 through December 31, 2013. Accomplishments for the reporting period are described below.

### **Research Project 1: Project Title and Purpose**

*Modifications of Histone H3 in Diabetic Retinopathy* - The overall purposes of this project are twofold. First we plan to define some of the changes in chromatin structure that occur in the retinas of an animal model of Type I diabetes. This will give us fundamental information about the range of retinal changes seen in this disease and will offer new insights into the types of change that need to be treated. The second objective is to monitor how treatment with insulin can reverse these changes and restore the retina to its normal state. This set of experiments will test the hypothesis that some of the retinal changes in diabetes become irreversible with time.

### Duration of Project

1/1/2010 – 6/30/2011

### Project Overview

The overall goal of this research project is to define a specific set of molecular changes that occur in a mouse model of Type I diabetes and to test the hypothesis that some of these changes become irreversible with longer periods of hyperglycemia. To achieve this goal the project has two specific aims.

Aim 1: We will test the hypothesis that two histone modifications, H3K9Ac and H3K4me2, will be detected at different sites in the genomes of normal and diabetic mouse retina. To test this hypothesis we will carry out three sets of experiments. First, to better define the appropriate ages for more detailed molecular experiments we will carry out an immunocytochemical analysis using antibodies that recognize the two modifications. We will test tissue from animals of 1 to 20 weeks of age. Second, we will take animals of defined ages and carry out a ChIP-seq analysis. The approximately 10 million short DNA sequences resulting from each experiment will be aligned to the mouse genome to give us a quantitative map of the frequency of occurrence of each modified histone at each site across the genome. We will then use custom algorithms to search for differences between control and diabetic samples. We will identify

genes associated with these modified histone changes by identifying coding sequences -2.5kb to +1kb from the modified histone binding sites. We will cluster genes associated with histone modification changes using bioinformatic approaches to identify any specific categories.

Aim 2: We will test the hypothesis that restoration of normal glucose levels by implantation of insulin pellets will cause some, but not all, epigenetic changes to revert to normal. The phenomenon of “metabolic memory” in which extended periods of poor glycemic control can lead to progressive retinopathy even after insulin therapy is an important issue as it affects the efficacy of any treatment. We will implant insulin pellets in mice either at the onset of hyperglycemia (4 weeks) or after retinopathy and vascular changes are well established (10 weeks). At 16 weeks, animals will be examined for reversion of changes in H3 modifications using the same ChIP-seq methods. In this way we will identify genes whose expression may be subject to metabolic memory. Such information is key to developing therapies to be used in conjunction with insulin to prevent retinopathy even after glycemic control.

### **Principal Investigator**

Colin J. Barnstable, DPhil  
Professor and Chair  
Penn State College of Medicine  
Department of Neural and Behavioral Sciences  
500 University Drive  
Hershey, PA 17033

### **Other Participating Researchers**

Evgenya Popova, PhD - employed by Penn State College of Medicine

### **Expected Research Outcomes and Benefits**

The anticipated outcomes of this project are 1) a description of two specific epigenetic changes across the whole genome that will define the retinal changes seen in a mouse model of Type I diabetes; 2) an understanding of how these changes might alter expression of genes in the retina; 3) a description of the effectiveness of insulin in restoring the epigenome and gene expression to a normal condition. The benefits from this project are twofold. First, the result will give us new information about the ways in which lack of insulin and hyperglycemia affect the structure of the retinal genome. From these results we will develop a fuller understanding of the ways in which diabetes can affect the expression of many genes in the retina. Second, we will have quantitative information about the ways in which insulin can reverse the retinal effects of diabetes at the early and late stages of the disease.

The health benefits of this project are that, first, we will define new therapeutic targets; second, we will define a set of biomarkers by which we can define the disease progression and the effectiveness of any therapy; and third, we will provide an accurate assessment of the ability of insulin therapy to reverse the damage to the retina at early and late stages of the disease. Together these outcomes will also speed the development and characterization of new therapies

to treat diabetic retinopathy.

## **Summary of Research Completed**

The overall goal of this research project is to determine whether there are a specific set of molecular changes in epigenetic postranslational modification of core histones H3 and H4 that occur in a mouse model of Type I diabetes, and to test the hypothesis that some of these changes become irreversible with longer periods of hyperglycemia in retina. During this year of the project we analyzed the ChIP-Seq data generated for several modifications of histones H3 and H4 for model of Type I diabetes,  $Ins2^{Akita/+}$  mice (Wang et al, J Clin Invest 1999; 103:27-37), in comparison with healthy littermates.

### Methods

*Chromatin isolation, ChIP and ChIP-Seq* analysis of retinal chromatin was performed with antibodies against H3K4me2, H3K9me3, H3K9ac, H3K27me3, H3K27ac, H4K12ac and H4K20me3. Chromatin immunoprecipitations with antibodies against acetylation modifications were done in presence of 5mM sodium butyrate. ChIP DNA libraries were sequenced on SOLiD™ 3 system (Applied Biosystem, Foster City, CA) at the Genome Core Facility, Huck Institutes for Life Sciences at the University Park Campus of the Pennsylvania State University. Data were analyzed with NexGENE software (SoftGenetics, State College, PA). All sequencing of ChIP libraries was performed in the Genome Core Facility, Huck Institutes for Life Sciences at the University Park Campus of the Pennsylvania State University. After sequencing ChIP DNA on the SOLiD sequencer, the reads were mapped to mouse genome with NextGENE software. Bed format for 136 genes was made for 4000bp around transcriptional start site (TSS) (+2000bp/-2000bp) with 200bp resolution and whole number of reads in 4000bp were calculated for each gene with NextGENE software.

### Results

#### ChIP-Seq analysis

To create and compare a comprehensive genomic map of the chromatin epigenetic status for  $Ins2^{Akita/+}$  and wild type littermate retinas ChIP-Seq was performed on mouse retina samples with antibodies against histone modifications implicated in heterochromatin formation: H3K9me3, H4K20me3 and H3K27me3 and histone modifications that are marks of euchromatin and actively transcribed genes: H3K9ac, H3K4me2, H3K27ac, H4K12ac. The reads from each experiment were mapped to mouse genome and analyzed with NextGENE software. The average of 9 millions reads was mapped to mouse genome for each ChIP-Seq sample.

#### Changes in epigenetic status of promoters or genomic regions

We performed the comparison analysis of epigenetic comprehensive maps for  $Ins2^{Akita/+}$  and wild type littermates ChIP-Seq data. We analyzed the distribution of histone modifications at loci of six categories of genes: photoreceptor-specific genes, progenitor-specific genes, genes not active in rod photoreceptors, constitutively active genes, genes involved in chromatin formation and histone/ DNA modification and genes implicated in diabetes (Freeman et al, J OculBiolDis Inform 2009; 2:202-13 and Fort et al, Mol Cell Proteomics, 2009; 4:767-79). Bed format for

these 136 genes was made for 4000bp around transcriptional start site (TSS) and we calculated and compared amount of reads for each histone modifications on this 4kb region genes for  $Ins2^{Akita/+}$  and wild type littermates samples. Genes that have maximum changes (decreased or increased by 1.5 times) around TSS are shown in tables 1-4.

Tables 1 and 2 summarize the distributions of active marks H3K4me2 and H3K27ac that are known to accumulate effectively on promoter regions of actively transcribed genes. Increase of accumulation of these marks in promoter could suggest more open chromatin structure in diabetes. Examples of genes TSS with decreased occupancy for the active mark H3K4me2 are shown on Figure 1a, b, and increased occupancy for the same mark are shown on Figure 1c, d. Tables 3 and 4 summarize distribution of inhibitory marks H3K27me3 and H3K9me3 in gene promoters. Decrease of accumulation of these marks is an indication of a more open chromatin structure. Genes marked with an asterisk have changes in histone modification in  $Ins2^{Akita/+}$  mice in agreement with transcriptome comparison study in mouse models of diabetes (Freeman et al, *J OculBiolDis Inform* 2009; 2:202-13 and Fort et al, *Mol Cell Proteomics*, 2009; 4:767-79). Examples of genes TSS with decreased occupancy for inhibitory mark H3K27me3 are shown on Figure 2a, b, and increased occupancy for the same mark are shown on Figure 2 c, d.

We conclude from these comprehensive genomic maps of the chromatin status for 3 repressive and 4 active epigenetic modifications in retinas of  $Ins2^{Akita/+}$  and wild type littermate mice that there are changes in promoter occupancy for multiple genes. While this dysregulation affects many genes, it is clear that not all genes are affected equally. Our study provides fundamental information about the range of retina epigenetic changes seen in diabetes.

#### Assessing the epigenetic status of loci implicated in type 2 diabetes by human GWAS

Recent progress in genome-wide association studies (GWAS) implicated group of human genes (or genomic regions in close proximity to these genes) in development of type 2 diabetes in human (Cox et al, *Dis Model Mech*. 2011, 4:155-164). We compared a list of these 45 genes with the retina developmental transcriptome (Zang et al, *BMC Dev Biol*, 2006,6:48) and found that 11 mouse homologs of these genes are expressed in the retina. Bed format for these 11 genes was made for 4000bp around promoter or other genomic loci implicated in regulation of the genes. We calculated and compared a number of reads for each histone modification through this 4kb region for  $Ins2^{Akita/+}$  and wild type littermates samples. Overall more genes (table 5) show epigenetic upregulation – a more open chromatin structure in diabetic animals. Examples of genomic loci with more open chromatin structure in diabetic animal are shown in figure 3 a, b. For the *Cdkal1* gene the H3K4me2 mark is increased in  $Ins2^{Akita/+}$  mice, while the inhibitory H3K27me3 mark is decreased. The *Fto* gene is an example of the region with more of the inhibitory mark H3K27me3 in  $Ins2^{Akita/+}$  mice (Figure 3c).

Assessing the epigenetic status of loci implicated in type 2 diabetes by human GWAS shows different accumulations of epigenetic marks for some of these loci suggesting that changes in histone modifications could play a role in diabetic retinopathy and metabolic memory phenomenon.

Table 1		H3K4me2	
Decreased in Akita		Increased in Akita	
gene	wt/akita	gene	wt/akita
Cbx5	4.10	SelenBP1*	0.20
Elov14	2.93	Mll2	0.26
GRM6	2.87	ccne	0.32
sag	2.43	setd7	0.48
H1d	2.36	KDM5c	0.48
Actb	2.28	ATP5j	0.51
PKCa	2.28	Cbx1	0.53
Chat	2.28	NSBP1	0.55
Gapdh	2.19	Tead2	0.55
H1b	2.15	Rbcc1	0.58
SNAP-25	2.05	Plscr2*	0.64
Grb10	1.86	Prph2	0.65
gngt1	1.82	Ifi2712a*	0.65
myc	1.82	Itrp3*	0.65
suv39h2	1.82	Aipl1*	0.66

Table 2		H3K27ac	
Decreased in Akita		Increased in Akita	
gene	wt/akita	gene	wt/akita
Arr3	3.70	Xpo1	0.17
Adamts19	2.44	tubb5	0.22
Cryba2	2.43	Rom1	0.24
H1e	2.36	IRS1	0.24
suv39h2	2.36	Suv39h1	0.24
Hbb	2.25	HMG2	0.31
H1c	2.17	Gad1	0.36
Tulp1	2.11	RGS9	0.40
Cryab	1.99	Mll2	0.40
Guca1a	1.92	MeCP2	0.42
Pde6b	1.91	dlg4*	0.42
PDE6g	1.89	Cryba4*	0.42
B2M	1.84	setd7	0.44
Sfrp2	1.78	Ano1*	0.45
crabp2	1.68	SNAP-25	0.46
ABCA4	1.68	GRM6	0.50
Jarid2	1.68	Clec7a*	0.50
Chat	1.68	Ror2*	0.51
RBP3	1.68	ATP5j	0.56
H2abl	1.68	IGF2	0.57
Cryaa	1.68	Igf2bp1	0.57
opnmw	1.55	Csrp3	0.59
Sox11	1.54	Kdm6b	0.59
LgalS9	1.52	Mbd2	0.59

Figure 1a

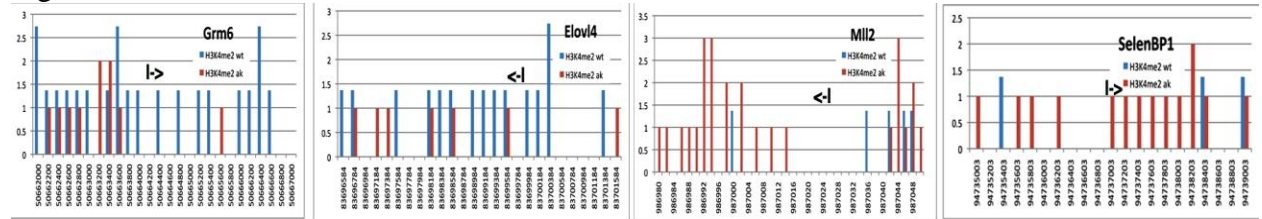


Table 3	H3K9me3		
Decreased in Akita		Increased in Akita	
gene	wt/akita	gene	wt/akita
EZH2	5.64	Cryba2	0.14
Cryba4*	5.64	Smagp	0.25
Pisd	5.08	Suv39h1	0.38
H1e	4.51	myc	0.40
Ifitm2*	3.67	ATP1a	0.42
Kdm5b	3.57	CBX3 / HP1a	0.42
LgalS9	3.39	Adams19	0.43
RB1	3.10	H1d	0.45
sag	3.01	H2abl	0.47
H2AZ	2.82	GNAT1	0.48
setd7	2.82	NRL	0.48
MII3	2.82	Tulp1	0.48
Got1	2.82	Igf2bp1	0.49
Ano1*	2.82	Guca1b	0.49
Arr3	2.54	Tbx	0.51
Cryab	2.45	opnmw	0.51
Actb	2.26	DNMT3a	0.52
Abi3bp*	2.26	Gucy2f	0.56
Gad2	2.12	Ror2	0.56
gngt1	2.12	Gucy2e	0.56
Cryaa	2.12	Rom1	0.56
RPSA	1.98	Csrp3	0.62
Stat3	1.98	Hbb	0.63
Cobll1*	1.98	Pde6b	0.64
Syn1	1.98	H1c	0.64
Rbcc1	1.92	MII2	0.64
Tor3a*	1.88	vamp2	0.66
Cmb1*	1.88	Guca1a	0.67

Table 4	H3K27me3		
Decreased in Akita		Increased in Akita	
gene	wt/akita	gene	wt/akita
Tor3a*	10.14	dlg4	0.07
Hbb	8.11	Tead2	0.10
Guca1b	8.11	Actb	0.14
LSD1/ kdm1	5.41	Gucy2e	0.17
PKCa	3.38	PDHb	0.26
Csrp3	3.21	Ifi2712a	0.27
Kdm5b	2.70	RPSA	0.32
Gapdh	2.70	GNAT1	0.34
G9a /ehmt2	2.70	H1c	0.34
Guca1a	2.70	Arr3	0.34
MII3	2.36	HMG2	0.34
tubb5	2.36	Ano1	0.37
setd7	2.03	Gad1	0.38
PDE6g	1.86	MII2	0.40
ccne	1.80	CRX	0.41
Cbx5	1.80	SelenBP1	0.41
Cbx1	1.69	vamp2	0.43
Stat3	1.69	Rho	0.45
IRS1	1.69	H1b	0.45
Elov14	1.58	II17rd	0.47
Abi3bp*	1.58	MDK	0.48
Jarid2	1.52	H19	0.48
H1a	1.52	Smagp	0.48

Figure 2a

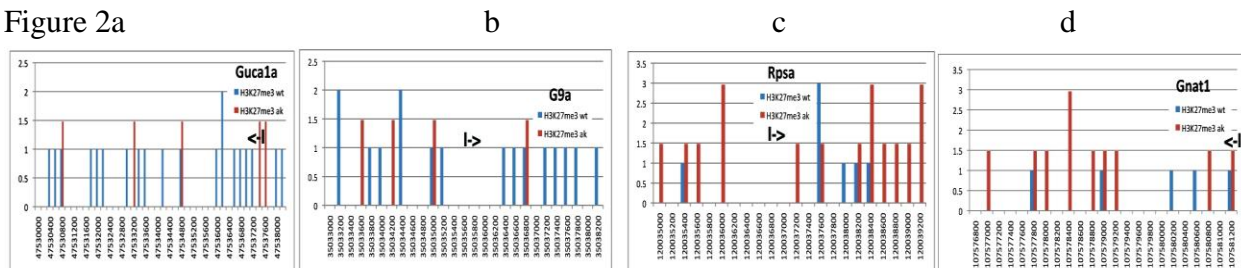
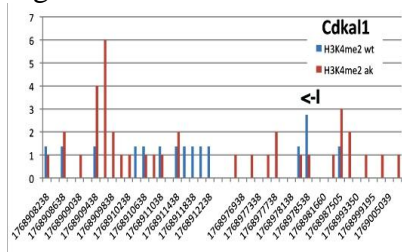
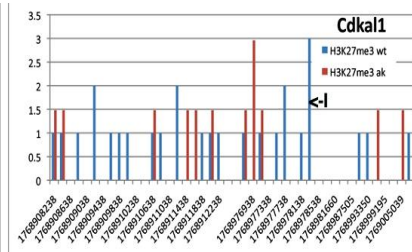


TABLE 5		Up in	Down
gene	location	Akita	Akita
Notch2	promoter		
Notch2	intron		1
Notch2	end of gene	111	1
Iris	promoter	11	1
Prox1	promoter		11
Bcl11a	promoter	1111	
Cdkal1	promoter	111	
Cdkal1	intron	1	
Adcy5	promoter	11	11
Tctf7l2	promoter	1	1
Tctf7l2	2 promoter		11
Camk1d	promoter	11	
Camk1d	Cdc123		
Wfs1	promoter		1
Pparg	promoter	1	
Fto	promoter	11	
Fto	Rpgrip11	111	11

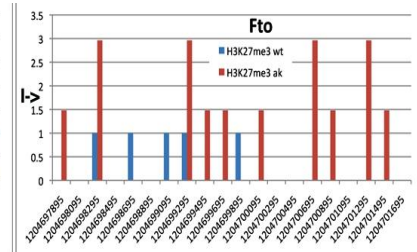
Figure 3a



b



c



## Research Project 2: Project Title and Purpose

*Brain and Behavior in Early Iron Deficiency* - Aggressive iron repletion following iron deficiency in infancy will result in excessive accumulation of this potential neurotoxin in the brain and is associated with alteration in brain genomic level and myelin composition. The purpose of this project is to determine if aggressive dietary iron intervention to replenish brain iron concentrations in formerly iron deficient animals is neurotoxic.

## Anticipated Duration of Project

1/1/2010 – 12/31/2011

## **Project Overview**

Our *long-term objective* is to determine *when and how much iron to give* to prevent the long-term neurobehavioral sequelae of early iron deficiency (ID). There is the potential for neurotoxicity if excessive iron is given to treat early ID. Thus, the *specific aim* of this study is to determine if larger amounts of iron taken up by brain tissue during aggressive dietary iron treatment result in changes in brain genomic and structural sequelae. We *hypothesize* that aggressive iron intervention during lactation is associated with neurotoxicity.

*Strategies:* We will assess the early ID in rat pups by cross-fostering of rat pup to mothers given <5 ppm Fe (ID group) or 50 ppm Fe diet (control group). Pups with early ID will receive the 50 ppm (control) or 1000 ppm iron diet (high iron treatment) between P8 and P21. We chose P8 to represent the rodent neuronal equivalency to the intervention being done in the human study at 6 weeks post-partum. The dietary levels of iron to achieve “iron loading” of the brain through this route was estimated from published data where lactating dams were provided from 400-20,000 ppm Fe.

To determine the consequences of aggressive iron repletion, we will measure brain iron concentration, targeted gene expression profiles for oxidative stress and myelin-associated protein expression at P21, P90 and 6 months of age. We chose P21 to document the model’s acute effects, P90 to document the persistence of the genomic and myelination and 6 months of age to document long-term effects of aggressive iron repletion. Brain iron concentration will be measured with atomic absorption spectrophotometry. The gene expression profile of the brain will target the oxidative stress gene and be determined with gene array. We will use RT-PCR to verify the changes from the gene array experiments. Myelin analyses will be focused on the expression of myelin-associated proteins (Myelin Base protein, CNPase and Proteolipid protein) in white matter regions. Measurements of brain iron concentration, gene expression and myelin composition in two iron treatment groups (50 and 1000 ppm Fe) will be compared to the control groups (never ID) and H67D mice. We will include H67D mice because the H63D HFE or hemochromatosis gene variant is associated with iron overload and increased oxidative stress and it has been proposed as a genetic modifier for risk of neurodegenerative disorders. Therefore, comparing gene expression and myelin-analyses of the P8 treated group given severe iron intervention (1000 ppm) to H67D mice will further elucidate the potential for neurotoxicity if excessive iron is given to treat early ID.

## **Principal Investigator**

James R. Connor, PhD  
University Distinguished Professor and Vice Chair  
Neurosurgery, H110  
Pennsylvania State University College of Medicine  
500 University Drive, PO Box 850  
Hershey, PA 17033-0850

## Other Participating Researchers

Wint Nandar - employed by Pennsylvania State University College of Medicine

## Expected Research Outcomes and Benefits

We anticipate that similar to H67D mice, which have significant increases in brain and liver iron concentration (preliminary data), P8 treated group given the severe degree of iron treatment (1000 ppm) will have increased brain iron concentration due to enhanced iron transport upregulated by the early ID. The cause of the increased transport will be a future direction for our analyses. P8 treated rats given 1000 ppm iron are also expected to have alterations in gene expression in the brain and myelin composition compared to the control groups (50 ppm Fe treatment and never ID groups). The interpretation is that aggressive iron repletion is associated with potential neurotoxicity if P8 treated rats given severe iron intervention display increased iron concentration and have similar pattern in alteration in expression of genes and myelin-associated proteins as H67D mice, an *in vivo* model for human H63D mutation, which is proposed to be a genetic modifier for risk of neurodegenerative diseases.

Therefore, this project will reveal if aggressive repletion of iron is associated with neurotoxicity. From the gene array analysis, we will learn the molecular footprint of brain iron overload resulting from aggressive iron intervention and the potential use of an antioxidant therapy with the iron supplementation. These data will help inform the future analyses being performed at the protein level suggesting mechanisms underlying these higher order analyses, including behavior, and the level at which intervention strategies must be targeted. The project may narrow down the optimal dosing and timing of iron treatment that is sufficient but not neurotoxic. Therefore, findings from this study will inform the non-human primate and human projects with respect to the efficacy and safety of iron treatment in young mammals and it may also have important public health implications.

## Summary of Research Completed

Our overall long-term goal is to evaluate when and how much iron to give to prevent the long-term neurobehavioral sequelae of early iron deficiency (ID). We focused our analyses on determining whether dietary iron replenishment during lactation is associated with neurotoxicity particularly the effect of aggressive iron repletion on oxidative stress and myelin composition.

We first assessed the early ID in rat pups by cross-fostering of rat pups to mothers given < 5 ppm iron (ID group) or 40 ppm iron diet (control group). The early ID pups were separated into 4 groups. Between postnatal day 8 (P8) and P21, the first group received 40 ppm iron (normal diet or diet 1), the second group received 400 ppm iron (high iron treatment or diet 2), the third group received 1000 ppm iron (aggressive iron repletion) and the last group did not receive the dietary iron intervention (ID group or diet 4). Rat pups cross-fostered to mother given 40 ppm Fe diet served as the control in the analysis (diet 0 group). We then harvested brain samples from all diet groups at postnatal days 21, 36 and 92. Table 1, 2 and 3 summarize the number of samples we have harvested from each diet group at different ages during the past year.

We are now in process of completing the sample collection from all diet groups at different ages. We are currently evaluating the gene expression profile of the brain particularly targeted to the oxidative stress pathway.

We have made significant progress on the analysis of the H67D mice. These mice show iron accumulation in liver and brain and therefore the mutation is functional. We have focused on the consequences of the excessive iron in these mice which will be evaluated in context of the mice fed the high iron diet. In particular we have focused on ER stress and expression of TDP-43 a protein whose expression may be tied to ER stress and neuron degeneration.

In order to demonstrate that the dysfunctional HFE protein would impact the glutamatergic system, we examined the expression of cystine/glutamate antiporter (system xc-) expression, which exchanges intracellular glutamate for extracellular cystine used in glutathione synthesis in H67D mice. Increased xCT antiporter level was observed in brains of H67D/H67D compared to wild-type mice.

These data demonstrated ER stress, caspase activation and increased TDP-43 were present in the lumbar spinal cord of H67D transgenic mice. Additionally, increased xCT expression was observed in the brain of H67D mice, suggesting a disturbance of extracellular glutamate homeostasis. These data strongly support the hypothesis that H63D HFE establishes a permissive milieu to increase neuronal vulnerability for ALS.

Table 1: Brain samples (age group: 21 days old)			
Control group – diet 0	Gestation Fe deficient until p8 and switch on to the control mother (Fe 40ppm) – diet 1	Gestation Fe deficient until p8 and switch on to the mother (Fe 400ppm) – diet 2	Total iron deficient – diet 4
6 females	6 female	6 female	6 females
6 males	5 male	6 male	6 males

Table 2: Brain samples (age group: 36-48 days old)			
Control group – diet 0	Gestation Fe deficient until p8 and switch on to the control mother (Fe 40ppm) – diet 1	Gestation Fe deficient until p8 and switch on to the mother (Fe 400ppm) – diet 2	Total iron deficient – diet 4
9 females	0 female	0 female	8 females
7 males	0 male	0 male	8 males

Table 3: Brain samples (age group: 92-102 days old)			
Control group – diet 0	Gestation Fe deficient until p8 and switch on to the control mother (Fe 40ppm) – diet 1	Gestation Fe deficient until p8 and switch on to the mother (Fe 400ppm) – diet 2	Total iron deficient – diet 4
19 females	14 females	10 females	9 females
9 males	13 males	12 males	13 males

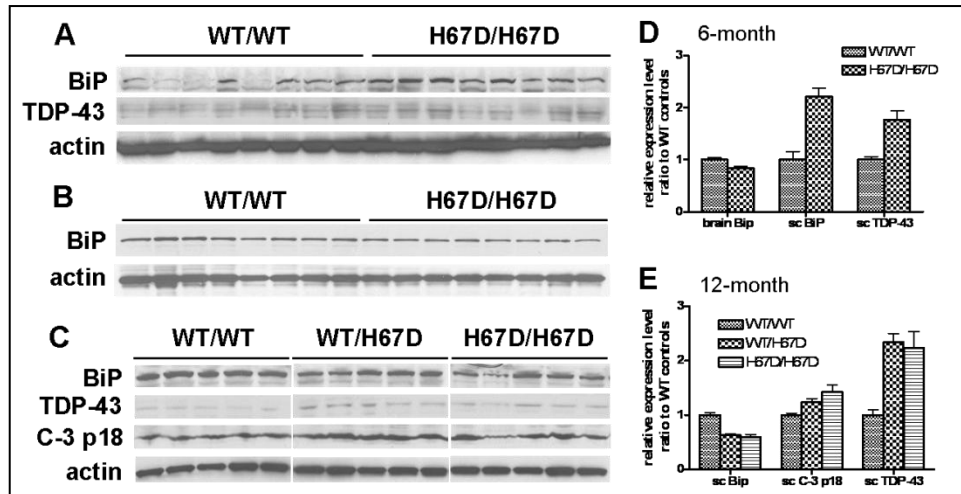


**Figure 1. Increased ER stress, activated Caspase and up-regulated TDP-43 in H67D mice.**

Western blot to monitor protein expression level in the homogenates of lumbar spinal cord (A), whole brain (B) from 6-month old and lumbar spinal cord from 12-month

old (C) wild-type or H67D mice. Quantification of the blots from 6-month (D) or 12-month old mice (E). The expression level of Bip, Caspase-3 and TDP-43 were normalized by actin level and calculated as the ratio to the wild-type controls ( $p < 0.05$ ,  $n = 5-8$ ).

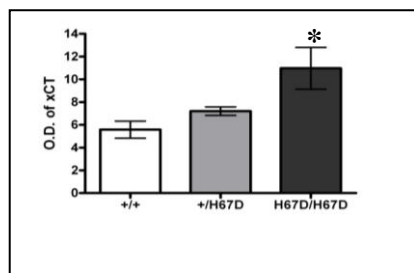


**Figure 2. Increased xCT expression in H67D/H67D compared to the wild-type mice.** The expression of the cystine glutamate antiporter (system xc- or xCT), was determined by Western blot in 6-month-old wild-type (+/+), heterozygous (+/H67D) and homozygous (H67D/H67D) mice. Bars represent mean  $\pm$  standard error. (\* =  $p < 0.05$ ;  $n = 4-6$  per genotype).

### **Research Project 3: Project Title and Purpose**

#### *Cell Signaling Mechanisms Necessary for High-Fidelity Replication of Repetitive Sequences -*

The integrity of an organism depends on faithful replication of the genome with every cell division. The human genome contains six billion bases, many of which can be present in structures that make it difficult for replicative enzymes to work efficiently and accurately. Human cells have 15 different DNA polymerases that function to copy the genome. Mutations caused by polymerase errors within repetitive microsatellite sequences pose a significant threat to genome integrity, as is evident in colorectal cancers. The goal of this project is to elucidate the polymerases and cell signaling mechanisms that are necessary for high-fidelity replication of microsatellites. Understanding the dynamics of microsatellite replication will lead to new approaches for detecting and treating colorectal cancer, one of the most common cancers in the United States and Pennsylvania.

#### **Duration of Project**

1/1/2010 - 12/31/2010

## **Project Overview**

Broad objective: To elucidate the polymerases and cell signaling mechanisms that are necessary for high-fidelity replication of microsatellites.

Specific Aim: To test the hypothesis that Y-family polymerases, Pol  $\kappa$  and Pol  $\eta$ , are required for accurate microsatellite replication, using a human cell culture model system.

Subaim 1: To determine the effects of altered Y-family polymerase levels on microsatellite mutagenesis.

Subaim 2: To determine the effect of mutations in the ubiquitin binding zinc-finger (UBZ) domain of Pol  $\kappa$  on microsatellite mutagenesis.

*Rationale:* Replicative polymerases are inhibited by microsatellite sequences, and other DNA sequences that form non-B structures require Pol  $\kappa$  and/or Pol  $\eta$  for effective replication. Our working model is that the faithful replication of microsatellite sequences necessitates coordination of several polymerases, including Y family polymerases. Switching among cellular polymerases has been proposed to be regulated by ubiquitination.

*Experimental approach:* To examine the roles of Pol  $\kappa$  and Pol  $\eta$  in microsatellite replication (Subaim 1), we will engineer human colorectal carcinoma cell lines to increase and decrease levels of the two polymerases Pol  $\kappa$  and Pol  $\eta$ , both individually and in combination. To determine the role of monoubiquitination of PCNA in signaling polymerase switching (Subaim 2), colorectal carcinoma cell lines will be created in which the conserved aspartic acid (D644) of the Pol  $\kappa$  UBZ domain is mutated to alanine. To measure mutagenesis in both aims, we will use a shuttle vector assay developed in our laboratory for determining mutation frequencies of both microsatellite and non-repetitive coding sequences. Mutation rates at the microsatellite sequences will be compared with those in the coding region of the HSV-tk gene in at least three independent determinations for each parental cell line and derivative.

## **Principal Investigator**

Kristin A. Eckert, PhD  
Professor  
Pennsylvania State University College Of Medicine  
500 University Drive, HO59  
Hershey, PA 17033

## **Other Participating Researchers**

Beverly A. Baptiste, MS - employed by Pennsylvania State University

## **Expected Research Outcomes and Benefits**

The immediate scientific outcome of this project is to define the specific roles of Pol  $\kappa$  and Pol  $\eta$  in human genome stability. The importance of Y-family DNA polymerases to genome stability is illustrated in disorders resulting from their absence. For example, DNA Pol  $\eta$  is mutated in the

hereditary cancer syndrome, xeroderma pigmentosum-variant; these patients are very susceptible to sunlight-induced skin cancers. Previous research on Y-family polymerases has focused almost exclusively on DNA damage tolerance. Our working hypothesis states that microsatellite sequences are recognized by a cell in a similar manner as damaged DNA, and that Y family polymerases are activated to assist in replication of microsatellites. Our work will determine whether altered DNA polymerase levels are tolerated in tumor cells, and what mutational effects can be expected by alterations in their regulation.

After this model system is established, it can be used to explore the role of other polymerases in microsatellite replication as well as the role of the cell cycle regulators, p53 and p21. Several potential health benefits of our research can be expected in the long-term. First, by determining the mechanisms of DNA polymerase alterations in tumors, new clinical tests may be developed to aid diagnosis and prognosis, especially of colorectal cancers that display microsatellite instability. Second, since altered DNA polymerase levels are implicated in resistance to cancer therapy, our research could be used to individualize patient treatment options, with the goal of optimizing an anti-tumor response.

## **Summary of Research Completed**

### *Manipulation of Y family polymerase levels in human cancer cell lines (Subaim 1)*

#### Summary of cell lines created for use in the model

Three parental cell lines were used in this study: two colon carcinoma cell lines, HCT-116 and DLD-1, and one osteosarcoma cell line, U2OS. Gene expression vectors were created for three Y family polymerase genes: POLH (Pol  $\eta$ ), POLI (Pol  $\iota$ ) and POLK (Pol  $\kappa$ ). All genes were cloned into the pTRE-tight, doxycycline regulated vector (Clontech). HCT-116 and DLD-1 cells were stably transfected with the pTetOn regulation vector; U2OS cells carrying the regulatory vector were purchased from Clontech. All experimental treatments with doxycycline were performed in media containing Tet-free fetal bovine serum.

Overexpression of Y family polymerases in human cancer cell lines. A summary of our experimental results to date is given in Table 1. We successfully isolated and characterized one stable, U2OS/POLI doxycycline-inducible clone (Figure 1A). Although doxycycline-inducible POLI expression was observed transiently after transfection of HCT-116 cells with pTRE/POLI (Figure 1A), no stable, dox-inducible HCT116 clones have yet to be isolated (Table 1). To date, we have been unable to observe doxycycline-induced overexpression of either POLH or POLK, transiently or stably, in either U2OS or HCT116 cell lines. An example of the lack of induction is shown in Figure 1B. We did not isolate any DLD-1 clones that displayed inducible expression of our pTRE-GFP plasmid; therefore, this cell line was not evaluated further.

We have examined several reasons for the lack of POLK and POLH overexpression results (data not shown). First, we sequenced the corresponding pTRE vectors, but found the DNA sequence to be correct for each construct. Second, we analyzed POLH mRNA levels with and without doxycycline treatment, in U2OS clones stably transfected with the pTRE/POLH vector by RT-PCR. We observed no differences between untreated and treated cells. Third, we examined the genomic DNA of the U2OS clones and verified integration of the pTRE/POLH vector, using

PCR and primers specific to the vector sequence.

siRNA knock-down of Y family polymerases in human cancer cell lines. To test the ability of HCT-116 cells to undergo siRNA-mediated gene silencing, we purchased siGLO RNAs to Lamin A/C from Dharmacon. Transfection of HCT-116 cells with this control siRNAs was successful, as determined by cellular fluorescence, and successful knockdown of Lamins A/C was observed by Immunoblot analyses 3 days after transfection (data not shown). We are in the process of repeating this protocol using siRNAs targeted to POLK and POLI.

#### SV40 origin-dependent HSV-tk shuttle vector assay (Subaims 1 and 2)

We previously reported the initial characterization of a new HSV-tk shuttle vector mutation assay, based on the SV40 origin of replication. This new assay was necessary, as we found that the oriP vectors used in our established mutagenesis system do not replicate in cancer cell lines. We have used the SV40 assay to quantitate spontaneous mutation frequencies after DNA replication in HCT-116 and U2OS cancer cells. We observed a very large increase in the HSV-tk mutation frequency after replication of the pGSV-tk vector in the tumor cells, compared to the *E. coli* background mutation frequency (Table 2, Method 1). The vast majority of plasmids (75%) obtained from the human cells contained large rearrangements involving the HSV-tk gene, rather than inactivating point mutations. We modified our experimental method by targeting mutation selection to a small region of the HSV-tk gene (~200 basepairs) surrounding the enzyme's ATP-binding domain. Our rationale was that this approach may improve detection of inactivating HSV-tk point mutations. Similar mutation frequencies were observed (Table 2, Method 2), and again, the majority of mutants obtained after replication in the tumor cell lines were large rearrangements (75-100%). Next, we measured the mutation frequency of a [GT/CA]<sub>19</sub> microsatellite-containing vector in the mismatch repair-deficient cell line, HCT116. This cell line has been well characterized, and displays a microsatellite instability high (MSI-H) phenotype at [GT/CA] markers. Accordingly, we observed a high mutation frequency after replication of the pGSV-GT19 vector in HCT-116 cells (Table 2). DNA sequence analyses revealed that 85% of the mutations occur within the [GT/CA]<sub>19</sub> repeat, consistent with an MSI-H phenotype.

#### Progress towards goals and Discussion

One of our goals was to determine whether altered Y family DNA polymerase levels are tolerated in tumor cells. Our results clearly demonstrate that increased levels of Pol  $\iota$  can be sustained (Figure 1). In contrast, our studies suggest that overexpression of either Pol  $\eta$  or Pol  $\kappa$  may not be sustainable with tumor cell viability. Although future studies are clearly warranted to definitively test the role of these polymerases in tumor cells, our results are consistent with the recent publication demonstrating that overexpression of the *E. coli* homolog to POLK, *dinB*, is lethal in bacteria (Uchida et al. 2008). Experiments are in progress to assess the effects of decreased Y family polymerase expression in our experimental system.

Our second goal was to establish a mutational assay to monitor the effects of alterations in Y family polymerase regulation on microsatellite mutagenesis. We have successfully achieved this goal. The SV40-based HSV-tk shuttle vector assay was used to readily measure microsatellite

instability in the HCT-116 colorectal carcinoma-derived cell line (Table 2). We are in the process of using this approach to measure microsatellite mutagenesis in U2OS cells under native and Pol  $\iota$  overexpressing conditions. To our knowledge, no published studies have examined the impact of Pol  $\iota$  expression levels on microsatellite mutagenesis. Importantly, Pol  $\iota$  overexpression has been reported in uterine, gastric and prostate cancers, relative to adjacent normal tissues (Albertella et al. 2005). Recently, decreased expression of Y family polymerase genes (POLH, POLI and POLK) has been reported in colorectal carcinoma tissues, relative to adjacent normal tissue (Pillaire et al. 2010). In the near future, we plan to use our SV40-tk shuttle vector assay to measure the mutational consequences of POLK and POLI down-regulation. The results of our studies will provide insight into the cellular consequences of altered Y family polymerase expression in human cancers.

**Table 1. Summary of Y family polymerase overexpression experimental results**

Experiment	U2OS	HCT-116	DLD-1
Transient expression pTRE-GFP	<b>Yes</b>	<b>Yes</b>	No
Transient overexpression pTRE/POL I (Pol $\iota$ )	<b>Yes</b>	<b>Yes</b>	n.d.
pTRE/POLK (Pol $\kappa$ )	No	No	+/-
pTRE/POLH (Pol $\eta$ )	No	No	n.d.
Stable overexpression pTRE/POL I (Pol $\iota$ )	<b>Yes</b>	No	n.a.
pTRE/POLK (Pol $\kappa$ )	No	No	n.a.
pTRE/POLH (Pol $\eta$ )	No	No	n.a.

n.d., not done; n.a., not applicable

Protein expression levels were assessed by fluorescence microscopy (GFP) or immunoblot analyses (polymerase)

**Table 2. Mutation frequencies obtained in the SV40 origin-HSVtk assay after shuttle vector replication in human cancer cell lines.**

Vector	Method <sup>a</sup>	HSV-tk Mutant Frequency		
		HCT116	U2OS	E. coli <sup>b</sup>
pGSV-tk	1	$8.5 \times 10^{-3}$	$14 \times 10^{-3}$	$1 \times 10^{-7}$
	2	$3.5 \times 10^{-3}$	$68 \times 10^{-3}$	$3.3 \times 10^{-4}$
pGSV-GT19	1	$14 \times 10^{-3}$	n.d.	$3.6 \times 10^{-4}$

<sup>a</sup> Method 1: Isolation of plasmid from human cells 48 hours after transfection, followed by DpnI digestion.

Method 2: Isolation of plasmid from human cells 48 hours after transfection, followed by isolation of a ~200bp MluI-EcoRV small fragment encoding part of the HSV-tk gene.

<sup>b</sup> Transfection of E. coli directly, without replication in human cells.

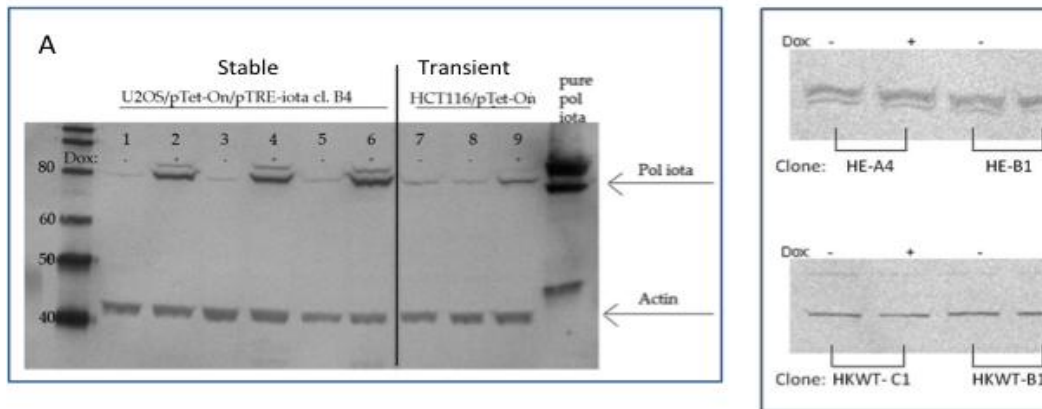


**Figure 1. Immunoblot analyses of doxycycline-induced Y family DNA polymerase protein overexpression in tumor cell lines.** (A). Overexpression of POLI (Pol  $\iota$ ) in U2OS cells (lanes 1-6, stable expression) and HCT-116 cells (lanes 7-9, transient expression). Lanes 3 and 4 are cytoplasmic fractions; the remaining lanes are nuclear fractions. Lanes 1, 3, 5, 7, and 8 show endogenous expression levels; lanes 2, 4, 6 and 9 shown increased levels in the presence of doxycycline. (B). Representative HCT-116 cell line clones that were stably integrated with pTRE-POLH (top) or pTRE-POLK (bottom) expression vectors. No doxycycline-inducible clones for these two polymerases have been isolated to date from either HCT-116 or U2OS cell lines.

#### **Research Project 4: Project Title and Purpose**

*Impact of the Penn State Diabetes Patient Registry* - Disease registries (or electronic patient databases) are being implemented extensively by health care systems with the goals of improved records management, individualized patient care, and population-based disease management. They are a central feature of improving quality care for chronic illnesses and feature prominently in the national effort towards redesigning primary care as the Patient Centered Medical Home (PCMH). Although used extensively, little data are available on the overall impact of registries on care. The Penn State Diabetes Registry (PSDR) was first implemented in the Penn State Hershey system in 2002 to achieve the aforementioned goals and to simultaneously provide a research network for patient recruitment for diabetes research. The purpose of this project is to identify the value of this chronic illness registry for quality improvement of clinical outcomes, to examine its effectiveness in promoting high quality clinical research and to identify opportunities for PSDR refinements through assessments of the impact of the PSDR.

#### **Anticipated Duration of Project**

5/1/2010 - 12/31/2011

## **Project Overview**

Despite widespread use of diabetes registries for a variety of functions, little is known regarding the value of these registries to improve clinical care, foster research recruitment, and determine what factors facilitate adoption and implementation. The current project has the following specific aims:

- 1. Evaluate the impact of introductions of a chronic disease registry (Penn State Diabetes Registry - PSDR) to improve clinical care.* As the PSDR is introduced into new clinics, pre-post comparisons of clinical parameters (Hemoglobin A1c (A1c), Blood Pressure (BP) and LDL-cholesterol (LDLc) and process measures (annual testing and screening) for the patient populations will demonstrate the impact of this implementation on diabetes care.
- 2. Evaluate the impact of the PSDR for subject recruitment for research trials.* A process approved by the Penn State Human Subjects Institutional Review Board allows researchers to make patients aware of opportunities to participate as human subjects in new research through letters sent by care providers using the PSDR. Consort diagrams constructed for each research project will enable comparisons of response, enrollment and completion rates, while using trial participation requirements such as time, risks and discomfort as co-variables.
- 3. Evaluate facilitating factors and identify barriers for the adoption and implementation of the PSDR within individual clinics.* Focus groups, surveys and related qualitative data on PSDR usage will be analyzed to identify factors that determine the success of PSDR implementations. As the PSDR and similar electronic medical record systems become standard in health care settings, this knowledge is important for new improvements.

## **Principal Investigator**

Robert A Gabbay, MD, PhD  
Professor of Medicine  
Penn State College of Medicine  
500 University Drive  
PO Box 850  
Hershey, PA 17033-0850

## **Other Participating Researchers**

Jan Ulbrecht, MD, Scott Mincemoyer, RN, Lorraine Mulfinger, PhD, Dave Mauger, PhD - employed by Penn State University

## **Expected Research Outcomes and Benefits**

The expected *outcomes* of this research are:

1. Assessment of the impact of a chronic disease registry (PSDR ) on patient care;
2. Identification of barriers to acceptance and use of a chronic disease registry for diabetes (PSDR) by health care providers;

3. Identification of specific elements most crucial for both clinical and research applications of the PSDR;
4. Summary of the effectiveness and identification of opportunities for process improvement in the use of registries as a research recruitment tool; and
5. Modification of the PSDR as appropriate to improve and enhance its usefulness for both clinical and research applications.

Based on these outcomes, the benefits expected are:

1. Dissemination of key features required for chronic disease registries as part of ongoing PCMH efforts throughout the commonwealth and nationally;
2. Modifications of the PSDR to improve usage compliance and enhance the PSDR design to more readily integrate it into the clinical setting;
3. Modifications of the PSDR that will enhance its usefulness to researchers;
4. Publication and dissemination of these results to support improvements to other registries;
5. Dissemination of these findings to the Pennsylvania Chronic Care Commission to improve the diabetes registry implementation process that is part of the Commonwealth's healthcare reform initiative;
6. Identification of the most successful process for using chronic disease registries to inform providers and patients about research opportunities while minimizing the burdensome aspects of clinician involvement; and
7. Identification of the data fields most crucial for both clinical and research processes to encourage clinician compliance with their use.

### **Summary of Research Completed**

This research aims to evaluate usage of the Penn State Diabetes Registry (PSDR) to improve clinical care, understand practice implementation of the registry, and evaluate use of the registry for research subject recruitment. Much has been accomplished in regards to each of these aims. Accomplishments to date are described below. Work is continuing on all three fronts.

*Aim #1: Evaluate the impact of introductions of a chronic disease registry (PSDR) to improve clinical care.*

Introduction: The hypothesis is that a longitudinal study of disease registry use, using the PSDR as an example, will show improved diabetes outcome measures (A1C, blood pressure, LDL). Studies to date on whether or not use of disease registries has translated into improved control of the disease have shown mixed results.

Methodology: De-identified data sets were collected from the PSDR for 18 practices using the PSDR following each practice's implementation of the PSDR through 2009. Statistical analyses in SAS were conducted to determine whether registry use was correlated with a change in outcome (A1C, BP, LDL) measures.

For data from 2008 and 2009, registry use was based on calculating the number of instances where new data was entered into the registry as an indicator of use by clinicians. This was then divided by the total number of visits billed using an ICD-9 diabetes diagnosis code. Outcome

measures were calculated as the number of patients meeting each measure specification divided by the total number of visits billed with the ICD-9 diabetes diagnosis code.

Results: Through a concerted multi-faceted intervention, registry use dramatically improved, increasing from less than 20% usage at the beginning of 2007 to nearly 70% usage at the end of 2009. While trend lines suggest improvement in patient A1C levels starting in 2007, statistical analysis found no significant correlation between registry use and A1C levels. Likewise, there was no correlation between registry use and LDL. There was, however, a significant correlation between blood pressure and registry use. Patient blood pressure levels improved as the level of registry use improved. Upon initial analysis, there were few significant correlations between registry use and A1C, blood pressure, or LDL at the individual clinic level, but the large datasets involved from these practices with over 8,000 patients requires further validations to further examine the associations.

Discussion: The use of a registry displaying longitudinal blood pressure values appears to have led to better blood pressure control in this cohort of patients from 18 clinics in central PA. Although the LDL data showed no correlation with registry use, this analysis was limited by the fact that the LDL variable was measured in years and the other variables were measured in quarters. There were many fewer data points to use for the LDL analysis.

In addition, adoption of the PSDR was variable in the practices, with some using it more than others. We plan to explore what correlations in outcomes may exist. It is possible that registry use is higher than reported if practices have not submitted updated patient profiles following each visit.

Conclusions: Blood pressure is the most critical predictor of morbidity and mortality in diabetes and use of a registry appears to be correlated with better blood pressure management. While still ongoing, this analysis indicates that it may take more than a registry to improve diabetes care for other parameters. Both the Chronic Care Model and Patient Centered Medical Home (PCMH), two of the leading models to strengthen the health care delivery system, consider use of a registry to be just one of several essential components to improving care. It is notable that registry use more than doubled in 2009, the year that four of the primary care practices using the PSDR began participating in a state-led Chronic Care and PCMH initiative.

The correlation between registry use and blood pressure improvement indicates that a registry may help providers overcome clinical inertia. By graphically tracking data over time, the PSDR enables both providers and patients to more easily see non-improving or declining trends that demand a change in medications or therapies. Blood pressure levels also are routinely assessed at every patient visit so that information is immediately available whereas the most recent A1C or LDL test results may not be.

Finally, there is typically a longer lag in outcomes measure improvement than process measure improvement. A longer time span is needed to evaluate correlations between registry use and outcomes measure improvement, particularly because registry use was low (below 30%) until 2009.

*Aim #2: Evaluate the impact of the PSDR for subject recruitment for research trials.*

Introduction: Recruiting subjects for research is challenging. Previous work has shown that recruitment may be affected by a number of factors, including time requirements and invasiveness of the study, access to knowledgeable personnel, as well as enlistment and reimbursement of personal physicians involved in the recruitment process.

The Penn State Institute for Diabetes and Obesity (PSIDO) offers investigators two resources to facilitate the recruitment of human subjects for studies on diabetes, obesity, and related conditions: a volunteer database and the PSDR. The volunteer database contains names, contact information, and limited clinical data on nearly 700 adults with diabetes and related conditions who have self-identified as open to participating in research. This study evaluated the relative merits of both recruitment modalities for studies at Penn State.

Methodology: An initial analysis compared 4 studies using the volunteer database to 4 studies using the PSDR for participant recruitment. Contact rates, response rates, and enrollment rates were analyzed according to study design, extent of subject involvement, and sample population characteristics.

Results: Average recruitment rates for both groups of studies was positive and compared favorably to other studies using patient registries to recruit individual chronic care patients. However, wide variation between sample populations and the methods of the studies clouded qualitative judgments about the relative recruitment efficacy of either database. Table 1 describes the extent of subject involvement and the numbers of criteria and criteria matches, letters sent and contact rate, replies and response rate, and enrollees and enrollment rate for all 8 studies.

Discussion: There were a number of difficulties with this analysis. All four studies using the volunteer database screened criteria matches before contact was made with potential enrollees; none of the studies using the PSDR pre-screened enrollees. Only studies that completed the enrollment phase were included. At least 7 additional studies are using the PSDR for subject recruitment.

Conclusions: Additional analyses involving more studies are needed to determine the relative merits of using either the PSDR or the volunteer database for research participant recruitment.

*Aim #3: Evaluate facilitating factors and identify barriers for the adoption and implementation of the PSDR within individual clinics.*

Introduction: This study aimed to determine the perspectives of health care providers and staff on the usefulness and barriers to use of disease registries through their experience with the PSDR. A manuscript on this study has been accepted for publication in the *Journal of Clinical Outcomes Management*.

Methodology: This mixed-methods study used both a survey assessment and semi-structured individual interviews and focus group sessions. The survey examined five domains: (1) time efficiency, (2) clinician-system interaction, (3) quality of patient care, (4) research, and (5)

improvements. Separate web-based surveys were distributed to providers (physicians, NPs, and PAs) (n=52) and staff (medical assistants, LPNs, RNs, clerical) (n=51). Surveys included 38 Likert-type scale questions (0=total disagreement, 10=total agreement); 12 questions were excluded from the staff survey due to specificity of providers' experiences. Surveys were anonymous, but respondents were given the opportunity to share their identity for follow-up with an interview or focus group.

Individual interviews were conducted with 10 providers, and there were 4 focus groups of staff. Purposeful sampling was used to recruit participants who used the registry. The interviews and focus groups explored four domains: (1) general perspectives of registries, (2) quality and efficiency of care using a registry, (3) research applicability of registries, and (4) orientation and feedback from a registry.

Survey Results: The provider survey response rate was 49.5%. As shown in Table 2, overall provider satisfaction with the PSDR was positive, with a median (min, max) of 7 (2, 10). The providers felt that the PSDR increased the efficiency of the diabetes patient visit (8 (1, 10)) and facilitated better adherence to evidence-based guidelines (8.5 (2, 10)). They felt that the PSDR patient profile was easy to understand and complete (8 (3, 10)), with 88.5% reporting filling out the profile and 76.9% reporting distributing the profile to their patients.

Less positive areas of registry use included increased time needed for documentation (6 (0, 10)), inadequate training in the use of the registry (5 (1, 10)) and inadequate IT help with the registry (5 (1, 10)). The providers who were satisfied with the PSDR believed that it did not increase documentation time and that it increased the efficiency of the diabetes patient visit and improved the health of their patients. Specific aspects of the PSDR that were highly correlated with satisfaction were the helpfulness of reminder prompts and the increased ability to follow evidence-based guidelines.

The staff survey response rate was 26.2%. Like providers, staff were overall satisfied with the PSDR (7 (3, 10)). They thought the patient profile was easy to understand and complete (8 (4, 10)) and that the online user interface was intuitive and easy to use (7 (0, 10)). Fewer staff than providers reported filling out the PSDR profile (54.9%,  $p<0.001$ ), but more reported having signed into the online system for data entry or printing of the patient profiles (64.7% for staff vs. 32.7% for providers,  $p<0.01$ ).

Like providers, staff were not very positive about PSDR system training (5 (0, 10)) or about the adequacy of available IT help (5 (0, 10)). As with providers, staff who were most satisfied with the registry believed that it increased the efficiency of the diabetes patient visit.

Interview/Focus Group Results: The data from the interviews and focus groups were combined in analysis. Many participants remarked about a registry's ability to help provide comprehensive evidence-based care. They appreciated the ability to display patient data graphically as a tool to explain clinical significance. They also viewed performance reports from the registry positively and noted using them to identify and set specific interventions to improve care and for intra-office benchmarking and sharing of best practices. Most providers said that having data available regarding a chronic condition ready for the patient visit was a time-saving feature that can

increase time for patient counseling, improve coordination of care, and facilitate clinic teamwork.

The most prevalent challenges associated with implementation of the PSDR were dealing with “double documentation” and the preconception of the registry being “more work.” Some mentioned the lack of integration with an electronic medical record to be problematic. One physician said, “The registry needs to be coordinated with my note. So right now, it’s a separate piece of paper, a separate thing that I’ve got to circle and put information on, or take information off of, and I’ve got to redo it for my note.” Another said, “There is a hump to get over with the staff because ... we were asking our staff with the registry to do things differently than they’ve always done them. It’s perceived frequently as more work and there’s always a limited amount of time to do the job.” However, there were also providers and staff who recognized that the work gets easier and that it comes with returns.

When implementing the PSDR, there was a lack of knowledge about the importance and purpose of the registry as well as using the features to the fullest extent. Some providers and staff said they didn’t initially understand the importance of completing the patient profiles, but later learned the features and powerful tools of the registry. There were also concerns about the accuracy of the data in the registry.

In addition, participants mentioned the value of using the registry to identify research subjects and as a data pool for retrospective data. Even so, there was recognition of the potential risk of soliciting patients for participation in research based on their health status.

Discussion: The prevailing attitude of providers and staff is that the diabetes registry has improved their ability to deliver quality care and improve the efficiency of the patient visit. Providers also felt that the patient profile was helpful for patients’ self-management of their diabetes. A key process improvement present in many offices is the printing of the profiles for every diabetes visit. This requires delegation, revised job duties, and team-based effort and is difficult to achieve.

Conclusions: Overall, registries can aid in improving chronic disease care by increasing adherence to evidence-based guidelines, providing performance reports for quality improvement, decreasing the time of patient visits, and assisting in clinical organization and care delivery design. They can also help in academic settings through their applicability toward research, whether retrospective data analysis or prospective study recruitment. Training and education about the use and benefits of the system is crucial, however, to realizing the full potential and power of the tool. Future adoption of registries is likely to be driven by the federal government’s “meaningful use” criteria for all future electronic health records.

Table 1: Research Participant Recruitment Using the PSDR vs. Volunteer Database

Source	Name	Sessions	Procedures	Criteria	Criteria Matches	Letters Sent	Contact Rate	Replies	Response Rate	Enrollees	Enrollment Rate
PSDR	SHADE	11	BG, A1C, Physical, Interview	4	844	844	100%	32	3.79%	15	1.78%
PSDR	Making Meaning of Diabetes Mellitus	9	3x A1C & BP, Interview	5	83	83	100%	8	9.64%	5	6.02%
PSDR	DYNAMIC	10	A1C, LDL, Lifestyle Intervention, Motivational Interviewing	4	1778	1778	100%	1012	56.92%	550	30.93%
PSDR	Diabetes Mellitus Values and Preferences	1	Telephone Interview	2	127	127	100%	40	31.50%	40	31.50%
Volunteer	Endometrial Hyperplasia	1	Physical, Transvaginal Ultrasound, Uterine Biopsy	5	60	10	16.67%	10	100%	5	50.00%
Volunteer	Incorporating Comorbidities	1	Focus Group	3	130	21	16.15%	13	61.90%	13	61.90%
Volunteer	Food: Focused Ethnographic Interview	1	Interview	1	34	11	32.35%	8	72.73%	8	72.73%
Volunteer	PDA	6	Height, Weight, 2x FG, Seminar, Interview	4	157	32	20.38%	24	75.00%	8	25.00%

Table 2: Comparison of Averages and Standard Deviation of Provider and Staff Surveys

Question	Provider Survey Median (Min, Max)	Staff Survey Median (Min, Max)	P value*
The PSDR increases time needed for documentation.	6 (0, 10)	5 (0, 10)	0.4876
The PSDR increases the efficiency of the patient visit.	8 (1, 10)	8 (4, 10)	0.7054
Do you fill out the PSDR form?***			
YES	46 (88.5%)	28 (54.9%)	0.0003
NO	6 (11.5%)	23 (45.1%)	
If yes to previous question, the PSDR form is easy to understand and complete.	8 (3, 10)	8 (4, 10)	0.8417
The adoption process of the PSDR into everyday practice was overall positive.	7 (0, 10)	6 (1, 10)	0.2205
There was adequate training in using the PSDR.	5 (0, 10)	5 (0, 10)	0.2812
There is adequate IT help in dealing with the PSDR.	5 (1, 10)	5 (0, 10)	0.0468
Have you ever signed into the PSDR system?			
YES	17 (32.7%)	33 (64.7%)	0.0017
NO	35 (67.3%)	18 (35.3%)	
If yes, the user interface is intuitive and easy to use.	7 (1, 10)	7 (0, 10)	0.5446
Do you receive feedback for population disease management from the PSDR?			
YES	24 (46.2%)	14 (27.5%)	0.0535
NO	28 (53.8%)	37 (72.5%)	
The reminder prompts for patient care from the PSDR are helpful.	8 (3, 10)	7 (0, 10)	0.0333
The PSDR helps to follow evidence-based guidelines for diabetes care.	8.5 (2, 10)	n/a	
The PSDR patient profiles present all the information necessary for effective management of diabetic patients.	7 (0, 10)	n/a	
Do you distribute the patient version of the PSDR patient profile to your patients?			
YES	40 (76.9%)	32 (62.7%)	0.1226
NO	12 (23.1%)	19 (37.3%)	
If yes, the PSDR patient sheet provides support to patients for self-management of their disease.	7 (2, 10)	n/a	
If yes, the patients seem satisfied with the information given to them in the patient profile.	7 (5, 10)	n/a	
Are you satisfied with the PSDR overall?	7 (2, 10)	7 (3, 10)	0.4779

\*The comparison between the provider and staff responses in common survey items were analyzed by performing a Mann-Whitney-Wilcoxin test. The p-values given are for the t Approximation value of the MWW test.

\*\*\*For purposes of data analysis, these responses were coded as 1 for yes, and 2 for no.

## **Research Project 5: Project Title and Purpose**

*Epigenetic Changes in Myeloid Differentiation and Acute Myeloid Leukemia* - The purpose of this project is to identify changes in epigenetic mechanisms controlling myeloid differentiation and transcription in order to predict and prevent the progression of acute myeloid leukemia (AML), a highly malignant blood cancer. Recent development of high-throughput “next-generation” genomic sequencing technologies such as ChIP-sequencing provided a dramatic breakthrough in whole-genomic mapping of epigenetic markers such as histone methylation and acetylation and their abnormalities. Here we propose to conduct a detailed whole-genomic characterization of the localization and expression of one such marker, histone H3 methylation, which is altered in AML cells, and to identify clusters of genes involved in epigenetic changes marked by this histone modification and transcriptionally deregulated in leukemia.

### **Anticipated Duration of Project**

1/1/2010 – 6/30/2012

### **Project Overview**

Acute myeloid leukemia (AML) is a highly malignant blood cancer with an estimated 12,810 new cases in 2009 and the lowest survival rate (23.4%) among the four major types of leukemia. This disease is caused by a combination of genetic rearrangements and epigenetic changes. Based on our previous studies of developmentally-regulated epigenetic and transcriptional changes associated with myeloid differentiation and leukemia as well as other data known from the literature, we hypothesize that epigenetic changes manifested in mis-localization of a repressive histone modification, histone H3 dimethylation at lysine 9 (H3K9me2) may interfere with transcription during myeloid differentiation and promote AML.

In this project we will conduct a detailed whole-genomic characterization of the localization and expression of H3K9me2 and identify clusters of genes involved in epigenetic changes marked by this histone modification. This project has two specific aims.

Specific aim 1 is to map genome-wide topography of histone H3(K9) demethylation and its transitions in the process of normal myeloid differentiation. We will use ChIP-sequencing to map this histone modification over the genomes of normal myeloid precursors and differentiated granulocytes. Our analysis should reveal sites of H3K9 dimethylation involved in normal myeloid differentiation.

Specific aim 2 is to determine spatial and functional relationship between histone H3(K9) methylation and transcriptional changes in AML. This work includes an innovative application of the cutting-edge genomic sequencing and bioinformatics analysis to study association of chromatin modification topographies with transcription in leukemia and is expected to reveal new chromosomal loci altered in AML that can be served for the disease prognosis as well as targets for its epigenetic therapy.

## **Principal Investigator**

Sergei A. Grigoryev, PhD  
Associate Professor  
Department of Biochemistry and Molecular Biology H171  
Penn State University College of Medicine  
500 University Drive  
Hershey, PA 17033

## **Other Participating Researchers**

Thomas P. Loughran, Jr., MD, David Claxton, MD, Sarah Correll - employed by Penn State University College of Medicine

## **Expected Research Outcomes and Benefits**

The initial causes of several known forms of AML are different and often include cytogenetically distinct chromosomal mutations that result in uncontrolled proliferation and incomplete differentiation of the affected cells. There is also a growing line of evidence that leukemia and many other cancers originate from epigenetic changes that often include deregulated silencing and mis-localized heterochromatin resulting either in inactivated tumor suppressors or activated genes promoting tumor growth.

Our studies should reveal: a) which particular genes or chromosomal loci in the whole human genome are affected by spontaneous epigenetic changes associated with particular forms of AML and with individual patients, and b) which genes and chromosomal loci can be modified by epigenetic protein factors and/or epigenetic therapy. Since several chromatin remodeling and gene regulating agents such as inhibitors of DNA methylation 5-azacytidine and decitabine and histone deacetylase (HDAC) inhibitors are already used for “epigenetic therapy” of AML, identification of their potential genomic targets may lead either to development of new chromatin-targeting therapeutic approaches promoting normal myeloid differentiation or to understanding the adverse effect(s) of these drugs on hematopoietic system.

## **Summary of Research Completed**

*Work on Specific Aim 1: To map genome-wide topography of histone H3(K9) dimethylation and its transitions in the process of normal myeloid differentiation.*

*a) Cells and fixation.* Normal polymorphonuclear granulocytes (predominantly neutrophils with less than 3% eosinophils) were isolated from discarded fresh white blood cells (buffy coats) from unidentified healthy donors collected at Hershey Medical Center Blood Bank using standard OptiPrep density centrifugation in Grigoryev laboratory (IRB protocol # HY03-136EP-A). Freshly thawed cells were fixed by 1% formaldehyde when suspended in PBS buffer to prevent nucleosome sliding. For initial analysis, we used  $5 \times 10^6$  primary blood cells for one experiment. However, we realized that we need more cells for efficient ChIP (see below) so all our successful experiments were conducted with no less than  $1 \times 10^7$  cells.

*b) Nuclear Isolation.* Cell nuclei were isolated using a new protocol that we adapted to ChIP analysis that employed physiological salt rather than low-salt RSB buffer during the nuclear lysis and purification through sucrose layer. This nuclear preparation was readily digested with micrococcal nuclease to ~150-180 bp (optimal for SOLiD) chromatin sizes (Figure 1), supernatant was collected and discarded and the pellet resuspended in SDS-containing lysis buffer by sonication. A typical yield for granulocyte nuclei was ~ 0.5 mg DNA for  $10^8$  cells. The solubilized material was immunoprecipitated with specific antibodies against H3K9me2.

*c) Immunoprecipitation.* We conducted several experiments to test antibody efficiency for immunoprecipitating chromatin labeled by H3K9me2. First, we conducted ChIP using two different commercially available types of antibodies at the same concentration: Abcam, ChIP Grade, ab1220 and Millipore 05-1249. We observed that for the same concentration of antibody used, the yield for Abcam antibodies was, on average, 1.84 fold higher so that in subsequent experiments we used only Abcam ab 1220. As Abcam antibodies are IgG2a type that could potentially react with protein A and protein B, we set experiments to test which type of immobilized protein is best suited for immunoprecipitation. For this analysis, we tested similar amount of sonicated material (35,800 ng) to react with the same amounts of Abcam antibodies (1.8  $\mu$ g) and immunoprecipitated with a) Protein A beads b) protein G beads c) Protein A-G combination. We observed that protein A was most efficient of immunoprecipitating H3K9me2 chromatin but combination with protein G was able to increase the efficiency by 20% (Figure 2A). In all subsequent experiments we employed combination of protein A-G beads.

Next we tested the optimal concentration of antibodies for immunoprecipitating of fixed amount of material (each sample contained 35,800 ng of DNA) with variable concentration of antibodies (0 - 3.6  $\mu$ g/ml). We found that the maximal amount of antibody was most efficient to pull down material for deep sequencing (Figure 2B). In all subsequent experiments we used 3.6  $\mu$ g/ml of antibodies that appeared to be a cost-efficient way of conducting ChIP for H3K9me2.

Finally, we determined the number of cells providing necessary yield by keeping the amount of antibody constant (2.7  $\mu$ g/ml) and changing the number of cells taken from 0 to  $1 \times 10^7$  per sample. We estimated that we need minimum  $0.2 \times 10^7$  cells to generate enough DNA, 200 ng, needed for one sequencing (Figure 2C).

*d) Sequencing and analysis.* From a sample containing 165,200 ng of total DNA, we were able to collect 380 ng of granulocyte ChIP-recovered DNA. We used this DNA to prepare the Input and ChIP samples (200 ng each) for genomic sequencing. The DNA samples were submitted for preparing fragment libraries and their amplifications using Applied Biosystems reagents and deep sequencing ( $10 \times 10^6$  reads per sample) using SOLiD sequencer at Penn State Genomic core facility (University Park). Sequencing of granulocyte DNA is currently in progress. For bioinformatic analysis of primary ChIP-seq data generated by genome SOLiD, we have acquired license for NextGENe software from Softgenetics (University Park, PA) specifically adapted for ChIP-sequencing. We have successfully tested the *Alignment* and *Peak identification* tools to map the ChIP-recovered H3K9me2-modified chromatin to the annotated human genome (included in the NextGENe software package) and identified the expressed peaks. We have also used the *Search* tool to locate particular genes of interest and *Expression* tool to compare peak intensity between the input genome and the ChIP-recovered chromatin (see results below).

*Work on Specific Aim 2: Spatial and functional relationship between histone H3(K9) methylation and transcriptional changes in AML.*

*a) AML-derived myeloid progenitors.* We have examined 11 samples from unidentified AML patients. Cells have been previously isolated from acute leukemia human bone-marrow samples by Ficoll-Paque density gradient centrifugation and cryopreserved at Claxton laboratory (IRB protocol 2000-186). Each sample contained more cells than needed for one ChIP-sequencing experiment ( $5 \times 10^6$  cells). Cryopreserved AML cell samples were thawed and immediately fixed by 1% formaldehyde. Cell nuclei were isolated using a new protocol that we adapted to ChIP analysis and digested with micrococcal nuclease to ~150-180bp (Figure 3). Supernatants were collected and discarded and the pellets resuspended in SDS-containing lysis buffer by sonication. Yields of total chromatin varied in the range 0.14 - 1.2 mg DNA for  $10^8$  cells (Table 1). The sonicated material was immunoprecipitated with 3.6  $\mu\text{g/ml}$  Abcam, ChIP Grade, ab1220 specific antibodies against H3K9me2 and combination of protein A-G beads. Total yield of ChIP-recovered DNA was in the range of 420 - 4200 ng and ratio of ChIP to input was between 0.45 and 3.4% (Table 1). These variations are consistent with natural variations of H3K9me2 levels in leukemia blood cells described by us before (Popova et al., 2006, Exp Hematol. 34:453-462).

*b) Cultured leukemia cells:* We have grown and characterized three new acute myeloid leukemia model cell lines, K562-HP1 $\alpha$  and K562-MNEI, overexpressing two factors affecting heterochromatin structure and transcription: HP1 $\alpha$  and MNEI as well as control cell line transfected with GFP-expression vector. These cells were grown and crosslinked with 1% formaldehyde *in situ*. Cell nuclei were isolated as above and digested with micrococcal nuclease to ~180bp (Figure 4). Supernatants were collected and the pellets resuspended in SDS-containing lysis buffer by sonication. Ratio of ChIP to input was between 0.02 and 0.1 % (Table 2) i.e. dramatically lower than within AML cells consistent with low level of H3K9me2 in K562 cells detected by Western blotting (Popova et al., 2006, Exp Hematol. 34:453-462). Interestingly, overexpression of two heterochromatin proteins, HP1 $\alpha$  and MNEI was able to increase the level of this histone modification approximately 5-fold compared to the K562-GFP control (Table 2).

*c) Sequencing and analysis.* From all 11 samples of AML cells and 3 samples of cultured leukemia cells, we were able to collect at least 200 ng of ChIP-recovered DNA. We prepared the Input and ChIP samples (200 ng each) and submitted for genomic sequencing using SOLiD sequencer at Penn State Genomic core facility (University Park). Sequencing and analysis of most samples is currently in progress. For extensive bioinformatic analysis of the first two AML samples generated by SOLiD (126 and 274), we used the *Alignment* and *Peak identification* tools to map the ChIP-recovered H3K9me2-modified chromatin to the annotated human genome and identified the expressed peaks. We have also used the *Search* tool to locate particular genes of interest and *Expression* tool to compare peak intensity between the input genome and the ChIP-recovered chromatin. We were able to observe three types of site-specific changes in H3K9me 2 levels:

- i. non-coding regions containing mostly repeated DNA and associated with more than 100-fold enrichment of H3K9me2 reads (Figure 5).
- ii. Open coding regions of genes that have been previously not known to be associated with AML such as RASA4P (Figure 6). Identification of these genes shows them as potential candidates for subsequent gene expression studies.

iii. Experiments by Drs. T. Loughran and D. Claxton helped us to identify a number of genes associated with AML and also co-regulated by MNEI and HP1 such as ETS1, G0S2, STC2, ITGB2, ANGPT1, and NSBP1. Using our ChIP-seq analysis, we were able to identify specific peaks of H3K9me2 in some leukemia-associated genes such as STC2 sample but not in others such as NSBP1 (Figure 7). As the AML-associated genes also show wide expression variations among different AML samples our subsequent analysis of 9 AML samples that is currently in progress should clarify correlation of epigenetic changes of these genes with expression variation.

In summary, in the past period we: established conditions for efficient chromatin isolation from formaldehyde-crosslinked live and cryopreserved myeloid cells; tested and established conditions for efficient immunoprecipitation resulting in recovery of amounts of DNA sufficient for deep genomic sequencing; prepared samples and conducted ChIP from 12 primary myeloid cells samples including 11 AML patients and 3 cultured myeloid cell samples; sequenced and conducted genome-wide mapping of H3K9me2 in the genomes of two AML patients; and observed accumulation of peaks of H3K9me2 methylation associated with genetic loci altered in AML.

AML	126	150	176	218	245	248	267
Cell x10 <sup>8</sup>	1.2	1.2	1.2	1	1	0.9	1.6
DNA ng nuclei	1405000	275000	186000	760000	1137000	817000	711000
DNA ng input	403200	86333	92167	136267	125300	115500	70467
DNA ng ChIP	4280	924	418.8	2184	1824	1452	1416
ChIP/input	0.0106	0.0107	0.0045	0.0160	0.0146	0.0126	0.0201
AML	274	329	424	452	472	482	
Cell x10 <sup>8</sup>	1	1.2	1.1	1	0.96	0.78	
DNA ng nuclei	1205000	171000	630000	1022000	402500	456000	
DNA ng input	336000	29400	62300	90067	73266	55533	
DNA ng ChIP	1840	993.6	721.2	1344	1548	472.8	
ChIP/input	0.0055	0.0338	0.0116	0.0149	0.0211	0.0085	

**Table 1.** Yield of chromatin immunoprecipitation from AML-derived myeloid progenitors with H3K9me2 antibodies.

Cell line	K562 + HP1	K562 + MNEI	K562 + GFP
Cell #x10 <sup>8</sup>	3.4	1	1.5
DNA ng (nuclei)	4680000	1365000	2172000
DNA ng input	651000	812400	999600
DNA ng ChIP	678	829.2	193.9
ChIP/input	0.00104	0.00102	0.00019

**Table 2.** Yield of chromatin immunoprecipitation from cultured leukemia cells line K562 expressing HP1a-GFP, MNEI-GFP, and control GFP.

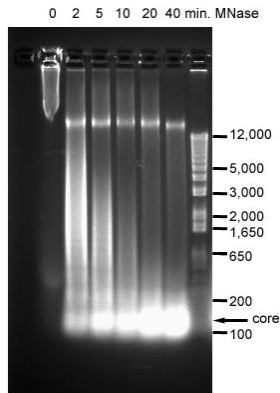


**Figure 1.** Agarose gel electrophoresis shows DNA from granulocyte nuclei in the process of Micrococcal nuclease (MNase) digestion for 0 – 40 min. as indicated. MNase converts granulocyte chromatin into nucleosome cores containing ~150-180 bp DNA fragments suitable for ChIP and genomic sequencing by SOLiD.

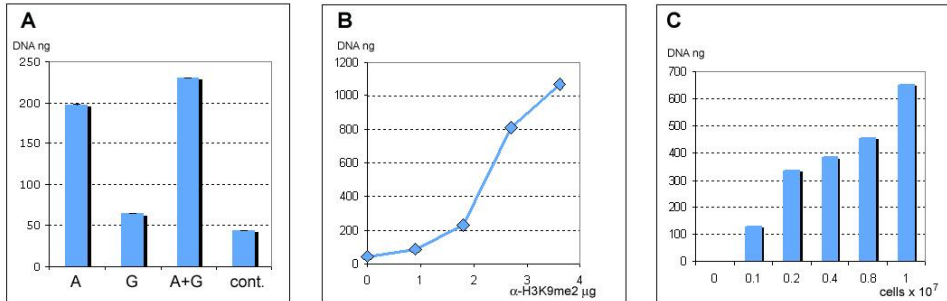


**Figure 2.** Testing and optimizing conditions for chromatin immunoprecipitation with H3K9me2 antibodies. A: similar amount of chromatin (35,800 ng by DNA) were reacted with 1.8 μg of Abcam ab 1220 antibodies and immunoprecipitated with Protein A beads, protein G bead, and Protein A+G combination. Control immunoprecipitation contained no antibodies and A+G beads. B: chromatin samples each containing 35,800 ng of DNA were reacted with variable concentration of α-H3K9me2 antibodies as indicated. C: Chromatin samples isolated from different number of cells (indicated at the X-axis) were reacted each with 2.7 μg α-H3K9me2 antibodies. Y-axis shows the amount of DNA recovered by ChIP.

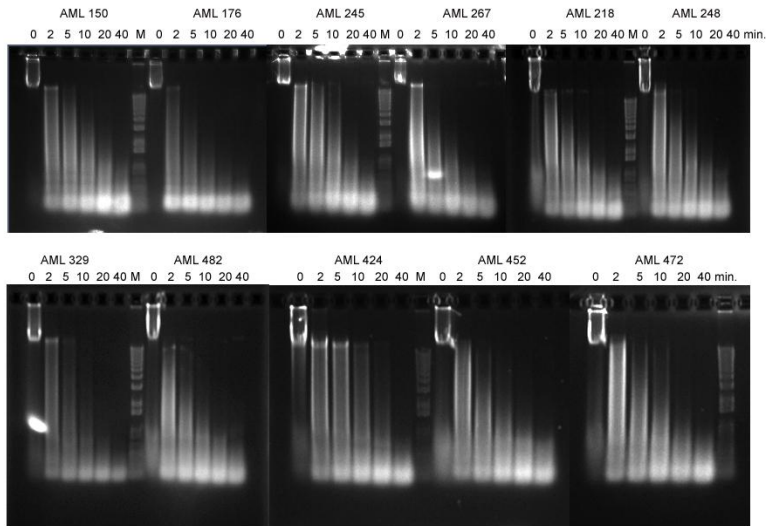


**Figure 3.** Agarose gel electrophoresis shows DNA from nuclei of 11 different human AML samples in the process of Micrococcal nuclease (Mnase) digestion for 0 – 40 min. as indicated.

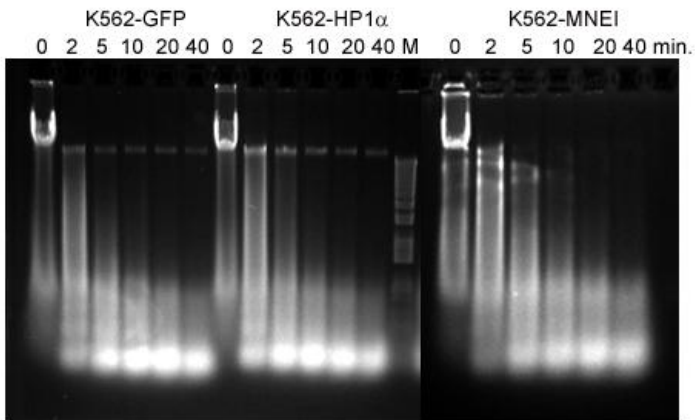


**Figure 4.** Agarose gel electrophoresis shows DNA from nuclei of K562 cells expressing GFP control, GFP-HP1 $\alpha$  and GFP-MNEI. Nuclei were digested with Mnase for 0 – 40 min. as indicated.



**Figure 5.** Example of an AML genome locus showing high enrichment with H3K9me2. Top panel: low-resolution map of a human chromosome locus (48737000-52895000 on human chromosome 4) showing two intergenic regions containing strong peaks of H3K9me2 (gray downward bars) resulting from ChIP-sequencing of AML 274. Transcribed regions are shown with blue arrows. Middle panel: high resolution mapping of human chromosome 4 locus 49118680-49119360 showing positions of actual sequence reads recovered by ChIP. Bottom panel: Expression comparison report for human chromosome 4 locus 49049000-49205000 showing a dramatic enrichment of H3K9me2 in the ChIP (purple) vs. Input DNA (red).

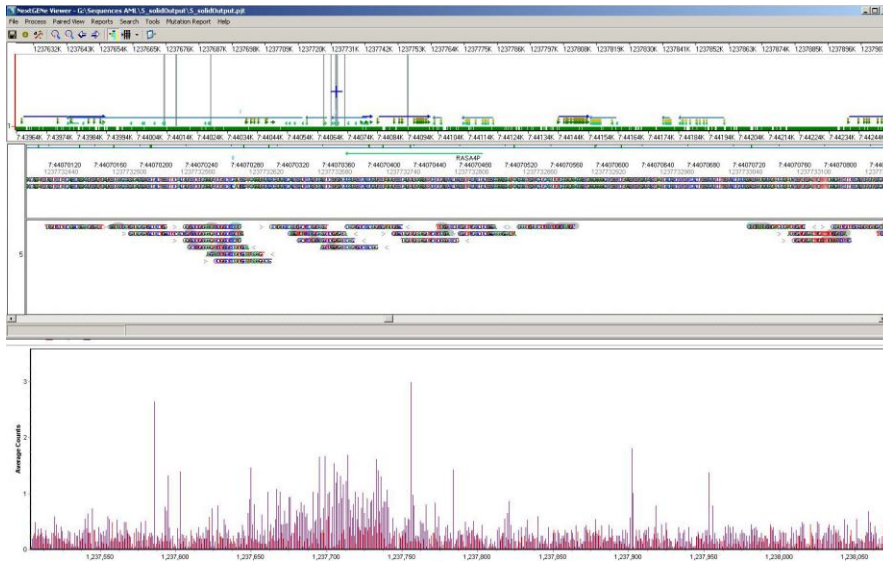


**Figure 6.** Example of an AML genome locus showing moderate enrichment with H3K9me2 over a gene ORF. Top panel: low resolution map of a human chromosome locus (43964000-44244000 on human chromosome 7) showing ORF of RASA4 gene regions (blue cross) containing several moderate peaks of H3K9me2 (gray downward bars) resulting from ChIP-seq on AML 274. Middle panel: high resolution mapping of human RASA4 locus 440701120-44070840 showing positions of actual sequence reads recovered by ChIP. Bottom panel: Expression comparison report for human chromosome 4 locus 43960000-44250000 showing a dramatic enrichment of H3K9me2 in the ChIP (purple) vs. Input DNA (red) in the area containing RASA4 ORF.

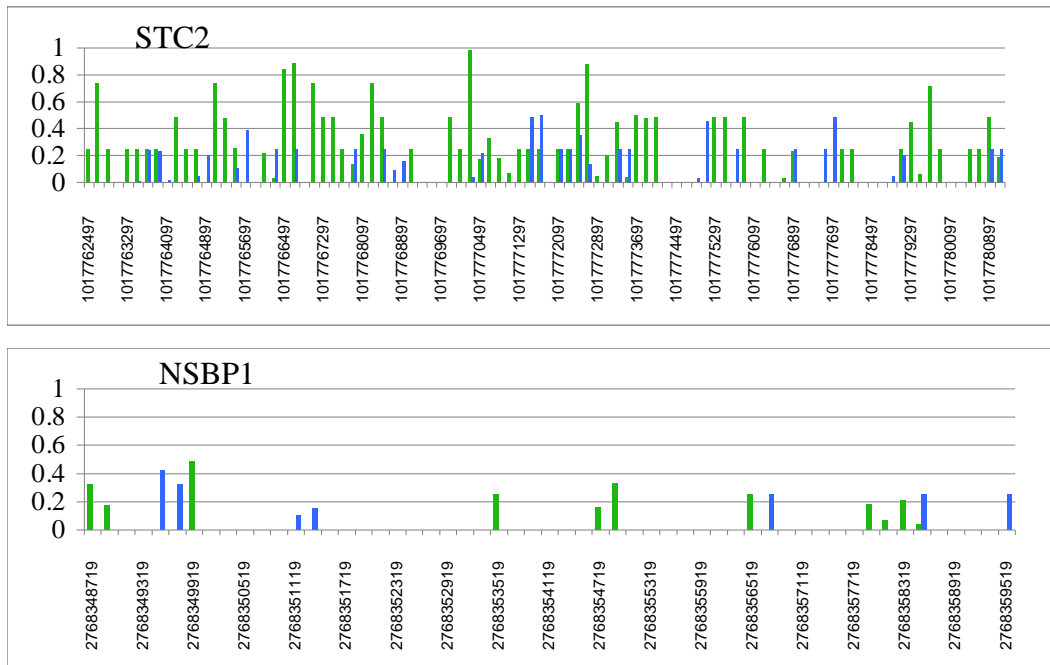


**Figure 7.** Examples of AML-associated genes showing variable levels of H3K9me2 over the gene's ORF. Top panel: expression comparison report for human STC2 locus showing a significant enrichment of H3K9me2 resulting from ChIP-seq on AML 126 (green) vs. Input DNA (blue). Bottom panel: human NSBP1 locus showing no enrichment of H3K9me2 Chip from ChIP from 126 (green) vs. Input DNA (blue).

## **Research Project 6: Project Title and Purpose**

*Bridging the Gap between Label-Retention and Mammary Stem Cell Properties* - Breast cancer patients frequently suffer relapse after prolonged periods of clinically undetectable disease. Whether dormant breast cancer is comprised of quiescent cells versus cycling cells, whose proliferation is offset by cell death, remains unknown. When modeling dormant breast cancer by reversing Wnt1-initiated mammary tumorigenesis in transgenic mice, we found that minimal residual disease (MRD) lesions harbor both latent malignant potential and mammary gland reconstitution capacity. Moreover, our preliminary data demonstrate that MRD lesions harbor a slow-cycling mammary epithelial cell (MEC) population. We propose to demonstrate that these quiescent cells are enriched for expression of validated mammary stem cell markers.

### **Duration of Project**

7/1/2010 - 6/30/2011

### **Project Overview**

A diverse set of observations suggest that stem cells within normal and malignant mammary epithelium may be capable of entering into and emerging from prolonged periods of quiescence. However, it is not yet clear whether mammary stem cells cycle infrequently relative to other mammary epithelial cells (MECs).

We hypothesize that both normal and malignant mammary epithelium harbor a relatively quiescent MEC compartment with stem cell-like regenerative capacity. Here, we propose to demonstrate that these quiescent cells are enriched for expression of validated mammary stem cell markers by completing two specific aims. In Specific Aim 1, we will generate normal and neoplastic mammary tissue in transgenic mice and identify the relatively quiescent label-retaining cells (LRCs) using an H2B-GFP reporter transgene. In Specific Aim 2, we will determine whether H2B-GFP LRCs possess stem cell-associated biological features.

### **Principal Investigator**

Edward J. Gunther, MD  
Associate Professor of Medicine  
Pennsylvania State College of Medicine  
Biomedical Research Building, H059  
500 University Drive  
Hershey, PA 17033

### **Other Participating Researchers**

None

## Expected Research Outcomes and Benefits

The cell-of-origin that gives rise to breast cancer remains elusive. One influential model of breast carcinogenesis posits that mutations responsible for initiating tumorigenesis accrue in a long-lived, slow-cycling mammary stem cell compartment. Remarkably, though great strides have been made in delineating the mammary epithelial cell developmental hierarchy, it remains unclear whether mammary stem cells are actively cycling or relatively quiescent. Our studies will identify slow cycling mammary epithelial cells in transgenic mice and determine whether these relatively quiescent cells express the cell surface markers associated with mammary stem cells.

## Summary of Research Completed

Identifying Mammary Epithelial Cell (MEC) Compartments Using Cell Surface Markers. First, we tested whether immunophenotyping using the CD24 and CD49 cell surface markers would resolve cell populations derived from our transgenic mouse mammary glands into discrete mammary cell compartments. Mammary glands from MMTV-rtTA/Tet-O-H2BGFP bitransgenic female were harvested at necropsy, and then processed to generate single-cell suspensions. Briefly, the glands were subjected to mechanical mincing, followed by serial enzymatic digestions with collagenase and dispase. After further purification using centrifugation and filtration steps, immune and endothelial cells were removed using immunomagnetic beads. Finally, the samples were incubated with fluorophore-conjugated antibodies, washed, and analyzed by flow cytometry.

As expected, 2-parameter plots permitted identification of discrete cell populations (Figure 1A). Consistent with previous reports, we found that the CD24<sup>High</sup>/CD49<sup>Low</sup> subset is highly enriched for luminal MECs (see below). We also identified the CD24<sup>Low</sup>/CD49<sup>high</sup> subset, which is comprised of basal MECs. This basal MEC subset is known to include both a small population of putative mammary stem cells and a much larger population of differentiated myoepithelial cells. Lastly, we identified the CD24<sup>Low</sup>/CD49<sup>low</sup> subset comprised of non-epithelial stromal cells. This immunophenotyping strategy was subsequently used to define the mammary cell compartments occupied by quiescent versus cycling mammary cells derived from 25 MMTV-rtTA/Tet-O-H2BGFP female mice.

Pulse-Chase H2B-GFP Labeling Permits Monitoring of MEC Proliferation History. Previously, Fuchs and colleagues used doxycycline (Dox)-dependent expression of an H2B-GFP transgene to perform pulse-chase labeling studies in mouse skin, thereby permitting discrimination between quiescent and cycling cells. To test the feasibility of adapting this strategy to permit pulse-chase labeling of mouse MECs, we generated a cohort of MMTV-rtTA/Tet-O-H2BGFP mice and analyzed mammary GFP signal intensity on a per-cell basis under pulse and pulse-chase conditions. Briefly, 10 week-old bitransgenic female mice were fed Dox-impregnated chow for 3 days, then either sacrificed immediately (pulse condition) or switched to Dox-free chow for a period of Dox withdrawal (pulse-chase condition) prior to sacrifice and tissue harvest. Freshly collected mammary glands were then processed to generate single cell suspensions, which were immunostained and analyzed by flow cytometry as described above.

Pulse treatment of bitransgenic mice with Dox reproducibly yielded robust H2B-GFP labeling of a discrete subset of MECs (Figures 1B, 2). This GFP<sup>High</sup> population was restricted to the CD24<sup>High</sup>/CD49<sup>Low</sup> luminal compartment. We tested whether cell proliferation history could be inferred from the extent of H2B-GFP washout measured by flow cytometry under pulse-chase conditions. Glands from mice pulsed with Dox yielded a reproducible fraction of GFP-labeled cells residing in a single high-intensity (GFP<sup>High</sup>) peak on single parameter plots. In contrast, glands from mice subjected to the pulse-chase condition reproducibly yielded numerous discrete peaks of lower GFP intensity, and these GFP<sup>Low</sup> peaks reliably created regular sawtooth patterns on single parameter plots (Figure 1B).

We speculated that the discrete peaks in GFP intensity identified under pulse-chase conditions might reflect the partitioning of GFP-labeled histones during cell division. To test this notion, we analyzed both 2-week and 3-week chase data by plotting the median intensities of successive peaks against peak number on a binary logarithmic scale. These plots yielded very high correlation coefficients ( $R^2 > 0.999$ ), strongly suggesting that the sawtooth pattern elicited by H2B-GFP washout derives from successive halving of GFP intensity. As such, each two-fold, step-wise decrease in GFP intensity very likely reflects one additional cell division undertaken during the chase. Importantly, this methodology permits discrimination between cells that are relatively quiescent (i.e., GFP<sup>High</sup>; zero or one cell divisions) versus those that are cycling (i.e., GFP<sup>Low</sup>; multiple cell divisions).

H2B-GFP Labeled Luminal MECs Remain Luminal in Character Whether Quiescent or Cycling. Having validated our strategies for immunophenotyping and pulse-chase labeling of MECs, we next performed these combined analyses on a cohort of MMTV-rtTA/Tet-O-H2BGFP mice subjected to timed chases (Figure 2). Mammary glands from at least 5 mice were analyzed at each of 5 chase time points (0, 2, 3, 4, and 5 weeks), and the resulting data were analyzed using the gating schemes depicted in Figure 1. H2B-GFP labeling was restricted to the luminal MEC compartment during pulse, as expected. Notably, labeled cells continued to reside in the luminal compartment, regardless of the degree of H2B-GFP washout (Figure 2). Thus, the luminal MECs labeled in our experiment remained lineage-restricted for at least 5 weeks, whether quiescent or cycling.

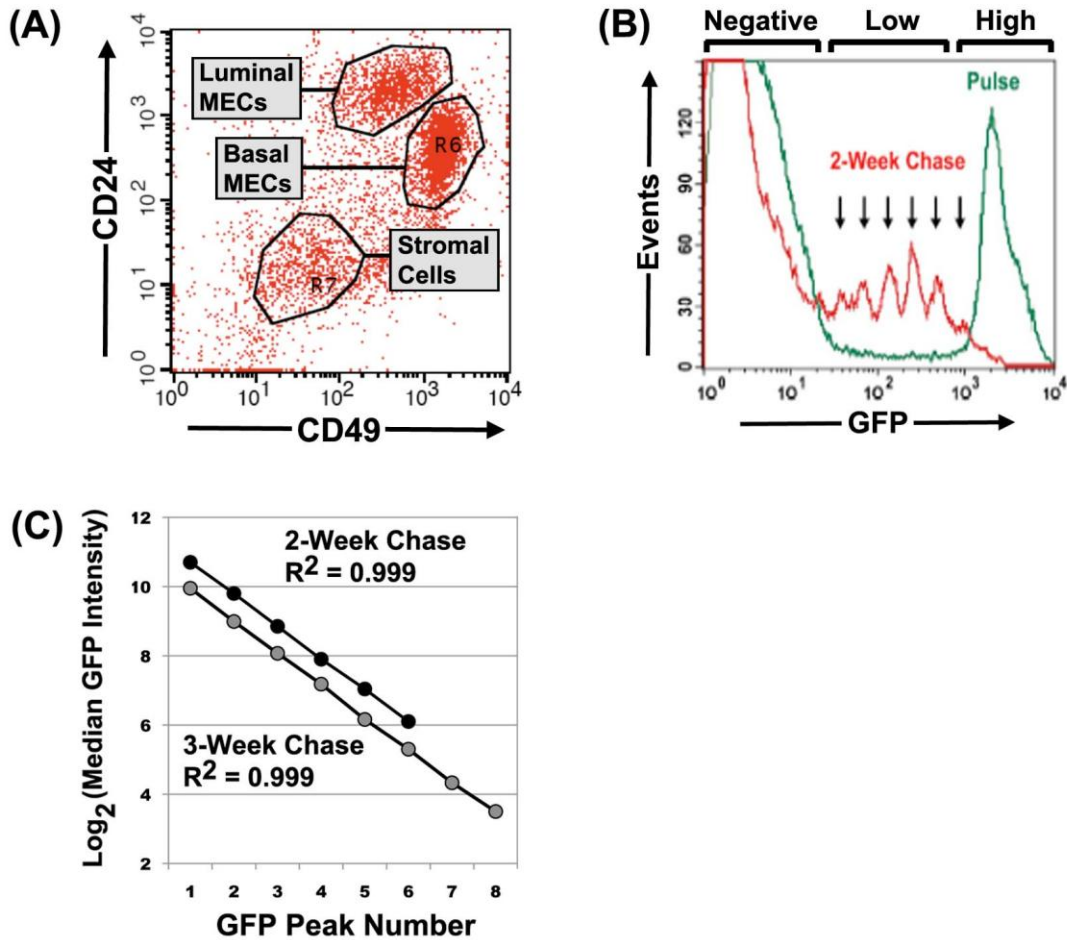


**Figure 1. Validation of Immunophenotyping and Pulse-Chase Labeling Strategies.** *A. Immunophenotypes of discrete MEC compartments.* Single-cell suspensions derived from transgenic mouse mammary glands were immunostained for the CD24 and CD49 cell surface markers and analyzed by flow cytometry. The panel depicts a representative two-parameter plot with population gates. *B. Pulse-chase H2B-GFP labeling in MMTV-rtTA/Tet-O-H2BGFP mice.* Mammary glands from adult virgin bitransgenic mice were harvested under the pulse-chase conditions indicated. After preparing single cell suspensions, samples were analyzed by flow cytometry and single-parameter plots were generated. The panel depicts data derived from two mice, which are representative of more than 30 animals analyzed. Downward pointing arrows denote GFP peak intensities within the sawtooth pattern that reproducibly arose during chase. *C. GFP peaks arising during chase show step-wise halving of GFP intensity.* The panel shows 2-week and 3-week chase data from representative mice depicted graphically. The median intensities of successive peaks identified on single-parameter histograms were plotted against peak number on a binary logarithmic scale.

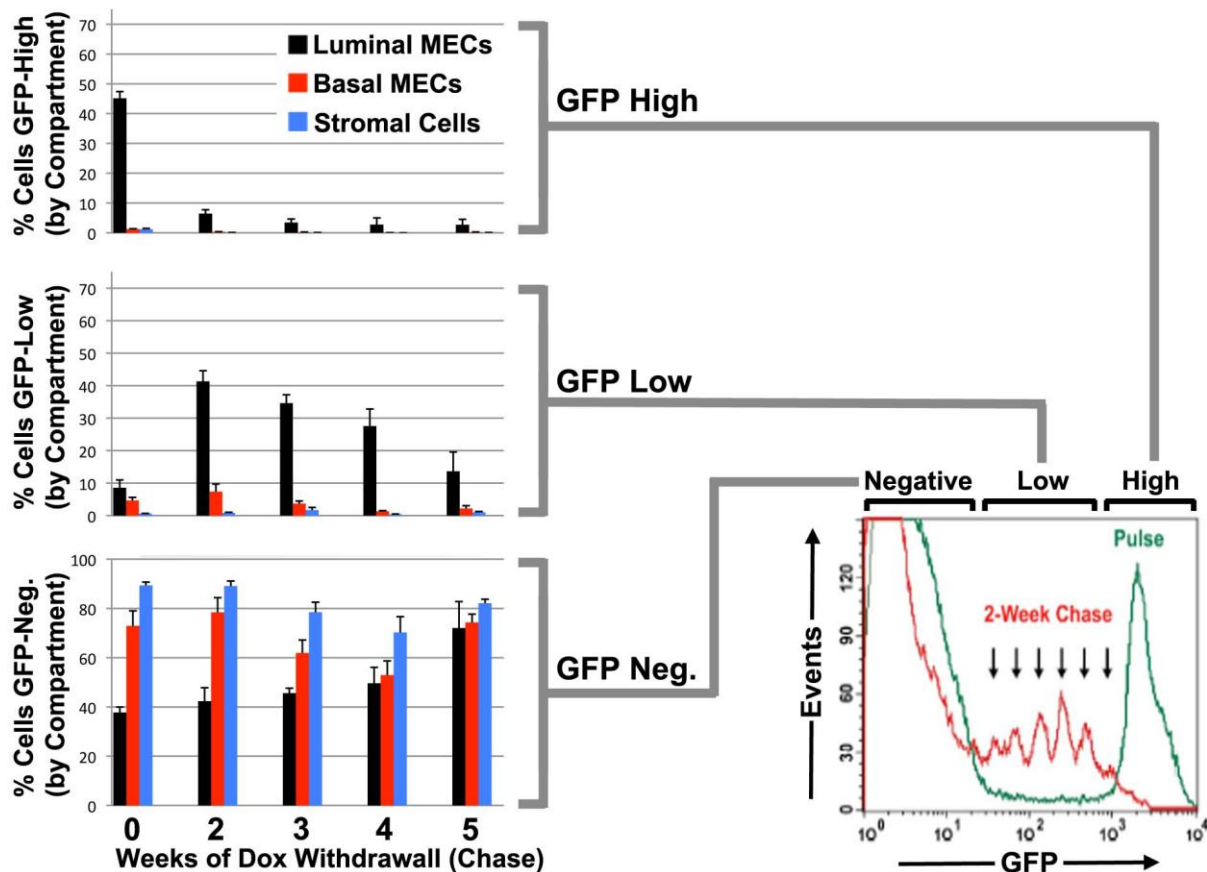


Figure 2. H2B-GFP Labeled Luminal MECs Show Lineage Fidelity Whether Quiescent or Cycling. Bars depict the mean values obtained by analyzing 5 or more mice for each pulse-chase condition. Error bars depict the SEM. The panel at lower right is reproduced from Figure 1 to illustrate the boundaries used to separate GFP high vs. low vs. negative.

**Research Project 7: Project Title and Purpose**

*Neural Control of Breathing by a Signal Encoding Venous Pressure: Implication in Heart Failure* - Respiratory symptoms such as chronic hyperventilation are dominant expressions of cardiac insufficiency. Hyperventilation induced hypocapnia also has the potential to disrupt sleep architecture and to provoke central sleep apnea, further limiting quality of life in these patients. Distension of the venous system, a common feature of cardiac failure, leads to the activation of neural afferent fibers located in the adventitia of the post capillary bed, which in turn increases breathing. The proposed studies are intended to establish, in an animal model, the involvement of such a mechanism at rest and during muscle activity.

**Anticipated Duration of Project**

7/1/2010 – 12/31/2011

**Project Overview**

Profound changes in the control of breathing accompany the syndrome known as ‘heart failure’

(HF). The mechanism(s) responsible for the excessive stimulation of breathing in HF which precipitate hypocapnia, Cheyne-Stokes breathing and dyspnea, are far from being understood. Given HF is a condition which affects millions of people in the United States, there is an urgent need for research which will aid in the development of effective therapies for treating or reducing the respiratory-related consequences of this disease state. Our research group has proposed that, in the absence of pulmonary oedema, the excessive ventilation that is observed in HF patients is caused by an increase in systemic venous pressure. My experiments will specifically determine whether an increase in systemic venous pressure, leads to a stimulation of breathing, independently of changes occurring in the systemic pulmonary and systemic arterial circulation. I will also determine the mechanism through which breathing is stimulated. Using a novel, spontaneously breathing, anesthetized sheep preparation, I will employ a combination of venous occlusion and veno-venous shunt techniques in order to measure the ventilatory response to changes in systemic venous pressure.

*Specific Aim 1:* To determine the magnitude of the increase in pulmonary ventilation caused specifically by an increase in pressure (load) in the systemic venous system. I will use a veno-venous circulatory bypass with a venous reservoir bag to isolate the contribution of increased venous pressure in the hind limb tissues, and determine the effects of the resulting increase in systemic venous pressure on ventilation. I predict that an increase in systemic venous pressure achieved only via increasing the load imposed upon venous return will stimulate breathing and lower PaCO<sub>2</sub>.

*Future direction:* The next step will be to investigate the mechanism through which an increase in systemic venous pressure causes an excessive level of pulmonary ventilation. These experiments will directly test the hypothesis that the stimulation of breathing which results from an increase in systemic venous pressure arises from a stimulation of mechanosensitive afferents in the muscle tissue that respond to changes in vascular distension. Infusions of various agents into the hind limbs will be used to block the activation of mechanogated ion channels on group III and IV muscle afferents and transient receptor **potential vanilloid receptors**.

### **Principal Investigator**

Philippe Aaron Haouzi, MD, PhD  
Professor of Medicine  
Penn State Hershey Medical Center  
Pulmonary Medicine  
500 University Drive  
Hershey, PA 17033

### **Other Participating Researchers**

Harold James Bell, PhD – employed by Penn State University College of Medicine

### **Expected Research Outcomes and Benefits**

Approximately 5 million Americans suffer from heart failure. Somewhat surprisingly, it is

pulmonary symptoms that have the most impact on the quality of life of these patients. People with heart failure breathe more in comparison to people without heart failure, and they often complain of feeling ‘breathless’, or ‘unable to catch their breath’. At present, in many patients, little can be done to decrease this “feeling” since many various and different, yet poorly understood, mechanisms can account for these respiratory symptoms. We have good reason to believe that one of these mechanisms is an increase in the pressure that blood exerts in the venous system. Heart failure causes an increase in the pressure that is present in the veins because the heart is less efficient, which causes a tendency for blood to ‘back up’ in the circulation. The experiments I describe in this project will determine how much this increased pressure in the veins can stimulate breathing and may help to explain the resulting sensation of breathlessness in heart failure. Should we find that this mechanism is an important one, then we can work upon developing new treatment strategies that will greatly improve the quality of life in people living with heart failure.

## **Summary of Research Completed**

### Introduction

As presented in our project, we have proposed that one of the causes of the excessive respiratory stimulation observed in cardiac patient is related to the distension of the peripheral venous/venular system, via the stimulation of a specific population of muscle afferent nerve endings. We referred to this homeostatic control system as *the ‘vascular distension hypothesis’*. The specific goal of the present project was to determine whether the gain of the ventilatory response to vascular distension is affected when central venous return to the heart is decreased, due the opposing effect the cardiac mechanoreceptors and of arterial baroreflex. We have developed a novel experimental model in spontaneously breathing, anaesthetized sheep which allows us to dissociate venous return from venous distension. The sheep were equipped with extracorporeal circuit comprising an external venous reservoir that allows independent control over the rate of venous return to the heart during the obstruction of the venous outflow from the hindlimbs (Figure 1).

### Methodological Basis

The extracorporeal circuit is presented in Figure 1. The circuit connected the inferior and superior vena cava (IVC and SVC, respectively) via 2 pumps with a large venous reservoir bag (3 liters) interposed between the pumps. Pump 1 withdrew blood from the inferior vena cava to the reservoir bag and pump 2 reinjected the blood at the same rate. The circuit was primed with a solution containing heparin before any data collection is performed. An intravenous occlusion catheter was placed in the IVC to obstruct venous outflow and create a distension of the hindlimb circulation. The protocol applied is the one presented in the project.

### Results

Nine sheep have been studied. Out of the 9 animals studied, data from 7 sheep could be analyzed:

#### *Change in Venous Return without distending the Peripheral Venous System (no venous distension and low cardiac output)*

As shown on Figure 2, reducing venous return was obtained by stopping pump 2. The effects

were a reduction in venous return to the heart, a decrease in blood pressure and an increase in the volume of blood in the reservoir bag. We found that there was very little effect on breathing as we have previously reported. In some cases ventilation actually dropped but the changes in ventilation were not significant ( $-8\% \pm 12$  from baseline). End tidal PCO<sub>2</sub> decreased by  $12 \pm 4$  Torr reflecting the reduction in venous return. Restoring venous return restored arterial blood pressure.

*Peripheral Venous Distension (venous obstruction) with low venous return (venous distension and low cardiac output)*

The pumps (P1 and P2) were stopped while the IVC was occluded. In all instances breathing started to rise progressively by  $65 \pm 8\%$  (Figure 2). End tidal CO<sub>2</sub> dropped. In other words, for a reduction in blood pressure similar to condition 1, ventilation was systematically stimulated when the venous system was distended.

*Peripheral Venous Distension (venous obstruction) while restoring venous return (venous distension and “normal” cardiac output)*

When Pump (P2) was allowed to restore venous return while pump 1 was stopped and IVC was occluded, ventilation decreased to baseline (Figure 2).

*Peripheral Venous Distension while increasing central venous return to the heart (venous distension and high cardiac output)*

Figure 3 illustrates the effects of venous occlusion in condition of very high venous return. This condition resulted in all instances in a stimulation of breathing which averaged  $153 \pm 27\%$ , along with a reduction in end tidal CO<sub>2</sub>.

Conclusion:

Our results are showing that there is a genuine stimulation of breathing triggered by peripheral venous distension which interacts with the stimulation of other receptors located in the central circulation when venous return increases changes. The conditions created by these models are aimed at mimicking some of the elementary changes in hemodynamic changes in right sided or global heart failure. When venous return was restored along with venous distension, ventilation returned to baseline. Conditions of high venous return produced an abrupt increase in breathing when associated with venous distension.

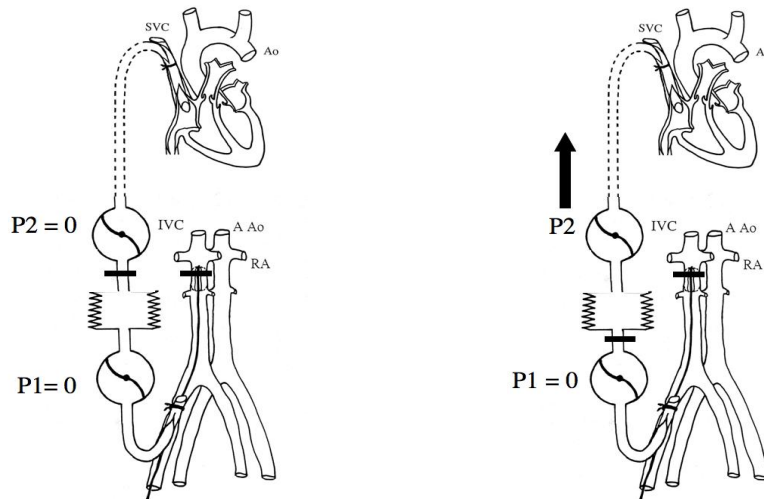


**Figure 1:** Schematic representation of the model where the inferior vena cava (IVC) was occluded. The reservoir bag contains venous blood at the same composition as the blood returning from the hindlimb circulation. During the occlusion of the inferior vena cava, the flow of blood from pump 2 (P2) was adjusted so that cardiac output will lower *Left panel (P2 was stopped)*, the same or higher than in *baseline conditions (Right panel)*.

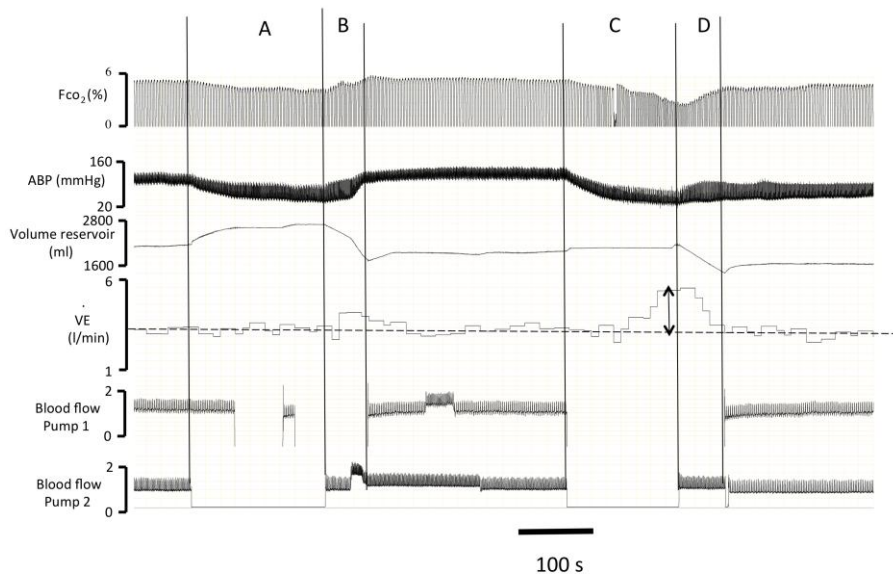


**Figure 2:** **A** responses to the reduction in venous return. Pump 2 was stopped, as pump 1 was still working venous return decreased, leading to a decrease in cardiac output and blood pressure (ABP). Minute ventilation (VE) did not change in this example. **B** Venous return was restored. **C** The vena cava was occluded while pump 1 and 2 were stopped. ABP decreased just like in condition A, but ventilation was progressively stimulated. Restoring venous return in **D** decreased ventilation to baseline levels.

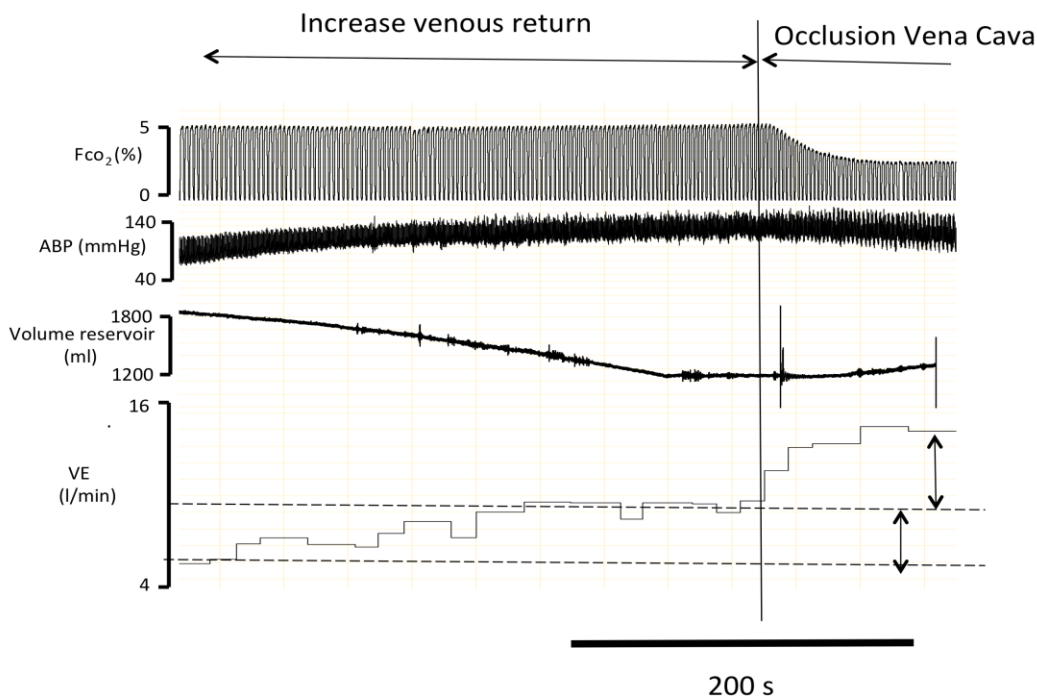


**Figure 3:** Venous return was increased by about 50 % of baseline (decrease in the volume of the reservoir bag), ventilation was stimulated. Occluding the vena cava produced a rapid and large increase in ventilation

### **Research Project 8: Project Title and Purpose**

*Influence of Brain Astrocyte Glutamate Concentrations on Neurotransmission* - The most abundant type of cell in the brain is the astrocyte. Astrocytes may control neurotransmitter traffic by lowering the concentration of neurotransmitter glutamate in synaptic spaces. Vesicular glutamate released from presynaptic neurons into the synaptic space stimulates depolarization and electrical signal transduction by post-synaptic neurons. The synaptic space barrier is composed of membranes from both presynaptic and post-synaptic neurons and astrocytes. Astrocytes rapidly remove glutamate from the synaptic space which would otherwise prolong signal transmission and cause excitotoxicity. The study examines the properties of the glutamate transporter in the astrocyte membrane to evaluate the influence of the intracellular astrocyte glutamate on inward transport and examines how cytosolic concentrations of glutamate are regulated by astrocytic enzymes.

### **Duration of Project**

1/1/2010 – 6/30/2011

## **Project Overview**

Glutamate in the brain acts as a source of nutrient energy and as an excitatory neurotransmitter. This project focuses on mechanisms that ensure optimal use of glutamate as a neurotransmitter, by providing optimal maintenance of low glutamate concentrations in astrocytes. Astrocytes form part of the boundaries of the synaptic spaces. Na<sup>+</sup>-linked glutamate transporters in the astrocyte plasma membranes provide the energy for the “pump” that keeps glutamate in the low  $\mu$ molar range in the synaptic space. We will test the hypothesis that maintenance of low concentrations of glutamate in the astrocyte cytosol augments the capacity of the astrocytes to transport glutamate from the synaptic space and into astrocytes.

First, we will measure the rate of [U-<sup>14</sup>C] glutamate entry into cultured astrocytes as a function of astrocytic, cytosolic glutamate. The external, [U-<sup>14</sup>C] glutamate will be held constant at 2 $\mu$ M. The intracellular glutamate will be varied by preliminary incubations of cultured cells with unlabeled glutamate (these concentrations will be varied from 0-20mM). Glutamate-loaded cells will be rinsed in glutamate-free Krebs Ringer bicarbonate solution. Glutamate will not leak out because of the presence of the Na<sup>+</sup>-linked glutamate transporter in the plasma membrane. The rate of transport of glutamate into the cells may be faster when intracellular glutamate is low and we expect to be able to determine the cytosolic glutamate concentration that results in half maximal inhibition of <sup>14</sup>C-glutamate entry into the cells.

Secondly, we will investigate the ability of astrocytic enzymes such as malic enzyme (ME1) and phosphoenolpyruvate carboxykinase (PEPCK2) to maintain low levels of glutamate in astrocytes. These enzymes are expressed mainly in brain astrocytes and they irreversibly convert malate to pyruvate. Since glutamate is rapidly converted to malate in astrocytes, these enzymes act as glutamate drainage sinks. The activities of ME1 and PEPCK2 probably play a significant role in maintaining low astrocyte glutamate levels.

We plan to use gene silencing techniques to lower expression of these two enzymes individually and together. The necessary siRNAs are available commercially. Cells will be exposed to the inhibitory nucleotides either separately or together. We expect that they will lower astrocyte glutamate levels to concentrations that stimulate entry of external glutamate into the astrocytes. If that happens, we will conclude that these enzymes are important for brain function and search for drugs that influence their activity *in vivo*.

## **Principal Investigator**

Kathryn F. LaNoue, PhD  
Distinguished Professor  
Pennsylvania State University Hershey Med Center  
Department of Cellular and Molecular Physiology  
500 University Drive  
P.O. Box 850, MC H166  
Hershey, PA 17033-0850

## Other Participating Researchers

None

## Expected Research Outcomes and Benefits

In this project we will learn how cytosolic glutamate levels are regulated in astrocytes and whether low cytosolic concentrations are critical for neurological health. Three enzymes in astrocytes lower astrocytic glutamate pool sizes. These are glutamine synthetase (GS), ME1, and PEPCK2. Inhibition of glutamine synthetase will slow neurotransmission, lower glutamine levels, increase astrocytic glutamate, and deplete neuronal glutamate but will not induce glutamate excitotoxicity, seizures or neuronal cell death. Therefore, our focus is on ME1 and PEPCK2.

Disruption of glutamate uptake from synaptic spaces, perhaps due to excess glutamate within astrocytes, may play a role in neurological disorders including cerebral ischemia, neurodegeneration, migraine, cerebral edema, and hepatic encephalopathy. Astrocytic dysfunction has also been cited as a cause of seizures in the brain. Excitotoxicity of glutamatergic neurons has been implicated in Alzheimer's disease, possibly induced by malfunction of the astrocytes and of the glutamate glutamine cycle. If trials using siRNA to slow ME1 and PEPCK2 in the cultured astrocytes succeed and lower astrocyte glutamate levels, we will search for drugs that inhibit the activity of these enzymes in the brain such as the PEPCK inhibitor, sulfoacetate, which may be effective in treatment of the neurological diseases cited above.

In future studies, we may also evaluate the roles of these enzymes in neurological health by generation of mice with disruptions of the ME1 or PEPCK2 genes. Determination of the resistance of these mice to neurological stresses such as chemically induced seizures or cerebral ischemia will reveal the importance of efforts to find ways to lower astrocytic glutamate *in vivo*.

## Summary of Research Completed

Studies of glutamate metabolism in the central nervous system (brain and retina) were initiated to evaluate the role of glial cells in prevention of glutamate excitotoxicity. Glutamate is the most abundant neurotransmitter in the brain and retina but it has dual roles because it acts both as a neurotransmitter and as an energy generating metabolite. Glutamate can enter neuronal and glial cells (astrocytes in brain, Müller cells in the retina) where it is transaminated to  $\alpha$ -ketoglutarate. When glutamate increases outside the cells due to rapid neurotransmission or anoxia, the extracellular glutamate can excite post synaptic neurons, produce excessive calcium in the cytosol, hydrolyze cell membrane lipids and cause neuronal death. Central nervous systems glial cells act as safeguards preventing glutamate excitotoxicity by removing glutamate from the extracellular fluid and converting it to glutamine. Our studies show that glutamate levels in astrocytes remain surprisingly constant when challenged with increasing amounts of extracellular glutamate. We have published a report of glutamate metabolism in control and diabetic retinas, (Gowda, K., Zinnati, WJ and LaNoue, KF, 2011) which was supported by funds from this grant. We demonstrated in that report the existence of an important glutamate buffering system in

Müller cells of the retina. The buffer prevents accumulation of intracellular glutamate in Müller cells which would otherwise slow influx of glutamate.

### Studies Undertaken and Completed

To monitor the influence of diabetes on glutamate metabolism, we measured 1). Glutamatergic neurotransmission, 2). Glutamate synthesis from  $^{14}\text{CO}_2$  and pyruvate (anaplerosis) and 3). [U- $^{14}\text{C}$ ] glutamate conversion back to  $^{14}\text{CO}_2$  and  $^{14}\text{C}$ -pyruvate cataplerosis. The data suggested the existence of a glutamate buffering anaplerotic/cataplerotic metabolic cycle in astrocytes which is uncoupled by diabetes. In retinal Müller cells, anaplerosis is initiated by a small pyruvate pool which is also the product of cataplerosis. In cells from diabetic rats the cataplerotic pathway, (glutamate conversion to  $\alpha$ -ketoglutarate and then to pyruvate) is reduced by 90% because glutamate transamination by branched chain aminotransferase is competitively inhibited by elevated branched chain amino acids (BCAAs). Branched chain amino acids, but not the ketoacids, were almost twice as high in diabetic rat retinas compared to euglycemic rat retinas. The data suggest that glutamate levels in retinal Müller cells from diabetic rats are elevated due to the presence of excess branched chain amino acids, and that the elevated glutamate in Müller cells causes glutamate excitotoxicity.

In order to monitor glutamate formation and pool sizes in the retina and to understand the metabolic changes in retinas of diabetic rats, we measured three metabolic pathways for glutamate in excised control and diabetic retinas. These metabolic processes were neurotransmission, de novo anaplerotic glutamate synthesis from pyruvate and  $\text{CO}_2$  and cataplerotic, irreversible disposal of glutamate to form pyruvate and  $\text{CO}_2$ . Glutamate neurotransmission was quantitated by measuring flux through the glutamate/glutamine cycle as we have done previously (Xu et al. 2007). We also measured rates of de novo synthesis of glutamate from  $^{14}\text{CO}_2$  and pyruvate which is catalyzed by enzymes expressed in retinal Müller cells and is dependent on ATP and pyruvate carboxylase (PC). We traced the carbon flow of anaplerosis by incubating excised retinas with  $^{14}\text{CO}_2$  and measuring incorporation of carbon 14 into the products. Fig 1A illustrates the pathways. Most of these enzymes are expressed in Müller cells in the retina and in brain they are expressed predominantly in astrocytes (Vogel et al. 1998; Vogel et al. 1998; Waagepetersen et al. 2002). Malic enzyme but not pyruvate carboxylase is also active in brain neurons (Olstad et al. 2007). Fig 1A illustrates glutamate entry into the Müller cells from the neurons and the return of the glutamate carbon (as glutamine) to the neurons. Finally, we measured the reversal of anaplerosis, (i.e. cataplerosis). This is the process that converts glutamate and citric acid cycle intermediates to pyruvate and  $\text{CO}_2$ . Cataplerotic carbon flow was monitored by including [U- $^{14}\text{C}$ ] glutamine in the medium and following appearance of carbon 14 (as a function of time) into pyruvate/lactate. The pathways of cataplerosis, including activities in both Müller cells and neurons and the flow of labeled metabolites between neurons and Müller cells are illustrated in Fig 1B. Cytosolic malic enzyme (ME1) and phosphoenolpyruvate carboxykinase (PEPCK2) both catalyze cataplerosis. These enzymes are expressed in Müller cells in the retina and astrocytes in the brain (Schmoll et al. 1995; Cruz et al. 1998; Vogel et al. 1998). Because anaplerosis and cataplerosis are likely to be present in the same cell type (Müller cells in the retina), and have overlapping substrates (pyruvate), they can catalyze a futile cycle. Still the site of expression of malic enzyme remains unresolved (Olstad et al. 2007). Cataplerotic/anaplerotic cycling together are sometimes referred to as pyruvate recycling (Cruz et al. 1998). Interaction between the two processes (anaplerosis

and cataplerosis) can only occur when they are present in the same cell type. They influence each other, and the anaplerotic and cataplerotic fluxes are similar in magnitude. We focused on glutamate metabolism in the Müller cells because Müller cells remove glutamate from synaptic spaces. They express Na<sup>+</sup> linked glutamate transporters which remove of glutamate from the extracellular synaptic spaces.

To monitor glutamate de novo synthesis, we measured rates of anaplerosis in the retinas. Pyruvate carboxylase (PC) is the first and rate limiting enzyme in the pathway of anaplerosis. PC initially converts pyruvate and CO<sub>2</sub> to oxaloacetate. The oxaloacetate enters the citric acid cycle and increases the citric acid cycle intermediates including  $\alpha$ -ketoglutarate and glutamate (Fig 1A). Excessive activity of this pathway causes glutamate excitotoxicity, because an increase in glutamate in the Müller cells interferes with uptake of glutamate into the Müller cells from the extracellular spaces. However the pathway was not increased, it was decreased in the diabetic retinas.

We also evaluated cataplerosis which catalyses the reversal of anaplerosis. If cataplerosis was decreased it could cause glutamate excitotoxicity. To do so we incubated retinas with [U-<sup>14</sup>C] glutamine. The rate limiting enzymes of cataplerosis are cytosolic malic enzyme (ME1) and mitochondrial phosphoenol pyruvate carboxykinase (PEPCK2). The carbon pathway is shown in Fig 1B. The anaplerotic pathway (Fig 1A) increases citric acid cycle intermediates and glutamate starting with CO<sub>2</sub> and pyruvate. The cataplerotic pathway (Fig 1B) decreases citric acid cycle intermediates and glutamate starting with glutamine. The products of the cataplerotic pathway are the same as the substrates of the anaplerotic pathway (i.e. CO<sub>2</sub> and pyruvate). Measurements of anaplerosis showed that de novo synthesis of citric acid cycle intermediates and glutamate were low in the diabetic retinas. The initial rate of cataplerosis in control retinas was  $1.29 \pm 0.08$  nmoles/mg min compared to the rate of anaplerosis ( $1.00 \pm 0.09$  nmoles/mg min). Thus the rates of anaplerosis and cataplerosis were similar in controls and both rates reduced in the diabetic retinas. The similarity of the rates of anaplerosis and cataplerosis in control retinas suggest the existence of a cycle where pyruvate connects the two pathways. The initial rate of anaplerosis was decreased from  $1.00 \pm 0.09$  nmoles/mg min in controls to  $0.58 \pm 0.06$  nmoles/mg min (~ 42%) in the diabetic.

The initial rate of cataplerosis was decreased from  $1.29 \pm 0.08$  nmoles/mg min to  $0.26 \pm 0.13$  nmoles/mg min (~90%) in the diabetic retinas. We conclude that the low amounts of [U-<sup>14</sup>C] lactate generated by diabetic retinas, incubated with [U-<sup>14</sup>C] glutamine is due to a decrease in the carbon 14 products of glutamate following inhibition of Müller cell glutamate transamination. [U-<sup>14</sup>C] glutamate conversion to  $\alpha$ -ketoglutarate is likely inhibited by BCAAs. Branched chain amino acids compete with glutamate for transamination in Müller cells. The BCAAs compete with glutamate for the amino acid binding site on BCATm (Hall et al. 1993). The Km of leucine for BCATm is ~0.8mM, for isoleucine it is 0.6mM, whereas Km for glutamate is 12mM (Conway et al. 2004).

In Müller cells,  $\alpha$ -ketoglutarate is produced not only by transamination of glutamate entering the cells, but also by pyruvate carboxylase. The source of nitrogen in the brain for conversion of  $\alpha$ -ketoglutarate to glutamate is debated, but in most studies it is either BCAAs or alanine (Sakai et al. 2004; Bak et al. 2005; Yudkoff et al. 2005). Therefore, our data and that of Frayser and Buse

(1978) suggest that neither alanine nor aspartate is the source of the excess nitrogen used for glutamate synthesis in diabetic retinas.

Since BCAAs provide much of the amino nitrogen for retinal transamination of  $\alpha$ -ketoglutarate to glutamate (LaNoue et al. 2001), increased levels of BCAAs will increase the pool size of glutamate in the Müller cells, just as they do in cultured brain astrocytes (McKenna et al. 1998), and perhaps interfere with uptake of glutamate from the synaptic spaces.

In the diabetic retinas, the decrease in conversion of [U-<sup>14</sup>C] glutamine to [U-<sup>14</sup>C] lactate and pyruvate (cataplerosis), ~90%, was accompanied by a decrease in anaplerosis ~42%. This may be because the products of cataplerosis are the substrates of anaplerosis and the enzymes are in the same cell type. When cataplerosis was inhibited the rate of anaplerosis declined, suggesting recycling. We define recycling here as the combination of anaplerosis and cataplerosis. For pyruvate recycling to influence Müller cell metabolism and buffer glutamate excitotoxicity, it must involve PC and ME1 in the same cell type. If anaplerosis and cataplerosis are active in the same cell and there is only a very small pool of pyruvate, increases in glutamate pool size will be determined by availability of pyruvate entering from the extracellular fluid. If cataplerosis did not supply most of the pyruvate needed by the anaplerotic pathway, anaplerosis and cataplerosis would be independent. The data show that the two pathways are dependent on each other. Our previous studies and those of others show that pyruvate is not generated glycolytically in the Müller cells and therefore is not present in excess in Müller cells as it is in neurons. In Müller cells, pyruvate is not the product of glycolysis because Müller cells do not express a malate aspartate cycle (LaNoue et al. 2001; Ramos et al. 2003; McKenna et al. 2006; Xu et al. 2007; Contreras et al. 2009). Therefore, in Müller cells, NADH generated glycolytically is not consumed by mitochondria (LaNoue et al. 2001; Xu et al. 2007) but instead is used to reduce pyruvate to lactate and the lactate is transported into the extracellular fluid (Pellerin 2008).

Thus we speculate that the two pathways anaplerosis and cataplerosis are present in the same cell types and are tightly linked by a small pool of pyruvate. We believe the cycle acts as a buffer to prevent large swings in the concentration of a Müller cell cytosolic glutamate. The two arms of the buffer are equal in the control retinas but not equal in the diabetic retinas. This may reflect loss of buffer capacity and the existence of glutamate excitotoxicity in the diabetic retinas.

It has been puzzling to us for some time that the glycolytic pathway from glucose to pyruvate is inactive in brain and retinal glial cells. Glycolysis is active in the glia but it only produces lactate which is exported to the neurons. The inability of the glia to oxidize lactate to pyruvate is due to the lack of a malate aspartate cycle in the glia. The “electrogenic” malate aspartate cycle provides a pathway to reduce cytosolic NAD<sup>+</sup> to NADH. Otherwise, the conversion is energetically unfavorable because the NADH/NAD ratio in the mitochondria is so much higher than in the cytosol. Thus, the glial cells sacrifice the energy they could get from oxidation of pyruvate in order to provide the proposed glutamate buffering system.

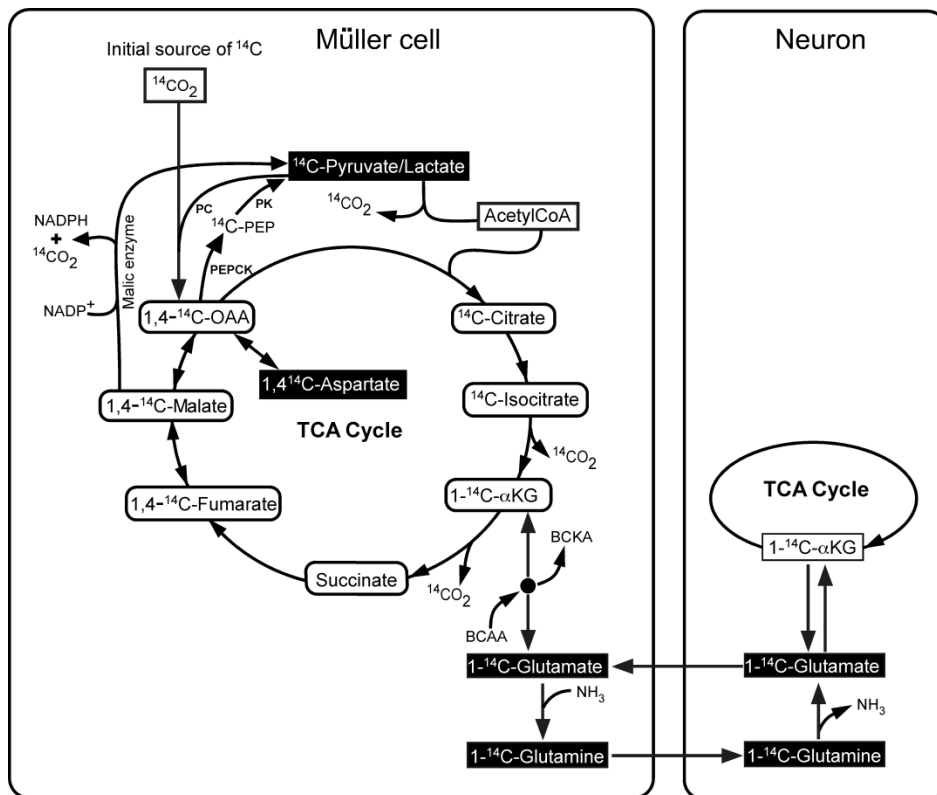


Figure 1A. Flow chart of metabolism in Müller cells involved in  $^{14}\text{CO}_2$

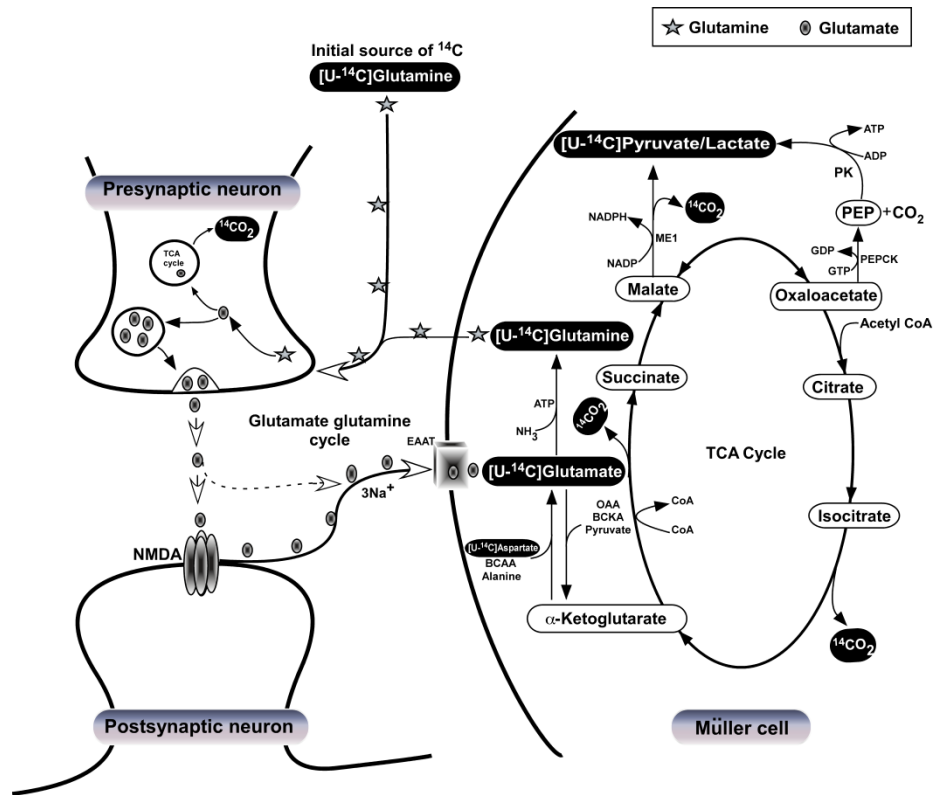


Figure 1B. Flow chart of retinal metabolism of glutamine including reactions that are catabolic.

## **Research Project 9: Project Title and Purpose**

*Identification and Function Study of Inflammatory Bowel Disease-associated DNA Methylation -* Inflammatory bowel disease (IBD), with Crohn's disease (CD) and ulcerative colitis (UC) as its two major forms, is a complex human disease. In the US, about 1.4 million people are affected with IBD. Currently, there is no known specific cause and no medical cure for the disease. Although more than 32 genes have been identified as IBD-associated genes, the total number of genetic factors discovered so far can only account for less than 20% of the overall genetic risk. It is clear that other factors make a significant contribution to the disease process. In this project we will examine the role of DNA methylation in IBD. DNA methylation is a modification of DNA molecules and has emerged as an important player in human development and diseases.

## **Anticipated Duration of Project**

7/1/2010 – 12/31/2011

## **Project Overview**

We hypothesize that DNA methylation plays a role in IBD pathogenesis. The objectives of this project are to identify DNA methylation CpG sites in IBD which would further add to the understanding of underlying pathophysiology and to provide a potential clinical application in

terms of disease diagnosis.

**Specific Aims:** 1) To identify IBD-specific DNA methylation in naïve B cell and mucosal tissues with a HumanMethylation27 BeadChip microarray, and 2) To demonstrate the effect of DNA methylation on gene expression and thus potential contribution to disease pathophysiology.

**Research Design and Methods:** The generally accepted mechanism of IBD pathophysiology is that there is a dysbiosis causing an inappropriate immune response in a genetically susceptible individual. Naïve B cells and mucosal tissues will be used in this study, as both play vital roles in the immune response. Furthermore, they are easily accessible via blood draws and tissue biopsies. In Aim 1, 96 samples (48 B cells and 48 mucosal tissues) will be used for methylation identification. In Aim 2, 200 samples (100 B cells and 100 mucosal tissues) will be used for the study on the correlation of DNA methylation with gene expression. For comparison, the study samples will include 1) naïve B cells and EBV-transformed B cell lines from IBD (CD and UC) and non-IBD siblings, 2) diseased and non-diseased mucosal and intestinal tissues classified by a pathologist from IBD (CD and UC) patients, and 3) unrelated healthy controls. In Aim 1, genomic DNA will be isolated and converted by bisulfite with Qiagen kits. The converted DNA will then be used for a HumanMethylation27 BeadChip assay. The BeadChip covers 27,578 CpG sites of 14,000 genes which have been validated in human studies. In Aim 2, we will target 4 genes (P2RX7, PPARG, RAP1A, and CRK) that are identified as having IBD-associated methylation in our preliminary study using the Illumina Goldengate Beadsarray. The levels of gene expression will be studied at mRNA transcription by RT-PCR and real-time PCR, and at protein translation by Western blot in the above clinical samples; and the correlation of methylation with gene expression will be statistically analyzed. All the human tissues are ready for the project, and our lab is well experienced in conducting such experiments.

### **Principal Investigator**

Zhenwu Lin, PhD  
Assistant Professor  
The Pennsylvania State University, College of Medicine  
Department of Surgery  
500 University Drive  
P. O. Box 850, H137  
Hershey, PA 17033

### **Other Participating Researchers**

Gerrit John, PhD, Yunhua Wang, BS, Arthur Berg, PhD - employed by The Pennsylvania State University, College of Medicine

### **Expected Research Outcomes and Benefits**

Specific Aim 1. We will identify inflammatory bowel disease-associated DNA methylation sites and investigate the distribution of DNA methylation in patients with inflammatory bowel disease. The knowledge gained from these results will contribute to understanding the cause of

IBD from modifications of human inherited molecules. The identified DNA methylation could be used as biomarkers for disease diagnosis and also provide target molecules for drug discovery and in developing strategies for clinical therapy.

*Specific Aim 2.* We will show that the levels of DNA methylation are correlated with gene expression in clinical samples in 4 target genes. These results will demonstrate that DNA methylation can affect gene expression, and thus contribute to IBD pathophysiology. This will also lead to further study on potential mechanisms of methylation related to the cause and/or severity of IBD. Determining how to control the methylation status of specific IBD genes will benefit disease prevention and treatment through regulation of the methylation process (methylation or demethylation), with drugs currently available.

## **Summary of Research Completed**

In the past year, we completed the Specific aim 1 for identification of IBD-specific DNA methylation with a HumanMethylation27 BeadChip microarray, and started the experiments for Specific aim 2.

### 1. Study sample modified

In the proposed research plan, the Specific aim 1 is to use 48 B cells and 48 mucosal tissues to identify IBD-specific DNA methylation with a HumanMethylation27 BeadChip microarray. As the progress of DNA methylation studies in our laboratory as well as others for other human diseases, we made an adjustment for the study samples, using 96 intestinal tissues from 3 disease groups, Crohn's disease (CD) in small intestine, CD in colon, and ulcerative colitis (UC) in colon. The reasons for the modification are the following:

1) Well characterized intestinal tissues from IBD patients are available in our laboratory; 2) Our results with Goldengate Beadchip from the intestinal tissues have been published in *Clinical Genetics* 2011(80):59-67. Therefore we plan to continue to use intestinal tissue for our future investigation as well as for a NIH R01 grant application; 3) Aim to identify disease subtype- and tissue-specific DNA methylation; 4) B cells are not from where disease is located, and EB-virus transformation may affect in vivo methylation status of B cells; and 5) Only a few or no mucosa tissues can be collected from the disease area in most of the surgery tissues. It is very difficult to collect 48 mucosa samples within a one year period of time.

### 2. DNA isolation and DNA bisulfite conversion

Frozen tissues were pulverized in liquid nitrogen and the tissue powder was used for genomic DNA isolation. DNA was isolated with QIAamp DNA Mini Kit (Qiagen Inc. Valencia, CA) according to the manufacturer's instruction. The isolated genomic DNA was converted by bisulfite using the Methylation-Gold kit (Zymo Research, Orange, CA) according to manufacturer's recommendations.

### 3. Human methylation27 BeadArray assay and data analysis

The BeadChip covers 27,578 highly informative CpGs from more than 14,000 genes. The BeadArray assay was performed at the Institute of Molecular Medicine, Cleveland Clinic. Briefly, single stranded PCR products were prepared by denaturation, and then hybridized to a

Sentrix® Array Matrix. The array hybridization was conducted under a temperature gradient program, and arrays were imaged using a BeadArray Reader 1000 scanner.

DNA methylation microarray data analysis was performed using Illumina BeadArray technology. A  $\beta$  value (0-1.0) signifying the methylation level was reported for each CpG site calculated by subtracting background using negative controls on the array and taking the ratio of methylated signal intensity to the sum of both methylated and unmethylated signals. IBD specific DNA methylation was identified by comparison of DNA methylation profile of B cells from IBD patients vs. non-IBD siblings. To assess the differences between diseased and non-diseased groups, Wilcoxon-signed rank test was used to compare  $\beta$  values due to small size in this experiment and violation of normality assumption. We isolated the DNA from these 96 tissues, and prepared bisulfite converted DNA for microarray assay.

#### 4. Disease-associated DNA methylation identification

In this study, IBD subtypes CD and UC are divided into 3 groups based on disease type and location: CD-TI (CD occurs at terminal ileum), CD-colon (CD occurs at colon), and UC-colon of 14, 9, and 15 patients, respectively. We identify disease-associated DNA methylation in diseased tissues by comparing the methylation level of disease tissues vs. matched nondiseased tissues from the same IBD patients. Considering that the comparison is between tissues from the same individual, we used the threshold as FDR (fault discovery rate)  $<0.25$  for CD-TI and CD-colon for cutoff. For UC group, the minimal FDR is 0.372, we used the rawp (raw data p value)  $<0.0005$  as an additional criteria for cutoff.

The matched nondiseased tissue is adjacent to the diseased. Although it looks normal, it may be already changed at the molecular level including DNA methylation at early stage of disease initiation and development. To detect these changes, we included small intestinal and colon tissues from 10 unrelated individuals without gastrointestinal diseases as health controls. We identify disease-associated DNA methylation from nondiseased tissues by comparing the nondiseased vs. health tissues. Considering that the comparison is between tissues from IBD patients and unrelated controls, we used a stringent threshold  $FDR < 0.03$  for cutoff.

After the disease-associated CpGs were identified, we examined the methylation status in other disease groups and tissues. For such comparison, we considered a change of DNA methylation in other disease groups as significant when  $FDR \leq 0.372$  and  $rawp \leq 0.010$  for diseased tissues, and  $FDR < 0.05$  for nondiseased tissues. The reason for using less stringent criteria is to detect a significant change and collect information as much as possible.

#### 5. Summary of the results

First, we identified disease-associated CpG methylation by comparison of diseased to nondiseased tissues from the same patients. For the group of CD-colon, we have identified 9 disease-associated methylated CpGs ( $FDR < 0.25$ ,  $rawp \leq 7.14E-05$ ) from diseased colon tissues. For the group of CD-small intestine, we have identified 12 disease-associated methylated CpGs ( $FDR < 0.025$ ,  $rawp < 0.0001$ ) from diseased small intestinal tissues. For the group of UC-colon, we have identified 17 disease-associated methylated CpGs ( $FDR = 0.3172$ ,  $rawp < 0.0005$ ) from diseased colon tissues.

Then we identified disease-associated CpG methylation by comparison of nondiseased tissues from IBD patients to healthy controls. For the group of CD-colon, we have identified 365 CpG methylation that is associated with disease (FDR<0.03). For the group of CD-small intestine, we only identified 7 disease associated CpGs (FDR<0.03, rawp≤7.26E-05). For the group of UC-colon, we have identified 95 disease associated CpG methylation (FDR≤0.022, rawp≤4.09E-05 for the top 30 CpGs).

In summary, we have identified 505 disease-associated methylated CpGs, 38 from diseased tissues (9 for CD-colon and 12 for CD-TI at FDR<0.25, and 17 for UC-colon at FDR=0.371, rawp<0.0005) and 467 from nondiseased tissues (365 for CD-colon, 7 for CD-TI, and 95 for UC-colon at FDR<0.03). Based on the results, a manuscript titled as “Disease-associated DNA methylation in inflammatory bowel disease subtypes Crohn’s disease and ulcerative colitis” is under preparation.

In the top 105 CpGs, 5 are observed in both CD-TI and CD-colon, 5 in both CD-TI and UC-colon, 23 in both CD-colon and UC-colon, and one in all the three disease groups, suggesting DNA methylation as a common mechanism in IBD pathology. The identification of disease-associated DNA methylation from nondiseased tissues indicates that DNA methylation occurs at the disease stages at which the tissue appears to be normal. The comparison of disease-associated methylation between intestine and colon affected by CD, and between CD and UC occurring at colon, indicates that the DNA methylation is preferentially regulated by disease subtype and tissue type affected, and colon is more subjective to methylation.

Three genes from the top 97 disease-associated genes, UBE2K rs652162, CPA5 rs17164838, and TRPV3 rs7219780, have been identified to be associated with CD (WTCC, *Nature* 447 (2007)661-8). According to gene function the major groups of these genes are: immune and inflammation (8 genes), transcriptional regulation (15), cell signaling (13), cell adhesion (8), and transport (15). The role of the methylation in these genes in intestinal physiology and IBD pathogenesis are current unknown.

The specific Aim 2 of the project is “To demonstrate the effect of DNA methylation on gene expression and thus potential contribution to disease pathophysiology.” We will select target genes from our new results from humanmethylation27 Beadarray instead of previously proposed P2RX7, PPARG, RAP1A, and CRK for the Illumina Goldengate BeadArray. The genes will include the 3 genes UBE2K, CPA5, and TRPV3 that are genetically associated with IBD and one gene THYN1 that is associated with all three IBD groups studied.

### **Research Project 10: Project Title and Purpose**

*Allogeneic CMV CTL for Refractory Glioblastoma Multiforme* - The purpose of this project is to determine the safety as well of the clinical and immunological effects of infusing allogeneic, cytomegalovirus (CMV) specific cytotoxic lymphocytes (CTL) in patients with refractory, CMV positive glioblastoma multiforme (GBM). Patient tumors will be tested for the presence of CMV pp65 and IE-1, and if the tumors are positive and the patients meet other eligibility criteria they will receive CMV CTL from an HLA partially matched donor. We will determine the duration and magnitude of CMV specific T cell function and donor cell microchimerism, the latter using

PCR assays. We will also determine the incidence of clinical responses to this intervention, and correlate these clinical responses with donor cell chimerism and CMV specific immunity post-infusion.

### **Duration of Project**

1/1/2010 - 1/17/2011

### **Project Overview**

Glioblastoma multiforme (GBM) is the most aggressive primary brain tumor affecting adults, with a median survival of approximately one year, and over 95% of patients surviving less than two years. Recently, several investigators have detected CMV proteins pp65 and IE-1 on GBM tumors, but not from normal brain tissue. While CMV is not thought to be oncogenic, the presence of these highly immunogenic CMV antigens indicates that there is the potential to intervene with CMV antigen specific immunotherapy. Since many patients with refractory GBM may have significantly compromised cellular immunity, using CMV specific cytotoxic T lymphocytes (CTL) from healthy donors would expedite the culture of CTL for these patients.

The purpose of this study is to examine the clinical and immunological effects of allogeneic CMV specific CTL for patients with refractory GBM. Patients with GBM will have their tumors tested for the presence of CMV pp65 and IE-1, and if they meet other eligibility criteria will have related donors screened for human leukocyte antigen (HLA) typing and CMV serology. We will administer HLA haplo-identical, CMV pp65/IE-1 specific CTL to patients with GBM whose tumors are refractory to primary therapy and test positive immunohistochemically for one or both of these antigens. Subjects will receive a lympho-depleting regimen consisting of single fraction total body irradiation (100 cGy) and cyclophosphamide to promote donor CTL chimerism. We will recruit 10 subjects to determine the safety of this approach, the incidence of tumor responses, and the duration and magnitude of donor CTL chimerism and CMV specific immune responses post-infusion. Since over 50% of individuals with disease progression or relapse would be expected to succumb from their disease within 2 months, a positive outcome will be defined as  $\geq 50\%$  of these subjects having disease stabilization, a partial response, or a complete response at 2 months post infusion. We will determine microchimerism post-infusion using a quantitative PCR assay for mismatched HLA alleles, and assess CMV specific immune function by performing cytotoxicity assays and cytofluorometry for intracellular cytokine production, correlating these findings with clinical responses.

### **Principal Investigator**

Kenneth G. Lucas, MD  
Professor of Hematology/Oncology  
Pennsylvania State University Hershey Medical Center  
500 University Drive, HO85  
Room C7830  
Hershey, PA 17033-0850

## Other Participating Researchers

Kim Dunham – employed by Pennsylvania State University, Hershey Medical Center

## Expected Research Outcomes and Benefits

This project will test a novel treatment strategy in patients with a highly lethal brain tumor. It is possible that allogeneic, CMV specific CTL could recognize and kill CMV positive GBM cells in patients whose tumors test positive for CMV pp65 or IE-1. First, we will determine the safety of infusing CMV antigen specific T cells into patients with therapy resistant glioblastoma multiforme (GBM). We will also determine the incidence of clinical responses to this form of therapy, and will correlate the duration of donor cell chimerism post-infusion with tumor responses. We expect that this form of therapy should be well tolerated, as allogeneic, antigen specific CTL have been used in other patient populations, namely those with EBV related lymphomas. We also expect that a number of these subjects may have detectable donor cells post-infusion, but the duration of this finding is unknown. It will be considered highly significant if some of these patients, who would otherwise be expected to die, experience several months of progression free survival. Since the median progression free survival for patients with refractory GBM is only two months, a significant finding would be having over half of the CTL recipients experiencing either stable disease, partial, or complete responses at two months post-infusion. This study will provide important information regarding the feasibility of this approach. If a correlation is seen between donor cell persistence and clinical responses, a future strategy would be to intensify the pre-CTL preparative regimen, or to increase the cell dose.

## Summary of Research Completed

*Introduction.* Glioblastoma multiforme (GBM) is the most aggressive primary brain tumor affecting adults, with a median survival of approximately one year, and over 95% of patients surviving less than two years. Recent studies have shown that CMV DNA can be detected in colon cancer, malignant glioma, and some prostate cancers. Three groups have demonstrated that CMV pp65 and IE1, two of the most immunogenic CMV antigens, are present in GBM, but not in normal brain tissue. There is no data to indicate that CMV is oncogenic, but it may have an oncomodulatory role in the progression of some tumors, causing dysregulation of key transcription factors, tumor suppressor proteins, or intracellular signaling pathways. Irrespective of the role of this virus in GBM, if immunogenic CMV antigens are expressed on these tumors, these antigens can be used as a target by adoptively transferred, antigen specific CTL. The purpose of this study was to determine the extent to which CMV pp65 and IE1 are expressed on newly diagnosed GBM, and if positive, treat patients with therapy refractory, CMV positive GBM with CMV specific cytotoxic T lymphocytes (CTL).

*Immunohistochemistry.* All immunohistochemical analysis was performed on 3-4µm thick sections from formalin-fixed, paraffin-embedded tissue. Tumors were from archived pathologic specimens of newly diagnosed patients with GBM at Penn State Hershey Medical Center from 2001-2009. The diagnosis of GBM was confirmed by a neuropathologist (CS) prior to being used for these studies. Immunohistochemistry for cytomegalovirus pp65 (NCL-CMVpp65, clone 2 and 6, Leica Microsystems, Newcastle, UK) and IE1 (MAB810, clone 8B1.2, Millipore,

Temecula, CA) was performed by first using heat-induced epitope retrieval in 10 mM citrate buffer pH 6.0 (IE1) or 1 mM EDTA pH 8.0 (pp65) for 20 minutes, followed by blocking for 10 minutes with 3% peroxidase.

Immunofluorescence (IF) analysis. T98G and U251 cells (American Type Culture Collection) were maintained in serum free medium and were trypsinized and replated onto glass coverslips in 12-well tissue culture plates ( $1 \times 10^5$  cells per well). After infection, the coverslips were harvested and rinsed in PBS. The cells on the coverslips were then fixed with 4% paraformaldehyde (in PBS) at room temperature for 5 minutes, permeabilized with 0.2% Triton X-100 (in PBS) at room temperature for 15 minutes, washed in PBS, and then blocked with 0.25% BSA in PBS at room temperature for 60 minutes. The cells on coverslips were incubated overnight with the same primary antibodies (Abs) used for immunohistochemistry. After extensive washes in PBS, coverslips were incubated with the secondary antibody (Dylight 488 AffiniPure Donkey Anti-Mouse IgG; Jackson ImmunoResearch, West Grove, PA). Following repeated washes in PBS, nuclei were counterstained with Hoechst dye, washed, and the coverslips were mounted in Aqua-Poly/Mount.

CMV Culture. Human CMV was obtained from ATCC, and virus was propagated in human skin fibroblasts (SF). The initial infection was at an MOI of 0.1. Five days after cytopathological effects appeared in more than 90% of cells, the virus-containing media were collected, passed through a 0.45-mm filter, and cryopreserved in liquid nitrogen. The viral titer was between  $10^6$  and  $10^7$ /mL by plaque assays in human SF.

Cell lines, and cell infection with CMV. T98G (human glioblastoma cell line; ATCC CRL-1690), U251 (Human glioma, kindly provided by Dr. Song Lee at Penn State Hershey Medical Center, Hershey, PA) were grown in Dulbecco Modified Eagle Medium (DMEM; GIBCO BRL). All media were supplemented with 10% fetal bovine serum, and cells were maintained at 37°C in a humidified atmosphere containing 5% CO<sub>2</sub>. All cell lines were maintained in DMEM without serum for 2 days prior to infection. Cells were replated and were infected at a multiplicity of infection (MOI) of 10. The cells were incubated with virus for 12 to 16 hours, re-fed with fresh medium with serum, and harvested 72 hours after infection for analysis.

Decitabine (DAC) and Interferon- $\gamma$  (IFN- $\gamma$ ) treatment. Prior to treatment with IFN- $\gamma$  or DAC, the cells were plated in 10-cm dishes. On the day of treatment the media was removed and replaced with media containing 1 $\mu$ M of 5-Aza-2'-deoxycytidine (DAC) (Sigma-Aldrich, St. Louis, MO) or 100 ng/ml human recombinant IFN- $\gamma$  (R&D systems, Minneapolis, MN). After incubation with DAC or IFN- $\gamma$  for 5 days, the cells were harvested, counted, and then prepared for flow cytometry or chromium release assay.

T Cell Culture. CMV specific CTL were generated using CMV pp65 and IE1 pools of peptides (15mers overlapping by 11 amino acids) as described previously. Nonadherent peripheral blood lymphocytes (PBLs) were stimulated with adherent cells pulsed with either CMV pp65 or IE1 peptide mixes (JPT Peptide Technologies, Berlin), consisting of 138 and 120 overlapping 15mers, respectively. CMV specific CTL were analyzed by chromium release assays and flow cytometry for intracellular IFN- $\gamma$  production.

Chromium Release Assays. Targets for chromium release assays (CRA) included autologous B cell blasts (BB; used as a negative control) and BB pulsed with the pp65 peptide mix. To determine whether these effector cells recognized naturally processed and presented pp65 epitopes, we infected GBM tumor cell lines with HCMV strain AD 169, and a portion of the cells were treated with DAC or IFN- $\gamma$ . Targets were labeled overnight with  $^{51}\text{Cr}$  (100  $\mu\text{Ci}/10^6$  cells; PerkinElmer Life and Analytical Science, Boston, MA), washed in PBS, and dispensed in triplicate into 96-well V-bottom plates (ICN, Costa Mesa, CA) at  $4 \times 10^3$  cells/well, as previously described. CTLs were added at different responder:target ratios, and after pelleting and incubation for 4 hours, the supernatant was analyzed in a gamma counter.

Flow cytometry. Flow cytometry was performed with a FACScan (BD Biosciences, San Jose, CA) for MHC class I and Class II expression. MHC Class I and Class II expression was determined by staining with directly conjugated monoclonal antibodies (mAb), including PE conjugated anti-human HLA-ABC mAb to detect MHC class I and FITC conjugated anti-human HLA-DR, DP, DQ mAb (BD Biosciences, San Jose, CA) to detect MHC class II.

CMV CTL study in GBM patients. With the data described in last year's Annual Report, and having developed a technique for expansion of CMV pp65/IE1 CTL, we began a clinical trial of allogeneic CMV CTL in patients with refractory, CMV positive GBM. We screened 16 subjects for this study, of whom 7 were positive for CMV antigens. Due to the nature of their relapsed disease, the majority of eligible subjects progressed prior to the treatment phase of the study. One patient was treated with HLA identical CMV pp65/IE1 CTL following a regimen of fludarabine and cyclophosphamide, the latter 2 drugs to induce donor CTL chimerism. This patient had rapid progression of her tumor after study entry and died one month later due to brainstem involvement with her tumor. Due to her immunocompromised state, there was no evidence of CMV specific immune reconstitution. Due to the fact that the majority of these subjects were requiring corticosteroids for tumor control and were rapidly progressing, we have closed the study.

### **Research Project 11: Project Title and Purpose**

*Molecular Mechanisms of Olanzapine's Metabolic Side Effects in an Animal Model -* Understanding the mechanism of the metabolic side effects of atypical antipsychotics is very important to the patients taking these drugs and their families. This research will focus on how atypical antipsychotics lower free fatty acids and will provide data supporting our hypothesis that it both impairs lipolysis leading to increased adiposity and simultaneously increases lipid oxidation leading through substrate competition to hyperglycemia and apparent insulin resistance.

#### **Duration of Project**

1/1/2010 - 6/30/2011

#### **Project Overview**

The long-term goals of this project are to elucidate the mechanisms of the metabolic side effects

of atypical antipsychotics. These drugs (e.g., olanzapine) are used to treat psychoses and other psychiatric disorders. Over the last 15 years their use has grown significantly in adults and soared in children. The sharp rise in atypical antipsychotic use is troublesome because of their propensity to cause serious metabolic side effects including obesity, diabetes their co-morbidities. We hypothesize that these serious side effects are preceded by causal changes in peripheral circulating factors along with carbohydrate and lipid metabolism that drive the insulin resistance, hunger, adiposity and obesity-comorbidities. Our focus will be on those aspects that have been confirmed as metabolic side effects in humans. Interesting preliminary data generated in a high fidelity rodent model indicate that increased adiposity in males may develop in response to tissue specific changes in insulin sensitivity or lipolysis leading to energy repartitioning that directs fuel away from muscle and towards fat. Hunger seems to involve leptin lowering. Hyperglycemia appears to involve alterations in fuel selection that leads to metabolic inflexibility, mitochondrial overload by increased lipid metabolism. We will test these hypotheses and address the mechanism(s) that underlie the acute endocrine and metabolic changes brought about by olanzapine in the preclinical model.

The aims are Aim 1. Determine the effect of olanzapine on FFA oxidation (measure FFA uptake and Acyl carnitine species in vivo) and uncover the role of malonyl CoA in this effect and the underlying mechanism (AMPK activation, ACC inhibition, reduced anaplerosis). Aim 2. Determine the role of cAMP in the anti in vivo lipolysis effect of atypical antipsychotics. By the conclusion of this work, we will have developed an approach to rapidly predict the likelihood of obesity-related side effects in emerging compounds before they are tested in humans. This will aid in the design of next generation drugs with reduced side effects and may also reveal new therapeutic targets for the treatment of obesity and diabetes.

### **Principal Investigator**

Christopher Lynch, PhD  
Professor  
Penn State College of Medicine  
MC H166  
500 University Dr  
Hershey, PA 17022

### **Other Participating Researchers**

None

### **Expected Research Outcomes and Benefits**

In this project, we will focus on how atypical antipsychotics lower FFAs in humans. Atypical antipsychotics also cause insulin resistance, obesity and diabetes in humans, and those conditions are associated with elevated not lower FFA. We have found that fasting plasma FFAs were lower in a chronic model using male Sprague Dawley rats. They were similarly reduced acutely, indicating a rapid and body composition independent effect, as has been true, for changes in glucose infusion rate during an euglycemic hyperinsulinemic clamp. In these studies we will

examine the mechanism of this effect. Specifically we will examine how atypical antipsychotics impair lipolysis and concurrently elevate FFA oxidation. These could suggest strategies to interfere with these side effects such as blocking fat oxidation. These findings may also provide a potential mechanism explaining the acute hyperglycemia/ insulin resistance (substrate competition), a strategy for reversing the metabolic side effects and may also have implications for the mechanisms underlying the cardiovascular side effects of these drugs. We will also further elaborate a non invasive pre-clinical screening strategy for these side effects by examining the effects of drugs acutely in mice by monitoring changes in fed RQ values after drug administration.

### **Summary of Research Completed**

All of the aims of this project have been completed and publications have either appeared in paper or are in press, but have appeared on line. Another paper that represents an offshoot of this research is also planned.

*Aim 1. Determine the effect of olanzapine on FFA oxidation (measure FFA uptake and Acyl carnitine species in vivo) and uncover the role of malonyl CoA in this effect and the underlying mechanism (AMPK activation, ACC inhibition, reduced anaplerosis).*

Olanzapine and other side effect prone atypical antipsychotics rapidly increased FFA oxidation as indicated by several techniques including depressed respiratory exchange ration (RER, also called RQ), FFA flux studies and oral lipid tolerance tests. The FFA oxidation was elevated 2-fold into most peripheral tissues except the heart and RER dropped to 0.7 within minutes after olanzapine or other side effect prone atypicals (Figures 1-2). The affected tissues included gastrocnemius and soleus muscle, liver, kidney, duodenum, ileum, skin and various adipose tissue depots. It should be noted that only some of these tissues experience altered transport of glucose in response to changes in plasma insulin or insulin resistance. We will come back to this later as we conclude with a hypothesis on where these drugs are eliciting one of their metabolic side effects.

Figure 2 shows the effects of olanzapine and other atypical antipsychotics on RER in mice during the dark cycle when RER increases. We found that side effect prone atypical antipsychotics shared a rapid effect on RER. We wondered if this was due to not eating food because the drugs were sedative. As can be seen in Figure 2, food restriction alone with vehicle gavage also decreases RER however this effect occurs over a period of many hrs. The drop in the RER indicates a switch from using mostly carbohydrate as a fuel to using fatty acids as a fuel as expected as the animal moves into the fasted state. After about 5 hrs of food restriction RER reaches about 0.7 (Consistently, according to the NIH Mouse Metabolic Phenotyping Centers, fasting is felt to be achieved in mice within 5hr-URL: [MMPC Consensus on fasting mice-SOP](#)). In contrast to this longer time course observed with food deprivation, olanzapine, clozapine, ziprasidone and risperidone elicited a much faster effect on RER (Figure 2). Therefore their effects are non consistent with a simple effect on food restriction. Indeed during fasting refeeding studies in rats, olanzapine had no effect on food intake (Publication 1 below). However, aripiprazole, generally regarded to be more free of metabolic side effects (but perhaps less efficacious as an antipsychotic) and the typical antipsychotic, haloperidol, lowered RER with time courses consistent with sedation and food deprivation rather than the rapid time course seen with olanzapine (Figure 2). Activity analysis using a beam break system supported the

hypothesis that haloperidol and aripiprazole caused strong sedation (data not shown). Another atypical antipsychotic, sulpiride, which is a pure Dopamine receptor-D2 antagonist (also not reported to cause metabolic side effects), did not lower RER even at a very high dose (Figure 2, N.B. There is a general recognition that antipsychotic efficacy with the atypicals is directly related to their ability to cause metabolic side effects).

In summary rapid increased fat oxidation as measured by lowering of dark cycle RER appears to be a feature of atypical antipsychotics that are more prone to have metabolic side effects. At the same time whole body glucose intolerance, insulin resistance were observed as determined during euglycemic hyperinsulinemic clamps, insulin tolerance and glucose tolerance tests (see Table 1 and publications listed below). However this response was not associated with changes in insulin signaling as shown in Figure 3 (left panel) or AMPK activation as shown in Figure 3 (right panel).

The increase in FFA metabolic flux after acute olanzapine exposure could be explained by a ~50% decrease in malonyl Co-A, the negative regulator of the first and rate determining step in FFA metabolism catalyzed by carnitine palmitoyl transferase 1 (CPT1, Table 2). This is the same magnitude of decline observed in fasting and starved states. We wondered whether this malonyl-CoA lowering was associated with direct inhibition of isoforms of acetyl-CoA carboxylase (ACC). However where bona fide inhibitors blocked recombinant ACC-1 and -2, olanzapine failed to inhibit these enzymes Figure 4. However the decrease was associated with anapleurotic intermediates in or related to the TCA cycle required for malonyl-CoA synthesis. These changes would normally be expected in a starved state. Acyl Carnitine profiles were consistent with elevated FFA metabolism (Publication 1). Thus muscle from fed animals treated with olanzapine for 45 min quickly appeared as if they were starved.

What would happen if we blocked this elevated fat metabolism? As mentioned in last year's report we began efforts to do this with the CPT1 inhibitor TDGA and this year expanded the scope of those studies with another blocker, etomoxir. Furthermore this year we expanded the antipsychotic drugs evaluated to include risperidone and clozapine. Consistent with the results from last year's report we found that blocking the elevated fat metabolism with either TDGA, reported last year, or etomoxir, this year, results in a rapid decline in whole body metabolism after olanzapine is injected. Similar effects were observed with other atypical antipsychotics. To keep the animals from dying all together we had lower the doses of TDGA and etomoxir. These two drugs are non-competitive inhibitors (in contrast to malonyl CoA). Two doses separated by 12-24 hrs is sufficient to completely block CPT1. However a single dose appears to provide about a 60-70% block (data not shown). Another adaptation we had to add to our experimental design was to find doses of the antipsychotics that were less sedating, since sedation itself causes a decrease in energy expenditure (see Figure 5). We were able to find doses of these drugs that were less sedating having little effect on VO<sub>2</sub> by themselves (Figure 5). Nevertheless, a combination of even partial CPT1 blockade and lower dose of atypical antipsychotics was found to be rapidly toxic at the level of oxygen consumption (Figure 6). As can be seen in Figure 6, middle panel etomoxir and TDGA produce a similar pattern of response to olanzapine injection. The time course of decline in energy expenditure after CPT1 blockade and olanzapine administration was almost identical.

In conclusion, Olanzapine and other atypical antipsychotics cause metabolic side effects including diabetes, but paradoxically lower FFAs. In rats, olanzapine rapidly increases FFA flux into most peripheral tissues ~2 fold. Notably, even tissues that are insulin independent for glucose metabolism are affected. The consequent drop in RER after antipsychotic administration in mice corresponds to their propensities to give rise to metabolic side effects. Since increased FFA oxidation is associated with lower malonyl CoA, we wondered whether the switch to fat metabolism was due to a drug effect on anapleurosis needed to maintain malonyl Co-A or a block in glucose transport or glycolysis. To probe this we used CPT1 inhibitors. We expected if the drugs were merely promoting fat metabolism that the animals would not drop their RER and would turn back to using glucose as a fuel. In contrast, what we found was that after partial CPT1 blockade, the animals appear to have little available fuel. This in turn leads to metabolic toxicity associated with moribund appearance, loss of body temperature and greatly decreased oxygen consumption. The rapid increase in FFA metabolism and glucose intolerance appears to be a Randle Cycle effect. Our CPT1 inhibitor studies suggest that the target of the Randle Cycle effect is either at the level of glucose transport or an early step in glycolysis.

There are at least two implications of our findings. Prevention of glucose utilization while impairing lipolysis and lowering FFA could trigger the occasional reports of activated AMP kinase after treatment with atypicals, although we could not detect that here. Because fat oxidation generates more reactive oxygen species than carbohydrate oxidation, in humans, persistent elevation of lipid oxidation could potentially contribute, over time, to diabetes susceptibility by promoting mitochondrial dysfunction through elevated ROS, thus contributing to the increased diabetes in those taking these drugs for treatment of psychiatric disorders.

*Aim 2. Determine the role of cAMP in the anti in vivo lipolysis effect of atypical antipsychotics.* We measured cAMP before and during an isoproterenol challenge test in SD rats. Under these conditions an obvious impairment in lipolysis was evident. However no change in cAMP in adipose tissue frozen powders was detected using an assay kit from CisBio.

### Publications

1. Albaugh VL, Vary TC, Ilkayeva O, Wenner BR, Maresca KP, et al. (2010) Atypical Antipsychotics Rapidly and Inappropriately Switch Peripheral Fuel Utilization to Lipids, Impairing Metabolic Flexibility in Rodents. *Schizophrenia Bulletin*.
2. Albaugh VL, Judson JG, She P, Lang CH, Maresca KP, et al. (2011) Olanzapine promotes fat accumulation in male rats by decreasing physical activity, repartitioning energy and increasing adipose tissue lipogenesis while impairing lipolysis. *Molecular psychiatry* 16: 569-581.

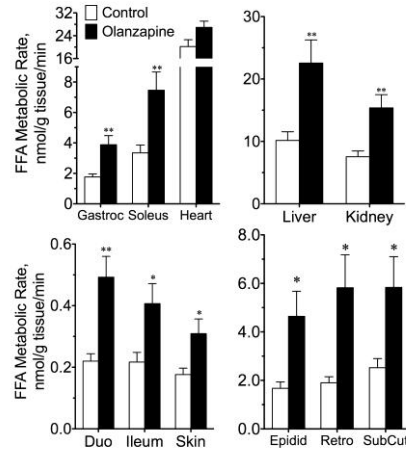


**Figure 1. Tissue uptake of free fatty acids following acute olanzapine administration in fed SD rats with *ad libitum* access to food and water.** On the second day of olanzapine (10 mg/kg) administration, animals received a bolus i.v. injection of [<sup>125</sup>I]-BMIPP and serial blood samples were drawn for calculation of plasma radioactivity and FFA concentration during a 40-min *in vivo* labeling period. Tissues sampled included skeletal and cardiac muscle, liver and kidney, proximal duodenum, terminal ileum, skin and three adipose tissue depots. Data represent the mean ± S.E. (n = 8); asterisks indicate significant differences (\*P<0.05, \*\*P<0.01).

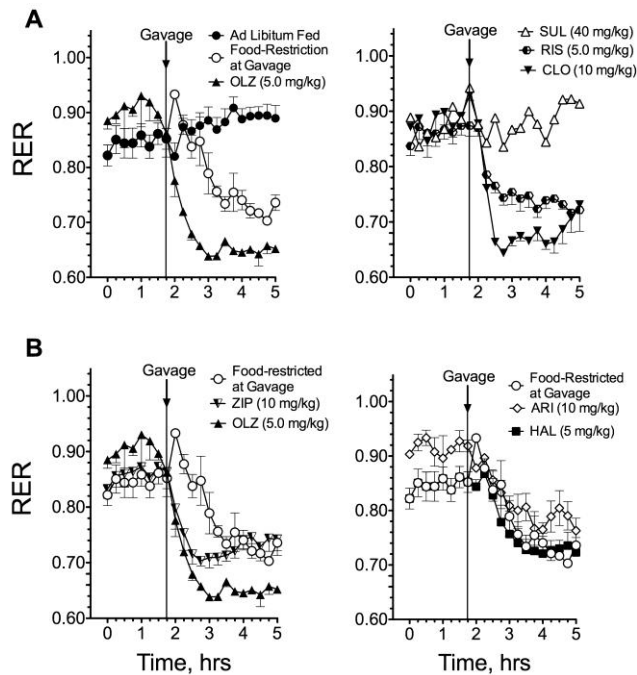


**Figure 2. Effect of antipsychotic drugs on respiratory exchange ratio (RER) in *ad libitum* fed mice.** Male mice were given a single dose of antipsychotic drug or vehicle via oral gavage (indicated by arrows) during the dark cycle following adequate food intake and normal rise in RER. Mice retained *ad libitum* access to food and water, except for a separate time-matched control group that was food-restricted following vehicle gavage (A-D). The effects of olanzapine (OLZ), sulpiride (SUL), risperidone (RIS), clozapine (CLO), ziprasidone (ZIP), aripiprazole (ARI) and haloperidol (HAL) in *ad libitum* fed mice were examined and compared to vehicle-treated mice that were either fed *ad libitum* or food-restricted. Data represent the mean ± S.E. (n = 5-6).

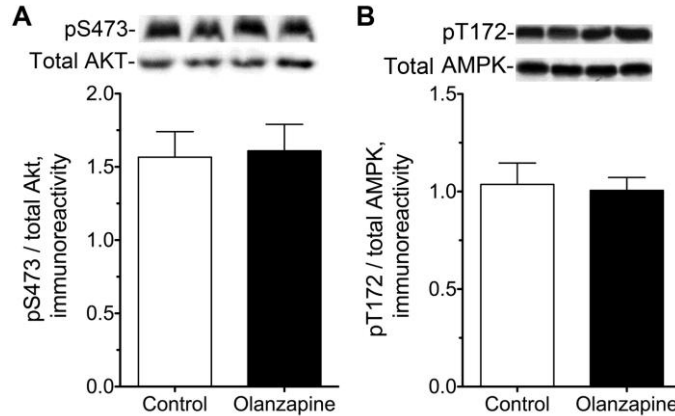


**Figure 3. Effect of olanzapine on AKT and AMPK phosphorylation in skeletal muscle of *ad libitum* fed male rats.** Gastrocnemius tissues were excised and immediately freeze-clamped approximately 2h after vehicle or olanzapine treatment. Tissue homogenates were subjected to Western blotting and quantified using chemiluminescence to measure the activity (ratio of phosphorylated (p) isoform to total protein isoform) of (A) AKT (Ser<sup>473</sup>) (B) AMPK (Thr<sup>172</sup>). Representative images from actual blots are shown along with relative quantification representing the mean intensity  $\pm$  S.E. (n = 8).

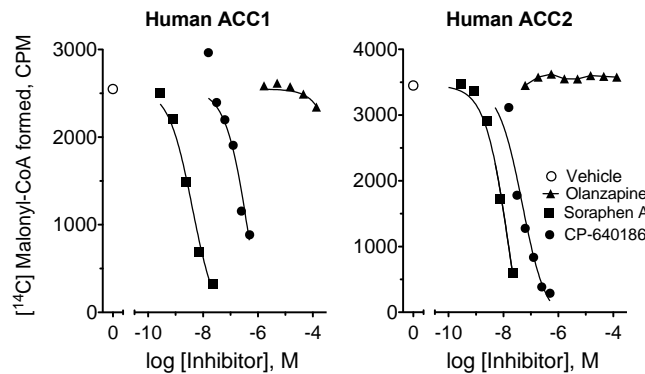


**Figure 4. *In vitro* inhibition assay of human acetyl-CoA carboxylase isoforms *hACC1* and *hACC2*.** Overall ACC activity in the *hACC* preparations was measured by following incorporation of [<sup>14</sup>C]-bicarbonate into malonyl-CoA. Potential inhibition of *hACC1* and *hACC2* by olanzapine, with concentrations of olanzapine up to 135  $\mu$ M, and inhibition by the known ACC inhibitors, Sorafen A and CP-640186, was measured.

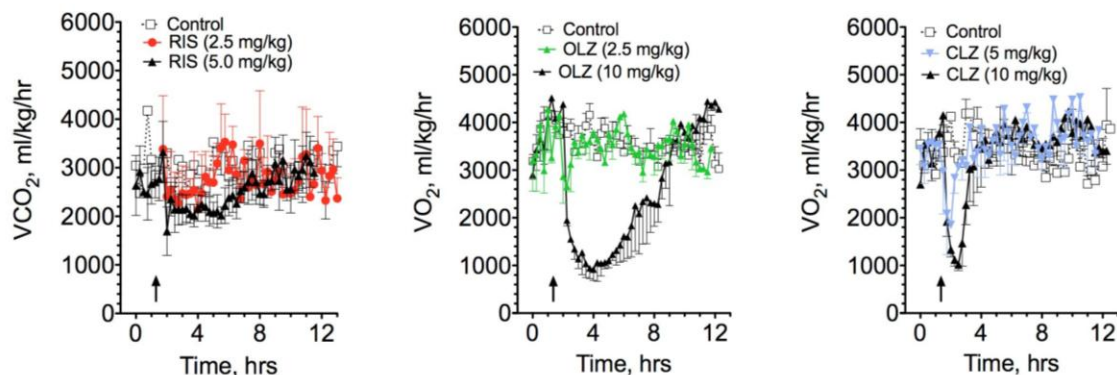


**Figure 5. Effect of vehicle and antipsychotic drugs on dark cycle  $VO_2$ .** Male mice were given a single dose of antipsychotic drug or vehicle via oral gavage (indicated by arrows) during the dark cycle with free access to food and water. Data represent the mean  $\pm$  S.E. ( $n = 5-6$ ).

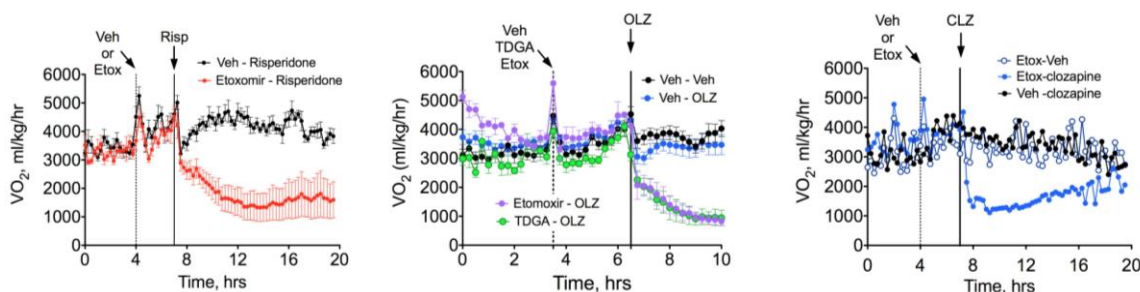


**Figure 6. Effect of partial CPT1 blockade or low dose atypical antipsychotic on energy expenditure.** Mice were acclimated to receiving gavage saline or water for several days before each experiment and acclimated to metabolic cages for 30 hrs or more. Multiple doses of etoxomir (Etox) or TDGA are frequently used to bring about a complete block of CPT-1. We found little effect on  $VO_2$  with these protocols; however multiple doses of these compounds when followed by an atypical antipsychotic led to rapid loss of body temperatures associated with dramatic drops in  $VO_2$  and morbidity. To investigate this further, we used a single dose of CPT1 inhibitor (30mg/kg by gavage) 3 hrs before the administration of Risperidone (Risp, 5 mg/kg), Olanzapine (OLZ, 5 mg/kg) or Clozapine (CLZ, 3mg/kg). The antipsychotic was given during the dark cycle around 9PM. RERs declined in both the Vehicle and CPT1 blocker group to the same extent because only partial CPT1 blockade was used (not shown).

**Table 1.** Plasma FFA, Glycerol, Insulin Tolerance Test Areas Under-the-Curve (ITT-AUC), and Euglycemic Clamp Glucose Infusion Rate after Chronic or Acute Olanzapine Treatment in male, Sprague-Dawley Rats.

Treatment Day	Dose mg/kg/day	Food Restriction	Endpoint	Condition	
				Control <sup>a</sup>	Olanzapine <sup>a</sup>
28 (Chronic)	Ramp, 4-12 <sup>b</sup>	14h	FFA	0.91 ± 0.05	0.58 ± 0.04***
			Glycerol	1.79 ± 0.13	1.34 ± 0.12*
			ITT-AUC	6,226 ± 564	3,797 ± 569**
2 (Acute)	4	5h	FFA	0.63 ± 0.05	0.38 ± 0.02***
			Glycerol	1.95 ± 0.08	1.61 ± 0.05**
			ITT-AUC, GIR	6,054 ± 344 81.4 ± 5.3	4,436 ± 415** 43.2 ± 5.5***

<sup>a</sup>Values are means ± SE; n= 10-12. Asterisks indicate statistical difference from Control group (\*P<0.05, \*\*P<0.01, \*\*\*P<0.001). Parameters reported in SI Units: FFA, mM; glycerol, mM, (GIR) Glucose Infusion Rate, mmol/kg/min, ITT-AUC (Time ! % Change from Baseline Glucose)

**Table 2.** Abridged muscle metabolomic findings from rat muscle after acute treatment with olanzapine.

Abridged muscle metabolomic findings			
Metabolite	Muscle concentration (nmol/g protein)		P value
	Control	Olanzapine	
Malonyl CoA	36 ± 6.3	16 ± 4.0	0.017
Succinyl CoA	47 ± 8.6	23 ± 5.1	0.031
Citrate	643 ± 36	221 ± 26.7	0.0024
a-ketoglutarate	6622 ± 290	4953 ± 278	0.0007
Glu & Gln	16 ± 0.80	13 ± 0.65	0.039

All data represent the mean ± S.E. P values < 0.1 are shown. Gastrocnemius samples from Figure 1 fed rats (n=8/grp) were analyzed for Coenzyme-A (Co-A) species and other metabolites were measured from a separate cohort of rats not infused with radioactivity (n=10/grp).

## **Research Project 12: Project Title and Purpose**

*Genetic Analysis of Papillomavirus Virion Morphogenesis* - The central hypothesis of this project is that the capsid proteins of human papillomavirus (HPV) have specific functional domains for morphogenesis of infectious viral particles in a differentiation-dependent manner. When completed, this project will provide new insight into the molecular mechanisms of virion morphogenesis in a system capable of reproducing the natural complex process and differentiating environment of native HPV virion (NV) morphogenesis and infection.

## **Duration of Project**

1/1/2010 – 11/30/2010

## **Project Overview**

The long-range goal of this project is to define the genetic and molecular events of human papillomavirus (HPV) virion morphogenesis. Specific Aim #1 is designed to biochemically assess the stability and structure of NVs derived from temporally distinct organotypic tissues. Specifically, NVs will be purified on Optiprep density gradients and assessed for gross morphological changes via transmission electron microscopy (TEM), and analyzed for differences in stability via partial chemical reduction and tryptic digests followed by Western blot analyses of L1 protein expression. To probe for distinct capsid assembly stages, we will utilize redox-altering reagents, which have been shown to alter DNA encapsidation efficiencies and infectivity titers of NVs and pseudovirions (PsV), and pulse tissues with these chemicals at various time points to determine when DNA encapsidation and formation of mature NVs finalize. Specific Aim #2 is designed to genetically analyze the role of capsid protein cysteine residues in capsid assembly. We propose to test cysteine mutants by purifying them on Optiprep density gradients followed by observation of gross morphological differences via TEM. Then, we will test their stabilities by partial chemical reduction and tryptic digest experiments followed by Western blot analysis of L1 expression. Specific infectivity of each mutant NV will also be assessed and we will determine how each cysteine substitution affects the tissue-dependent capsid assembly processes described in Specific Aim #1.

## **Principal Investigator**

Craig M. Meyers, PhD  
Professor  
Penn State University College of Medicine  
500 University Drive C6767  
Hershey, PA 17033

## **Other Participating Researchers**

Michael J. Conway, BS - employed by Penn State University College of Medicine

## **Expected Research Outcomes and Benefits**

Our expertise with the organotypic virus culture system, which is capable of supporting the complete human papillomavirus (HPV) life cycle, puts us in a unique position to initiate the first studies to directly compare capsid assembly of *in vitro*-derived papillomavirus particles with HPV virions produced in stratified and differentiated epithelial tissues (i.e. native virions). Our studies will provide a foundation to investigate whether the molecular requirements for the production of *in vitro*-derived papillomavirus particles are the same as native virions. We will test hypotheses developed from atomic structures, in addition to genetic, molecular, and biochemical studies of *in vitro*-derived papillomavirus particles using native virions from our organotypic virus culture system. Our studies will provide direction for future atomic structure studies of *in vitro*-derived papillomavirus particles, therefore, developing a synergy between atomic structure and genetic analysis of native virions. When completed, this project will provide new insights into the molecular mechanisms of HPV virion morphogenesis in a system capable

of reproducing the natural complex process and differentiating environment of HPV morphogenesis and infection. Further, such an understanding of HPV capsid assembly within human tissue will facilitate the future production of therapeutics which will inhibit the spread of HPV infection.

## **Summary of Research Completed**

The long-range goal of this project was to define genetic and molecular events of human papillomavirus (HPV) morphogenesis.

### Specific Aim #1

The first aim proposed to biochemically assess the stability of structure of native viruses (NVs) derived from temporally distinct organotypic tissues. Numerous viral preparations were harvested and purified using Optiprep density gradients and then attempts were made to assess gross morphological changes using transmission electron microscopy (TEM). In order to produce native human papillomavirus (HPV) virions continuously, HPV infected human keratinocyte cell lines needed to be grown in organotypic raft epithelial tissue culture. Three raft tissues were pooled and virus was released from the tissue by dounce homogenization followed by centrifugation. This process typically provided viral stocks containing  $10^8$  or more viral particles per ml. Three raft tissues produced approximately 0.7 ml of viral stock. We had previously demonstrated that virus isolated from raft tissues grown for 10-days was less stable than virus isolated from raft tissues grown for 20-days. One goal was to use TEM to visually observe differences in 10-day and 20-day virus that may be correlated to the differences in stability. Unfortunately, several attempts were made, but we unable to visualize the virus. After discussions with experts in imaging and physical analyses of virus we came to the conclusion the chemicals that are part of the Optiprep gradient may be interfering with the procedure. In the past we had used ultra-thin tissue sections or cesium chloride gradient purified virus and were able to observe particle structure by TEM. Additionally, imaging experts newly recruited to the Penn State College of Medicine have discussed with us additional techniques that we could try. Therefore we have future goals to pursue these techniques.

Along with visualizing differences in 10-day and 20-day virus by TEM, attempts were also made to analyze differences in stability via partial chemical reduction and tryptic digests followed by Western blot analyses of L1 protein expression. In a nonreducing Western blot L1 dimers and trimers were formed only in wild-type 20-day virus preparations and not in 10-day virus. Analyses of differences in stability via partial chemical reduction and tryptic digests were attempted but we have no clear results at this time. Instead of pursuing this further, time and efforts were put into pursuing goals of Aim #2, which resulted in two manuscripts.

We then decided to try to ‘visualize’ differences in 10-day and 20-day virus by using minor capsid protein L2 specific antibodies. Many labs are pursuing using the L2 protein as a potential wide-spectrum vaccine agent to prevent HPV infection. Presently, there are two HPV vaccines, both of which are directed against the major capsid protein L1 and do not cross-protect against HPV types not contained in the vaccine. In the process of testing for a L2-based vaccine, portions of the L2 protein have been used to raise antibody. We have taken advantage of these antibody preparations to visualize differences in 10-day and 20-day virus. Our studies have led to

a manuscript “Cross-neutralization potential of native human papillomavirus N-terminal L2 epitopes”, which has been accepted for publication in the journal PLoS ONE. HPV capsids are composed of 72 pentamers of the major capsid protein L1, and an unknown number of L2 minor capsid proteins. An N-terminal “external loop” of L2 contains cross-neutralizing epitopes, and native HPV16 virions extracted from 20-day-old organotypic tissues are neutralized by anti-HPV16 L2 antibodies but virus from 10-day-old cultures are not, suggesting that L2 epitopes are more exposed in mature, 20-day virions. This current study was undertaken to determine whether cross-neutralization of other HPV types is similarly dependent on time of harvest and to screen for the most effective cross-neutralizing epitope of L2 in the native virion. Although HPV16 L2 epitopes were only exposed in 20-day virions, HPV31 or HPV18 epitopes behaved differently. Conversely, HPV31 and HPV18 L2 epitopes were exposed in 10-day virions and remained so in 20-day virions. In contrast, presumably due to sequence divergence, HPV45 was not cross-neutralized by any of the anti-HPV16 L2 antibodies. We found that the most effective cross-neutralizing antibody was a polyclonal antibody named anti-P56/75 #1, which was raised against a peptide consisting of highly conserved HPV16 L2 amino acids 56 to 75.

The final goal of the first Aim was to utilize redox-altering reagents to determine when DNA encapsidation and formation of mature NVs is finalized. Previous studies have shown that treatment of HPV-infected organotypic raft cultures with 5mM GSSG enhances capsid maturation (Conway et al, *Virology*, 393:295-303 and Conway et al, *Journ of Virol* 83:10515-26). We found that a mild oxidizing agent, DMSO also gave similar results as GSSG. The reducing green tea extract, epigallocatechin gallate (EGCG), was added to raft cultures and shown to have a negative effect on the maturation of HPV. EGCG greatly lowered viral titers, again demonstrating the importance of the oxidizing environment for virion maturation.

### Specific Aim #2

This aim proposed to test the role of capsid protein cysteine residues in capsid assembly. Besides observation of particle structure by TEM (for reason described above in Aim #1) we have accomplished all the goals and more of this aim. Our efforts have resulted in two manuscripts; therefore these papers will be used to summarize the accomplishments of this aim.

### Manuscript #1: “Differentiation-Dependent Interpentameric Disulfide Bond Stabilizes Native Human Papillomavirus Type 16”

This manuscript is in revision and will be resubmitted by the end of January 2011. Genetic and biochemical analyses of human papillomavirus type 16 (HPV16) capsids have shown that certain conserved L1 cysteine residues are critical for capsid assembly, integrity, and maturation. Since previous studies utilized HPV capsids produced in monolayer culture-based protein expression systems, the ascribed roles for these cysteine residues were not placed in the temporal context of the natural host environment for HPV, stratifying and differentiating human tissue. Here we extend upon previous observation, that HPV16 capsids become stabilized over time (10-day to 20-day) by utilizing a tissue-spanning redox gradient and by identifying temporal roles for individual L1 cysteine residues. Specifically, the C175S substitution severely undermined wild-type titers within 10 and 20-day tissue, while C428S, C185S, and C175,185S substitutions severely undermined wild-type titers only within 20-day tissue. All mutations led to 20-day virions that were less stable than wild-type and failed to form L1 multimers via nonreducing SDS-PAGE; however, only Optiprep-fractionated 20-day C428S, C175S, and C175,185S

capsids appeared permeable to endonucleases in comparison to wild-type and C185S capsids. In addition, since treatment of raft cultures with oxidized glutathione (GSSG) or exposure to the natural tissue-spanning redox gradient failed to enhance infectious titers of any of the cysteine mutants compared to wild-type, we hypothesize that a complex, temporal interplay of disulfide bond formation, disruption, and reformation occurs between C175, C185, and C428 during migration of virions from the suprabasal compartment to the cornified envelope within stratifying and differentiating human epithelial tissue.

Manuscript #2: “Roles for HPV16 L1 cysteine residues 379, 161, and 229 in DNA encapsidation”

This manuscript is ‘In Preparation’ and should be submitted for review by the end of February 2011. Human papillomavirus (HPV) capsids are formed through a network of inter- and intra-pentameric hydrophobic interactions and disulfide bonds. 72 pentamers of the major capsid protein L1 and an unknown amount of the minor capsid protein L2 form the structure of the capsid. There are 12 conserved L1 cysteine residues in HPV16. Although C428, C175, and C185 have been implicated in the formation of a critical interpentameric disulfide bond, no structural or functional roles have been firmly attributed to any of the other conserved cysteine residues. Here we show that substitution of cysteine residues C379, C161, and C229 for serine hinders the accumulation of endonuclease-resistant genomes as virions mature within stratifying and differentiating human epithelial tissue. Further, C229S mutant virions form, but are noninfectious, which supports previous data that this residue might be involved in downstream steps in the virus life cycle. These studies add further detail to the differentiation-dependent assembly and maturation steps that occur during the HPV16 life cycle.

### **Research Project 13: Project Title and Purpose**

*Epidermal Stem Cell Properties in Mice with Altered Polyamines* - Our research studies the role of the polyamine pathway in early skin cancer development. Since skin cancers are the most common form of malignancies world-wide, identification of possible targets for prevention is highly relevant to public health. Understanding the role of the polyamine pathway is also of great importance because the polyamine biosynthesis inhibitor difluoromethylornithine (DFMO) is a promising chemopreventive agent of human skin cancer.

#### **Duration of Project**

1/1/2010 - 06/30/2011

#### **Project Overview**

Our project will use subpopulations of primary keratinocytes derived from several transgenic mouse models to identify the downstream targets of polyamines that alter keratinocyte stem cell expansion and lead to tumorigenesis.

Previous work in our lab has shown that the upregulation of ornithine decarboxylase (ODC) through overexpressing constitutively active MEK in the skin results in expansion of epidermal stem cells, activation of progenitor cells, and increased skin tumorigenesis. Double transgenic

mice overexpressing Antizyme (AZ), an endogenous inhibitor of ODC, and MEK showed a reduction in the MEK-induced phenotypes, including stem cell expansion and tumor formation. These data strongly support the hypothesis that polyamines are critical regulators of stem cell expansion and activation of progenitor cells. However, the downstream targets of polyamines remain largely undefined. We hypothesize that MEK, a critical downstream effector of the *ras* oncogene, plays a critical role in stem cell activation by altering transcription in response to carcinogens, and these changes are mediated in a polyamine-dependent manner. Our aim is to examine the transcriptional profiles of CD34<sup>+</sup>/α<sub>6</sub>integrin<sup>high</sup> (immature stem cell enriched) and CD34<sup>+</sup>/α<sub>6</sub>integrin<sup>low</sup> (committed progenitor cell enriched) populations of cells isolated from AZ, MEK, and MEK/AZ mice. With these experiments, we hope to identify a pattern of gene expression in the keratinocyte stem cell population that responds to changes in intracellular polyamines. Our studies may thus lead to the identification of new targets for chemoprevention of skin cancer.

### **Principal Investigator**

Lisa M Shantz, PhD  
Associate Professor  
Penn State College of Medicine  
Dept of C&M Physiology H166  
500 University Drive  
Hershey, PA 17033

### **Other Participating Researchers**

Theresa D Carr, BS - employed by Penn State College of Medicine

### **Expected Research Outcomes and Benefits**

Although it is known that the mammalian epidermis is maintained by self-renewal of stem cells, the underlying mechanisms, and how these mechanisms change in cancer, are not yet well-defined. Therefore, increasing our understanding of the mechanisms responsible for stem cell proliferation and their differentiation into mature cells could lead to important new cancer therapies and modes of prevention. The ability to prevent the onset of non-melanoma skin cancer in high-risk groups by topical application of a drug like the ODC inhibitor DFMO would be of great interest to the general public.

### **Summary of Research Completed**

Our project aim is to identify polyamine-dependent gene expression changes within keratinocyte populations harboring activation of *ras*-dependent pathways, a common activating mutation in non-melanoma skin cancer (NMSC). Our ultimate goal is to perform these experiments on keratinocyte populations that are enriched in stem cells using FACs analysis with CD34 and α<sub>6</sub>integrin stem cell markers. These experiments have been technically challenging, and we have thus far been unable to isolate sufficient numbers of cells using the FACs system available to us at the College of Medicine that would allow us to do transcriptional profiling. Therefore, in a

logical extension of the proposed work, we have employed a targeted approach in a series of experiments using both unsorted primary keratinocytes isolated from newborn mice and keratinocyte-derived cell lines to test our hypothesis that activation of pathways downstream of *ras* induces a specific pattern of polyamine-dependent gene expression in keratinocytes, which leads to stem cell expansion and tumor development.

The stem cell expansion experiments described in this progress report used keratinocytes isolated from mice of the following genotypes: Wild-type, MEK, AZ and MEK/AZ. Keratinocytes were isolated 1-3 days after birth and established in low calcium medium. Briefly, epidermis and dermis were incubated in 0.25% trypsin overnight at 4°C. After removal of the dermis, epidermal keratinocytes were isolated and plated in standard growth medium consisting of Ca<sup>+2</sup>- and Mg<sup>+2</sup>-free EMEM (Biowhitaker) and 8% FCS treated with Chelex (BioRad Laboratories). Final calcium concentration was adjusted to 0.05 mM using CaCl<sub>2</sub>, and the culture medium was also supplemented with EGF (5ng/ml). Cells were harvested and assayed at the times described in the figure legends. While this approach does not specifically enrich for stem cell populations, the procedure allows isolation of cells only from the proliferating basal layer of the epidermis, which contains the stem cell population, and eliminates other more differentiated populations such as suprabasal cells.

The approach to these experiments was to validate gene expression changes in primary keratinocytes that we identified previously using Affymetrix gene arrays comparing skin tumors from MEK and MEK/AZ mice (Origanti and Shantz, unpublished observations). The gene expression pattern observed in these tumor samples suggested strongly that expression of AZ and MEK together within the hair follicle and the basal layer of the epidermis, where the putative stem cell population resides, results in not only a lower tumor number compared to MEK expression alone, but those tumors that form in MEK/AZ mice are more highly differentiated. This conclusion is based partly on the Keratin expression pattern, which showed increased levels of differentiation-related Keratins 1, 2 and 10 within MEK/AZ tumors, along with a decrease in expression of p63, an essential regulator of stem cell maintenance (all genes changed at least 2-fold).

To test our hypothesis that limitation of intracellular polyamines in MEK-overexpressing keratinocytes results in the expression of differentiation-associated gene products, we measured markers of early (Keratin 1) and late (Involucrin, Loricrin) differentiation in primary keratinocytes isolated at 1-3 days of age from mice of each genotype of interest. The results suggest that MEK expression substantially delays differentiation of keratinocytes in culture compared to wild-type cells, and this is completely reversed by the co-expression of AZ, which limits ODC activity and subsequent polyamine accumulation (Figure 1). Since these changes were originally identified at the transcriptional level in tumors, these results further suggest that polyamines regulate the expression of differentiation-associated genes in the keratinocyte, which ultimately results in a more highly differentiated tumor phenotype.

Further analysis of MEK and MEK/AZ tumor arrays revealed a downregulation (2.4-fold) of the ELAV1 gene, also known as HuR, in MEK/AZ tumors. HuR is a ubiquitously-expressed mRNA binding protein (RBP) that binds to *cis*-acting elements within the 3'UTRs of its targets, resulting in mRNA stabilization. Of interest to our studies, changes in intracellular polyamine

pools have been shown to affect the expression and intracellular localization of HuR, although the effects of polyamines on HuR expression and regulation in the skin have not been defined. HuR has been shown to bind to and stabilize numerous transcripts whose overexpression contribute to tumorigenesis, such as c-Myc, COX2, and VEGF, and a correlation between HuR localization and neoplastic transformation has been described. The studies described here were designed to measure the intracellular localization and expression of HuR in keratinocyte-derived cells and tumors with differing levels of polyamines.

The mouse keratinocyte cell model used in these studies is comprised of two cell lines: C5N cells have a wild-type keratinocyte morphology and contain no detectable mutations in the *H-ras* gene, which is mutated at a high frequency in non-melanoma skin cancer (NMSC). A5 carcinoma cells were isolated from the tumor of a mouse that had been subjected to the classical two-stage protocol of initiation with the carcinogen DMBA, which results in mutations in *ras* and high levels of MEK activation, and promotion with the phorbol ester TPA, which is known to induce ODC activity and polyamine accumulation in the skin. Thus, C5N cells express very low levels of ODC and polyamines, while A5 cells have induced ODC activity and higher polyamine content, particularly putrescine.

HuR is predominately nuclear and has been shown to shuttle between the nucleus and cytoplasm in response to various stimuli or intrinsic cellular conditions. In human tumors, both greater expression of HuR and accumulation in the cytoplasm correlates with increased tumor grade and decreased survival rate. This also fits with our tumor array analysis, which shows decreased HuR expression in the more differentiated MEK/AZ tumors compared to those expressing MEK alone. Based on this, we decided to investigate the content and cellular localization of the HuR protein in C5N keratinocytes and A5 carcinoma cells. The immunofluorescence results show that HuR is almost exclusively nuclear in C5N cells, whereas in A5 cells HuR is both nuclear and cytoplasmic (Figure 2). Since a mutated HuR protein has never been reported in cancer, our results suggest the possibility that HuR is post-translationally modified in A5 cells, thereby causing its cytoplasmic accumulation, where it can bind to a variety of target mRNAs.

Given that HuR is a stabilizing RBP and that its cellular localization is influenced by intracellular polyamine content, we decided to investigate whether HuR binds to the ODC mRNA transcript in our keratinocyte-derived cell lines. These studies were derived in part from the fact that upon examination of the ODC mRNA 3'UTR, we identified several adenosine- and uracil-rich elements (AREs), which are sequences classically located within the 3'UTR of labile mRNAs. These sequences behave as *cis*-acting elements for the binding of RBPs, and are located in numerous proto-oncogene, cytokine, and transcription factor mRNAs. The endogenous intracellular association of ODC mRNA and HuR was assessed through immunoprecipitation of HuR in an assay that allows the association between HuR and its target mRNAs in cytoplasmic ribonucleoprotein (RNP) complexes to be maintained. Little or no ODC mRNA was immunoprecipitated from the C5N keratinocyte cell line cytoplasmic lysate, but a strong ODC band was detected in the immunoprecipitated material from A5 cells (Figure 3). GAPDH was present at very low levels in both lysates, while the positive control c-Myc mRNA associated strongly with HuR protein in A5 lysates (Figure 3). The difference in HuR cellular localization likely accounts for the lack of association between HuR and the ODC mRNA in C5N cytoplasmic extracts. In fact, when C5N nuclear extracts were used to investigate HuR

binding to the ODC mRNA transcript, HuR was able to bind to the ODC 3'UTR (data not shown). Taken together, these data extend the idea that the stabilizing RBP HuR is regulated by intracellular polyamine content, and suggest that HuR present in the cytoplasm binds to the ODC transcript, further contributing to polyamine accumulation by stabilization of the ODC mRNA and subsequent increase in ODC protein and activity.

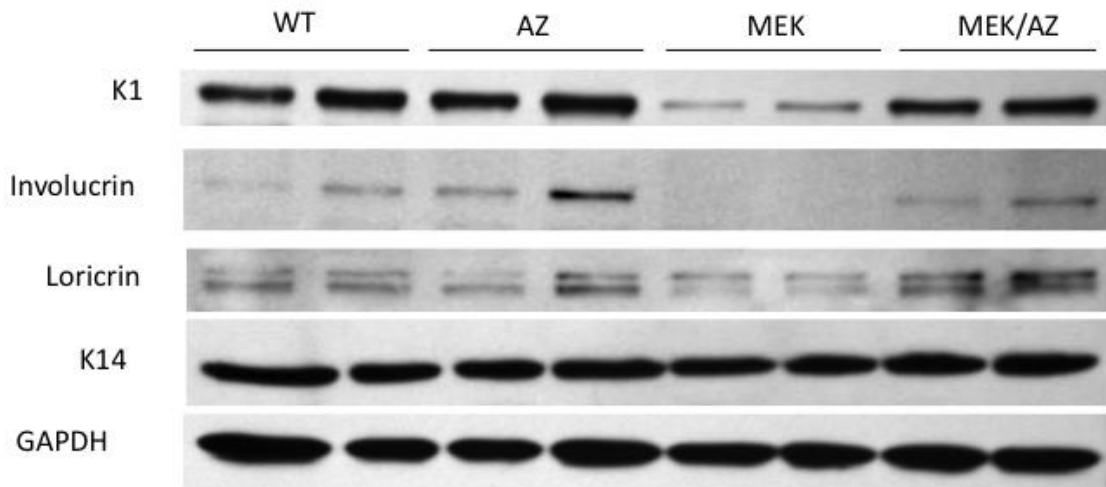


Figure 1. Limitation of ODC activity in the presence of activated MEK causes increased expression of differentiation-associated gene products. Primary keratinocytes from 1-3 day old pups were cultured for 7 days in low  $\text{Ca}^{+2}$  (0.05mM) media and harvested in RIPA buffer. The induction of differentiation markers was identified by Western blot analysis. All samples are presented in duplicate and each measurement was performed at least twice.

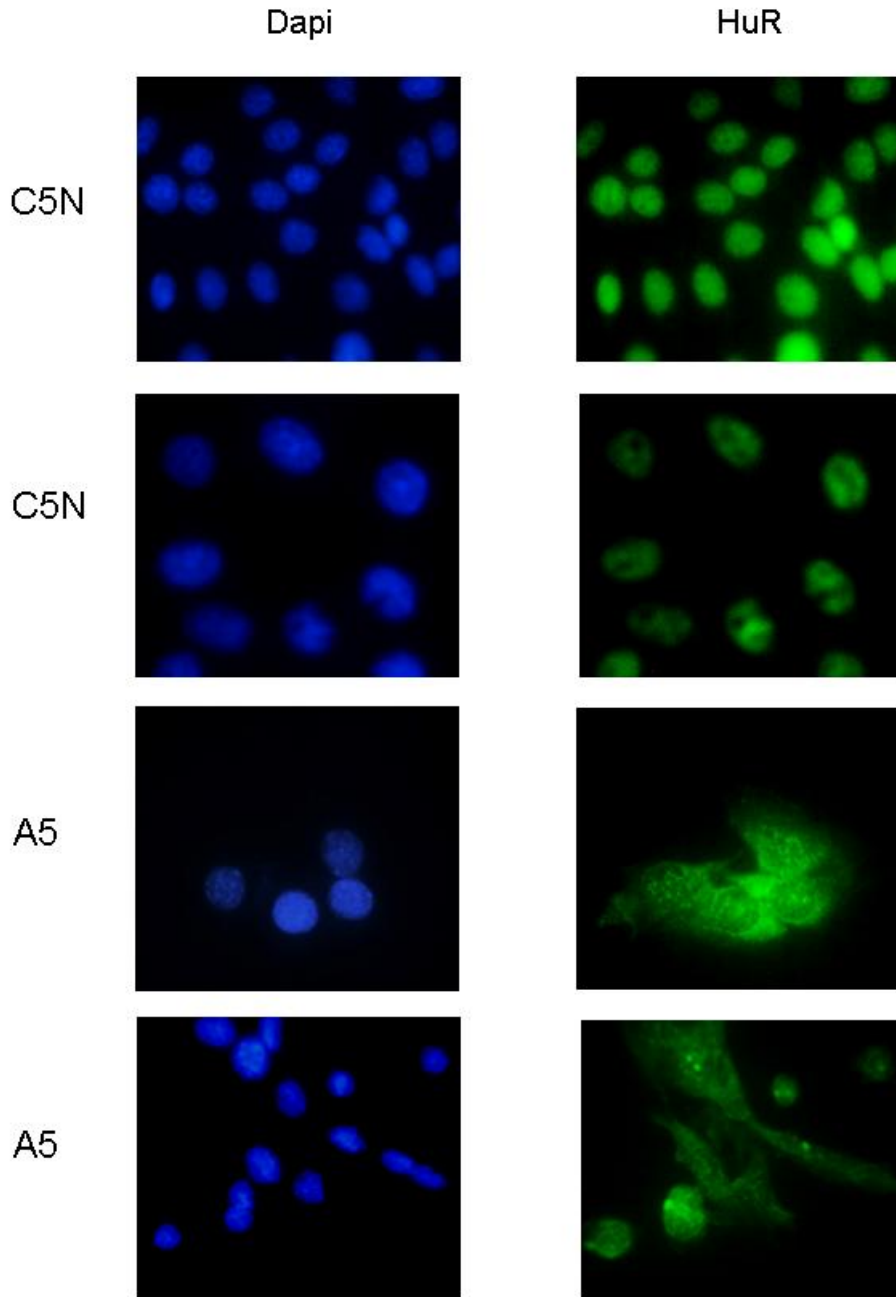


Figure 2. HuR is exclusively nuclear in C5N normal keratinocytes but is both nuclear and cytoplasmic in A5 spindle carcinoma cells. Cells were grown on glass coverslips as described in the Experimental Procedures. HuR protein was detected using anti-HuR antibody (1:500). Cy-2 secondary antibody was used (1:200) (green fluorescence). The nucleus was stained using Dapi (1:1000) (blue fluorescence). Images were taken at a 40X magnification. Representative pictures are shown. This experiment was done in triplicate with reproducible results.

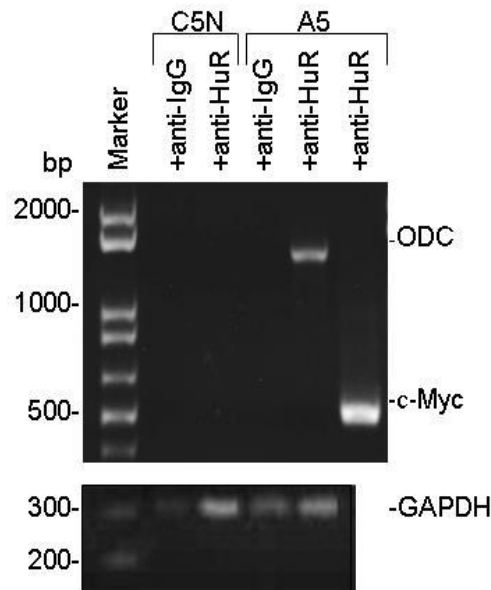


Figure 3. Association of endogenous HuR with endogenous ODC mRNA in A5 cells but not in C5N cells. Cytoplasmic lysates from C5N and A5 cells were used for immunoprecipitation (IP) with anti-HuR or nonspecific mouse IgG. RNA in the IP material was extracted using phenol chloroform extraction, used in a PCR reaction, and visualized on a 2% agarose gel. The levels of ODC mRNA and GAPDH mRNA were assessed by PCR using primers that were specific for their respective coding regions. The level of c-Myc bound to HuR was assessed as a positive control. This experiment was conducted in triplicate with reproducible results.

### **Research Project 14: Project Title and Purpose**

*Topical Application of Isoselenocyanates for the Prevention of Melanoma* – Malignant melanoma is the most fatal and invasive form of skin cancer. The cause of 60% of melanomas is yet to be determined, making development of effective targeted chemopreventive agents especially important. In spite of the widely appreciated magnitude of the problem, there is still a critical gap in knowledge regarding key deregulated signaling pathways causing melanoma and chemopreventive agents targeting these gene defects to prevent this disease. Therefore, the purpose of this project is to develop *a rationally designed chemopreventive agent targeting the Akt3 signaling pathway*. As a direct outcome of the investigation, we expect to validate the effectiveness of novel synthetic agents derived from naturally occurring chemopreventive agents as a topical agent that prevents early melanocytic lesion development.

### **Duration of Project**

7/1/2010 – 6/30/2011

### **Project Overview**

New strategies are urgently needed to prevent development of melanoma. Currently, surgical excision is the mainstay for eliminating early melanocytic lesions or preventing development of

more aggressive cancer. Despite these preventive strategies and increased use of sunscreen, incidence and mortality rates of melanoma continues to rise by about 4% per year in the US and worldwide. This makes melanoma the cancer with the second fastest rate of increase in this country.

Recently, we identified elevated Akt3 activity occurring in ~70% of sporadic melanomas compared to normal cells. Functionally, active Akt3 reduces responsiveness of early pre-malignant melanoma cells to agents that would normally kill via apoptosis, thereby promoting melanoma development. Unfortunately, no agents are available to inhibit the Akt3 signaling cascade in early melanoma cells. Use of sunscreen or body lotions containing topical agents with chemopreventive efficacy could be potentially useful for preventing cancer development. Therefore, novel topical chemopreventive agents with negligible systemic toxicity to prevent melanocytic lesion development would be highly significant. In order to meet this unmet medical need, potent anti-melanoma agents called isoselenocyanates (ISC) have been developed from naturally occurring isothiocyanates (ITC), which are derived from plants. In these agents, sulfur has been replaced with selenium and the alkyl side chain has been lengthened from 1 or 2 to 4 or 6.

The *central hypothesis* for this project is that targeting Akt3 signaling in early melanoma lesions would be an effective chemopreventive approach for preventing melanoma lesion development. The *hypothesis will be tested* by determining the chemopreventive utility of novel synthetic isoselenocyanate derivative as a topical agent that inhibits Akt3 signaling in a preclinical mouse model of melanoma. The *approach* to be used involves, evaluating effectiveness for retarding melanoma development in culture and animal models of this disease. Accomplishing these goals would be highly significant, providing novel insight into the chemopreventive potential of targeting a major signaling pathway promoting melanoma development, and provide solid rationale for initiating clinical trials with potent selenium-containing topical chemopreventive agent with significant potential to prevent melanocytic lesion in melanoma patients by targeting Akt3 signaling.

### **Principal Investigator**

Arati Sharma, PhD  
Assistant Professor  
Pennsylvania State University College of Medicine  
Penn State Hershey Cancer Institute-CH74  
500 University Drive  
Hershey, PA 17033

### **Other Participating Researchers**

None

### **Expected Research Outcomes and Benefits**

Currently, no effective chemopreventive agents exist to prevent /retard development of early into

more advanced melanomas in the skin. Research, models and technology contribute to emerging novel concepts that suggest development of unique synthetic chemopreventive agents that target Akt3 signaling to prevent early melanoma development within skin.

This research is expected to yield several outcomes: First, demonstrate that inhibition of Akt3 signaling in reconstructed human skin retards development of early melanocytic skin lesions; and second, validate that topical application of a selenium analog of isothiocyanate targets Akt3 signaling and prevents melanoma development in a transgenic melanoma mouse model. Thus, a novel topical chemopreventive agent inhibiting early melanomas would be identified, contributing a needed tool to the relatively small arsenal of chemopreventive agents currently available for preventing this disease.

For melanoma patients and the general public, these discoveries have the potential to significantly impact human health by decreasing the number of persons having melanoma, thereby directly decreasing mortality rates. The positive impact for reducing melanoma incidence and mortality rates would be significant.

### **Summary of Research Completed**

One manuscript describing project accomplishments using support from the PA Tobacco Settlement Fund has been accepted for publication in the AACR Journal, Cancer Prevention Research February 2011 Issue. One of the figures from this manuscript has been selected by the editor to be featured on the cover page of February issue of Cancer Prevention Research. The accepted article is listed below.

Nguyen N, Sharma A, Nguyen N, Sharma AK, Desai D, Huh SJ, Amin S, Meyers C, Robertson GP. Melanoma Chemoprevention in Skin Reconstructs and Mouse Xenografts using Isoselenocyanate-4. Cancer Prev Res (Phila). 2010 Nov 19. PMID: 21097713 [Epub ahead of print]

#### **Abstract**

Melanoma incidence and mortality rates continue to rise despite the use of sunscreen as well as screening programs for early surgical excision of premalignant lesions. The steady increase in melanoma incidence suggests that additional preventive approaches are needed to augment these existing strategies. One unexplored area involves targeting genes whose deregulation promotes disease development in order to prevent melanoma. The Akt3 signaling pathway is one key signaling cascade playing a central role by deregulating apoptosis to promote development of ~70% of melanomas. Isoselenocyanate-4 (ISC-4), derived from isothiocyanates by increasing the alkyl chain length and replacing sulfur with selenium, has been developed to target this important signaling pathway in melanomas; however, its chemopreventive potential is unknown. In this study, the chemopreventive efficacy of topical ISC-4 was evaluated in a laboratory generated human skin melanoma model containing early melanocytic lesion or advanced stage melanoma cell lines as well as in animals containing invasive xenografted human melanoma. Repeated topical application of ISC-4 reduced tumor cell expansion in the skin model by 80-90% and decreased tumor development in animals by ~80%. Histological examination of ISC-4 treated skin showed no obvious damage to skin cells or skin morphology and treated animals did

not exhibit markers indicative of major organ related toxicity. Mechanistically, ISC-4 prevented melanoma by decreasing Akt3 signaling leading to a 3-fold increase in apoptosis rates. Thus, topical ISC-4 can delay or slow melanocytic lesion or melanoma development in preclinical models and could impact melanoma incidence rates if similar results are observed in humans.

### **Research Project 15: Project Title and Purpose**

*Activation of STAT3 Protects Liver from Ischemia Reperfusion Injury* - Liver resection is the only curative option for liver tumors and liver transplantation is the only viable treatment for end stage liver disease. Warm ischemia/reperfusion (I/R) is a common clinical problem during both types of surgeries. Warm ischemia also occurs in trauma and shock. The liver is the most commonly injured abdominal organ in blunt and penetrating abdominal trauma. The management of trauma and shock frequently involves exposing the liver to varying periods of warm ischemia followed by reperfusion. I/R injury is significantly associated with morbidity and mortality in such conditions. Prevention or minimization of liver I/R injury is the clinical priority for our study, because there is still no safe and promising strategy to protect liver from I/R injury.

#### **Duration of Project**

1/1/2010 – 6/30/2011

#### **Project Overview**

Signal transducers and activators of transcription 3 (STAT3) is a major signaling molecule for a variety of genes in response to cell stimuli and plays a key role in many cellular processes such as cell growth and apoptosis. Recent studies have suggested that STAT3 activation is involved in protection of hepatocyte from I/R injury. Our goal is to understand the mechanisms of STAT3 in I/R injury. In this project, we hypothesize that STAT3 is an essential factor in protecting liver and in survival from I/R injury. Using STAT3 hepatocyte-specific deficient mice and their wild type control, we will examine this hypothesis in response to partial and total liver ischemia.

*Specific Aim 1: To demonstrate that STAT3 has hepatoprotective role from partial hepatic injury.* A persistent 90 minutes partial liver ischemia followed by reperfusion will be performed in both STAT3 hepatocyte deficient mice and wild-type littermates. STAT3 expression, serum transaminase level, liver degeneration (apoptosis) and regeneration (cell cycle reentry) will be monitored by molecular biochemical and immunohistochemical assays. Animals will be sacrificed at 6 hours (injury phase) and 48 hours (repair phase) after reperfusion. Liver enzyme level and liver pathology will be compared between STAT3 deficient mice and wild-type littermates. Histological changes will be examined using liver I/R injury score.

*Specific Aim 2: To demonstrate that STAT3 is essential for animal survival from total warm ischemic injury.* Total liver ischemia behaves differently from partial liver ischemia. It has been shown that all animals survived 60 minutes of total ischemia, whereas all died after 90 minutes of total ischemia. An intermediate time period of 75 minutes of total liver ischemia followed by

reperfusion will be performed in control and hepatocyte specific STAT3 deficient mice. A poor survival outcome is expected in the STAT3 deficient group compared to control group.

This study will provide direct evidence whether STAT3 activation is the essential process in liver protection and survival from I/R injury. In this application, we will be able to show the mechanisms of STAT3 on I/R injury not only at the cellular level but also at the in vivo level.

### **Principal Investigator**

Tadahiro Uemura, MD, PhD  
Assistant professor of Surgery  
Penn State Milton S. Hershey Medical Center  
500 University Drive  
P.O. Box 850  
Hershey, PA 17033

### **Other Participating Researchers**

Samuel Shao-Min Zhang, MD, PhD, John Liang, MD, Lucy Xi Lou, MD – employed by Pennsylvania State University

### **Expected Research Outcomes and Benefits**

To minimize blood loss during liver surgeries, hepatic vascular inflow is temporarily clamped (ischemia) and de-clamped after resection of tumors (reperfusion). This procedure is known as Pringle maneuver and it is a well-established and routine procedure during liver surgeries. However, Pringle maneuver causes I/R injury, which may cause liver failure.

Liver transplantation has significantly progressed during the past decades and it is the only viable treatment for end stage liver disease. More than 6,000 liver transplantations were performed in United States in 2008. In liver transplantation, the liver receives ischemic damage in cold preservation and the liver is exposed to reperfusion injury after implantation. I/R injury in liver transplantation is strongly associated with a non-functional liver, which is a life threatening condition and requires emergent liver re-transplantation.

I/R injury is a common clinical problem encountered during liver resection and liver transplantation. Warm I/R injury also occurs in trauma and shock. This study will provide direct evidence whether STAT3 activation is the essential process in liver protection and survival from I/R injury. We may be able to identify methods to minimize or prevent I/R injury as a result of this study.

### **Summary of Research Completed**

#### *1. Generation and expansion of STAT3 deficient mice specific in hepatocytes*

In collaboration with Dr. Zhang's lab, we have generated a tissue specific STAT3 deficient mouse model, where STAT3 has been deleted within hepatocytes using Cre-Lox recombination

driven by transthyretin (TTR) promoter (Moh et al., 2007). The exons from 18 to 20 encode the Src homology 2 (SH2) domain of STAT3, which is responsible for the protein's function as a transcriptional factor (Figure 1A). By flanking the SH2 domain (Figure 1B), exons 18-20, with a loxP (locus of x over P1) recognition signal targets the molecules for deletion through recombination of the DNA, which is catalyzed by the Cre (cyclization recombination) enzyme (Figure 1C). As a result of breeding a TTR promoter driven Cre recombinase gene transgenic mouse with a STAT3 lox-P (F/F) strain we created a conditional STAT3 deficiency specifically to hepatocytes (Figure 1C). This animal model is referred to as a STAT3 CFF mouse because it contains a homozygous allelic deletion of the SH2 domain (STAT3-loxP<sup>F/F</sup>) and a heterozygous C allele (Cre<sup>+/-</sup> gene). This STAT3(CFF) mouse is good for *in vivo* studies by ischemic induction. Littermates with STAT3(FF) or STAT3(F/+) genotypes were used as controls. Genotyping was performed the same as previously reported (Welte et al., 2003). The three small arrows in Figure 1 indicated primer location and directions.

## 2. Analysis of STAT3 activation in STAT3 wild type and deficient livers

Liver tissue collection from STAT3 wild type and deficient mice: Liver tissues were harvested from STAT3 wild type (STAT3FF) and hepatocyte STAT3 deficient (STAT3CFF) animals at 8 weeks after birth for both male and female, respectively. Liver tissues from individual animals were stored separately for eventual analysis. A 90 minute partial liver ischemia was performed on another set of animals, with the same genotype as above.

Cell lysate and Western blot: Fresh liver tissues were also used for full cell lysate. Whole cell extracts were prepared and Western blot assays performed as described previously with modification (Zhang et al., 2004, 2005). Briefly, liver cells from each experimental and control group were suspended in about 80ul T-PER tissue protein extraction buffer (Pierce, Rockford, IL) with protease inhibitor cocktail (Roche Applied Science, Indianapolis, IN). The tissue samples were homogenized and centrifuged at 10,000g under 4°C for 5 minutes. The supernatant was collected and protein concentrations were measured. Fifteen to 25ug of the whole cell extract were separated by SDS-polyacrylamide gel electrophoresis and transferred to Immun-Blot polyvinylidene difluoride membrane (Bio-Rad Laboratories, Hercules, CA). After blocking with 3% non-fat milk in washing buffer, membranes were incubated with primary antibodies. The primary antibodies include STAT3 (Santa Cruz, Santa Cruz, CA), and phosphorylated STAT3 (Cell Signaling, Danvers, MA). Following washes, they were incubated in anti-rabbit or anti-mouse IgG coupled to horseradish peroxidase. The immunoreactive bands were visualized using SuperSignal Chemiluminescent Substrate (Pierce, Rockford, IL) by developing films or using ChemiDoc XRS System (Bio-Rad Laboratories, Hercules, CA). Signal intensity was analyzed using Quantity One (Bio-Rad Laboratories, Hercules, CA).

Reduction of STAT3 expression and activation in STAT3 deficient livers: As shown in Figure 2, a clear reduction of STAT3 protein expression in livers from STAT3CFF mice were observed compared to their littermate wild type control STAT3FF mice. Similarly, the resting livers maintained a certain level expression of activated STAT3 with tyrosine phosphorylation, suggesting that a functional STAT3 exists routinely in liver. Beta- actin was a protein loading control in this study. This study also confirmed the successful deletion of STAT3 in STAT3CFF animals, which is a suitable model for STAT3 function in hepatocytes *in vivo*, although there are very lower level expression of STAT3 seen in the STAT3CFF liver, could contaminate by other

cell types of liver, such as endothelial cells, macrophages, or stellate cells.

To evaluate the function of STAT3 in response to ischemic injury: STAT3 is an immediate response gene, which is found first in livers. To evaluate the functions of STAT3 in livers from wild type or STAT3 deficient hepatocytes, we tested the level of STAT3 tyrosine phosphorylation in response to a liver ischemic injury. As shown in the Figure 2, both STAT3 protein expression and protein tyrosine phosphorylation were increased in the wild type animals while the levels in STAT3CFF mice showed only a slightly increase, indicating that the response of STAT3 to ischemic injury was abolished.

### 3) Examination of liver functions in response to ischemic injury

Liver partial ischemic injury: Mice were anesthetized (i.p.) with a mixture of 100mg/kg Ketamine and 10mg/kg Xylazine. A midline incision was made on the abdomen. The liver was exposed with retractors placed in the flanks. The blood supply to the medial largest lobe and lateral lobe of the liver (70% of liver) was temporally interrupted (ischemia) by applying a microclamp (RS-5435, Roboz Surgical Instrument, MD) to the vascular pedicle (Yadav et al, 1998). The blood supply was resumed by removing the microclamp after 90 minutes of ischemia.

Peripheral blood collection: As originally proposed, we have designed 6 and 24 hours as the time points for liver functional analysis. For monitoring the liver injury, serum was collected from each animal for enzymatic analysis at 6 hours after reperfusion. Serum level of alanine transaminase (ALT) was used for marker of I/R injury (Matsumoto et al., 2006) ALT was measured using serum multiple biochemical analyzer in clinical laboratories at 6 and 24 hours after reperfusion.

Alanine Transaminase (ALT) analysis 6 hours after liver ischemic injury: ALT was monitored as an indicator of liver I/R injury. We have examined a large range of STAT3 wild type and deficient animals 6 hours after ischemic injury. As shown in the Figure 3, we initially measured ALT at 6 hours after ischemia. There was no significant difference between those groups, as  $1146 \pm 608$  or  $927 \pm 412$  u/L from wild types or STAT3CFF, respectively ( $P=0.52$ ). *This is an unexpected result based on our hypothesis.* One possibility could be that STAT3 deficiency might be involved in the earlier stages. Then we decided to examine the ALT levels at 3 hours after ischemic injury instead of looking at the levels at 24 hours after ischemia.

ALT analysis 3 hours after liver ischemic injury: Two pairs of STAT3 wild type and deficient animals were used for the pilot experiment the same as above, but at the earlier time point. As shown in the Figure 4, a dramatically higher level of average ALT was seen in the serum from STAT3CFF animals ( $1576$  u/L) compared with their wild type controls ( $574$  u/L). Because of a delay in generating enough STAT3CFF animals, we had insufficient samples for statistical analysis, however, now that we have about 9 STAT3CFF and the same amount of controls, an additional experiment was performed to finish this study. The results from this pilot study suggested that STAT3 might function as an earlier factor in protecting liver damages in response to ischemic injury.

### 4) Histological analysis of hepatocytes in response to ischemic injury

Liver tissue collection and fixation 6 hours after liver ischemic injury: Although the earlier ALT

changes in STAT3CFF mice reflected a possible immediate damage of hepatocytes we have examined histologically the potential alteration. Liver tissues were collected at 6 hours after ischemic injury. Livers were fixed with 4% paraformaldehyde in PBS for at least 6 hours at 4°C. After three washes with PBS, fixed explants were dehydrated through a series of graded ethanols and embedded in paraffin. Liver specimens were stained with hematoxylin and eosin. Histological change was scored from 0 to 4 based on the degree of cytoplasmic vacuolation, congestion and necrosis using score of ischemic injury, Suzuki Score at 6 hours after reperfusion (Suzuki et al, 1993). Stained sections were imaged with a microscope (Carl Zeiss Meditec, Thornwood, NY; or Olympus Corp. of America, Lake Success, NY) equipped with a digital camera.

Histological examination and evaluation: The liver samples have been pathologically examined between wild type and STAT3CFF groups 6 hours after ischemic injury. Six animals were used for each group. As shown in the Figure 5, beside little nuclear condensation observed in STAT3 wild type liver sections (upper panel), a dramatic hepatocyte degeneration was seen in the liver sections from STAT3CFF animals (lower panel). The areas of cytoplasmic vacuolation, congestion, and necrosis were seen closer to portal triad (PT) and far from central veins (CV), which matched the basic pathological changes by portal vein ischemia. After TUNEL analysis, apoptotic cells were counted in the section with a high power field (HPF) in both wild type and STAT3CFF groups. A significantly higher apoptotic cells were found in STAT3CFF animals (average  $8 \pm 3$ /HPF) compared to their wild type controls ( $4 \pm 2$ /HPF), respectively ( $p < 0.05$ ). The results from this study suggested that STAT3 plays an important role to protect hepatocytes from ischemic injury.

Liver degeneration in STAT3 deficient animals: Using a semi-quantitated method, Suzuki scoring, which examines the histological changes by scoring from 0 to 4 based on the degree of cytoplasmic vacuolation, congestion and necrosis, we found that significant tissue damage in STAT3CFF sections were observed in all categories examined (Figure 6), such as vacuolation ( $p = 0.01$ ), congestion ( $p = 0.02$ ), and necrosis ( $p = 0.001$ ) compared to the scores of their controls. This strongly supported the role of STAT3 in protective ischemic hepatocytes.

##### 5) Confirmation of STAT3 inhibition in hepatocyte survival

STAT3 in immediately protection of hepatocytes: For evaluating the STAT3 functions under total ischemia injury as proposed in the Specific Aim 2, we used 2 mice of wild type. All mice died before completion of the experiment, suggesting a higher sensitivity in response to the completed block of blood flow. For this reason, we changed the focus and kept it on the STAT3 functions in liver protection for partial ischemic damages. Although the animal model with STAT3CFF provided a sufficient system to study hepatocyte *in vivo*, since the deletion of STAT3 happened from embryonic stages, it is unclear whether STAT3 is immediately required for protecting hepatocytes. In this study we examined the survival rate of a human hepatocyte cell line HepG2 in response to a specific STAT3 activation inhibitor.

Preparation of hepatocytes in culture: Human hepatoma cells (HepG2) were used to study effects of AG490, a STAT3 inhibitor *in vitro*. HepG2 cells were cultured in 6-well plates with Dulbecco's Modified Eagle Medium (DMEM) containing 1% Pen-Strep under atmosphere of 5% CO<sub>2</sub>. HepG2 cells were then moved to 96-well plate for AG490 challenge. 12 hours after

treatments cells were used for MTT analysis. Three repeats were used for all experiments. Reads from coloring were used for statistical analysis.

Inactivation of STAT3 declines hepatocyte survival: AG490 treatments were performed under a 10% FBS condition. Non-FBS group served as positive control for cell damages. As shown in Figure 7, we found that a significant reduction ( $p > 0.05$ ) of HepG2 cells 12 hours in response to AG490 treatment compared to untreated controls. The cell survival rates of AG490 treated groups were similar to non-FBS groups, indicating that STAT3 is required for immediate hepatocyte protection. The results from this project suggested that activation of STAT3 signaling is essential in protecting hepatocytes in response to warm ischemic injury, small molecule or other reagent, which trigger STAT3 activation in hepatocytes might help to preserve hepatocyte functions during liver surgery and transplantation.

Figure 1. The scheme of STAT3 deletion specific in hepatocytes.

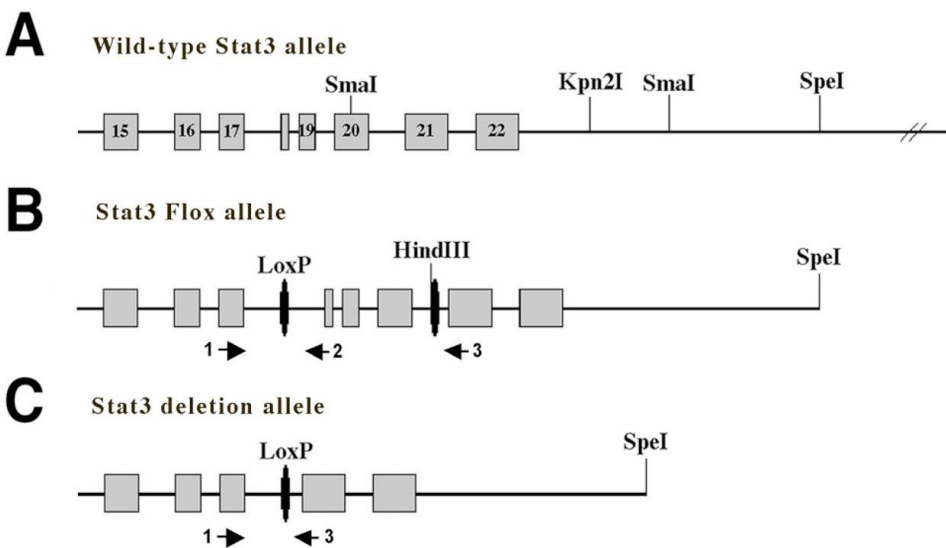


Figure 2. Reduction of STAT3 expression and activation in STAT3 deficient liver tissues compared to their wild type controls.

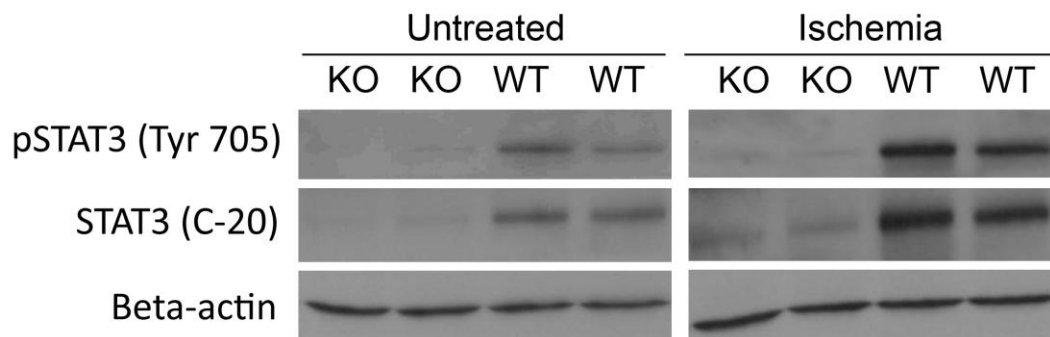


Figure 3. No significant difference of serum ALT changes between STAT3CFF and their wild type animals 6 hour after ischemic injury.

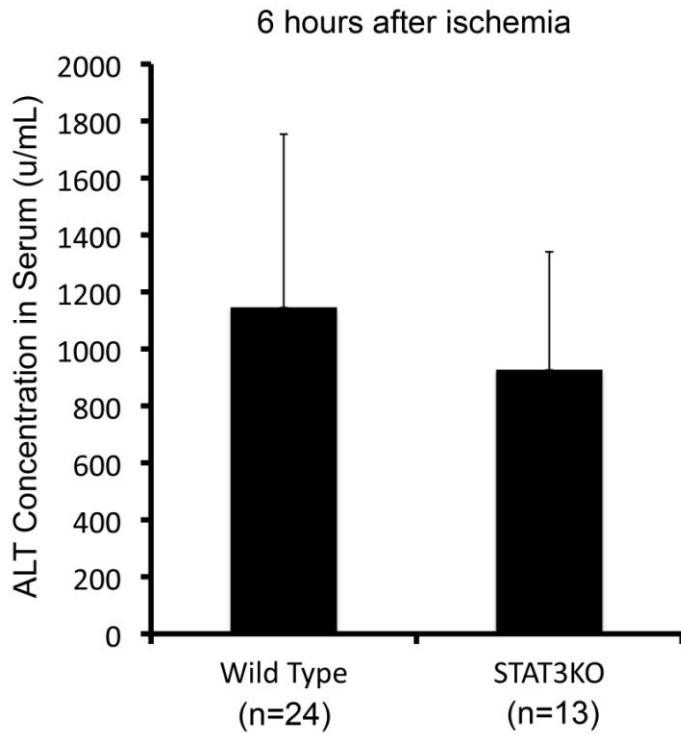


Figure 4. Increase of serum ALT levels in STAT3CFF animals 3 hour after ischemic injury compared with STAT3 wild type animals.

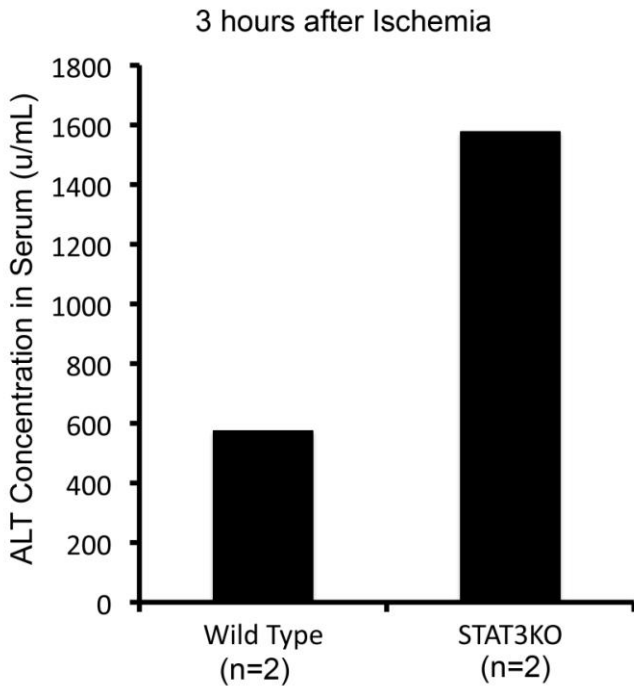


Figure 5. A significant congestion and necrosis found in STAT3CFF animals compared with their wild type control.

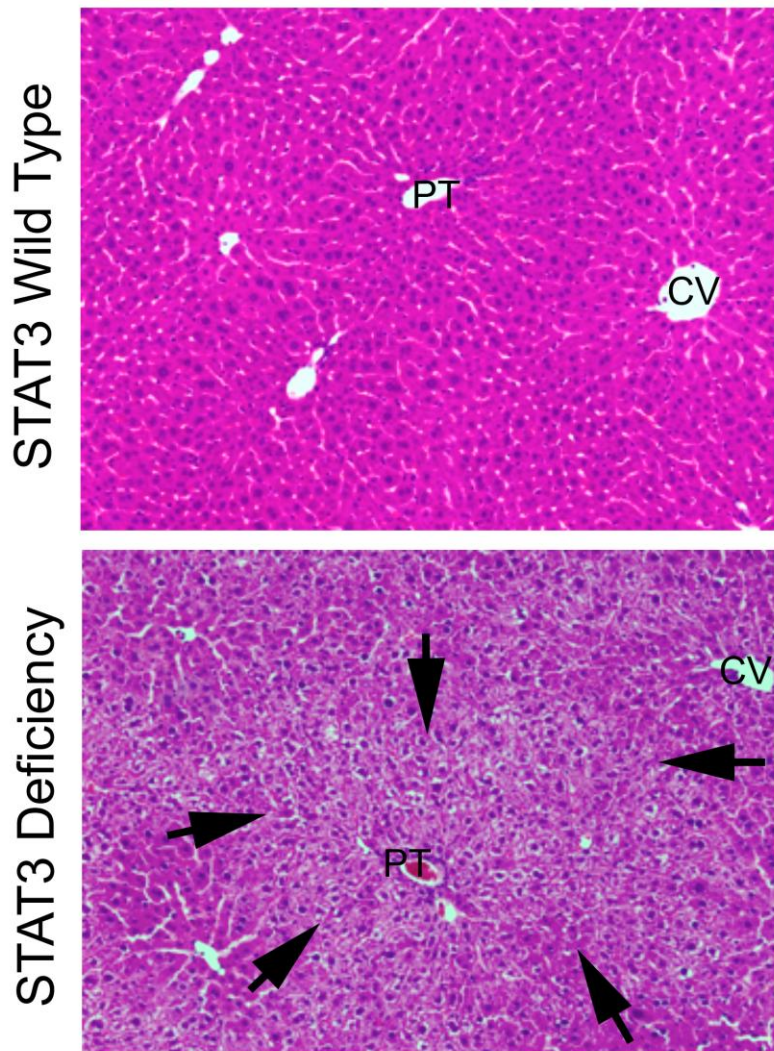
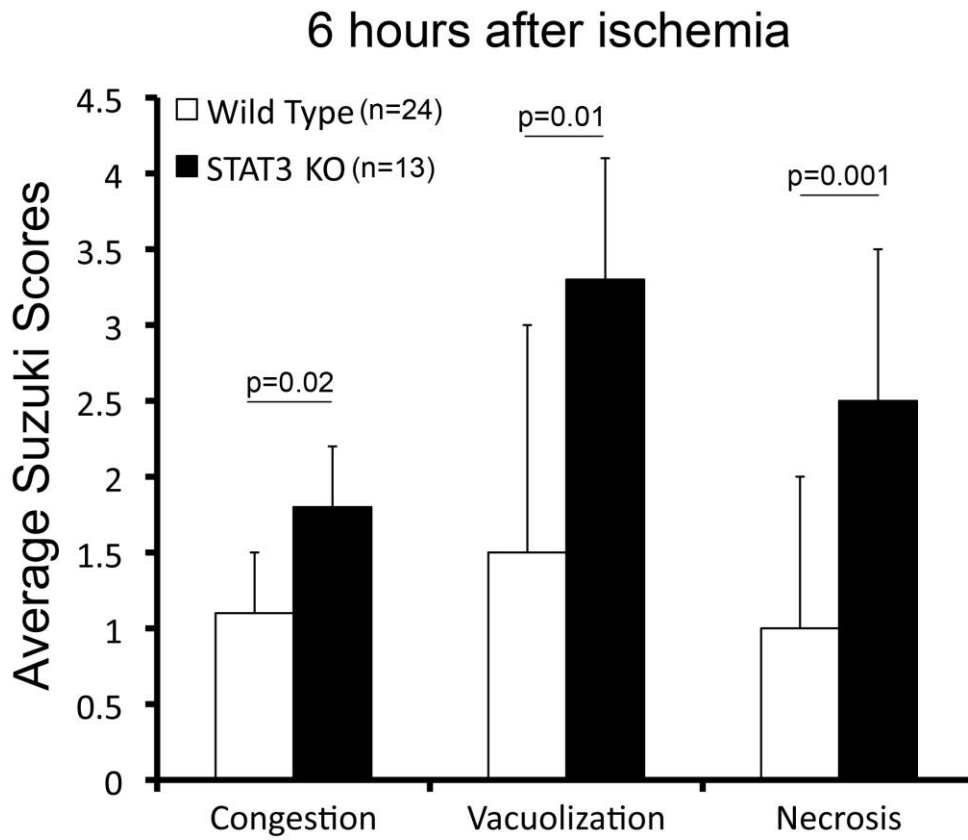
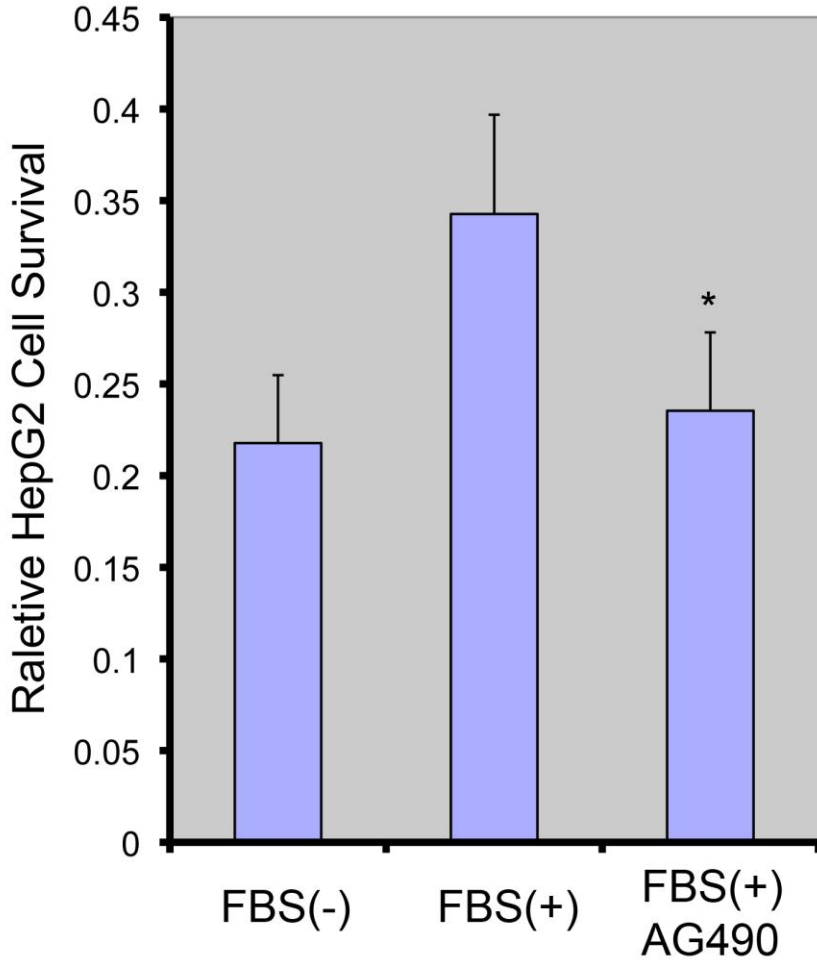


Figure 6. A significant increase of Suzuki scores in STAT3CFF animals compared to their wild type controls.



**Figure 7.** Inhibition of STAT3 activation by AG490 immediately reduced HepG2 cells survival by MTT assay.



**Research Project 16: Project Title and Purpose**

*Multifunctional Nanoparticles for Melanoma and Brain* - Malignant melanoma and glioblastoma multiformi (GBM) are invasive and deadly forms of skin and brain cancer respectively with no effective therapy to treat advanced disease, leading to poor survival rates. A P01 Program Project Grant is proposed consisting of 5 projects using “Multifunctional Nanoparticles” to develop a new category of agents to treat these cancers. This project will focus on developing preliminary data to be used in supporting the Program Project application and to illustrate advanced integration and improved synergy between the 5 projects incorporated in the Program Project Grant (PPG).

**Anticipated Duration of Project**

7/1/2010 - 12/31/2011

## **Project Overview**

The purpose of this project will be to develop preliminary research data in the following areas: Development of liposomes targeting genes, which when targeted together, will lead to synergistically acting cancer inhibition and, into which plasmids can be loaded to express lost genes in cancer cells. This project will also undertake siRNA screens to identify genes when targeted with H-ferritin will synergistically inhibit cancer cells. The project will further undertake studies to develop a cell culture based blood brain barrier model and study liposome movement across the barrier. Finally, this project will collect preliminary data in a study that focuses on the liposome uptake to circulating tumor cells in a flow system. The preliminary data obtained from this study will be used in a Program Project application. The P01 application will focus on Melanoma and GBM since both are deadly and invasive diseases frequently metastasizing to, or occurring in, the brain respectively. Furthermore, for both cancers, lack of effectiveness of untargeted therapies has led to the conclusion that targeted therapeutics are needed that inhibit multiple proteins or pathways causing these diseases. To accomplish this objective, multifunctional nanoparticles will serve as a single platform for delivering agents which will target multiple pathways that can also be used for imaging the cancer. As a direct result of this realization, the members of this PPG have chosen this platform to address important biological questions related to each disease. The PPG is centered on a funded R01 project (project 1), which focuses on developing synergistically acting nanoparticles targeting multiple proteins in order to more effectively treat melanoma. It should be noted that this R01 project was, in its initial phase, supported by a Pennsylvania Department of Health Research Grant. The use of multifunctional nanoparticles is a unifying theme focusing on developing synergistically acting nanoparticles targeting multiple proteins in order to more effectively treat melanoma. Use of multifunctional nanoparticles is also a unifying theme to solve important biological problems in melanoma and brain cancer. Interaction and sharing between projects will result in a cooperative and synergistic team effort.

## **Principal Investigator**

James Connor, PhD  
Pennsylvania State University, College of Medicine  
The Milton S. Hershey Medical Center  
Department of Neurosurgery, H 110  
500 University Drive. P.O. Box 850  
Hershey, PA 17033-0850

## **Other Participating Researchers**

Gavin P. Robertson, PhD; Cheng Dong, PhD; Rogerio Neves, MD, PhD; Nadine Barrie Smith, PhD; Siyang Zheng, PhD; Achuthamangalam B Madhankumar, PhD; Thomas Neuberger, PhD; Jason Liao, PhD; Richard Rauscher, MS; Melissa Tran, PhD; Anton Mulder, BCom; Arati Sharma, PhD - The Pennsylvania State University

## **Expected Research Outcomes and Benefits**

This project will be focused on obtaining preliminary data to be used in a P01 application. More specifically, it will be using Pennsylvania Department of Health Funds to develop research data that will support the liposome development for the respective projects of the P01 application. Preliminary research data will also be used to illustrate high levels of integration and synergy between the 5 projects incorporated in the proposed PPG application. This, according to the NIH, based upon a NIH visit (12/17/2009) and presentation of the proposed PPG, will significantly increase the probability of having this PPG funded. Funding of this PPG, over the long-term, will have a significant positive impact on the currently poor prognosis faced by advanced-stage melanoma and glioblastoma patients and will contribute to the availability of more effective therapeutic agents, which would increase the length and quality of life for these patients. Therefore, the positive impact on melanoma and glioblastoma therapeutic development will be significant. Expected deliverables of this PPG are:

1. Novel synergistically acting nanoparticles targeting multiple kinase targets to more effectively kill melanoma, which do not currently exist.
2. Novel nanoparticles that synergistically increase the sensitivity of glioblastoma cells to BCNU chemotherapy, which does not currently exist.
3. Novel nanoparticles for imaging and treating melanoma lymph node, which do not currently exist.
4. Novel imaging and therapeutic nanoparticles for measuring the efficacy of ultrasound for permeating the blood-brain barrier and shrinking glioblastoma or metastasized melanoma tumors, which do not currently exist.
5. Novel nanoparticles for targeting circulating tumor cells to disrupt extracellular interactions in order to decrease metastasis, which do not currently exist.

## **Summary of Research Completed**

The funds were used to provide 4 investigators the opportunity to gather data and perform research to develop a program project application to the National Cancer Institute. We were successful in developing an application that was submitted (1 P01 CA160005-01) and reviewed on 01/25/2011. The PO1 received a priority score of 65. Although a good working score for the original submission, the grant was not in the fundable range. The individual projects received impact factor scores ranging between 5.9 and 6.6. Discussion among the investigators to resubmit the application is ongoing. Considerable progress has been made and additional grant applications submitted.

### PROJECT 1: Sensitizing Glioblastomas to Chemotherapy and Radiation through the delivery of H-ferritin siRNA.

This project has resulted in one publication (Xiaoli Liu, A.B. Madhankumar, Jonas Sheehan, Nodar Surguladze, Becky Slagle-Webb, and James R. Connor. "H-ferritin siRNA Delivered by Cationic Liposomes Increases Chemotherapeutic Sensitivity for Treating Glioma." [Cancer Res.](#) 2011 Mar 15;71(6):2240-9. Epub 2011 Mar 8). The work in this paper is summarized as follows: Approximately half of all gliomas are resistant to chemotherapy and new therapeutic strategies are urgently needed to treat this cancer. We hypothesized that disrupting iron homeostasis in glioma cells could block tumor growth, based on an acute requirement for high levels of iron to

meet energy requirements associated with their rapid growth. Ferritin is best known as an intracellular iron storage protein, but it also localizes to tumor cell nuclei where it appears to protect DNA from oxidative damage and to promote transcription. In this study, we determined whether silencing the H-ferritin gene could increase tumor sensitivity to chemotoxins. To test this hypothesis, H-ferritin siRNA was delivered to several human cancer cell lines using cationic liposomes. H-ferritin siRNA decreased protein expression by 80% within 48 hours and this decrease was associated with a >50% decrease in the LD50 for DNA alkylating agent carmustine (BCNU), which is commonly used to treat glioma in clinic. In a subcutaneous mouse model of human glioma, intratumoral injections of liposomes containing H-ferritin siRNA reduced the effective dose of BCNU needed for tumor suppression by >50%. A plasmid supercoil relaxation assay demonstrated that H-ferritin specifically and directly protected DNA from BCNU treatment. H-ferritin siRNA additionally appeared to increase apoptosis in glioma cells *in vitro* upon H-ferritin knockdown. Overall, our results illustrate how silencing H-ferritin can effectively sensitize tumors to chemotherapy, also demonstrating the ability of cationic liposomes to serve as a novel *in vivo* delivery tool for siRNAs.

In addition to this published work, a second manuscript is nearing completion with a targeted submission date of end of August 2011. This study extended our findings of increased sensitivity of GBMs to chemotherapy to radiation. Specifically, our results demonstrated that exposing H-ferritin siRNA to U251 cells with 20 Gy of radiation results in a 50% increase in cell death. Intratumoral injections of cationic liposomes containing H-ferritin siRNA resulted in a 1000-fold increase in radiation efficacy compared to the same cationic liposomes delivering non-specific RNA. Because radiation is thought to kill cancer cells by damaging their DNA, the interaction of H-ferritin with DNA was investigated *in vitro* using a supercoil relaxation assay. This study demonstrated that H-ferritin maintained DNA in a relaxed and linear form in the presence of radiation, but not in the absence of H-ferritin. Overall, our data demonstrates that silencing the *H-ferritin* gene appears to be an effective way to sensitize glioma tumor cells for radiation. Thus, H-ferritin siRNA may provide a novel target for improving efficacy of radiation therapy for the treatment of GBMs. Since various malignant cancer cells typically express high levels of ferritin, the use of H-ferritin siRNA as an adjuvant therapy, this treatment can be used to treat other types of cancers and will not be limited to just for treatment of GBMs.

An R01 NIH application is under development to be submitted with Dr. Jeremy Rich of the Cleveland Clinic Neuro-oncology program.

#### PROJECTS 2 AND 4: Targeting Invasion and Triggering Apoptosis to Halt Lymphatic Spread of Melanoma

Significant progress has been made developing the nanoliposomal formulations required to deliver siRNA. The initial formulations to be used for projects 2 and 4 failed. We had to redesign and test new liposomal formulations to be able to accomplish project 2 and project 4. With the new formulations in hand, projects 2 and 4 are now proceeding forward. Despite this obstacle, a screen of kinases has been undertaken identifying those to be targeted in combination with Akt3 leading to synergistic inhibition. Furthermore, Calcsyn software has been used to analyze synergy between kinases identified from the screen validating combinations to target in combination with Akt3.

With the development of the new nanoliposomal formulation project 2 is now proceeding rapidly.

PROJECT 3: Enhanced Delivery of Imaging and Therapeutic Nanoliposomal Agents Across the Blood Brain Barrier Following Ultrasound Treatment to Treat Glioblastoma or Melanoma Metastasized to the Brain.

This technically challenging but potentially high reward project has made significant progress and has also attracted commercial interest. An NIH grant has been submitted (June 5, 2011). A brief description of project's goals: To deliver the MRI contrast agent selectively to the high grade brain tumors (glioma) for imaging them more effectively. The selective nuclear accumulation will also improve the radiosensitivity of the tumors. Another goal is to deliver a multifunctional liposomes carrying both imaging and therapeutic agent concomitantly to the high grade brain tumors overcoming the blood-brain barrier.

*In addition, this project has captured the attention of an industry partner and we have submitted an SBIR application with Luna Innovations. The title of this application is "Efficacy testing of a new glioblastoma theranostics".* The major goal of this proposal is to test newly made glioblastoma-targeting theranostics (GTTN) in which the diagnostic TMS is enclosed within glioblastoma-targeting IL-13-liposomes which can deliver a therapeutic payload of doxorubicin (dox).

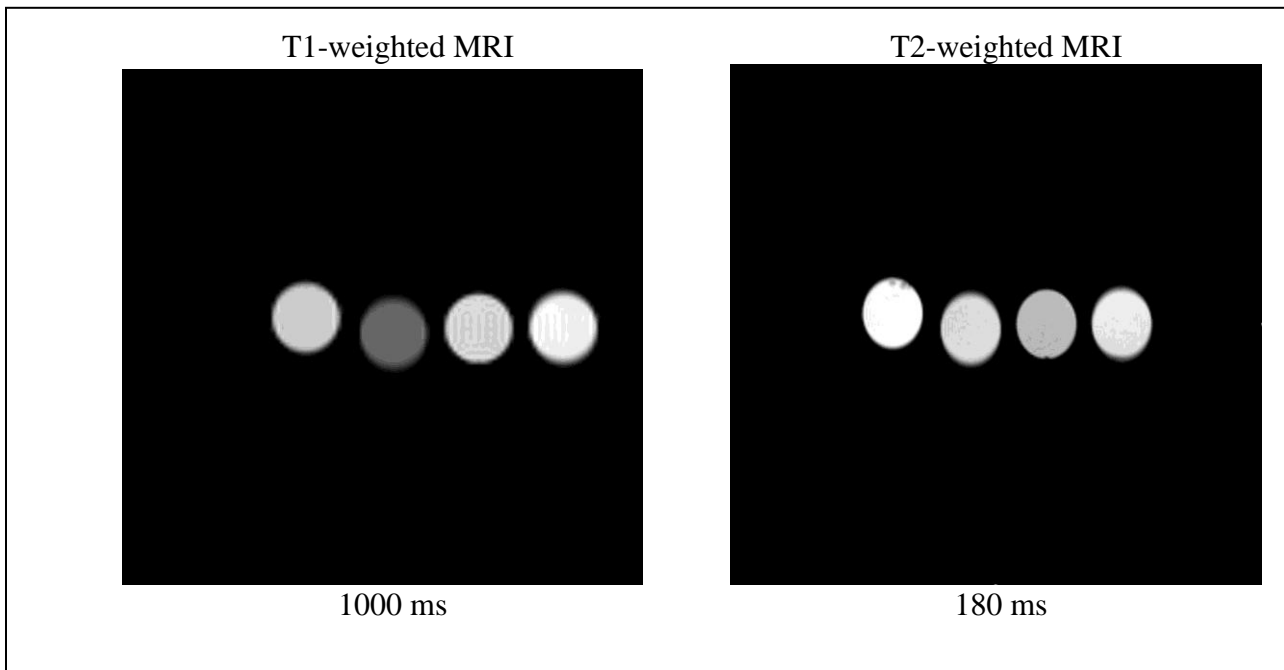
Figure 1 is an example that the formulation is working and Figure 2 is an *In vitro* analysis of relaxivity properties of gadofullerenes compared to the Magnevist control contrast agent and Magnevist-containing IL-13 liposomes

Gadofullerene sample was diluted in a 3:1 (v/v) chloroform and methanol solution. DPPC, Cholesterol, DSPE-PEG-2000, DSPE-PEG-Maleimide, and gadofullerene sample in the appropriate ratio were solubilized in methanol and t-butanol in 1: 1(v/v) ratio. The resulting solution was rotary evaporated at 40°C in a round-bottom flask to form a thin film, which was then dried under nitrogen for 30 minutes and in a desiccator for 30 minutes. The dried lipid was reconstituted in 4 mL of Tris buffer (20 mM, pH 7.4) and extruded through 200 nm and 100 nm membrane extruder for 5 times each. Human IL-13 protein was thiolated using imminothiolane HCL and then purified by Sephadex G-25M column. The thiolated protein, which will conjugate with maleimide moiety in the liposomes, was added to the liposome sample immediately, passed with nitrogen, and stirred overnight at 4°C. The liposomes were concentrated in a concentrator and passed through a Sepharose CL column to purify them of free, unconjugated protein. Then the conjugated liposomes were dialyzed for 24h against Tris with one buffer change to remove any free gadolinium in the liposome formulation. Finally they were again concentrated to a volume of 2 ml. The particle size of the resulting liposomes and the charge were measured using Malvern the Zetasizer

**Figure 1**



**Figure 2.** Representative T1 and T2 weighted MR images of the samples in the order of diluted magnevist in PBS, Tris buffer, gadofullerene in Tris buffer, and Magnevist liposome in PBS. These images were produced by diluting the samples to a 100 ug/ml concentration and imaging in NMR tubes.



## **Research Project 17: Project Title and Purpose**

*Parathyroid Hormone and Prostate Cancer Colonization of Bone* - There is a fundamental gap in understanding how osteosclerotic prostate cancer (PCa) metastases colonize bone, and the contribution of bone formation and parathyroid hormone (PTH) to this process. Our long term goal is to understand what regulates PCa colonization and establishment in bone, and to aid development of treatments that prevent bone metastases. The objective of this project is to identify the requirement(s) for PTH-enhanced bone formation in osteosclerotic PCa colonization and establishment in murine bone. Our central hypothesis is that osteosclerotic PCa colonization of bone, from the vasculature, requires enhanced bone formation. The rationale for this project is that once we know how enhanced bone formation facilitates the favorable interaction(s) between osteosclerotic PCa cells and bone, novel treatments can be developed to prevent such interactions.

### **Anticipated Duration of Project**

4/21/2010 - 12/31/2011

### **Project Overview**

The broad, long term objective of this project is to identify the requirement(s) for PTH-enhanced bone formation in osteosclerotic PCa colonization and establishment in murine bone. There are two specific aims of this project: 1) Identify the effect of intermittent parathyroid hormone (PTH)-zoledronic acid administration on SCID/Beige bone; 2) Isolate and characterize bone marrow endothelial cells from SCID/Beige bone.

Under aim I our working hypothesis is that PTH, zoledronic acid co-administration is anabolic to bone. To test this hypothesis we will employ the following approach. Twenty-four, 8-week old male SCID/Beige immune-compromised mice will be divided into four groups of six. Each group will be treated as follows: *Group one*, vehicle (control); *group two*, human PTH 1-34 (40 µg/kg per day); *group three*, zoledronic acid (ZA) (3 µg/day); *group four*, human PTH 1-34 combined with zoledronic acid (ZA). Mice in each group will be treated intermittently with 3 rounds. An intermittent treatment round is defined as: one subcutaneous injection each day for 5 days followed by two days of no injections. Thus, 3 treatment rounds span a total of 21 days.

Under aim II our working hypothesis is that human prostate cancer cell adhesion to murine bone marrow endothelial cells is enhanced following intermittent exposure to PTH, *in vitro*. To test this hypothesis we will employ the following approach. Six, 8-week old, male SCID/Beige immune-compromised mice will be used for the isolation and characterization of bone marrow vascular endothelial cells from the femur and lumbar spine. For endothelial cell isolation we propose to employ immunomagnetic selection using Dynabeads (Invitrogen) conjugated with mouse CD31, according to Fei et al., 1990, and Dong et al., 1997. Murine bone marrow endothelial cells (mBMECs) will be characterized: 1) morphologically; 2) by their ability to form tube-like structures when seeded on Matrigel; 3) by FACS analysis for their expression of von Willebrand factor, CD31, CD34, VCAM-1, and VE-cadherin, and PTH 1R. Cultures will be expanded for use in cell-cell adhesion assays.

The successful completion of these aims will establish the feasibility to conduct future experiments that seek to identify: 1) the requirement for enhanced bone formation in the colonization and establishment of human osteosclerotic PCa cells in murine bone; 2) the requirement for enhanced bone resorption in the colonization and establishment of human osteosclerotic PCa cells in murine bone; 3) mechanisms of osteosclerotic PCa cell colonization and establishment in murine bone.

### **Principal Investigator**

Ronald R. Gomes, Jr., PhD  
Pennsylvania State University, College of Medicine  
Orthopaedics and Rehabilitation, H089  
500 University Drive, PO Box 850  
Hershey, PA 17033

### **Other Participating Researchers**

Ari Muthusamy, PhD; Sarah Sheehan, BS - Pennsylvania State University

### **Expected Research Outcomes and Benefits**

*Expectations for aim I:* Our hypothesis predicts that bone formation parameters (osteocalcin, number of ALP positive osteoblast, bone mineral density, trabecular thickness, and separation) will be enhanced by co-administration of PTH with zoledronic acid relative to PTH alone. We predict ZA administration will reduce the number (TRAP staining) and activity (serum TRAcP 5b) of osteoclast in SCID/Beige bone and serum. Such outcomes will allow us to more directly test the role of osteoblast activity and bone formation, enhanced by PTH, in the colonization and establishment of osteosclerotic prostate cancer in bone.

*Expectations for aim II:* Our hypothesis predicts that the PTH 1R is expressed by mBMECs, and that incubation with PTH, intermittently, will enhance the ability of osteosclerotic prostate cancer cells to adhere, *in vitro*. In contrast, chronic PTH treatments will down regulate PTH 1R expression and correlate with attenuated prostate cancer cell adhesion *in vitro*. Besides direct in-growth into bone, it is well established that prostate cancer cells find their way to secondary targets of metastasis via the circulation. Bone marrow endothelial cells are thus a key cell type for prostate cancer cells to interact with prior to invading bone.

Prostate cancer metastasis to bone has been difficult to prevent or eradicate. What facilitates the favorable interaction between PCa cells and bone is unknown and is a critical barrier to solving the problem. Knowledge of how circulating osteosclerotic PCa cells metastasize to bone is critical for the development of therapeutics aimed at preventing their establishment in bone.

### **Summary of Research Completed**

Under aim II, our working hypothesis was that human prostate cancer cell adhesion to murine bone marrow endothelial cells will be enhanced following intermittent exposure to PTH, *in vitro*.

To test this hypothesis we first isolated and characterized bone marrow vascular endothelial cells from bones of male SCID/Beige immune-compromised mice, employing immunomagnetic selection using Dynabeads (Invitrogen) conjugated with mouse CD146. Next, we employed the bone marrow vascular endothelial cells in adhesion studies with prostate cancer cells, *in vitro*. Our hypothesis predicts that the PTH 1R is expressed by mBMECs, and that incubation with PTH will enhance the ability of osteosclerotic prostate cancer cells to adhere.

#### Methods:

Isolation of mBMECs: Reported in last year's Annual Report.

Capillary tube-like formation: Growth factor reduced (GFR) Matrigel was added to wells of ice-cold 96-well plates (70  $\mu$ l/well) for 6 seconds. Excess was removed, leaving a thin coating. Plates were incubated for 6 minutes on ice, 20 minutes at room temperature, and finally warmed for 20 minutes at 37°C. Bone marrow endothelial cells were seeded (6,500 cells/well) in serum free RPMI 1640 media containing 1% (w/v) penicillin/streptavidin, 2 mM glutamax without growth supplements. After 18 h, the cells were fixed (4% (v/v) paraformaldehyde), stained with SYTO13, or DAPI and tube-like formation was photographed with a SPOT CCD camera affixed to an inverted microscope equipped for epifluorescence.

Prostate cancer cell:mBMEC adhesion assays: For heterotypic cell adhesion assays, mBMECs are allowed to form confluent monolayers in 48 well plates. On the day of the adhesion assay, C4-2 cells, released from the culture surface (0.5 mM EDTA containing 1 mM glucose, and 12.5 mM HEAPS in PBS, pH = 7.0), are re-suspended in fresh serum free RPMI media containing 5 mM Calcein AM. After 15 minutes, labeled cells are washed twice in serum free RPMI and counted. For the adhesion assay, mBMECs are overlaid with 125,000 labeled C4-2 cells, under serum free conditions. After 3 hrs, the plates are washed twice, under gentle agitation, the adherent cells lysed and fluorescence quantified (485/515 excitation/emission).

Invasion assays: In this transwell invasion assay, confluent mBMECs seeded on an 8  $\mu$ m porous membrane, are overlaid with 60,000 Calcein AM or DiI labeled C4-2 prostate cancer cells. After 24 hrs, the C4-2 cells that migrated through mBMECs to the bottom of the membrane are collected, lysed, and fluorescence quantified. Note: the chemotaxic stimulus is serum containing media, initially present in the lower chamber.

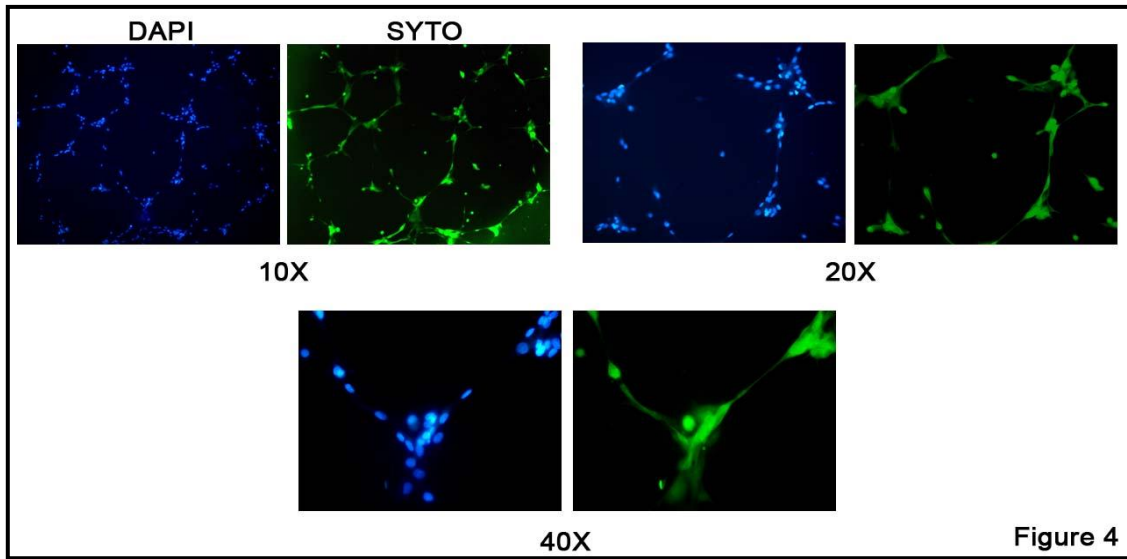


*Figure 1. Primary mBMECs form capillary tube-like structures, in vitro.* Capillary tube-like formation by mBMECs after 18 h culture on surfaces coated with growth factor reduced Matrigel. The cells were fixed, and then stained with DAPI (blue) or the green fluorescent nucleic acid stain SYTO 13 (green). The Tube-like formation was photographed with a SPOT CCD camera affixed to an inverted microscope equipped for epifluorescence.

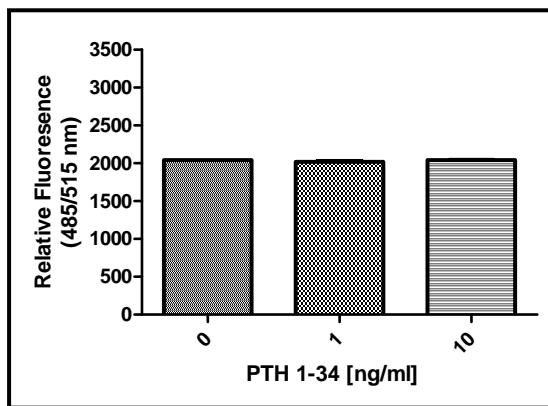


*Figure 2. PTH 1-34 exposure does not alter C4-2 cell adhesion to hBMECs.* Confluent mBMECs, pre-treated with 0, 1, or 10 ng/ml PTH 1-34 were overlaid with Calcein AM labeled C4-2 cells. After 3 hrs, the plates are washed twice with gentle agitation, the adhered cells lysed, and fluorescence read under 485/515 excitation/emission. Data are shown as the mean fluorescence units  $\pm$  SD for triplicate observations.

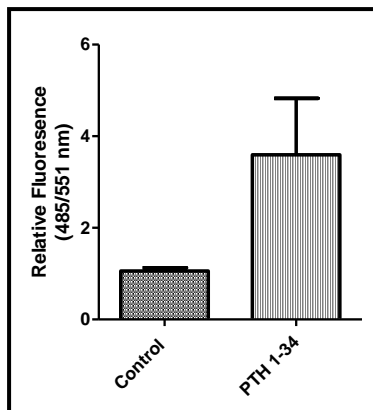


*Figure 3. PTH 1-34 pre-treatment of hBMECs enhances C4-2 cell invasion, in vitro.* In this trans-well invasion assay, monolayers of mBMECs, seeded on a 8  $\mu\text{m}$  porous membrane were untreated or pre-treated with PTH 1-34 [10 ng/ml], then overlaid with Calcein AM labeled C4-2 cells. After 24 hrs, the C4-2 cells that migrate through mBMECs to the bottom of the membrane are collected, lysed, and fluorescence quantified. Data are shown as the mean fluorescence units  $\pm$  SD for triplicate observations. Control = untreated mBMECs; PTH 1-34 = mBMEC pre-treatment with hPTH 1-34. These data suggest that hPTH 1-34 interactions with mBMECs facilitate C4-2 invasion, *in vitro*.

### **Research Project 18: Project Title and Purpose**

*Perlecan Regulation of Synovial Hyperplasia* - In patients with arthritis, synovial hyperplasia (SH) gives rise to pannus formation, invasion and erosion of articular cartilage, leading to joint destruction and chronic pain. There is a fundamental gap in understanding what regulates SH. The objective of this proposal is to identify a role for the HSPG, perlecan, in modulating SH.

### **Duration of Project**

4/21/2010 – 2/28/2011

### **Project Overview**

The long term goal of our laboratory is to understand the role of basement membrane and extracellular matrix molecules in regulating articular cartilage health, and use this knowledge in the treatment and prevention of joint disorders. The objective of this project is to identify a role for the heparan sulfate proteoglycans (HSPG), perlecan (Pln), in modulating SH. Our central hypothesis is that Pln regulates the bio-availability and activity of heparin-binding growth factors important for initiation and development of SH. This hypothesis is predicated upon our strong preliminary data and a published report demonstrating: 1) Pln expression is enhanced in diseased synovial tissues; 2) Fibroblast growth factor binds to purified forms of full length and recombinant domain I of Pln; 3) binding interactions are heparan sulfate dependent. Our rationale for this project is that Pln, a regulator of heparin-binding growth factor bio-availability, is a likely candidate involved in pathomechanism(s) of SH. Yet, a role for Pln in regulating SH has not been examined. Guided by a dedicated team, and strong preliminary data, our central

hypothesis will be tested pursuing the following specific aim: Determine if perlecan regulates synovial hyperplasia by modulating fibroblast growth factor bio-availability and activity. Under this aim: 1) human Pln isolated from synovial tissues will be employed in binding studies with exogenous fibroblast growth factors to identify how binding differs in diseased tissues; 2) primary synoviocytes, isolated from patients, will be employed to identify the effect of exogenous Pln +/- FGFs on synoviocyte survival, proliferation and migration; and 3) primary synoviocytes cultured in the presence of exogenous Pln +/- FGFs will be employed to identify requirement(s) for Pln's modulation of FGF-induced signaling. The planned project is innovative in its approach as no published studies have demonstrated interactions between human synovial tissue derived Pln and FGFs and/or their receptors. This research is significant, because it is expected to advance our understanding of how HSPGs bind to and modulate the activity of heparin-binding growth factors in synovial tissues, knowledge needed to develop novel pharmacologic strategies that aim to regulate such factors in slowing or preventing cartilage degradation.

### **Principal Investigator**

Ronald R. Gomes, Jr., PhD  
Pennsylvania State University, College of Medicine  
500 University Drive, PO Box 850  
Hershey, PA 17033

### **Other Participating Researchers**

Charles M. Davis, III, MD, PhD; Arivalagan Muthusamy, PhD; Cara L. Schengrund, PhD;  
Christopher Niyibizi, PhD - Pennsylvania State University

### **Expected Research Outcomes and Benefits**

Upon completion of the planned studies, we expect to know if Pln isolated from RA synovial tissues has the capacity to bind and modulate FGF activity, *in vitro*. From the studies planned in *sub-hypothesis I*, we expect that Pln isolated from all tissues will bind heparin-binding FGFs in a heparan-sulfate dependent manner; however, Pln isolated from RA synovium will be poorly sulfated and demonstrate weak binding of FGFs relative to Pln from non-diseased and OA synovial tissues.

From the studies proposed in *sub-hypothesis II*, we expect the exogenous addition of Pln/FGF mixtures to synoviocytes in culture will enhance cell survival, proliferation, and migration. However, enhanced cell survival, proliferation, and migration are expected to be greater for Pln isolated from RA tissues (RA>>OA> non-diseased). FGF sequestration will be greatest for Pln isolated from non-diseased tissues.

From the studies proposed in *sub-hypothesis III*, we expect exogenous Pln, isolated from RA tissues, will poorly modulate FGF induced phosphorylation of FGFRs relative to Pln from OA and non-diseased tissues. We also anticipate that RA tissue derived Pln/FGF mixtures will enhance synoviocyte survival by activating the AKT pathway.

Together, our expected observations would suggest that Pln isolated from RA tissues has lost much of its ability to bind and sequester FGFs, and thus regulate activity. If supported, our hypothesis would suggest that approaches seeking to restore and/or mimic Pln's ability to bind and sequester FGF activity could slow or attenuate the development of SH.

### **Summary of Research Completed**

Our central hypothesis is that Pln regulates the bio-availability and activity of heparin-binding growth factors important for initiation and development of SH. We propose to test this hypothesis by addressing the following specific aim: Determine if perlecan regulates synovial hyperplasia by modulating fibroblast growth factor bio-availability and activity. Under this aim: 1) human Pln isolated from synovial tissues will be employed in binding studies with exogenous fibroblast growth factors to identify how binding differs in diseased tissues; 2) primary synoviocytes, isolated from patients, will be employed to identify the effect of exogenous Pln +/- FGFs on synoviocyte survival, proliferation and migration; and 3) primary synoviocytes cultured in the presence of exogenous Pln +/- FGFs will be employed to identify requirement(s) for Pln's modulation of FGF-induced signaling.

#### **Methods:**

*Perlecan Extraction from Synovial Tissues.* Mince synovial tissue to ~1 mm size pieces, and add to lysis buffer (20 ml, containing 1M Sodium acetate [pH 6.0], 2% CHAPS, 2M Amino hexanoic acid, 0.5M EDTA [pH 8.0], and protease inhibitors [i.e., 100 mM each NEM, PMSF, and Benzamidine. HCl]). After stirring 15 min (4°C) an equal volume (25 ml) of 8M guanidine HCl is added to the suspension and left to stir overnight. Following the addition of fresh protease inhibitors the suspension is centrifuged at 19,000 rpm for 30 min at 12° C. The supernatant is then collected and the density of the solution is adjusted to 1.22 g/ml with CsCl, and then centrifuged at 46,000 rpm for 29 hrs at 14°C. After fractionation, the density, uronic acid, protein and nucleic acid of the each fraction was determined. The first six fractions were pooled and density adjusted to 1.3341 g/ml with CsCl and spun again. Samples were again fractionated (1 ml each) and the uronic acid, protein and HSPG2 (using anti-HSPG2 specific antibodies) identified. Fractions containing HSPG2 were pooled and dialyzed (72 hrs) against cold double distilled water (4°C) with frequent changes. The final product was lyophilized for later used.

*Enzyme Linked Immunosorbent Assay (ELISA).* To determine the ability of synovial tissue derived perlecan (SnPln) to bind heparan binding growth factors, wells of microtiter plates were coated with SnPln (200 ng/well) in 50 µl coating buffer (0.05 mM sodium carbonate and bicarbonate buffer, pH 9.3), and incubated overnight (4°C). After washing (PBS) to remove unbound material, a blocking solution (3% BSA in PBST [PBS containing 0.05% Tween-20]) was added for 60 min at room temperature. In the meantime heparin binding growth factors were pre-incubated with/without different concentrations of heparin [1000- 0.01 ug/ml] in 50 µl sterile PBS for 30 min at room temperature. After the blocking buffer is removed, growth factor with/without heparin is added to each well and incubated for 3 h at room temperature. After washing 50 µl of anti-growth factor antibodies is added to each well and incubated for 1 hr at RT on a shaker. After extensive washing, 50 µl of anti-mouse IgG-HRP antibodies is added to each well and incubated for 40 min at RT on a shaker. To visualize secondary ab binding 50 µl of TMB substrate is added to each well and incubated for 15-20 min at RT. To stop the reaction 50

$\mu$ l of 1N HCl is added to each well. To quantify binding, the absorbance of each well is read (450 nm).

*Primary Synoviocyte Isolation and Culture.* Human synovium procured immediately after surgery will be minced into small pieces. Tissue pieces will be suspended in balanced salt solution containing Hepes buffer, 0.5 mg/ml collagenase, and 0.15 mg/ml deoxyribonuclease then stirred for 1 h at 37°C. The suspension will be filtered through a sterile sieve (80 mesh) to remove undigested debris. The filtrate will be spun down through a cushion containing 22% Percoll and 0.15 mg/ml DNase I in a balanced salt solution. After washing with RPMI 1640 medium containing 10% FCS and 50 IU/ml penicillin/streptomycin (pen/strep), cells will be seeded in tissue culture flasks ( $5 \times 10^5$  cells/ml), and incubated at 37°C for 6-16 h (5% CO<sub>2</sub>). Non-adherent cells will be removed by gentle washing with media. Adherent cells will be trypsinized, washed and frozen down. Cell Passages between 3-5 will be used for the studies proposed.

*Proliferation Assays.* Human synoviocytes seeded at  $10^5$  cells/well in 96 well culture dishes were cultured overnight in RPMI1640 media containing 1% FCS and 1% pen/strep. Cells will be carried in fresh, serum free, media containing BrdU +/- Pln (5  $\mu$ g) and/or FGF(s) (40 ng/ml) then incubated for 0-144 h. Cells will be fixed and denatured, then incubated with anti-BrdU antibodies. After 1 h, the wells will be washed, and then incubated with goat anti-mouse IgG HRP conjugated secondary antibodies. Bound anti-bodies will be visualized after incubation with a fluorogenic substrate (325 nm/420 nm, excitation/emission). Wells without cells, media only, will be used as controls.

## Results:

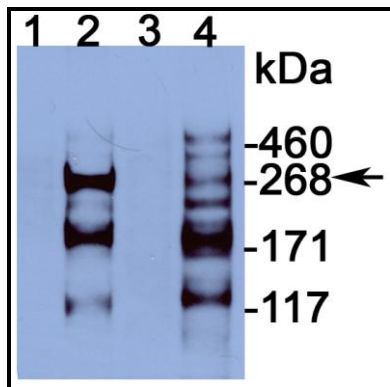


**Figure 1.** *Western blot of perlecan isolated from synovial tissues.* Lanes 1-2, perlecan isolated from normal synovial tissue. Lanes 3-4, perlecan isolated from synovial tissue of osteoarthritic patient. Lanes 1 and 3, undigested; lanes 2 and 4 heparinase cocktail and chondroitinase ABC pre-treated perlecan. Heparinase cocktail is a mixture of heparinases I, II, and III. Arrow denotes protein core of perlecan released after heparinase cocktail and chondroitinase ABC digestion.

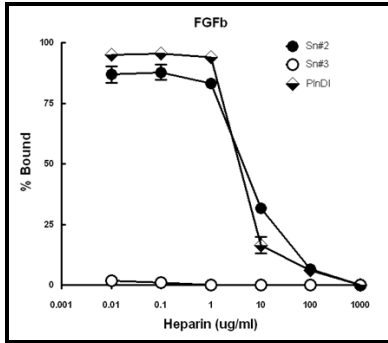


**Figure 2. *Perlecan from synovial tissues of osteoarthritic patients does not bind FGFb.*** Perlecan, isolated from synovial tissues of normal (Sn#2, ●) and osteoarthritic (Sn#3, ○) patients was immobilized on a microtiter plate and overlaid with FGFb [10 ng/ml] in the presence of increasing concentrations of heparin [0.01-1000 ug/ml]. FGFb bound to perlecan was detected and quantified using an ELISA based approach employing FGFb specific monoclonal antibodies. Data are presented as a percentage of total bound. Specific binding was determined by subtracting the background binding of FGFb to the microtiter plate from total bound. FGFb binding to recombinant domain I of perlecan (PInDI) was employed as a positive control.

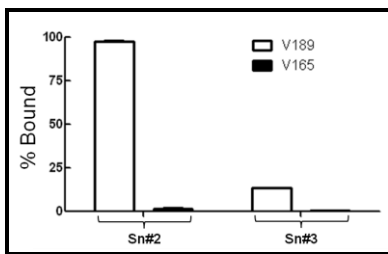


**Figure 3. *Perlecan from synovial tissues of osteoarthritic patients poorly binds VEGFs.*** Perlecan, isolated from synovial tissues of normal (Sn#2) and osteoarthritic (Sn#3) patients were immobilized on a microtiter plate and overlaid with either VEGF<sub>165</sub> or VEGF<sub>189</sub> [20 ng/ml]. VEGFs bound to perlecan were detected and quantified using an ELISA based approach employing VEGF<sub>165</sub> and VEGF<sub>189</sub> specific monoclonal antibodies. Data are presented as a percentage of total bound. Specific binding was determined by subtracting the background binding of VEGF to the microtiter plate from total bound.

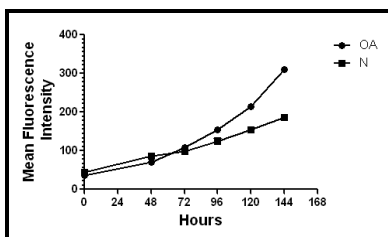


**Figure 4. *Primary synoviocytes, from osteoarthritic patients have a higher rate of proliferation, in vitro.*** Growth curves for human synoviocytes isolated from patients with normal and osteoarthritic joints. The data represent the mean fluorescence intensity (MFI) of triplicate cultures at each time point.

## **Research Project 19: Project Title and Purpose**

*A Multi-Center Randomized Single Blind Trial of Intravenous Fluids during Labor* - To determine if intrapartum use of a glucose-containing solution will improve the outcome of labor and reduce operative deliveries.

### **Anticipated Duration of Project**

4/21/2010 - 6/30/2013

### **Project Overview**

This will be a multi-center, prospective, single-blind randomized trial of two types of IV fluids for maintenance hydration during labor to determine if intrapartum use of a glucose-containing solution will improve the outcome of labor. This study will randomize 1524 women at greater than or equal to 36 weeks in spontaneous labor attempting vaginal delivery and will be conducted at 4 sites: Reading (Reading Hospital), Allentown (Lehigh Valley), Hershey (Penn State College of Medicine), and York (York Hospital). The primary analysis will use an intent-to-treat approach to examine differences between the two IV fluid treatments in the proportion of deliveries requiring cesarean section. We assume the proportion of deliveries requiring cesarean section will be 0.24 in the arm receiving the non-glucose-containing (i.e., lactated Ringer's) solution and 0.18 in the arm receiving the glucose-containing (i.e., D<sub>5</sub> lactated Ringer's) solution (i.e., a 25% relative reduction in the proportion of cesarean deliveries). We anticipate a 5% dropout rate for this study. Secondary efficacy parameters will include incidence of ketosis and influence of ketonuria on the primary outcome, incidence of prolonged labor, need for oxytocin augmentation, incidence of operative vaginal delivery, incidence of chorioamnionitis, indications for cesarean birth, maternal nausea/vomiting in labor, reduced umbilical artery pH/fetal acidemia, increased umbilical artery CO<sub>2</sub>/fetal hypercarbia, neonatal hypoglycemia, neonatal intensive care unit admission, and difficulties with initiating breast feeding. A total of 28 months will be required to complete the study. This will be accomplished by enrolling 15 women per center per month over the two-year enrollment period, and for 3 months to clean and analyze the final data.

### **Principal Investigator**

Richard S. Legro, MD  
Pennsylvania State University  
500 University Drive, H103  
Hershey, PA 17033

### **Other Participating Researchers**

John Smulian, MD; Meredith Rochon, MD - Lehigh Valley Hospital  
James Hole, MD - York Hospital  
George Neubert, MD - Reading Hospital  
Allen Kunselman, MA; John Repke, MD - Penn State University

## **Expected Research Outcomes and Benefits**

We propose that even in the presence of adequate hydration, inadequate carbohydrate replacement in labor may contribute to prolongation of labor and increased need for operative delivery. Glucose is the main energy substrate for the pregnant uterus. Physiological requirements for glucose during labor are estimated to be around 10 grams per hour. Adequate supplies of glucose are needed to maintain exercise tolerance and muscle efficiency, which are important factors in the progress of labor. However, there are no data to precisely quantify the glucose needs of the human uterus during labor.

Dysfunctional labor or dystocia, which is the leading indication for primary cesarean delivery, is primarily caused by uterine forces insufficiently strong or inappropriately coordinated to efface and dilate the cervix. Dystocia can be a result of inadequate voluntary muscle effort in the second stage of labor. Supplying carbohydrate fuel for working uterine and skeletal muscle may improve progress in labor and, therefore, diminish the need for cesarean delivery. Importantly, with dysfunctional labor, there are increased risks for other intrapartum interventions and complications such as high doses of Pitocin, chorioamnionitis, postpartum hemorrhage and fetal compromise.

Our expected outcomes are that - Hydrating patients with an intravenous fluid during labor containing glucose will :1) Lower operative deliveries, i.e. cesarean section; 2) Reduce the incidence of dysfunctional labor; and 3) Reduce the incidence of fetal and maternal morbidity related to dysfunctional labor or operative delivery.

## **Summary of Research Completed**

The protocol is now up and running at all three sites and we are actively recruiting. Our site had recruited our first subject in May 2010, Reading's first subject was not recruited until July 2010 and Lehigh Valley went through such an extended IRB review process that they did not receive IRB approval until February 2011 and recruited their first subject in March 2011. To date we have randomized 107 subjects: PSU currently has 83 participants, Reading Hospital has recruited 13 subjects and Lehigh has recruited 11 subjects.

At Penn State Hershey Medical Center we have initiated some innovative ways for recruitment to reach our recruitment goals. We have picked up momentum and recruitment has increased as of March 2011 and we feel will continue to increase until our projected completion date. PSU is involving the Obstetrics and Gynecology (ObGyn) faculty and Residents in the Residency Training Program in this project. For example, ensuring that all Residents and Faculty complete IRB training and receive approval to participate in this study was a substantial hurdle in this trial. We have met with the Residents to review with them the trial and its inclusion/exclusion criteria. Further, we will be reviewing with them on a monthly basis their ongoing recruitment reports in our Clinical Trials Monthly Journal Clubs. We have had meetings with the Labor and Delivery nurses in March in the daytime and evening hours and weekend shifts to discuss with them the trial and have them also help identify those subjects who may be eligible. We have begun reviewing this with faculty members on a regular basis at our monthly staff meetings and on a face to face basis. Additionally, we are trying to leverage the resources we have available from

this grant and our own funds to provide some study coordinator assistance to this trial. We have achieved success in increasing enrollment at Hershey as noted in Figure 1.

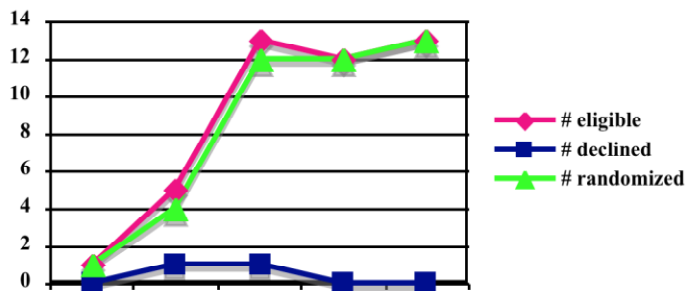
Our impression is that part of the reason for the slow recruitment, is that there are few eligible patients who meet our criteria for presenting in early uncomplicated labor who are candidates for vaginal delivery. Most patients who are screened are eligible and also consent to the study (Figure 1). To explore this possibility of fewer eligible patients than projected, we developed an expedited protocol in which to examine the prevalence of subjects who are eligible for the study. We have received IRB approval here at PSU and Reading is still waiting for IRB approval for this expedited protocol. We will start the data collection shortly on the approved number of subjects at PSU over our recruitment time period to further adjust our expectations for completion of this trial.

We continue to have monthly phone conferences with all three sites to discuss and resolve any issues that any of us may be experiencing and are sharing plans and suggestions with each other and we are in the process of scheduling another Face to Face meeting by August 2011. We are sharing plans and suggestions with our other sites, Lehigh Valley and Reading Hospital and we are optimistic that once all three sites initiate and put some of these actions into place, enrollment will pick up as we have seen here at PSU over the past few months. We note that the author of the protocol, Dr. John Smullian, is located at Lehigh Valley Hospital and is fully dedicated to increasing enrollment in the protocol. He is currently acting Chair and in our monthly phone conferences has expressed the commitment to devote the resources and personnel to complete recruitment at Lehigh Valley Hospital, which is the largest obstetrical hospital in our network.

We have established a web based data entry system through WebUQ as developed and maintained by our biostatisticians, Allen Kunselman and Christy Stetter, and have been entering the data on consented subjects in a timely fashion. We review the progress of this during our monthly phone conferences. We have formed a DSMC consisting of representatives of each medical center for a total of 3 members who will review enrollment, outcomes and safety data by treatment arm. Adverse Events (AE's) will be categorized and percentage of patients experiencing these AE's and Serious Adverse Events (SAE's) during the treatment period will be detailed in addition to the primary outcome. To date, we have had no AE's to report, however we have had 1 SAE. This was a subject who was randomized into the D<sub>5</sub>Lactated Ringer's solution and delivered a newborn with a congenital malformation; extra digit on right foot. This event is not related to the study; however we must report every congenital malformation as a Serious Adverse Event to our IRB.

Thus we have made significant progress over the last year and remain committed to completing this project, though clearly it will take longer than projected.

**Figure 1: Monthly Recruitment at Hershey Medical Center for RARHY study thru May 2011**



### **Research Project 20: Project Title and Purpose**

#### *Identification and Characterization of Regulatory Factors of the Human Telomerase Gene -*

Normal human somatic cells age due to the fact that telomere is limiting, and telomerase is stringently repressed in these cells. The human telomerase reverse transcriptase (*hTERT*) gene, which encodes the limiting catalytic subunit of telomerase, is primarily regulated at the level of transcription. It is highly expressed in pluripotent stem cells but silenced in most somatic cells. Hypomorphic alleles of the telomerase gene, found in patients of dyskeratosis congenita, cause severe abnormalities in multiple organs and tissues. On the other hand, telomerase activation in tumor cells leads to limitless proliferation, a hallmark of all cancers. Our research is to reveal how telomerase is repressed during development and activated in cancer cells. Specifically, we have identified several candidate genes involved in telomerase regulation and plan to understand how telomerase is regulated by these genes. This study will lead to a better understanding of cancer and age-related diseases, and ultimately better therapeutic strategies for these diseases.

### **Anticipated Duration of Project**

4/21/2010 - 9/30/2011

### **Project Overview**

Our long-term objective is to determine the mechanisms of hTERT gene repression during development and differentiation. The hTERT gene is highly expressed in pluripotent stem cells, but stringently repressed in most adult somatic cells. Despite intensive investigation in the past decade, the mechanism of its repression in somatic cells, including cis-regulatory elements and trans-acting factors involved in hTERT repression remain to be elucidated. Our data indicated that the hTERT locus was embedded in a condensed chromatin domain in many somatic cells, including both telomerase-positive and -negative cells. Such a compacted domain was not detected in the mouse TERT locus, which is more loosely regulated than the hTERT gene. We hypothesize that (1) establishment of an appropriate chromatin environment and local nucleosomal architecture is essential for hTERT repression in somatic cells and (2) de-repression or partial de-repression of the hTERT promoter leads to telomerase activation during cellular

immortalization. To study the mechanisms of hTERT repression, we developed a novel technical platform, the recombinase-mediated BAC targeting or RMBT, for targeted integration of a single-copy bacterial artificial chromosome (BAC) reporter into specified chromosomal sites. Using this technique, we demonstrated that chromosomal integration of a BAC construct containing the hTERT locus resulted in the establishment of a surrogate chromatin setting in which the hTERT promoter was tightly repressed and recapitulated its endogenous counterpart in human fibroblasts. In this project, we plan to accomplish the following three specific aims.

*Aim 1. Validation and characterization of novel repressors of the hTERT gene.* In a recent screen for regulatory factors of the *hTERT* gene, we identified several candidates that are likely involved in the repression of the hTERT promoter. We plan to validate their regulation of the endogenous *hTERT* gene and determine their roles in telomerase regulation during cell differentiation.

*Aim 2. Characterization of the hTERT BAC reporter in transgenic mice to demonstrate that the BAC clone contains sufficient regulatory elements.* In this aim, we propose to determine the expression profile of the transgenic hTERT promoter during embryonic development.

*Aim 3. Development of a genetically amendable system for studying the epigenetic regulation of the hTERT gene in mouse embryonic stem cells.* Because lentiviral viruses are not silenced in pluripotent stem cells, we proposed to generate a lentiviral vector and establish mESC acceptor lines for RMBT.

### **Principal Investigator**

Jiye Zhu, PhD  
Pennsylvania State University, College of Medicine  
500 University Drive, C4605  
Hershey, PA 17033

### **Other Participating Researchers**

Yaunjun Zhao, PhD, Longgui Chen - Pennsylvania State University

### **Expected Research Outcomes and Benefits**

Telomeres - the ends of linear chromosomes- are important determinants of human aging. Telomerase, the enzyme that elongates telomeres, is expressed in about 95% of cancer cells but is rarely found in normal human cells. In fact, ectopic expression of hTERT, the catalytic subunit of telomerase, is able to stabilize the telomere, immortalize human cells, and convert pre-neoplastic cells into tumorigenic cells. Therefore, understanding the mechanisms on how telomerase is suppressed in normal cells and activated in immortal and cancer cells will elucidate one of the key steps during the multi-step tumorigenesis. The knowledge will also help us to understand how we age and benefit the treatment of many age-related diseases.

## Summary of Research Completed

### Aim 1. Determine the roles of the Polycomb group (PcG) pathway in the repression of hTERT gene.

Progress on Aim 1 was described in last year's Annual report.

### Aim 2. Characterization of the hTERT BAC reporter in transgenic mice to demonstrate that the BAC clone contains sufficient regulatory elements.

Telomerase is tightly regulated in humans relative to mice, owing to the differential regulation of *TERT* genes. To explore hTERT regulation *in vivo*, we engineered mice with a 160-kb transgenic BAC spanning the *hTERT* locus with a *Renilla* luciferase (*Rluc*) cassette downstream of its promoter. Analysis of multiple founder lines revealed that the *Rluc* expression profile from the transgenic hTERT reporter locus reproduced that of the native *hTERT* gene in all tissues and organs examined, demonstrating that genetic sequence determined the species-specific developmental regulation of the *hTERT* gene and that mouse epigenetic and transcription machineries faithfully regulated hTERT transcription. Thus, these mice allowed detailed analyses of developmental hTERT regulation. Both the transgenic hTERT reporter and the endogenous *mTERT* locus were expressed in early embryonic stages and their mRNA levels progressively decreased throughout embryonic and postnatal development. Whereas hTERT transcription was much lower than mTERT expression in most organs, it increased significantly during postnatal development of thymus, testis, and ovary. In testis, the *Rluc* mRNA was enriched in elongating spermatids of seminiferous tubules. Additionally, the transcription of transgenic hTERT reporter, but surprisingly not the endogenous *mTERT* gene, was activated during Wnt1-induced mammary tumorigenesis, allowing the monitoring of tumor development via non-invasive bioluminescent imaging. Collectively, our results demonstrate that the hTERT transgenic reporter system recapitulates the developmental regulation of the *hTERT* gene in a chromosomal position-independent manner and serves as legitimate model to explore telomerase regulation in the development of normal and neoplastic tissues *in vivo*. This work has been published in

Jia, W., et al. A BAC transgenic reporter recapitulates *in vivo* regulation of human telomerase reverse transcriptase in development and tumorigenesis (2011) *FASEB Journal* 25(3):979-89.

### Aim 3. Development of a genetically amendable system for studying the epigenetic regulation of the hTERT gene in mouse embryonic stem cells.

Acceptor vector. Our published RMBT technique was a two-step procedure: generation of acceptor loci by retroviral transduction and Cre-mediated BAC integration (Figure 1) (Wang et al. *Nucleic Acids Res* 37(17):e111). Though successful in fibroblasts, the strategy was inefficient in ESCs due to retroviral silencing. Thus, we constructed a lentiviral acceptor vector, as lentiviruses are not silenced in ESCs. Briefly, a floxed CMV promoter/tkNeo cassette was used to replace eGFP in the lentiviral vector pLL3.7 and a 1.2-kb chicken  $\beta$ -globin insulator cHS4 inserted into the enhancerless 3' LTR. The resulting lentiviral vector is similar to the original retroviral vector pML-2 except for the lack of CreER. Upon transduction, the 3' LTR is copied

to the 5' end, surrounding the acceptor locus with insulators and thus shielding it from potential chromosomal position effects (CPE).

Acceptor lines. One strain of HM1 mESCs, adapted to grow on gelatin-coated plates under feeder-free conditions for easier selection and clonal expansion, was transduced with the acceptor lentivirus at a low MOI (multiplicity of infection) to minimize multiple infections in a single cell. Neomycin-resistant colonies were isolated and genomic DNAs subjected to Southern analysis (Figure 2 A&B). Clones with single-copy proviral insertions (labeled by stars in Figure 2B) and normal karyotypes were chosen as acceptor lines.

BAC integration. Reporters 117B23-cFtR and 183M22-cFtR will be transfected into HM1 ESC acceptor lines, with a Cre-expressing plasmid pCAGGS (Figures 1), followed by a 3-day selection by puromycin (Puro) and a 2-day selection by ganciclovir (GCV). Drug-resistant colonies with both *Fluc* and *Rluc* activities will be expanded and their genomic DNAs examined by Southern analysis to identify correctly targeted clones. In the past six months, we have worked out the RMBT conditions in mESCs using a 14-kb BAC backbone vector (pBACpuroF). PCR analysis of junction sequences in Puro/GCV-resistant clones showed that at least two acceptor loci (HM1A1&A2) recombined with the vector readily (Figure 2 C&D).

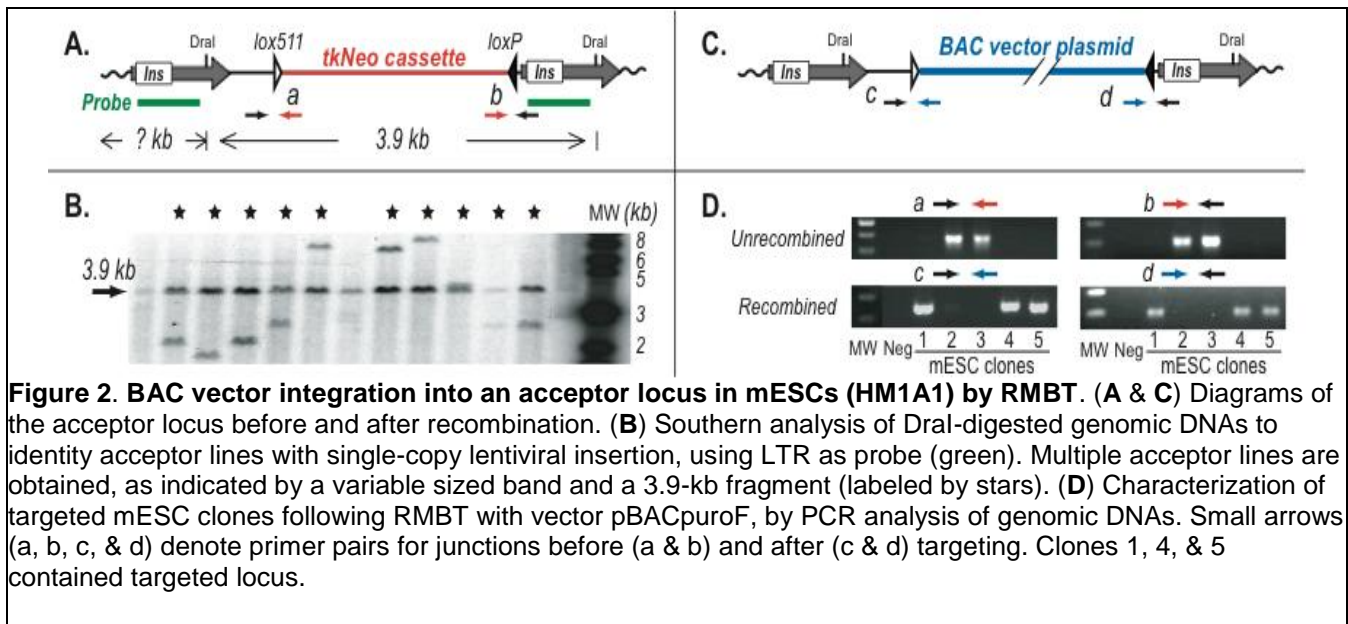
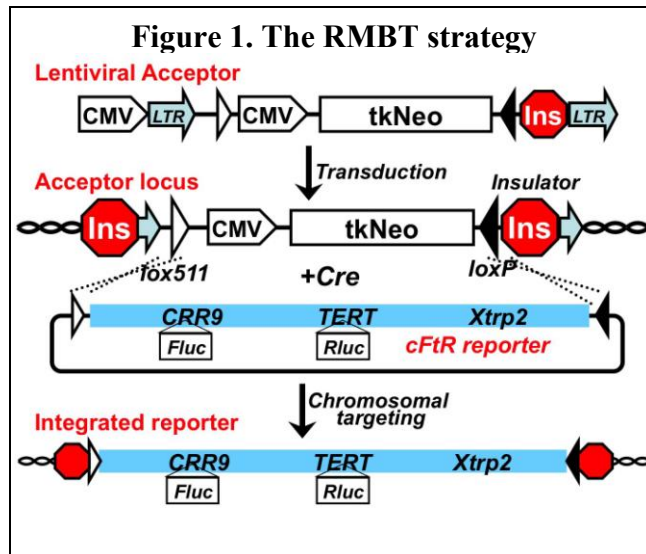


**Figure 2. BAC vector integration into an acceptor locus in mESCs (HM1A1) by RMBT. (A & C)** Diagrams of the acceptor locus before and after recombination. **(B)** Southern analysis of Dral-digested genomic DNAs to identify acceptor lines with single-copy lentiviral insertion, using LTR as probe (green). Multiple acceptor lines are obtained, as indicated by a variable sized band and a 3.9-kb fragment (labeled by stars). **(D)** Characterization of targeted mESC clones following RMBT with vector pBACpuroF, by PCR analysis of genomic DNAs. Small arrows (a, b, c, & d) denote primer pairs for junctions before (a & b) and after (c & d) targeting. Clones 1, 4, & 5 contained targeted locus.

## **Research Project 21: Project Title and Purpose**

*Biomechanical Failure and Loosening Characteristics of a Novel Posteriorly Augmented Glenoid Component* – The objective of this study is to characterize the mechanics of novel and standard cemented Total Shoulder Arthroplasty glenoid implants subject to cyclic mechanical loading. We have developed a novel glenoid implant that includes a posterior augmentation to compensate for posterior bone loss often found in shoulder osteoarthritis. We seek to understand the loosening resistance and micro-mechanics of the bone-cement-implant interface in both this implant and standard glenoid implants. Micro-computed tomography will be used to image the implant fixation after various stages of controlled cyclic loading applied to simulate physiologic shoulder activity.

### **Anticipated Duration of Project**

9/1/2010 - 9/30/2011

### **Project Overview**

Loosening of the artificial glenoid implant is the most common complication following total shoulder arthroplasty. Glenoid component implantation is often difficult due to posterior glenoid bone loss associated with osteoarthritis. A novel posteriorly augmented step glenoid implant which compensates for bone loss has been developed in our laboratory. The objective of this study is to biomechanically characterize the loosening performance of this novel implant subject to cyclic loading, as compared to a standard glenoid implant. In addition we expect to advance the general understanding of the loosening mechanics of the glenoid, and potentially other cemented orthopaedic implants, through novel analysis of high resolution X-ray microcomputed tomography (micro-CT) scans obtained at various stages of the fatigue process.

Specific Aim 1: Quantify number of cycles until initiation of fixation fracture for a novel posterior step glenoid implant and a standard three-pegged glenoid implant. An ASTM standard method for cyclically loading glenoid implants implanted in bone substitute will be modified to include an anterior-posterior directed mechanical load. We will perform novel micro-CT analysis of the bone-cement-interface at every 10,000 loading cycles until fracture initiation, and then at 70,000 cycles. Our hypothesis predicts an equivalent or greater number of cycles before initiation of a 5 mm fixation fracture crack for the posterior step glenoid compared to the standard implant.

Specific Aim 2: Quantify toggle displacement of the anterior and posterior glenoid articular rims for the posterior step glenoid implant and the standard implant. Using the cyclic loading protocol described above, implant toggle displacement will be measured before cycling, at fracture initiation, and after 70,000 loading cycles. Our hypothesis predicts equivalent or less toggle displacement for the posterior step glenoid compared to the standard implant.

Specific Aim 3: Repeat testing with the same loading protocol but with implanting the glenoid prostheses in a small number of cadaveric scapular bone specimens instead of the bone substitutes. We expect that the findings obtained in Specific Aims 1 and 2 will be supported.

## **Principal Investigator**

April D. Armstrong, MD, MSc  
Associate Professor  
Penn State University College of Medicine/Hershey Medical Center  
30 Hope Drive, Building A, EC089  
Hershey, PA 17033

## **Other Participating Researchers**

Gregory S. Lewis, PhD, Vikram M. Sathyendra, MD – employed by Penn State College of Medicine

## **Expected Research Outcomes and Benefits**

We expect this project to result in the furthering of understanding of the mechanics of glenoid implant loosening in total shoulder arthroplasty, and whether a novel posteriorly augmented glenoid implant can provide equivalent or improved loosening resistance. Glenoid loosening is the most frequent complication in total shoulder arthroplasty. Improving the lifespan of glenoid implants would greatly improve patient satisfaction and reduce health care costs associated with revision surgeries.

This project should also result in directing the focus of further studies. For example, if fatigue cracking is found to initiate at the implant-cement interface, we may focus future projects on altering glenoid implant material, or designing to minimize stress-risers. If loosening is instead initiated at the bone-cement interface we may focus on improving the interface strength by study of the cement-bone interlock mechanics.

## **Summary of Research Completed**

We have finalized the experimental loading apparatus and most of the data analysis procedures. We have loaded and imaged a series of specimens implanted in both synthetic bone and cadaver bone. A major finding, related to Aim 3, has been that porous synthetic bone appears to not have realistic mechanical properties under cyclic loading. Accordingly we are now focused on testing human cadaveric specimens. Although our sample size will be limited to seven to ten specimens because of much higher expense, we believe we are obtaining data that will be more translational and will better advance the understanding of glenoid loosening micromechanics. We have completed work in the following areas:

### ***(1) Design, fabrication, and troubleshooting of experimental cyclic loading machine.***

For this project we designed and constructed a machine that applies controlled combined loadings to glenoid implants. These loadings simulate physiologic “high load” activities of the shoulder, such as lifting an item up onto a shelf. Figure 1a shows a schematic of the loads applied, and Figure 1b shows the constructed apparatus. The glenoid prosthesis is shown implanted into cadaveric glenoid bone. A humeral head prosthesis is welded to a steel arm, and this arm is fastened to a load cell (force sensor) which is fastened to the vertical actuator of our

laboratory's servo-hydraulic mechanical testing machine (Interlaken/MTS, Eden Prairie MN). Two fundamental loads are applied to the glenohumeral joint (Figure 1a): a vertical cyclic displacement, and a horizontal constant compressive force. The vertical cyclic displacement has a magnitude of +/- 2.5 mm relative to the joint-centered position, a frequency of 1 Hz, and is controlled by the Interlaken/MTS machine. The specimen is oriented such that these displacements are in the anterior and posterior direction of the glenoid. The glenoid specimen is fastened to a carriage that rides on a horizontal linear bearing. Two additional linear bearing units are attached to the humeral head side of the device in order to prevent bending loading of the vertical actuator rod.

The horizontal compressive force has a magnitude of 750 N and is applied by a pneumatic cylinder. The pneumatic pressure is held constant (~41 psi) by a pressure regulator, and actuator friction is minimized by using a rolling diaphragm cylinder with ball bearings (ControlAir, Amherst NH). This pneumatic system enables us to hold the horizontal force nearly constant (+/-5 N), as the glenoid carriage slides back and forth during cyclic loading. The horizontal force is continuously monitored by a strain-gage based load cell, which is calibrated beforehand using stacked weights.

For cadaver bone tests, before prosthesis implantation, the glenoid bone is potted in a rectangular block shape for later gripping by the loading apparatus. We fabricated an aluminum mold box, which includes a series of set screws for holding the bone in place (Figure 2). The glenoid is positioned with its face orthogonal to the box sides, and acrylic cement is poured into the box and cures at room temperature. (The selection of potting material is described below.)

### (2) Development of micro-computed tomography (micro-CT) imaging approach and parameters.

We developed techniques for imaging the microstructure of the implanted constructs consisting of glenoid prosthesis, cement, and either cadaver bone or polyurethane bone substitute. Micro-CT scanning is performed on each specimen before cyclic loading, and then after 1000 (1k), 10k, 25k, 50k, and 100k loading cycles. Proper micro-CT settings including energy, matrix size, and field-of-view were determined in order to obtain low noise images covering the entire cement mantle (Figure 3). A resolution of 20 x 20 x 20 micrometers (microns) per voxel was obtained. For cadaver bone tests, a challenge was the radiopacity of the potting material which led to signal-to-noise ratio concerns. We experimented with several different potting materials and have found that poly methyl methacrylate (acrylic dental cement, Figure 2) results in good strength, workability, and it is radiolucent.

### (3) Development of toggle displacement measurement technique.

We developed a novel technique for measuring the toggle displacement of the glenoid implant while under load. Toggle displacements are derived from high-magnification digital photographs taken before cyclic loading, and after 1k, 10k, 25k, 50k, and 100k cycles. A digital SLR camera with macro lens is mounted to our testing apparatus (Figure 1a), and a plane mirror (first surface) is used to view downward at the top edge of the glenoid implant and bone/potting. For each toggle measurement session, images (e.g. Figure 4) are recorded with the joint under 750 N compression. Images are taken of both anterior and posterior sides of the glenoid, and under centered, anterior, and posterior eccentric joint loading. Resolution is ~5 micrometers per pixel. Images are analyzed using ImageJ software (National Institutes of Health) to determine

displacements of marks placed on the implant relative to marks on the bone potting. We have measured good intraobserver reliability using this method ( $r^2 = 0.98$ ). In an earlier design, we were using a miniature differential variable reluctance transducer (DVRT) gauge to measure implant toggle displacement. Because of accuracy concerns associated with the need to place an extension screw on the implant that could be reached by the DVRT, we switched to the photographic method above.

*(4) Fabrication of posterior-augmented glenoid implants, and refinement of implantation technique for these implants*

We have fabricated posterior augmented glenoid implants (Figure 5a). Posterior “steps” were machined from ultra high molecular weight polyethylene by an outside source (with geometry designed previously in our lab). A flexible, high strength special-purpose epoxy (Reltek, Santa Rosa CA) was selected for this project to fasten the steps to standard commercial implants (Zimmer, Warsaw IN) to create the augmented implants. The standard implants themselves are also being tested. We are implanting the prostheses using a combination of standard glenoid tools (Zimmer) and custom-built tooling. The custom-built tooling is used to cut a step into the glenoid bone, in order to accept the posterior augmented implant.

*(5) Experimental determination of glenoid loading parameters.*

The magnitude of  $\pm 2.5$  mm used for the vertical cyclic displacements was determined experimentally, based on convention from the literature, using two separate prostheses implanted in synthetic bone blocks (Pacific Research Laboratories, Vashon WA). A so-called subluxation distance, which is specific to the particular implant design, was determined by centering the humeral head on the glenoid within the loading apparatus, then translating the head until a peak vertical force was measured. The translation at this point was the subluxation distance. The average from multiple cycles, in both directions, from both specimens was determined, and 90% of this distance is being used to cyclically load the specimens.

*(6) Testing/imaging of several prostheses implanted in synthetic bone substitute.*

Three pilot specimens were prepared that consisted of standard glenoid prostheses implanted with cement into porous synthetic bone block (Pacific Research Laboratories, Vashon WA). Two were loaded in the anterior-posterior direction, and one in the superior-inferior direction. We found that mechanical strength and stiffness of the constructs appeared unrealistically low. In one specimen, early delamination (gapping) occurred at the interface of the implant and cement (Figure 6a). In another specimen, early cracking within the construct occurred (Figure 6b). We have also considered several alternative synthetic bone types. *Non-porous* material appears to provide sufficient mechanical properties, but the lack of pores prevents realistic cement penetration and interdigitation that occurs in cadaveric bone.

*(7) Testing/imaging of several prostheses implanted in cadaveric glenoid bone.*

Because of the concerns with synthetic bone found in our early experiments, we have switched our focus to testing with cadaver glenoid specimens. A total of four specimens including both implant types have been implanted, cyclically loaded, micro-CT imaged, and measured for toggle displacements at multiple time points. The first of these is considered a pilot specimen because of a different bone potting technique used. The next two specimens (#1 & 2) consist of standard prostheses implanted into cadaver bone. The most recent specimen consists of a

posterior augmented prosthesis in cadaver bone (#3).

The pilot specimen was loaded to 1000 cycles. A crack occurred and was identified by micro-CT. Specimen 1 was loaded for 100,000 cycles. Toggle displacement measurements remained consistent, within 0.5 mm, throughout the cycling (Figure 7a), indicating lack of loosening. This is also supported with the microCT assessment that showed no cracking. No cracking has been identified within the construct from inspection of the micro-CT scans. Loading of Specimens 2 & 3 is ongoing. Toggle displacement results thus far for Specimen 2 are also shown in Figure 7b.

(8) *Development of computational techniques for data analysis*

Each micro-CT scan (performed at 0, 1k, 10k, 25k, 50k, & 100k cycles) results in approximately 1600 slices of image data and requires about 13 gigabytes of storage. We have developed custom code (Matlab, Mathworks, Natick MA) for pre-processing the dataset so that it can be loaded in memory on a high performance PC and inspected as a single coherent dataset. The code includes optimizing image contrast, reducing from 16-bit to 8-bit grayscale, and resampling the data to result in 40 micrometer voxel size. We are in the process of verifying that the resampled data does not result in missed information compared to the original data.

We have also been developing a methodology for more quantitatively comparing micro-CT scans obtained at different time points, e.g. comparing the 100,000 cycle scan to the 0 cycle scan. Using a 3D visualization software package (Avizo, VSG US, Burlington MA), we first co-register (align) portions of the 3D bone image of the 100 k cycle dataset with the 0 cycle dataset. We then compute the absolute difference between the two datasets, at each voxel, and inspect the resulting 3D dataset. We have performed this process for Specimen 1 and have confirmed no differences between the scans and thus a lack of construct cracking, as demonstrated by a visibly black dataset except for noise and edge artifact (Figure. 8).

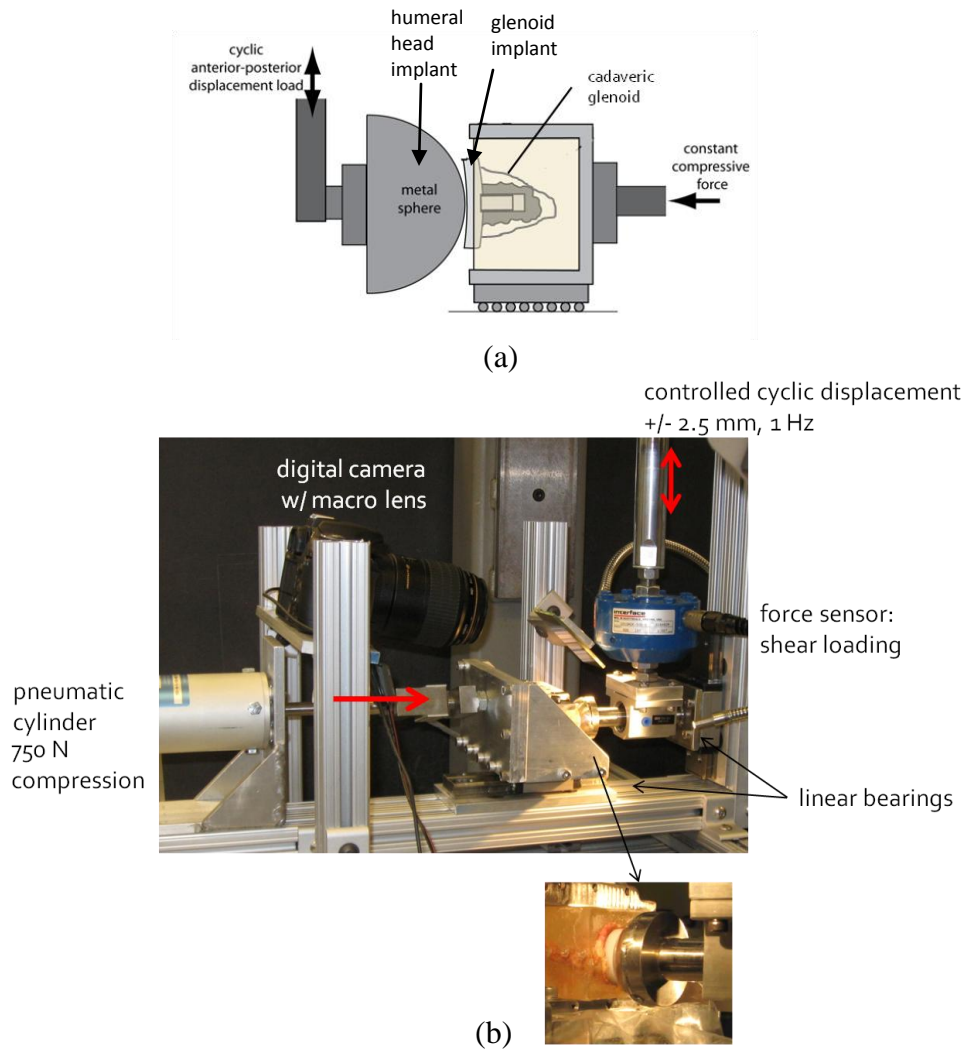


**Figure 1.** (a) Schematic of loadings applied to specimens; (b) Photograph of experimental apparatus used to apply loadings

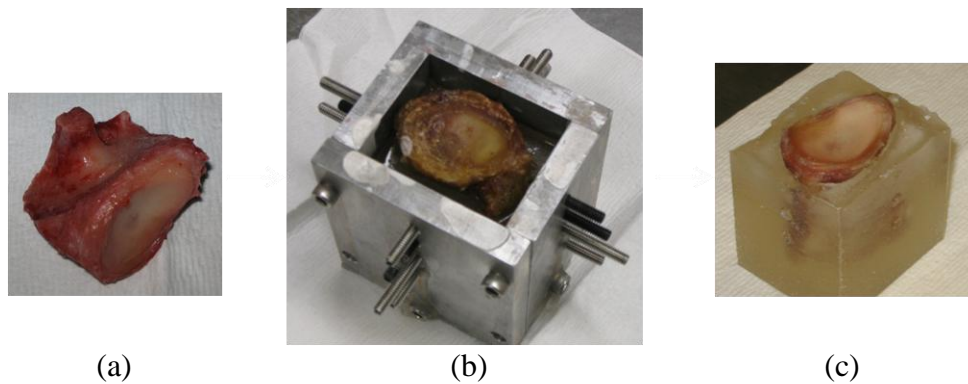


**Figure 2.** (a) Isolated glenoid cadaver bone; (b) potting box; (c) glenoid bone after potting in the acrylic cement (before prosthesis implantation)

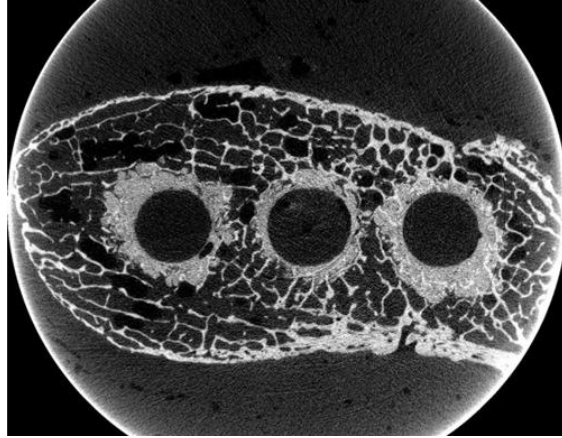


**Figure 3.** Example of a micro-CT image. Slices are obtained parallel to the glenoid face. The three fixation pegs of the implant can be seen, along with the grey cement mantles around them. The trabecular and cortical bone appears white, and the acrylic potting cement is outside the bone.

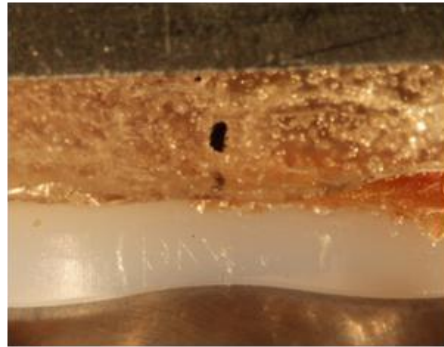
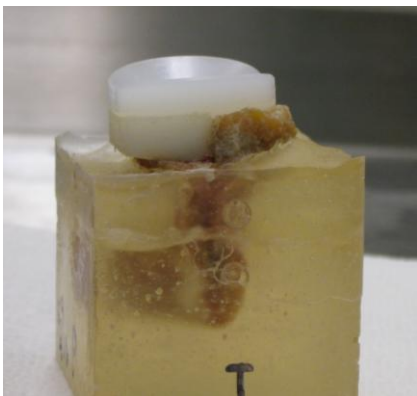
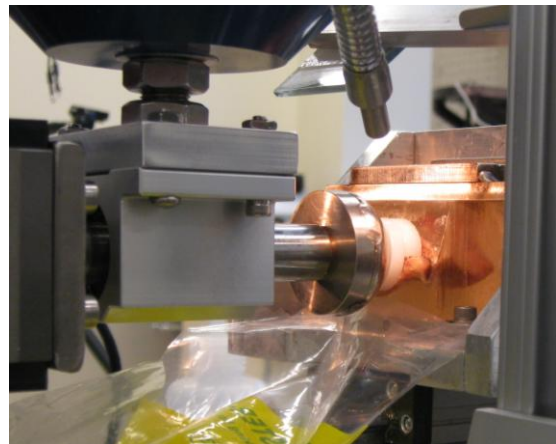


**Figure 4.** Example of a toggle displacement image. Software is used to measure changes in length between landmarks on the implant (appearing white) and bone potting (which is fixed to the bone, appearing orange).



(a)



(b)

**Figure 5.** (a) Posterior augmented prosthesis implanted into glenoid bone, and potted in acrylic. The prosthesis is formed by attaching a custom made step under the (left side) base of a standard glenoid implant. (b) The same prosthesis being cyclically loaded.

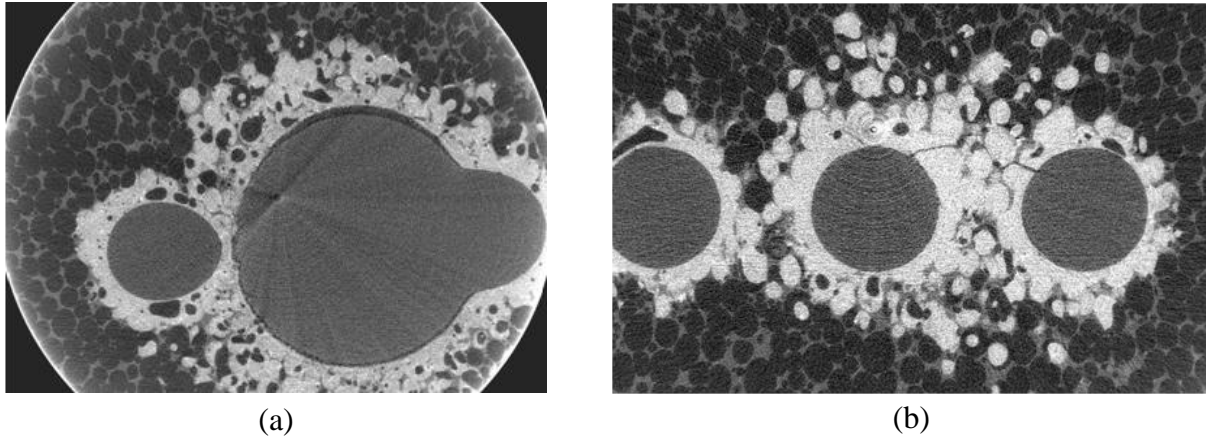


**Figure 6.** Micro-CT slices of porous synthetic bone specimens after cyclic loading, demonstrating (a) implant-cement delamination, and (b) cement mantle cracking.

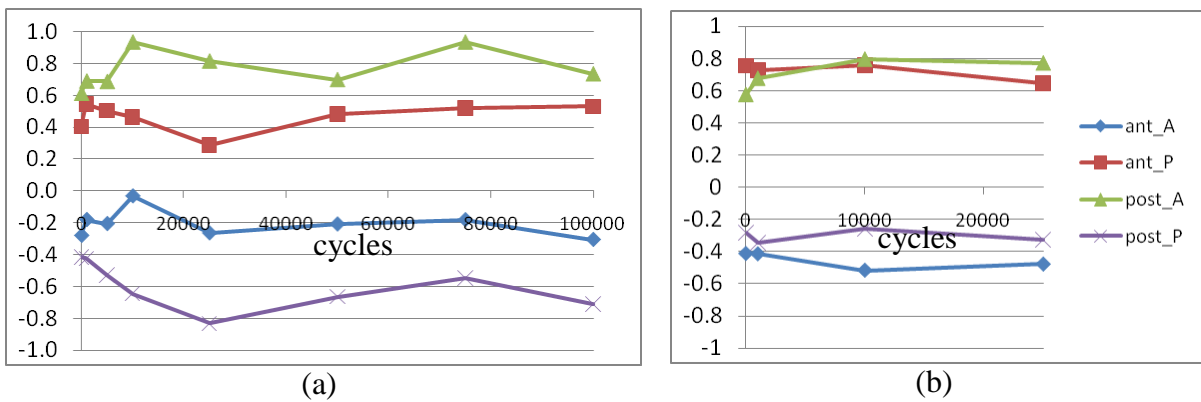


**Figure 7.** Toggle displacement measurements (in mm) of (a) Specimen 1, and (b) Specimen 2 (implanted cadaver specimens). In the legend, “ant\_P” indicates the posterior-side displacement while loading on the anterior side, and so on.

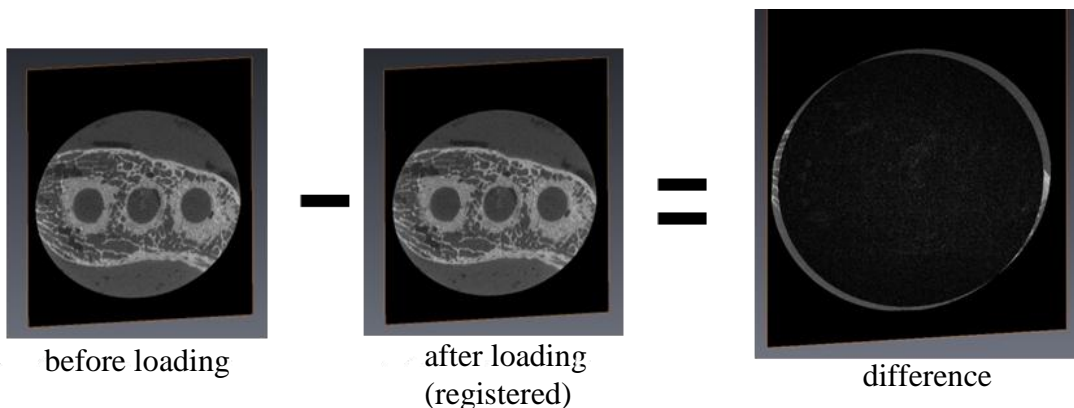


**Figure 8.** Example of micro-CT data processing for Specimen 1. The after-loading images are co-registered (aligned) with the before-loading images, and then the absolute differences are computed for all voxels in 3D space. Only a single slice of each 3D dataset is shown above. The lack of signal on the resulting dataset indicates no cracking due to loading.

## **Research Project 22: Project Title and Purpose**

*Delivery and Mechanism of Action of Novel Therapeutic Agents to Combat ALS* – Amyotrophic Lateral Sclerosis (ALS) is a progressive degenerative disease causing loss of spinal cord motor neurons and is almost always fatal within 3 -5 years of diagnosis. In this project we will use mutant SOD1 transgenic mice to test the actions of a well-established neuroprotective factor Pigment Epithelium Derived Factor (PEDF) that has a number of unique features about its structure and mode of action that strongly suggest it will succeed in treating ALS where studies of different growth factors or neurotrophic factors have failed. The outcome of this project will be new knowledge on ways of delivering drugs to combat ALS as well as an understanding of the molecular mechanisms by which PEDF can exert its protective action on spinal motor neurons.

### **Anticipated Duration of Project**

9/1/2010 - 6/30/2012

### **Project Overview**

Most cases of ALS are sporadic but the 20% of inherited cases have allowed the identification of some molecular changes that can cause the disease. One of the best studied is a mutation in the superoxide dismutase gene SOD1. Mice expressing the same mutation show many symptoms in common with ALS and undergo progressive degeneration until death.

In this project we will use mutant SOD1 transgenic mice to test the actions of a well-established neuroprotective factor PEDF. Pigment Epithelium Derived Factor was first isolated from the pigment epithelial cells of the eye and has since been found to be produced by a number of different tissues. It protects many types of neurons, including spinal motor neurons, from a wide variety of toxic insults. It has a number of unique features about its structure and mode of action that strongly suggests it will succeed in treating ALS where studies of different growth factors or neurotrophic factors have failed.

To define the action of PEDF in a mouse model of PEDF we will carry out four types of studies. First, we will develop encapsulated forms of PEDF that can release therapeutic doses of the factor over extended periods. Second, we will surgically implant pumps into the mutant mice that deliver the encapsulated PEDF to the cerebro-spinal fluid (csf) from which it can reach the motor neurons. We will measure the amounts of PEDF in the csf and also test the effect on the mice both by measuring muscle function and by studying the loss of cells anatomically. In a third set of experiments we will investigate the mechanisms by which PEDF may act on the neurons and glia of the spinal cord. We will study whether PEDF alters the induction of cell death pathways, alters the generation of toxic oxygen free-radicals or alters the accumulation of protein aggregates – all features of ALS degeneration.

## **Principal Investigator**

Colin J. Barnstable, DPhil  
Professor and Chair, Department of Neural and Behavioral Sciences  
Penn State University College of Medicine  
500 University Drive  
Hershey, PA 17033

## **Other Participating Researchers**

James Connor, PhD, Joyce Tombran-Tink, PhD, AB Madhankumar, PhD, Zachary Simmons, MD, Min Pang – employed by Pennsylvania State University

## **Expected Research Outcomes and Benefits**

The expected outcomes of this project will be new knowledge on ways of delivering drugs to combat ALS, as well as an understanding of the molecular mechanisms by which PEDF can exert its protective action on spinal motor neurons. Most importantly, this work is expected to show that PEDF is a powerful protective factor that can be used in clinical trials and has the potential to prolong the life of patients suffering from ALS.

## **Summary of Research Completed**

This is very much a progress report as a series of long-term experiments have been initiated but the results will not be obtained for several more months.

We prepared sufficient quantities of recombinant PEDF as described in our original aim 1. This has been highly purified and shown to be therapeutically active as defined by a number of in vitro assays.

After some delay we were able to obtain a sufficient number of mutant SOD1 transgenic mice from the Jackson Laboratory. These mice have been implanted with osmotic pumps delivering either PEDF or buffer. At present these mice are under daily observation and testing to determine the onset of ALS-like symptoms. Only when all mice have developed symptoms, or a group continue to show no symptoms at least two months after others have died, will the code be broken and the effects of PEDF determined. Other parts of the project, namely the histological analysis of control and PEDF-treated mice will not be carried out until the conclusion of the behavioral testing. The final aim of this proposal, the study of the mechanism of action of PEDF, will wait for the histological studies because this information will provide a critical indication of which cell types to use.

We are now just waiting for treated animals to develop symptoms - a process that could take several more months. Although this phase of the work requires daily testing and observation, i.e. a lot of time, it does not yield any results until the very end. We do expect to have all the animal testing completed by the end of the summer and so should complete the other phases of the project well within our expected completion date of 6/30/2012.

## **Research Project 23: Project Title and Purpose**

*Developing an Animal Model of Cognitive Bias to Study the Impact of Emotion on Health and Behavior* – Emotional states play a fundamental role in influencing health outcomes; individuals with a bias toward negative emotions, such as anger and depression, are more prone to health related problems. Furthermore, it has recently been shown that positive emotions help to protect against certain kinds of disease. Animal models provide a powerful tool to experimentally determine the processes involved in disease pathways. Such models are used to investigate the health consequences of states such as depression or anxiety, but current models of animal emotion are poor and incomplete because they take no account of the cognitive aspect of emotion - appraisal processes that bias an individual toward a more negative or positive outlook. This project aims to develop an improved animal model of emotion.

### **Anticipated Duration of Project**

9/1/2010 - 12/31/2011

### **Project Overview**

Using novel testing paradigms that directly measure rodent cognitive appraisal strategies, we will create a new animal model of emotional states. Our approach will quantify emotional state by simultaneously evaluating behavioral, physiological and cognitive biases. Specifically, this refined model will enhance our ability to determine the consequences of positive and negative affective states (analogous to optimism and pessimism in humans), and how these influence different health issues. There are two main objectives.

Objective (i) Demonstrate that cognitive biases in rats are associated with neuroendocrine and behavioral biases that accompany positive and negative affective states in humans. By doing so, we will develop a more comprehensive rodent model of emotion that includes assessment of cognitive as well as physiological and behavioral biases.

Objective (ii) Develop a rearing paradigm to create different populations of rats with contrasting long-term cognitive biases (i.e., groups of animals with either more positive or more negative tendencies). These rats can then be used to determine health consequences of cognitive bias. In this initial project we will investigate choice behaviors related to drugs of abuse, but future work will address how emotional state affects resilience and plasticity in response to different kinds of challenge such as compromised health, stress and pain.

In the current project, we will train rats to associate different stimuli with specific outcomes (i.e., one stimulus leads to a reward, a different stimulus leads to a punishment). We will then test rat response to ambiguous ‘in between’ stimuli. Previous work has shown that rats that appraise ambiguous events to be more like the rewarded stimulus generally have a positive affective state, whereas animals that assess ambiguous stimuli as more like the punishment stimulus have a negative affective state.

We will focus on determining how positive or negative emotional bias affects addiction to drugs

of abuse. By developing a more comprehensive method to quantify animal emotional state we will devise a more sophisticated and accurate model that can be manipulated to determine how emotional states influence health trajectories over an individual's life span.

### **Principal Investigator**

Victoria A Braithwaite, PhD  
Professor of Fisheries & Biology  
Penn State University  
410 Forest Resources Building  
University Park, PA 16802

### **Other Participating Researchers**

Sonia Cavigelli, PhD, Jennifer Graham, PhD, Patricia Sue Grigson, PhD, Christina Ragan, BS, Jamie Troupe, BS – employed by Pennsylvania State University

### **Expected Research Outcomes and Benefits**

The novel approach described in this project will allow us to create a superior model of animal emotion that encompasses the key component of cognitive bias – a part that is so far lacking in current models. By quantifying cognitive bias, we will characterize emotion more accurately and critically. Such animal models will allow us to address the effects that cognitive bias has on health including aspects relating to addiction. Much of the current focus in human research has been on the detrimental effects of negative cognitive bias, but recent research has shown that positive cognitive bias is likely to play an equally important role. Although optimism and pessimism are usually considered opposites, it now appears that these two states, while related, are distinct constructs. Our animal models will allow us to more systematically investigate these differences to provide us with a better understanding of the role played by cognitive bias and emotion on human health and behavior. In the future, we envisage using this model to investigate the consequences of positive and negative affective states and their effects on other health issues such as depression, anxiety and thresholds of pain.

### **Summary of Research Completed**

#### *Objective 1:*

We have successfully completed a series of temperament assays for 12 rats measured at different times and after different manipulations. We have tried to repeat a previously published demonstration of cognitive bias, but did not find that the training protocol worked effectively, we are therefore currently testing alternative methods (details below). Measures of neuroendocrine responses i.e. stress measured as changes in corticosterone production and serotonin assays from the brain stem are being run the last week of June 2011.

Objective 1 was based on repeating work originally performed in the UK with Lister Hooded rats. As we were unable to obtain the same strain without importing the animals from the UK, we selected a different hooded strain, Long Evans. Both are outbred strains with similar growth

trajectories. Twelve, Long Evans, male rats at 55 days of age were purchased. Rats were pair-housed and maintained on a 12:12 light:dark cycle. Each animal was handled daily and weighed. All cages were provided with corncob bedding as well as various, but identical, forms of enrichment; 2 tubes, a small, rubber dog-toy and wooden chewing blocks. Manipulation of the enrichment items (i.e. removal of enrichment) is being used in Objective 2 to induce a negative affective state as previously published work has shown that rats are sensitive to changes with cage enrichment. The rats have *ad libitum* access to food and water. Natural variation in body pattern markings was used to identify individual animals.

#### *Experiment 1a. Temperament behavior assays*

All rats were screened in two standard temperament assays ((i) Open field arena; (ii) Novel objects approach) at three different time points; (1) Prior to the first cognitive bias assay described below (experiment 1b); (2) at the end of a second cognitive bias assay (experiment 1c); (3) after cage enrichment removal (performed to explore the effect of a major environmental change on temperament).

Temperament assay (i) examined rat behavioral responses in an open field arena (a 118 cm x 119 cm white plastic arena with 30cm high walls). Individual rats were transported in one of the enrichment tubes from their home cage and then released into the arena in the middle of one side wall. An overhead video camera recorded the movements and paths made by the rat over a 10 minute observation phase. Anxious animals express strong wall-hugging responses rarely moving away from the arena walls (thigmotaxis). Less anxious animals begin to move into the middle of the arena as they explore the environment. The video films are then replayed to allow us to record time spent at outer edge, time before first moving into the middle and rate of movement.

Temperament assay (ii) was run the day after the open field trials and tested the latency of the rats to approach 2 novel objects placed in separate corners of the same arena used for the open field trails. Again, the rats are released at the edge of the arena and the time taken to approach and reach within one body-length of each novel object is measured for both object 1 and 2. More risk prone, exploratory animals tend to reach the objects before more timid, risk averse individuals.

By testing rats at different time points and after manipulations such as enrichment loss, we have investigated the stability of individual temperament traits. While these are assumed to be stable across time and contexts, we needed to determine whether anxiety-related responses were similarly consistent.

*Results:* The 12 rats exhibited considerable individual variation as expected in assays of temperament (e.g. range of time to leave the edge and explore the center of the first open field arena test was (2s - 91s). Despite the between individual variation, however, measures of within animal temperament were highly repeatable across time indicating that rats have stable temperaments that persist despite stressful disruption such as loss of cage enrichment. We are therefore confident that our assays provide reliable behavioral assays of susceptibility to anxiety.

### *Experiment 1b - Cognitive bias assay*

After 14 days of handling and acclimation to the laboratory rats were trained on a spatial discrimination task.

#### 5-armed maze:

We selected a 5-armed maze design as recently published work has indicated that rats learn to discriminate a rewarded and an aversive location more efficiently if the arms of a maze constrain general exploration. Otherwise the design of the paradigm was the same as we originally explained in the proposed plan of work.

The 5 arm-maze was constructed with a start box leading to the different arms (arm length 70 cm, width 10 cm, height 30 cm with a clear plexiglass lid fitted to prevent escape attempts during trials, but allowing us to film rat movements using a ceiling mounted camera. Maze arms 1 and 5 were positioned at 180° from each other while the other arms (2, 3 & 4) were evenly placed between these to create a semicircular radial maze. Arms 1 and 5 were assigned as the rewarded and aversive arms for training and were counterbalanced across rats. Arms 2-4 represent ambiguous locations in between the rewarded and aversive locations.

During training sessions individual rats were placed in a central hub start area and allowed to settle for 2 minutes before a guillotine door to arm 1 or 5 was raised. At the end of each arm the rats could examine a bowl, for the rewarded arm this contained four food pellets, whereas the aversive arm contained one quinine soaked pellet. Each animal was given 12 trials per day, 6 positive (i.e. access to 4 food pellets) and 6 aversive (i.e. access to a quinine soaked pellet).

Other researchers used latency to reach the food bowls as a measure of expectation (e.g. Burman et al. 2009 found a mean latency to approach rewarded bowl: 4.0s, mean latency to reach aversive bowl: 12.5s), *i.e.* if rats understand a specific arm is rewarded they approach the bowl faster than if they perceive it to contain a quinine pellet. However, our rats, even after 156 individual trials, did not show a difference in the time taken to reach rewarded or aversive food bowls (mean latency to approach rewarded bowl: 7.78 s, mean latency to approach aversive bowl: 7.29 s). There are several factors that may explain this result. For example, we are using a different strain of rat. Our rats were 3 months younger than those used in previously published work. Furthermore, the rats do not seem to find the quinine soaked pellets particularly aversive (in fact, some rats consumed part of all of these pellets). Alternatively, the training protocol using the 5-arm maze may make the discrimination task too difficult for the rats to solve.

*Experiment 1c:* This is an additional experiment that we used to determine why the maze discrimination did not work. To address age effects we purchased 12 rats that were 6 months old. To explore strain effects we now compared the performance of 6 Long Evans and 6 Sprague Dawley rats. Furthermore, we changed the cognitive bias paradigm to simplify the design. Individual rats are now placed in a start box that is connected by a meter long tube to a reward chamber. As the rats run down the tube they experience sandpaper of a specific grade, the grade (rough or smooth) indicates whether the reward will be a preferred half chocolate drop, or a less preferred piece of breakfast cereal (Cheerio). In this paradigm, intermediate grades of sandpaper then act as the ambiguous cues. The different trials are currently on going and we are waiting to see whether older rats, different strains or the different experimental design help us determine

cognitive bias.

*Experiment 1d:* To monitor the neuroendocrine response we have practiced collecting a time series of blood plasma samples (after 10, 20 and 45 minutes) from a tail snip. We are currently sacrificing the 12 original rats from Objective 1 (experiments 1a and b). Last week these animals had their enrichment removed, they were then tested in a final set of temperament assays and we will now compare peak corticosterone and brainstem serotonin transporter (SERT) mRNA expression to examine whether loss of enrichment affects neuroendocrine measures. We selected the two groups (enrichment loss versus no change) such that they have similar numbers of risk averse and risk prone (or bold versus timid) animals.

*Objective 2:*

Long term manipulation of affective state. Twelve, 4 week old, male, Long Evans rats have been purchased for Objective 2. These are pair housed with enrichment. From the age of 5 weeks, 6 rats have been exposed to standard housing with enrichment and handling while the remaining 6 have been treated with a chronic mild stress (CMS). To create a state of CMS we are exposing these rats to a series of unpredictable daily changes such as tilted cages, wet bedding, change of rat partner, short term isolation etc.. These unpredictable changes are expected to create a stressful environment. These animals have just become adults (i.e. 60 days of age) and so are about to begin their discrimination training to investigate whether the chronic mild stress during their juvenile phase has a long term effect on behavior.

*Summary of progress made in first 6 months*

We are on track to complete the schedule of work within 12 months. While the initial cognitive assay has been difficult to quantify, we are confident the change of experimental design will provide us with the data we require. Furthermore, we believe that our not being able to replicate the original finding suggests that there are some interesting strain or age differences that could influence cognitive bias training. We therefore propose to explore these at the same time as completing the originally planned work. To this end, we have an undergraduate summer assistant following up this aspect of the project.

### **Research Project 24: Project Title and Purpose**

*Structural Studies of Tight Junction Structure Function and Regulation* – Tight junctions (TJ) are supramolecular structures that form the cell-cell barriers required for tissue formation and in regulating the flow of solutes through paracellular spaces. Occludin (Occ) is a tetraspanning integral membrane protein in epithelial and endothelial tight junctions. This protein and its interacting extra- and intracellular partners are believed to be critical for regulating TJ properties. Specifically, Occ is proposed to act in signal transduction to adapt TJ properties to cellular and tissue need. Understanding the structure and function of Occ is critical for understanding its role in TJ biology. The results obtained from this project will lay the foundation for pursuing external grants, including one from the NIH membrane protein structure initiatives, where proposals that show purified, well behaved membrane proteins are generally well received.

## **Anticipated Duration of Project**

9/1/2010 - 12/31/2011

## **Project Overview**

TJs form the blood-brain and blood-retinal barriers. Loss of barriers increases fluid and solute transport across the brain and retinal vasculature is associated with a number of disease pathologies including brain tumors, stroke, diabetic retinopathy and age-related macular degeneration. In many cases, the increased TJ permeability associated with disease is correlated with changes in Occ phosphorylation and/or membrane localization. We have shown that Occ participates in VEGF regulated TJ remodeling in diabetic retinopathy. However, little is known how this multidomain transmembrane protein functions in this capacity. In two specific aims, we describe experiments to determine the role of the transmembrane (TM) domain and its extracellular loops that appear to be required for TJ formation and regulation. These loops are the binding site for a number of proteins including TGF $\beta$  receptor, claudin-1 and JAM-4, and cellular pathogens including Coxsackie virus and HCV. Encouraged by our initial success in the expression of the transmembrane domains of Occ in *E. Coli*, we propose two additional specific aims that seek to understand mechanisms by which both intra- and extracellular signals affect Occ function and alter TJ properties. In these experiments, we will focus on the intracellular domains of Occ which interact with the TJ scaffolding protein ZO-1 and the ubiquitin E3 ligase Itch. The four aims are as follows: *First*, we will optimize the expression, purification and reconstitution conditions for the preparation of a homogeneous sample suitable for structural studies by NMR and X-Ray crystallography. Gel filtration, light scattering, CD and 2D <sup>15</sup>N-TROSY will be employed to characterize the preparations. *Second*, we will determine the topology of the Occ through proteolysis, mass spectroscopy in conjunction with H/D exchange and NMR. *Third*, we will use NMR spectroscopy and small angle X-ray scattering to determine the structure of the ZO-1/Occ complex. *Fourth*, we will determine how ZO-1 binding affect the ability of Itch to access and ubiquitinate the C-terminal region of Occludin. These aims represent two distinct but synergistic projects that will advance our knowledge of TJ structure and function.

## **Principal Investigator**

John M. Flanagan, PhD  
Professor  
Penn State University College of Medicine  
500 University Dr.  
H171  
Hershey PA, 17033

## **Other Participating Researchers**

Fang Tian, PhD, Maria Bewley, PhD – employed by Pennsylvania State University

## **Expected Research Outcomes and Benefits**

The planned studies are designed to understand how Occ acts in regulating TJ structure and function. As a result of the project, we will have large quantities of the Occ-TM domain for subsequent structural and biochemical studies. This protein will be useful for our studies and for studies in the Bond laboratory. Moreover, this general procedure may be useful for studying other TJ TM proteins such as members of the claudin family. The availability of these proteins will allow a range of experiments that have not been previously possible and will lead to new insight into how they function in TJs including the initial characterization of its oligomeric state described in Aim 2. There is a large body of anecdotal evidence that the oligomeric state of Occ is functionally important, and that oligomerization involves residues in the second extracellular domain. Moreover, this loop has been implicated in Occ's interaction with other membrane proteins and with some viruses. With purified Occ-TM preparations, we will be able to study these interactions in detail. Studies focusing on the intracellular domains of Occ will shed light on how Occ is sensitive to both intra and extracellular signals in modulating TJ function. There is a body of evidence that both extra and intracellular signals affect Occ membrane localization and TJ properties via changes in the interaction of the intracellular domains with protein factors such as ZO-1 and Itch. If true, this makes Occ an ideal target for modifying TJ properties. The project will begin to address this possibility. Understanding these interactions will provide a first step in determining whether these interactions can be exploited in therapies targeted to TJs. Moreover, the experiments will provide the necessary starting material and biochemical and biophysical basis to compete for external funding. Specifically, they provide the foundations necessary to apply for NIH membrane protein Roadmap funds.

## **Summary of Research Completed**

During this reporting period, we have published a paper entitled “RDC derived protein backbone resonance assignment using fragment assembly” (PMID 21191805) that describes a novel method for NMR resonance assignments. The method is based upon the observation that experimental residual dipolar couplings (RDCs) in combination with structural models can be used in the protein backbone resonance assignment process because RDCs can be measured accurately and interpreted quantitatively. Here, we introduced an approach that allows resonance assignment based on optimal agreement between the experimental and calculated RDCs from a structural template that contains all assignable residues. To overcome the inherent computational complexity of such a global search, we have adopted an efficient two-stage search algorithm and included connectivity data from conventional assignment experiments. In the first stage, a list of strings of resonances (CA-links) is generated via exhaustive searches for short segments of sequentially connected residues in a protein (local templates), and then ranked by the agreement of the experimental  $(^{13}\text{C}(\alpha))$  chemical shifts and  $(^{15}\text{N}-(^1\text{H}))$  RDCs to the predicted values for each local template. In the second stage, the top CA-links for different local templates in stage I are combinatorially connected to produce CA-links for all assignable residues. The resulting CA-links are ranked for resonance assignment according to their measured RDCs and predicted values from a tertiary structure. Since the final RDC ranking of CA-links includes all assignable residues and the assignment is derived from a "global minimum", our approach is far less reliant on the quality of experimental data and structural templates. The present approach is validated with the assignments of several proteins, including a 42 kDa maltose binding protein (MBP) and

the PDZ-3 domain of the human ZO-1 protein using RDCs and structural templates of varying quality. Since backbone resonance assignment is an essential first step for most of biomolecular NMR applications and is often a bottleneck for large systems, we expect that this new approach will improve the efficiency of the assignment process for small and medium size proteins and will extend the size limits assignable by current methods for proteins with structural models.

We have also determined the solution structure, by a combination of small angle X-ray scattering (SAXS), nuclear magnetic resonance spectroscopy (NMR) and molecular modeling of the complex between the tight junction (TJ) proteins Occludin and ZO-1. This complex is thought to be a key regulator of TJ structure, properties and acts as an interface between the extracellular matrix, tight junctions and various signal transduction cascades. The SAXS model (Figure 1) indicates that the negatively charged “head” domain of the occludin coiled-coil domain (occCC) interacts with a region on the guanylate kinase domain (GuK) of ZO-1. In order to independently identify the region of occCC at the ZO-1 binding interface, we performed NMR cross saturation relaxation experiments to identify residues in the occCC domain that are in close (~4-6Å) proximity to ZO-1 in the complex. These experiments allowed direct distance measurements between residues within a fully deuterated protein and a fully protonated binding partner by measuring the reduction in intensity of backbone  $^1\text{H}$ - $^{15}\text{N}$  resonances due to the proximity of residues in the protonated partner. For the occCC/ZO-1 complex, perdeuterated occCC was mixed with fully protonated ZO-1 comprised of PDZ-3/SH3/GuK domains (PSG) at 1:1, 1:2 and 1:0.5 molar ratios and the reduction in intensity for each resonance was recorded. When compared to the TROSY-HSQC spectrum of occCC, the intensity of residues Tyr<sup>467</sup> and Ala<sup>478</sup> of occCC were consistently reduced in the complex compared to apo occCC and thus were located at the interface between the two proteins in the complex. These results provided further support for the placement of occCC in the complex by SAX. Together, the SAXS and NMR experiments demonstrate that the negatively charged head of occCC sits at the interface with the positively charged ZO-1 GuK domain in the binary complex.

The residues at the interface were verified by site-directed mutagenesis and *in vitro* and *ex vivo* (cell lysates) binding studies (GST-pulldowns Figure 2). In this analysis, charge reversal substitutions for four negatively charged residues in the head domain of occCC (D465, E469, E470 and E472) were each shown to markedly reduce complex formation with the ZO-1 PSG construct. Further, a peptide spanning residues 465-475 competitively inhibited occCC/ZO-1 complex formation. This region contains S471 which we have shown is phosphorylated in VEGF stimulated TJs. A phosphorylated (pT471) version of the 465-475 peptide was a 3-fold better competitor than the non-phosphorylated peptide in our *in vitro* and *in vivo* binding assays. Finally, treatment of confluent MDCK cells, which form robust TJs, with the non-phosphorylated peptide resulted in increased breakdown of the barriers as measured by changes in conductance. Together, these results identify the head domain of occCC as a site of interaction with ZO-1.

The identification of residues in the ZO-1 PSG construct that interact with occCC was based upon (1) the observation, by SAXS, that calmodulin (CaM) binding to a similar site on ZO-1 as occCC and (2) work by others showing that helix V in the GuK domain of ZO-1 was essential for CaM binding. To test this experimentally, binding assays were used to determine whether calmodulin can directly compete with GST-occCC for binding to his-tagged ZO-1 PSG. At a 1:1

molar ratio of CaM:GST-occCC, the binding between occludin and ZO1 PSG is reduced to 57% compared to the condition without calmodulin. This level is further reduced to 36% when a 2-fold molar ratio of calmodulin is added to the reaction and 23% of *wt* binding with a 10-fold excess of calmodulin. These results demonstrate that the occludin and calmodulin binding sites on ZO-1 overlap and that these two proteins are direct competitors for binding to the ZO-1 GuK domain *in vitro*.

Since CaM and occCC are direct competitors for binding to the ZO-1 GuK domain, we hypothesized that the same residues were responsible for directly mediating the interaction with both proteins. Previous work has identified a set of positively charged residues within the GuK domain that are necessary for the ZO-1:CaM interaction. In this assay, we created charge reversal mutations of two groups of these residues to determine their effect between GST-occCC and ZO-1 PSG *in vitro*. The first charge reversal variant, termed ZO-1 TM(D/E), contains lysine / arginine to aspartate / glutamate charge reversal mutations at Lys<sup>479</sup>, Arg<sup>752</sup> and Lys<sup>753</sup> (K749D / R752D / K753E) while the second, termed 2(D/E), contains charge reversal mutations at Arg<sup>760</sup> and Arg<sup>762</sup> (R760E / R763E). *Wt* ZO-1 PSG is able to bind GST-OccCC whereas capture of ZO-1 TM(D/E) was significantly compromised with a reduction to 9% of *wt* while the ZO-1 2(D/E) variant also reduced binding to 29% of *wt* (Figure 3). These results suggest that both sets of residues are necessary for the occCC:ZO-1 PSG interaction *in vitro* and confirm that CaM and occCC share the same binding site on ZO-1.

This work is being readied for publication.

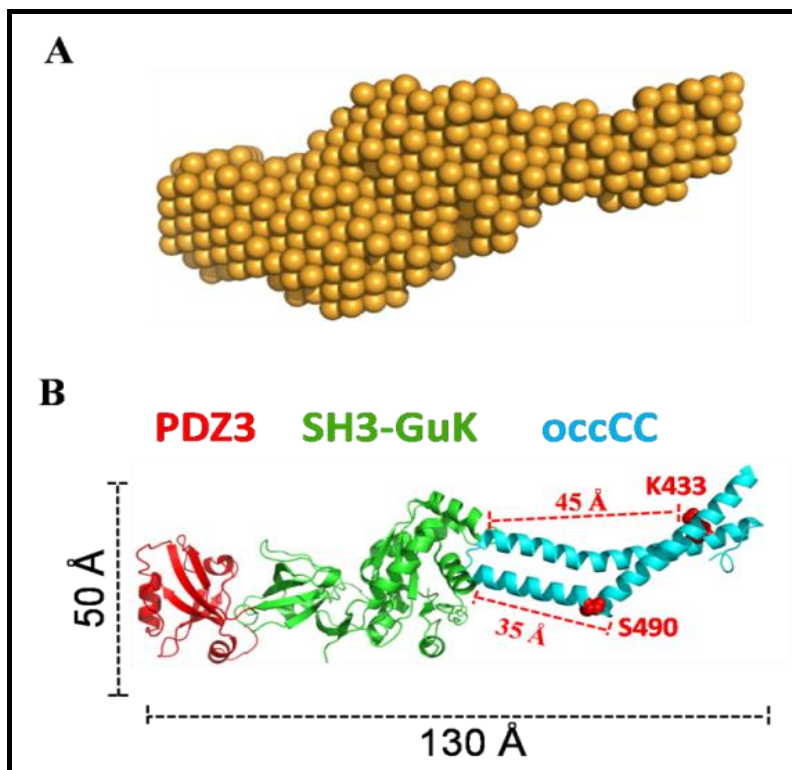
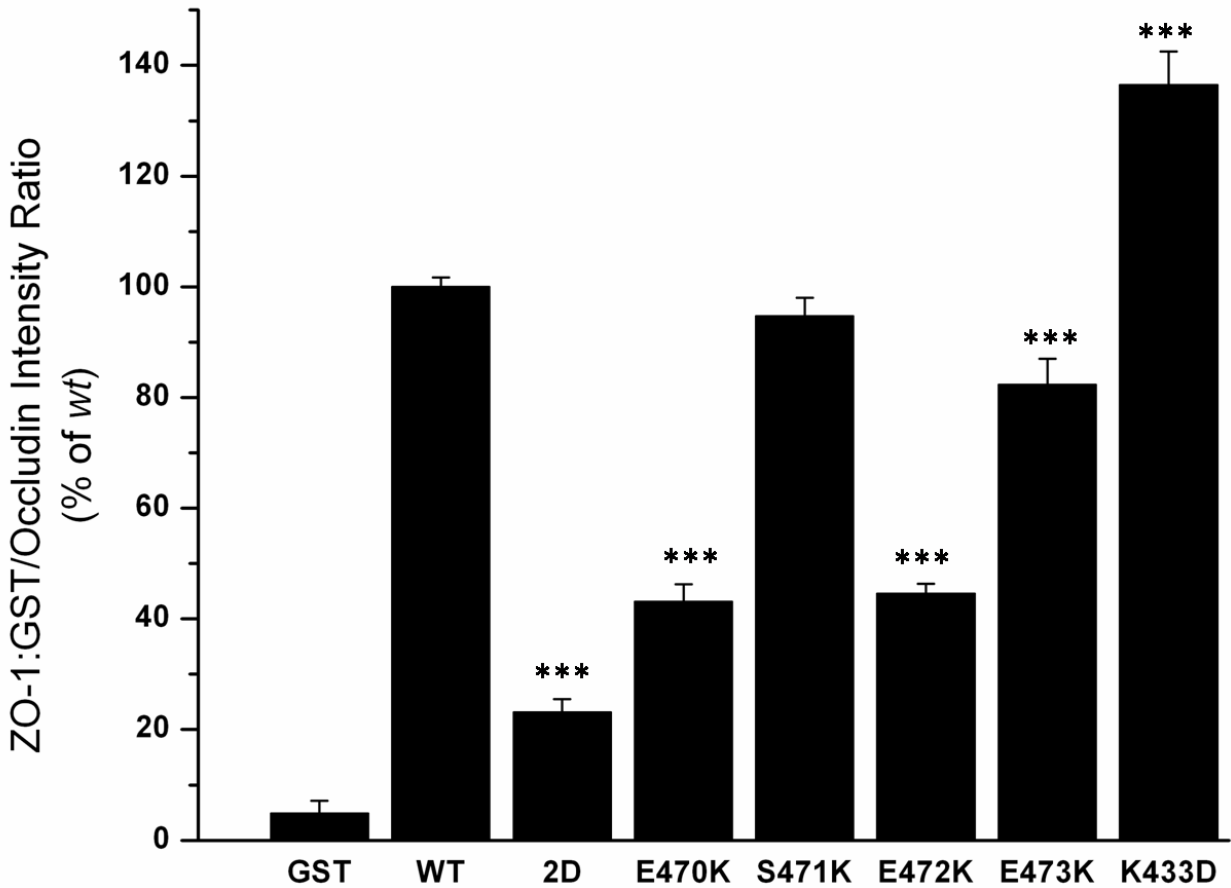
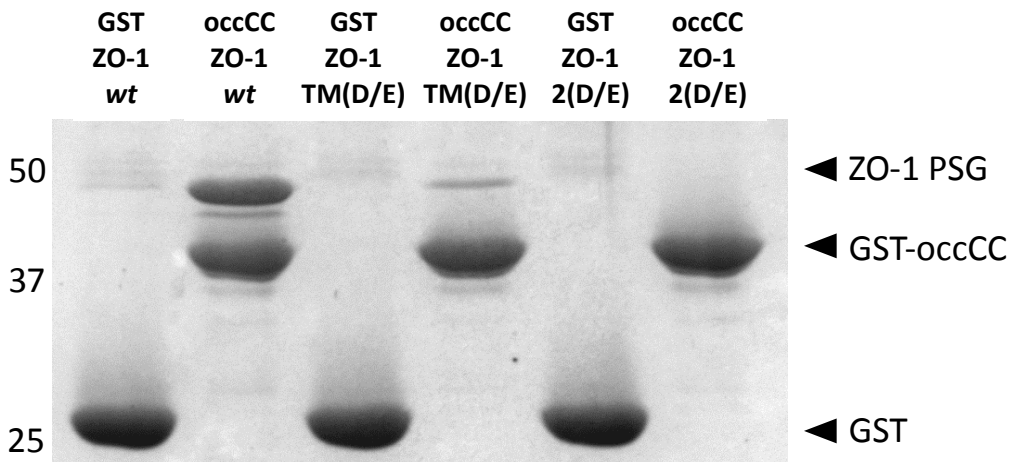


Figure 1. Solution structure of the occCC/ZO-1 PSG complex by SAXS. The figure is the reconstructed solution structure of the complex from the scattering data to  $q = 0.3\text{\AA}^{-1}$ . The chi-square value for this model is 1.2 indicating a good fit to the experimental data. Models were also determined for occCC and ZO-1 PSG alone. In both cases, the resultant models were in good agreement with the X-ray crystal structures of the constructs (data not shown).



**Figure 2.** In vitro GST-pulldown experiments for charge reversal substitution in occCC to determine their ability to interact with wild type ZO-1 PSG.



**Figure 3.** In vitro GST-pulldown experiments for charge reversal substitutions in ZO-1 PSG domain.

## **Research Project 25: Project Title and Purpose**

*Epigenetic Basis of Metabolic Memory in Diabetic Retinopathy* – Recent longitudinal studies demonstrate that despite achieving good control of blood glucose for ten years patients formerly under non-intensive insulin therapy continue to have a higher rate of developing diabetic retinopathy and other complications. With this background, we hypothesize that poor glucose control causes epigenomic changes that are not fully reversed with intensive insulin therapy. Demonstration of epigenetic changes in the retina, in response to diabetes, not reversible by insulin, would be an example of an innovative, high pay-off, paradigm-shifting outcome. Such information would open new avenues for understanding diabetic complications and developing treatments that, used in conjunction with homeostatic insulin replacement, would be capable of restoring the pre-diabetes epigenetic state and reducing the risk of complication development.

### **Anticipated Duration of Project**

9/1/2010 - 6/30/2012

### **Project Overview**

To date we have focused on a well-characterized spontaneous genetic Type I mouse model,  $Ins2^{Akita}$ , supported by a wealth of data on the functional and molecular effects of diabetes on the retina. We have also focused on DNA methylation as an epigenetic change because methylation changes are capable of persisting in the absence of a continued stimulus (e.g., hyperglycemia). Even small changes in methylation of DNA sequences can alter gene expression. We have performed an initial genome-wide discovery analysis of methylation levels in the  $Ins2^{Akita}$  retina. Non-diabetic, Untreated diabetic, and Insulin-treated diabetic groups were compared to identify DNA sequences differentially methylated in response to diabetes, methylation changes that were reversed by insulin treatment, and methylation changes that were not reversed by insulin treatment. In a preliminary study we identified 210 DNA sequences with differential methylation in Diabetics as compared to Non-diabetics. Comparing the Insulin-treated diabetic to the Diabetic group we found that only 10% of sequences with decreased methylation were fully normalized by insulin and 39% of sequences with increased methylation in Diabetics were fully normalized with insulin treatment. In this project we will generate a new set of samples including – Non-diabetic, Diabetic, Diabetic with Insulin treatment for the last 6 weeks (similar to the original experiment), and Diabetic with Insulin treatment for the last 11 weeks (approximately 1 week after the onset of hyperglycemia). We will validate methylation of DNA sequences associated with specific genes through sequencing of bisulfite treated DNA samples (bisulfite alters the structure of methylated nucleotides), and quantitative polymerase chain reaction amplification of methylated DNA (MeDIP qPCR) for ~10 high-priority genes. Priority will be based on relevance as suggested by biological function and the existing scientific literature. Bisulfite sequencing will also determine the specific nucleotides with methylation changes. We will measure differential mRNA expression from genes with validated methylation changes by qPCR to determine if the methylation change is functionally relevant. To date there are no published reports of DNA methylation changes in response to diabetes or after treatment with insulin. The anticipated outcome of the study is a set of confirmed genes that are regulated by an epigenetic mechanism, methylation. The functional role(s) of these genes in the development of

diabetic retinopathy can be addressed in future studies.

### **Principal Investigator**

Willard M. Freeman, PhD  
Assistant Professor  
Dept. of Pharmacology  
Penn State University College of Medicine  
500 University Drive, R130  
Hershey PA 17033

### **Other Participating Researchers**

Sarah K. Bronson, PhD, Melissa Bridi, Georgina Bixler – employed by Pennsylvania State University

### **Expected Research Outcomes and Benefits**

This project will allow us to incorporate an additional experimental group that will allow us to query the impact of sustained exposure to the diabetic state; permit validation of discovery findings by bisulfite sequencing and qPCR; and permit assessment of the functional consequences of the validated changes by measuring gene expression by qPCR. The deliverables of the experiments will be a demonstration of differential retinal DNA methylation in response to diabetes that is normalized with insulin treatment from the onset but is not normalized by later insulin treatment and that corresponds to altered gene expression. A possible benefit for diabetic patients is an increased understanding of how diabetic complications develop and the consequences of suboptimal blood glucose control. While this project will not directly test new therapies for diabetic retinopathy, defining a role for epigenetic mechanisms in diabetic retinopathy and other diabetic complications opens the door to new treatments that target this novel mechanism.

### **Summary of Research Completed**

For the reporting period the research completed falls into three major categories.

- 1) Characterization of metabolic memory prototypical retinal transcriptomic and proteomic changes.
- 2) Integrative analysis of transcriptomic and epigenetic alterations in DNA methylation levels with diabetes.
- 3) Grants submitted

Two reports of our work investigating metabolic memory prototypical retinal transcriptomic and proteomic changes were published in the past six months. In the first report:

VanGuilder HD, Bixler GV, Kutzler L, Brucklacher RM, Bronson SK, Kimball SR, Freeman WM. Multi-modal proteomic analysis of retinal protein expression alterations in a rat model of

diabetic retinopathy. PLoS One. 2011 Jan 13;6(1):e16271.

We extended on our previously reported duration-dependent changes in retinal vascular permeability, apoptosis, and mRNA expression with diabetes. The aim of this study was to identify retinal proteomic alterations associated with functional dysregulation of the diabetic retina to better understand diabetic retinopathy pathogenesis and that could potentially be used as surrogate endpoints in preclinical drug testing studies. A multi-modal proteomic approach of antibody (Luminex)-, electrophoresis (DIGE)-, and LC-MS (iTRAQ)-based quantitation methods was used to maximize coverage of the retinal proteome (Figure 1). Transcriptomic profiling through microarray analysis was included to identify additional targets and assess potential regulation of protein expression changes at the mRNA level. The proteomic approaches proved complementary, with limited overlap in proteomic coverage. Alterations in pro-inflammatory, signaling and crystallin family proteins were confirmed by orthogonal methods in multiple independent animal cohorts. In an independent experiment, insulin replacement therapy normalized the expression of some proteins (Dbi, Anxa5) while other proteins (Cp, Cryba3, Lgals3, Stat3) were only partially normalized and Fgf2 and Crybb2 expression remained elevated. These results expand the understanding of the changes in retinal protein expression occurring with diabetes and their responsiveness to normalization of blood glucose through insulin therapy. These proteins, especially those not normalized by insulin therapy, may also be useful in preclinical drug development studies, and are indicative of metabolic memory and the inability of restoring normoglycemia to correct all of the retinal molecular and biochemical changes that occur with a period of hyperglycemia.

In our next report:

Bixler GV, Vanguilder HD, Brucklacher RM, Kimball SR, Bronson SK, Freeman WM. Chronic insulin treatment of diabetes does not fully normalize alterations in the retinal transcriptome. BMC Med Genomics. 2011 May 15;4:40.

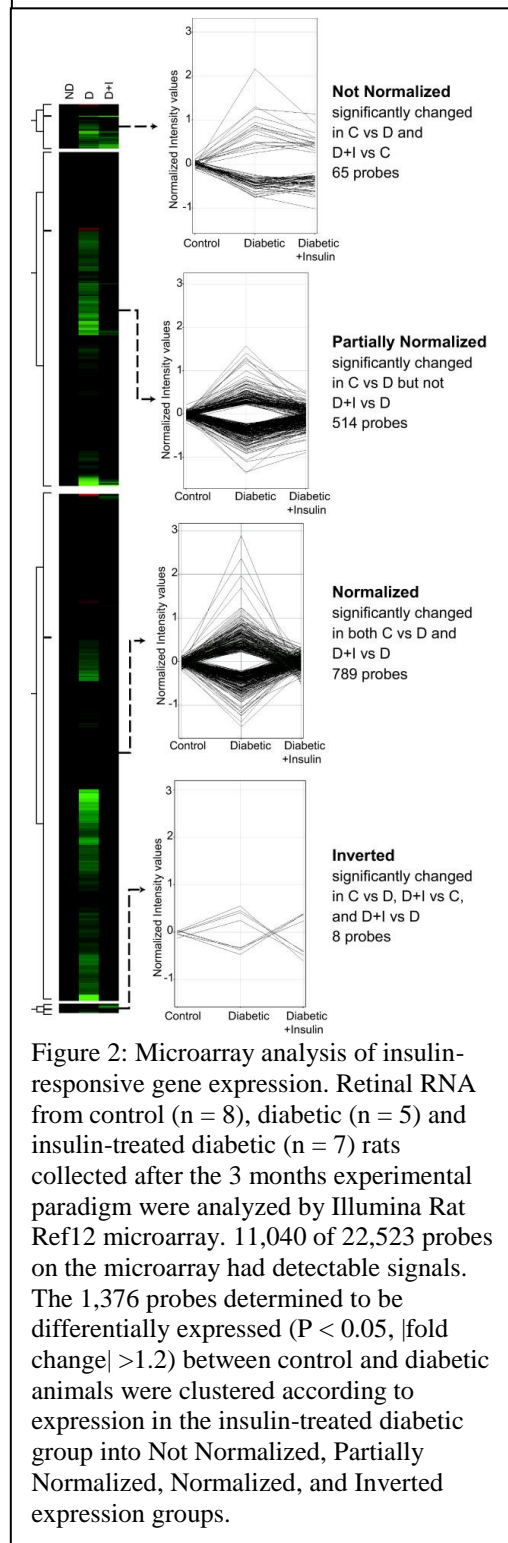
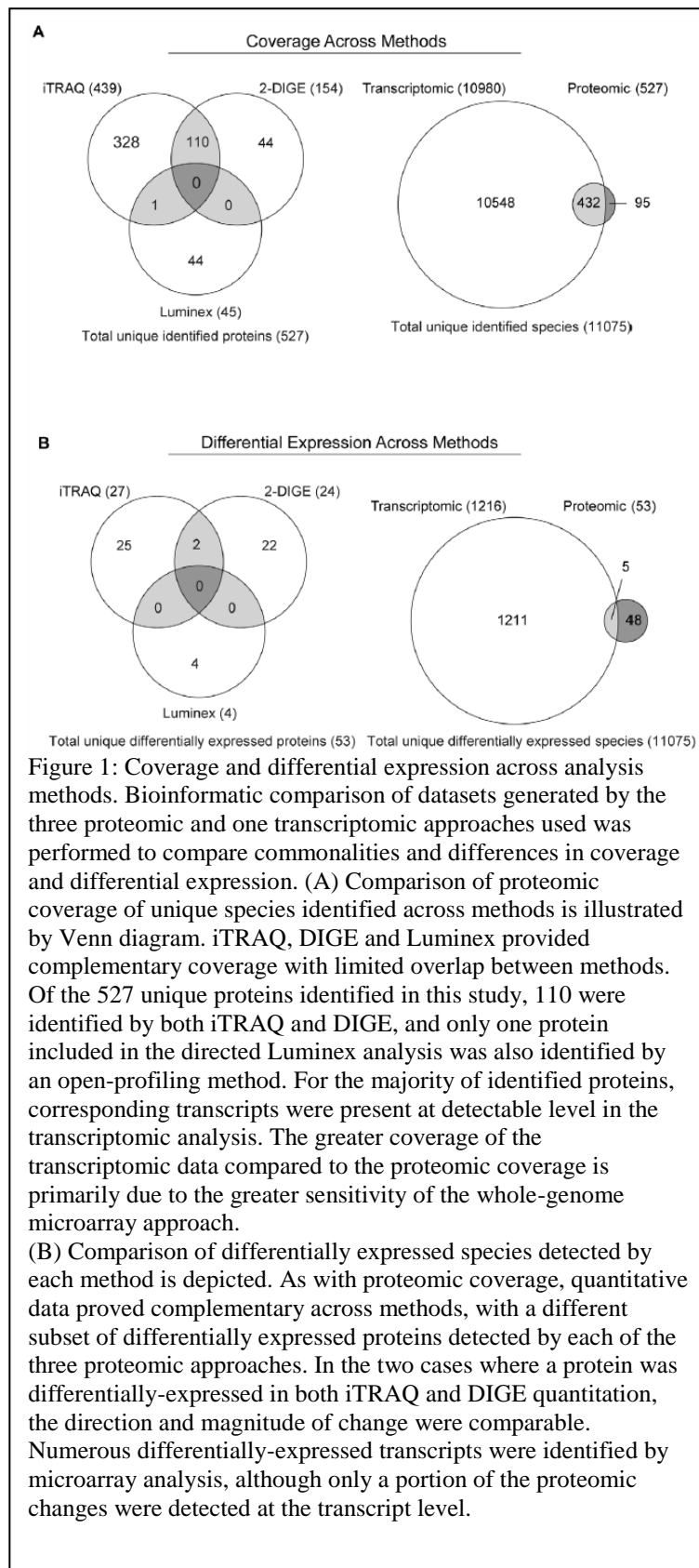
We identified, on a genome-wide scale, the molecular changes in the rodent retina induced by diabetes that are not normalized by insulin replacement and restoration of euglycemia. The retina transcriptome (22,523 genes and transcript variants) was examined after three months of streptozotocin-induced diabetes with and without insulin replacement for the later one and a half months of diabetes. Selected gene expression changes were confirmed by qPCR, and also examined in independent control and diabetic rats at a one month time-point. Transcriptomic alterations in response to diabetes (1376 probes) were clustered according to insulin responsiveness (Figure 2). More than half (57%) of diabetes-induced mRNA changes (789 probes) observed at three months were fully normalized to control levels with insulin therapy, while 37% of probes (514) were only partially normalized. A small set of genes (5%, 65 probes) was significantly dysregulated in the insulin-treated diabetic rats. qPCR confirmation of findings and examination of a one month time point allowed genes to be further categorized as prevented or rescued with insulin therapy. A subset of genes (Ccr5, Jak3, Litaf) was confirmed at the level of protein expression, with protein levels recapitulating changes in mRNA expression. These results provide the first genome-wide examination of the effects of insulin therapy on retinal gene expression changes with diabetes. While insulin clearly normalizes the majority of genes dysregulated in response to diabetes, a number of genes related to inflammatory processes,

microvascular integrity, and neuronal function are still altered in expression with restoration of euglycemia (Figure 3). Gene expression changes not rescued or prevented by insulin treatment may be critical to the pathogenesis of diabetic retinopathy, as it occurs in diabetic patients receiving insulin replacement, and are prototypical of metabolic memory.

Continuing on with this work, we have generated whole genome gene expression data for the same Ins2 Akita animals as our previous DNA methylation analyses (Figure 4). Having paired mRNA and DNA methylation data from the same animals will allow us to not only examine differential DNA methylation and its potential effects on mRNA expression but to also ask fundamental questions about the regulation of gene expression by DNA methylation levels. For example, we will be able to correlate the impact of the distance from the transcription start site on gene expression. These bioinformatics analyses are currently underway.

Additionally, we have been optimizing methods to perform cell-specific epigenetic and transcriptomic analyses. The advantage of this approach will be that changes in mRNA or DNA methylation will be isolated to specific cell type and there is also the potential to identify changes obscured in the whole retinal analysis. In the first study we used a retinal digestion and immune-capture approach to specifically isolate retinal endothelial cells (CD31+) from non-endothelial cells (CD31-). Specificity of isolation was confirmed by measurement of gene expression for endothelial, neuronal and microglial markers (Figure 5).

As this research has progressed we have also submitted federal and foundation proposals for additional funding. Currently proposals to the Juvenile Diabetes Research Foundation, American Diabetes Association, and National Eye Institutes (National Institutes of Health) are in review and we expect funding decisions this Fall.



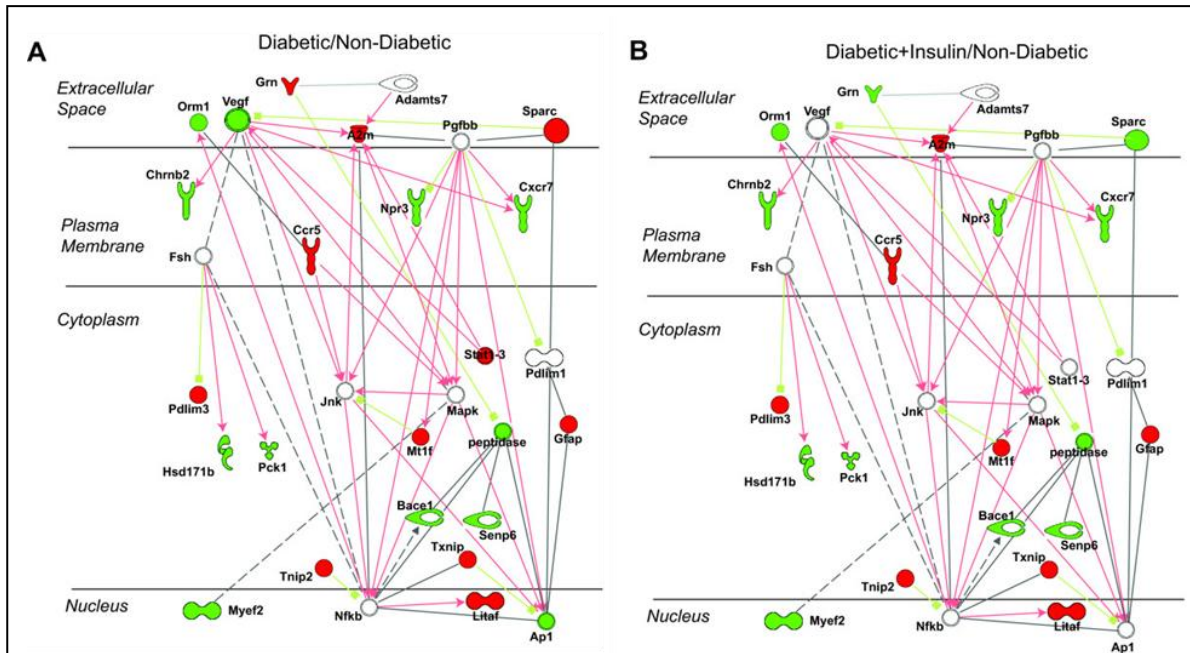
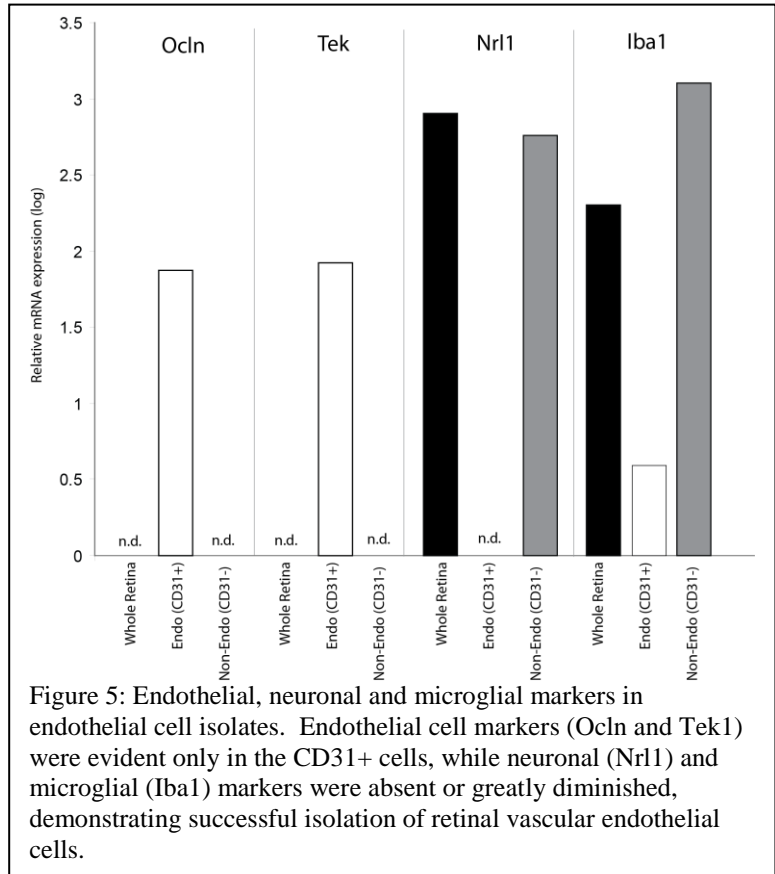
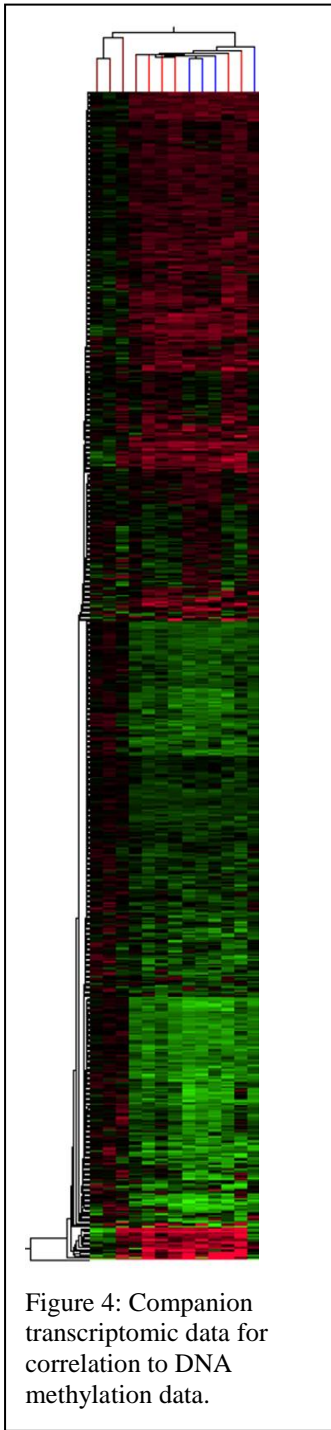


Figure 3: Network analysis of genes Not Normalized. Genes and expression values from the Not Normalized category were examined for networks of interrelated genes using Ingenuity Pathway Analysis software. One significant network was centered on Pdgf, Nfkb, and Jnk. Expression values for the control versus diabetic groups are presented in A and for the insulin-treated diabetic versus diabetic comparison in B. Relationships are presented as lines and arrows. Red lines represent activation or positive regulation of expression while green lines indicate inhibition or negative regulation of expression. Grey lines are known protein-protein interactions and dashed lines are indirect relationships. Gene symbols are coded as green for significantly reduced expression, red for significantly increased expression, and white for no change in expression



## **Research Project 26: Project Title and Purpose**

*Transplantation of Human Retinal Pigment Epithelial Cells (RPECs) in the Nucleus Accumbens of Rats* – The purpose of this research project is to determine, preclinically, whether rats with a history of cocaine self-administration can be rescued from the grips of this disease with focal bilateral transplant of 20 or 30 K/side of L-dopa producing fetal human (fh) Retinal Pigment Epithelial Cells (RPECs) into the nucleus accumbens. The potential effectiveness of the transplant in preventing relapse will be examined following 14, 30, and 60 days of abstinence. Given that transplant of these cells already is in Phase II Clinical Trials as a potential treatment for Parkinson's Disease, the long-term objective is to determine whether such a transplant into the reward, rather than the motor, pathway is a viable option for the treatment of addiction in humans.

### **Anticipated Duration of Project**

9/1/2010 - 6/30/2012

### **Project Overview**

Millions of Americans are addicted to drugs and alcohol. There is no cure and 90% of all addicts will relapse, most more than once. Addiction, however, is not a disease of will, but a disease of the brain. Studies show that chronic exposure to drugs and alcohol leads to damage to dopaminergic neurons in the 'reward pathway' that projects from the ventral tegmental area (VTA) to the nucleus accumbens (NAc) and this damage is thought to contribute to, if not to mediate, the signature symptom of addiction: chronic relapse. In a preliminary study, we found that a single transplant of 20K/side levodopa (L-dopa) producing retinal pigment epithelial cells (fhRPECs) into the medial shell of the NAc rescued drug-experienced rats from reinstatement of cocaine-seeking. This effect was quite striking when tested following 14 days of abstinence. The effect, however, needs to be replicated. In addition, given the chronic nature of the disease, we must examine whether the transplant also is effective at a later time point (e.g., after 30 or 60 days of abstinence). Finally, while we obtained effectiveness with a transplant of 20K RPECs/side, we think it important at this early juncture to examine the effectiveness of a larger transplant (i.e., 30K/side), particularly since we will be challenging the effectiveness of the transplant at longer time points after drug exposure. If a dose response is critical, this would be vital to determine as either underdosing or overdosing could be potentially deleterious to obtaining efficacious results in cocaine addiction. Such a dose response has been seen in many other transplant situations including Parkinson's Disease where a threshold dose is necessary to see benefits. *Specific Aim 1*, then, will use rats to test whether a transplant of 20K or 30K fhRPECs into the nucleus accumbens will prevent reinstatement following 14, 30, or 60 days of abstinence. *Specific Aim 2* will use instrumental responding for water to rule out a motor impairment and instrumental responding for sucrose to rule out a general motivational deficit. Finally, *Specific Aim 3* will use high performance liquid chromatography (HPLC) and tyrosine hydroxylase staining to test the hypothesis that increases in dopamine mediate the protective effects of the transplant. Addiction afflicts millions of Americans, costs hundreds of billions of dollars/year, and is a devastating life-long illness. Rescue of the drug-damaged reward pathway via fhRPEC transplant holds great promise as a novel potential therapeutic intervention.

## **Principal Investigator**

Patricia Sue Grigson, PhD  
Professor  
Neural and Behavioral Science Department  
Penn State University College of Medicine  
500 University Drive, MC H109  
Hershey, PA 17033

## **Other Participating Researchers**

Thyagarajan Subramanian, MD, Kala Venkiteswaren, PhD, Anand Rao, BS, Danielle Alexander, BA – employed by Pennsylvania State University

## **Expected Research Outcomes and Benefits**

In accordance with the preliminary data, transplant of either 20K or 30K fhRPECs into the NAc shell is expected to rescue rats with a history of high cocaine self-administration behavior. These rats are expected to make fewer infusion attempts and to exhibit less goal-directed behavior during extinction testing. The rats also are expected to be less willing to work for cocaine when tested on the progressive ratio schedule of reinforcement. Given the data showing that these fhRPeC xenotransplants are intact and functional at 18 months in parkinsonian animal models, including Sprague-Dawley rat models, we hypothesize that the protective effect of the 20K and 30K transplant also will be evident even at 30 and 60 days. We predict that the effect will be selective for drug-seeking and drug-taking behavior. Thus, transplanted rats will have no difficulty working for water or for a sweet. Overall, the effect is expected to be even more robust in rats receiving the 30K transplant. Finally, we predict that, like the dorsal striatum transplant with fhRPEC, the graft will be viable when assessed histologically out to our 60 d time point and it will be contained within the NAc shell. We expect upregulation of dopamine in the tissue punches that contain fhRPEC grafts and the NAc targets to be specific. If these hypotheses are confirmed, the results will provide the first evidence that rats with a history of high cocaine self-administration can be rescued via fhRPEC transplant from drug-seeking and drug-taking following an extended period of abstinence. This could lead to a translational effort to discover similar treatment strategies for drug addiction using focused cell transplants, including regulatable gene expression.

## **Summary of Research Completed**

In comparison to the myriad of studies designed to treat Parkinsonian symptoms with dopaminergic transplants of one sort or another, we are not aware of any cell transplantation experiments to ‘treat’ addiction. In the first replication of this study (described in our Strategic Plan), we found that bilateral transplants of fhRPEC into the medial shell and/or core of NAc rescue rats with a history of cocaine self-administration from drug-seeking when returned, after 2 weeks abstinence, to the drug-associated chamber under extinction conditions (i.e., no drug available). Thus, rats with a history of high cocaine self-administration, that received RPEC

transplants, exhibited the same degree of seeking for drug (i.e., relapse) as did rats with a history of low cocaine self-administration. The RPEC transplant, then, appeared highly protective.

Since this time, we have conducted 2 full replications of the study. This is a huge study, involving nearly all personnel of both the Grigson and the Subramanian laboratory. Unfortunately, on each occasion, for various reasons, we have failed to replicate the data because the transplants were placed outside of the target site. We have, then, planned a final replication to be completed in the Fall semester of 2011.

That said, we have successfully produced very interesting histological data. Histology was conducted on 75% of the rats that received a RPEC transplant (25% were saved for dopamine analysis) and the transplants were found to be located in the shell and/or the core of the NAc in both sides in all transplanted animals that had behavioral recovery from cocaine “addiction” (a representative coronal section stained with cresyl violet through the NAc is shown in Figure 1 below). Rats that received only unilateral accurate grafts did not appear to have behavioral benefits. Interestingly, in the last replication experiment, an equal number of animals transplanted with empty beads showed behavioral improvement making the statistics insignificant. We are using careful histology to investigate why such “control” animals had behavioral benefits.

Examination of the graft sites using tyrosine hydroxylase (TH) and dopa decarboxylase (DDC) also provides supportive preliminary data to these observations. We have thus far examined four RPEC transplanted rats and four vehicle rats and in all 4 RPEC transplanted rats, grafts in the NAc shell were visible. Figure 2 used unbiased stereology to show the percentage of change of TH positive cell bodies summed across the left and right VTA. Total counts for the VTA for cocaine inexperienced rats (n=2) was as predicted a mean 40,000 cells as reported in the literature. In comparison cocaine experienced rats that received the empty microcarrier vehicle transplant (Vehicle Only, n=3), showed a significant reduction (40%) in dopaminergic neurons. Cocaine experienced rats that received bilateral RPEC transplants (n=2) showed improved VTA TH cell counts (~25% reduction compared to 40% in vehicle treated animals) that was statistically significant for >5% in each VTA (2x6 versus 2x4), fisher exact test at p=0.03. These preliminary data suggest that there may be benefits to RPEC graft placement into the NAc.

We also noticed that when the graft was inserted into the NAc shell that the shell would stain much darker for TH. Moreover, the shell stained much darker than the shells of rats without RPEC transplants (see examples in Figures 3, 4, and 5). To see whether or not these observations were true, we used densitometry to find out which sections had a more intense TH staining. In this software, the higher the intensity of TH staining, the lower the optical density (OD) registered. As is evident from the data (see Table 1), the RPEC transplanted rats have significantly lower numbers than the rats without the transplant, *proving that RPEC does increase the TH levels in the NAc shell—implying that RPEC transplants effect the first step of dopamine production: turning L-tyrosine to levadopa*. This finding further supports our observation that VTA neuronal number for TH positive cells is upregulated in animals that received RPEC grafts as VTA neurons provide the axons in the NAc that supply the dopamine.

Another interesting trend we noticed in the DDC staining was that the total volume of the NAc

core that stains for DDC appeared to be more in vehicle treated rats compared to RPEC treated rats. To prove this observation we used unbiased Cavalari technique of stereology. These results are shown below (see Figure 6). This surprising finding suggests that vehicle treated rats have upregulation of DDC in the NAc core that is prevented by RPEC grafting into the NAc. *This finding could putatively explain the behavioral recovery noted in vehicle treated animals and suggests that there is a natural compensatory upregulation of DDC expression in some of these cocaine treated animals. Further, the lack of upregulation of DDC in the NAc core in RPEC grafted animals supports the notion that RPEC provides L-dopa locally into the NAc negating the need for upregulating DDC expression.*

The most likely explanation of the beneficial effects of NAc grafts on the TH positive neurons in the VTA is via the retrograde transport of beneficial trophic factors secreted by the RPEC via the remaining intact VTA-NAc axons and their neuritic processes. One such trophic factor secreted by RPEC is PEDF. The local effects in the NAc shell for TH immunostaining can also be attributed to potential secretion of growth factors by the RPEC grafts. Finally, the down regulation of DDC expression in animals that got RPEC grafts suggests that functional RPEC grafts actually ameliorate the dopamine deficit in cocaine “addicted” rats.

Additional studies are underway to investigate thoroughly these preliminary observations, quantify them and to investigate why the “empty bead” treated animals showed beneficial behavioral effects to the same extent as the “RPEC” treated group in the third cohort.

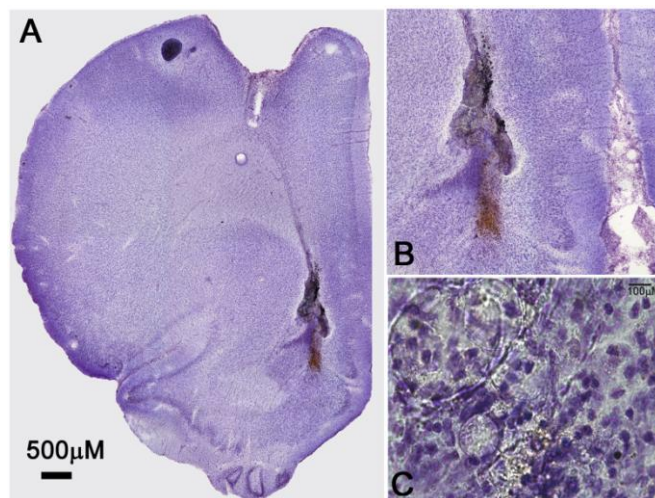


**Figure 1 Histology.** A. Representative coronal section stained with cresyl violet through the NAc in a rat that received RPEC transplants showing accurate placement of the graft into the NAc shell. Note the needle tract and the entry wound in the cortex. B. High power view of graft site with the collagen beads. C. Details of the graft showing viable large brownish purple cells attached to the bead matrix (round profiles). The brown color is due to the melanin pigment in these RPEC cells.

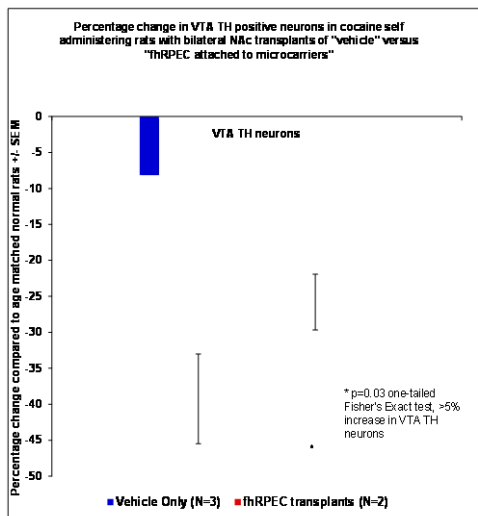


**Figure 2 Unbiased Stereology.** Percentage of change from design based unbiased stereology of TH positive cell bodies summed across the left and right VTA. Total counts for the VTA for cocaine inexperienced rats (n=2) was as predicted a mean 40,000 cells as reported in the literature. In comparison cocaine experienced rats that received the empty microcarrier vehicle transplant (Vehicle Only, n=3), showed a significant reduction (40%) in dopaminergic neurons. Cocaine experienced rats that received bilateral RPEC transplants (n=2) showed improved VTA TH cell counts (~25% reduction compared to 40% in vehicle treated animals) that was statistically significant for >5% in each VTA (2x6 versus 2x4), fisher exact test at p=0.03. This preliminary data suggest that there may be benefits to RPEC graft placement into the NAc.



10-G294: Graft enters right NAc shell  
Figure 3



10-G272: Graft enters left NAc shell  
Figure 4

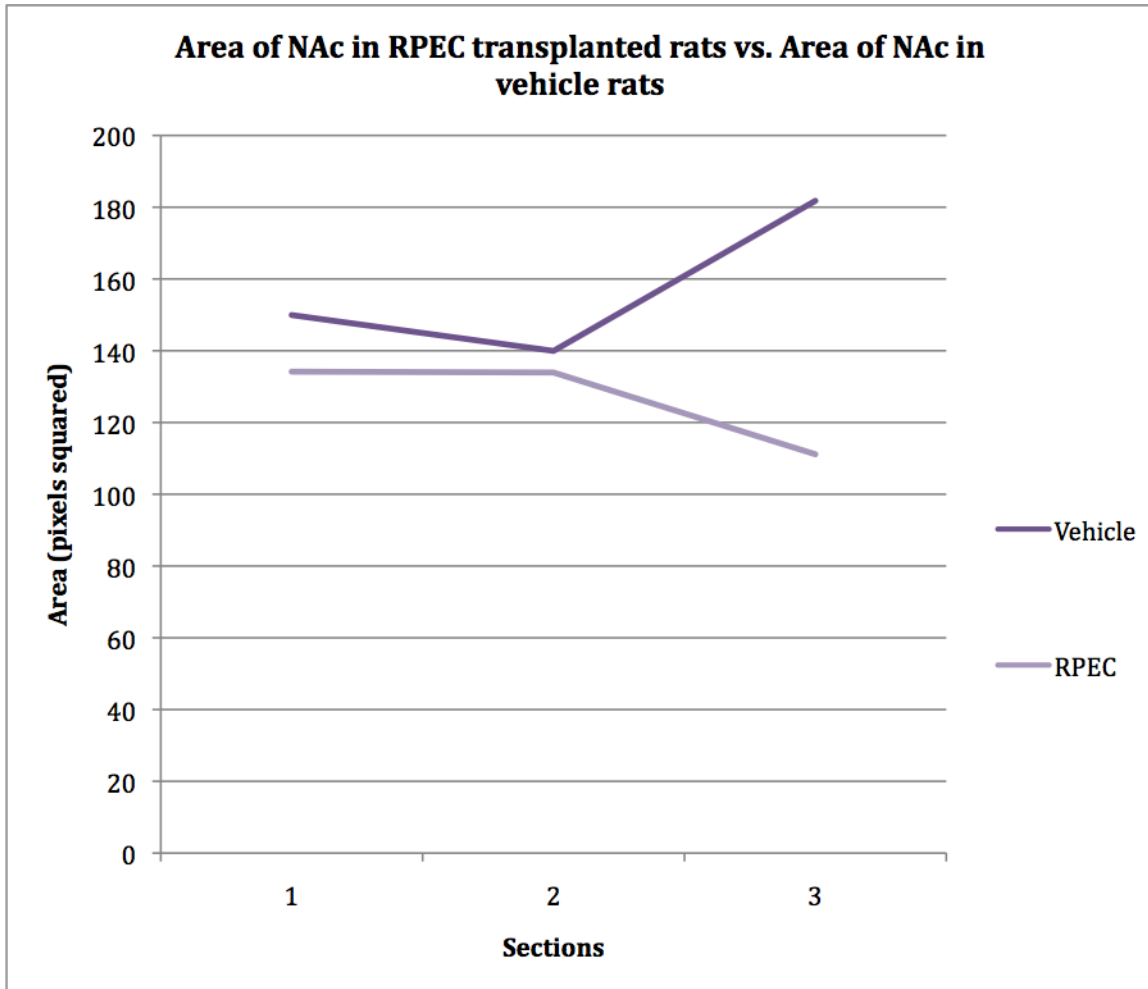


10-G253: Graft enters left NAc shell  
Figure 5

Table 1.

Rat Name	Type	Optical Density Units
10-G294	RPEC	134.178
10-G272	RPEC	133.936
10-G253	RPEC	111.140
10-G257	Vehicle	149.951
10-G263	Vehicle	139.950
10-G296	Vehicle	181.78

Figure 6



Average Area of NAc in RPEC (pixels <sup>2</sup> )	Average Area of NAc in Vehicle (pixels <sup>2</sup> )
466271.364	717100.22

## **Research Project 27: Project Title and Purpose**

*Interrogating the Role of Myoepithelial Cells in Mammary Carcinogenesis* – Breast cancers arise from mammary epithelial cells (MECs). Two distinct MEC compartments have been defined which occupy concentric layers in normal mammary ducts. An inner luminal MEC layer harbors milk-producing cells whereas an outer myoepithelial cell layer forms a contractile sheath that aids milk expulsion. The role of myoepithelial cells in breast carcinogenesis remains poorly defined. Some findings suggest that myoepithelial cells can themselves be transformed into cancer cells. Other findings suggest that normal myoepithelial cells protect against cancer by providing a barrier against luminal MEC invasion. By using novel transgenic mouse models, we will test whether myoepithelial cells promote or inhibit carcinogenesis. These studies will define whether prevention strategies ought to maximize or minimize myoepithelial cell number.

### **Anticipated Duration of Project**

7/1/2011 - 6/30/2012

### **Project Overview**

How basally-located mammary epithelial cells (MECs) participate in breast carcinogenesis remains unknown. It has been proposed that basal-type breast cancers may arise from basal MECs of the myoepithelial lineage, but the susceptibility of basal MECs to carcinogenesis remains poorly defined. Mouse models of breast cancer offer little insight into this question, as nearly all transgenic mammary tumorigenesis models rely on promoters that drive oncogene expression in a largely luminal MEC-restricted manner. Alternatively, basal MECs have been proposed to have a tumor suppressor role. Specifically, tumor cell non-autonomous changes in the microenvironment (e.g., loss of either basal MECs or a critical basal MEC function) may be essential for disruption of tissue architecture and the transition to an invasive breast cancer. Indirect support for this concept comes from studies showing that normal myoepithelial cells suppress malignant traits when propagated together with breast cancer cell lines in coculture experiments and xenograft studies. However, no studies to date have examined whether dropout of normal MECs directly triggers an invasive transition within neighboring mammary neoplasia. To interrogate the role of basal MECs in mammary carcinogenesis, we have designed novel transgenic mouse models that permit oncogene activation and cell ablation in an MEC compartment-restricted manner. These models will be used to explore the role of basal MECs in malignant transformation by completing the following aims:

Aim 1. Compare the cell fate changes initiated in basal versus luminal MECs upon oncogene activation in 3D organotypic culture.

Aim 2. Develop an inducible cell ablation strategy for testing whether normal MECs suppress malignant traits in neighboring cells.

## **Principal Investigator**

Edward J. Gunther, PhD  
Associate Professor of Medicine  
Penn State University College of Medicine  
Biomedical Research Building, H059  
500 University Drive  
Hershey, PA 17033

## **Other Participating Researchers**

Shelley A. Gestl, MS – employed by Pennsylvania State University

## **Expected Research Outcomes and Benefits**

The project is designed to clarify the role of myoepithelial cells in breast carcinogenesis. There is no consensus in the fields of mammary gland developmental biology and breast tumor biology as to whether myoepithelial cells contribute to, or protect against, the development of breast cancer. This knowledge gap has enormous clinical implications because researchers focused on breast cancer prevention have alternatively proposed strategies aimed at preserving or depleting the myoepithelial cell population in patients. The first aim of the project is to test the degree to which myoepithelial cells are susceptible to cancer-causing oncogenes. Mammary tissue derived from novel transgenic mouse models will be propagated in culture systems that permit oncogene expression to be restricted to either luminal cells or basal myoepithelial cells. By comparing the impact of oncogene expression in each cell type, we will gather data that will help discern whether myoepithelial cells are credible candidates for the cell of origin of breast cancers. Conversely, the second aim of the proposed research will explore whether myoepithelial cells are capable of suppressing the development of breast cancer in live mice. For these studies, transgenic mice were engineered to permit myoepithelial cells ablation within intact mammary glands. This experimental model will permit the first prospective test of whether myoepithelial cells serve a tumor suppressor function. Together, these research aims will provide information critical for the rational design of breast cancer chemoprevention strategies.

## **Summary of Research Completed**

The research has not yet started. The start of the research has been delayed by an unexpected disruption that hampered fertility within our transgenic mouse breeder colony for several months. The breeding disruption appears to be related to noise and vibrations associated with a construction project near our animal facility. Following completion of the construction project, we have begun to see a return to normal breeding patterns in our mouse colony. We expect to be capable of generating experimental mice in 10-12 weeks.

## **Research Project 28: Project Title and Purpose**

*Outcomes for Recurrent Thyroid Cancer in the Elderly* – The purpose of this project is to identify factors associated with variation in treatment for thyroid cancers in the Medicare

population, to estimate the impact of different treatments on cost of medical care for patients with recurrent thyroid carcinomas, controlling for tumor features, demographic characteristics, and co-morbid conditions, and to assess the impact of different treatments on overall and disease-free survival for patients with recurrent carcinomas. Results will inform and guide physicians as they consider treatment recommendations for individual patients and policy makers as they develop and refine treatment guidelines for Medicare patients. In addition, while these aims deal with recurrent thyroid cancer, the broader issues of treatment specific costs and effectiveness are also relevant for other cancers.

### **Anticipated Duration of Project**

9/1/2010 - 9/30/2011

### **Project Overview**

Objectives: Over the past 20 years the incidence of thyroid cancer has doubled to approximately 24,000 new cases diagnosed yearly. Despite the excellent prognosis of thyroid cancer in which the proportion of deaths has remained relatively constant over time, recurrence of thyroid carcinomas is not unusual. The objective of this project is to address deficiencies in the knowledge base about treatment outcomes for recurrent thyroid cancers. The research will lead to an understanding of the factors associated with variation in treatment, the costs of different treatments, the clinical outcomes of different treatments, and the relative value of alternative interventions. Specific Aims: 1) To identify factors associated with variation in treatment for thyroid cancers in the Medicare population, 2) To estimate the impact of different treatments on cost of medical care for patients with recurrent thyroid carcinomas, controlling for tumor features, demographic characteristics, and co-morbid conditions, and 3) To estimate the impact of different treatments on overall and disease-free survival for patients with recurrent carcinomas. Research Design: All information obtained and analyses performed will utilize the National Cancer Institute's Surveillance, Epidemiology, and End Results (SEER)-Medicare linked database, which has collected standardized data, covering approximately 14% of the U.S. population, from a number of population-based registries since 1973. The data that will be used include thyroid cancer diagnoses from 1986-2005 and their associated billing records that are available from 1986 to 2008. To achieve *Specific Aim 1* the univariate associations between thyroid cancer treatment and candidate predictor variables such as age categories, gender, stage, and co-morbidities will be analyzed. In *Specific Aim 2* we will first compute one-, two-, and five-year total costs for each patient. Costs will be defined as total Medicare payments. To estimate one-, two- and five-year costs a consistent estimator of the survivor function is obtained. This will be done using the Kaplan-Meier product limit method. Second, the average costs incurred on each day is estimated for patients who are at risk (that is, not censored). Finally, the sum of the product of these terms yields a consistent estimate of average cumulative costs. In *Specific Aim 3* we will perform survival analyses of patient survival and tumor free survival among patients with recurrent disease using the Kaplan-Meier method. Survivor functions will be stratified by treatment and comparisons will be made using the log rank test. We will then estimate survivor functions using the Cox proportional hazard model to control for demographic characteristics, tumor features, and co-morbidities.

## **Principal Investigator**

Christopher S. Hollenbeak, PhD  
Associate Professor of Surgery and Public Health Sciences  
Department of Surgery  
Penn State University College of Medicine  
600 Centerview Drive, A210  
Hershey, PA 17033

## **Other Participating Researchers**

David Goldenberg, MD, Melissa M. Boltz, DO, Eric Schaefer, MS – employed by Pennsylvania State University

## **Expected Research Outcomes and Benefits**

Approximately half of the 24,000 patients diagnosed with thyroid cancer yearly who develop recurrent thyroid cancer succumb to the disease. Thyroid cancers can affect the most basic and complex human functions, including breathing, swallowing, and communication. Treatment options depend upon tumor features, overall health of the patient, and patient and physician preferences. For thyroid cancer, little is known about recurrent disease, including risk factors, types of surgery performed and use of radioactive iodine therapy, as well as the public expenditures for treating recurrent disease.

We expect that with our research results we will be able to provide important information to clinical and health policy decision makers. So little is known about recurrent thyroid disease that much decision making is not made based on a solid foundation of evidence. Our results will show what factors are associated with treatment for thyroid cancer; what factors contribute to costs of thyroid cancer, including recurrent disease; and how outcomes for recurrent disease differ from other forms of thyroid cancer. This study is possible because of the linkage between the SEER cancer registry and the Medicare billing data. The billing data allow us to identify recurrence, albeit imperfectly, through the use of specific resource utilization. The linkage between these two data sets also allows us to estimate costs, which can facilitate cost-effectiveness and other forms of comparative effectiveness research for treatments.

## **Summary of Research Completed**

To date, we have completed two manuscripts that address the specific aims of the study. The first study focuses on estimating the rates of recurrence for thyroid cancer and the outcomes implications of recurrence, and the second manuscript estimates the cost of care associated with treatment choice and recurrence.

### *Introduction*

Although long-term survival of patients with well-differentiated thyroid cancer (WDTC) is common, little is known about the risk of tumor recurrence. We used data from the Surveillance Epidemiology and End Results-Medicare linked database to estimate the incidence of and

identify risk factors associated with recurrent thyroid cancer, and to assess the impact of recurrence on mortality as well as cost up to five years following diagnosis.

### *Methods*

Data: Data for this study were from the SEER-Medicare linked data of the National Cancer Institute (NCI). The SEER program is a national tumor registry that collects data on approximately 26% of the US population, and reports cancer incidence and survival in the United States. The SEER-Medicare linked data contains the subset of Medicare enrollees in the SEER registry. It then links these patients to all Medicare claims records. Thus, using the Medicare billing claims data it is possible to identify specific types of resource utilization in the combined SEER-Medicare data. Our analysis was limited to Medicare enrollees (65 years and older) diagnosed with a single primary thyroid cancer (papillary or follicular) between 1995 and 2007. A recurrence was considered if the patient had evidence of iodine-131, imaging for metastatic thyroid carcinoma, or completion thyroidectomy beyond one month of diagnosis.

Costs: The cost analyses take the perspective of Medicare as payer and represent actual payments made by Medicare for all-cause treatment of patients. All costs were adjusted for inflation to year 2009 dollars. We studied the impact of demographic and disease characteristics, comorbidities, and treatment choice on 1-year and 5-year costs.

### Statistical Analysis

*(Manuscript 1):* The statistical analysis was designed to identify risk factors for recurrent thyroid cancer in the SEER population, and estimate the impact of recurrence on cancer-specific and all-cause mortality, controlling for other patient and disease characteristics that may also impact survival. Summary statistics for patient characteristics, cancer stage, histology, and treatment were presented, and differences stratified by recurrence were compared using Student's *t*-test for continuous variables and chi-square tests for binary and categorical variables. Survivor functions were estimated using the Kaplan-Meier product limit method, with differences between strata compared using the log rank test. Multivariate analyses of survival were performed using Cox proportional hazards models. These models estimated the hazard (or point-in-time risk) of death due to recurrent thyroid cancer, controlling for the age, gender, ethnicity, location of residence, stage, histology, and treatment. Separate proportional hazards models were fit for cancer-specific mortality and all-cause mortality.

*(Manuscript 2):* Patients in the SEER-Medicare data have variable follow-up. Therefore, the approach to estimating costs at one year and five years was a method proposed by Bang and Tsiatis, which accounts for variable follow-up and patient censoring. This approach estimates costs for each patient at regular time intervals (monthly costs) and weights those estimates by the inverse of the probability that the patient is not censored. Bang and Tsiatis recommend a nonparametric estimator of the inverse probability. This is obtained from a Kaplan-Meier estimator of time to censoring. Using 60 monthly observation periods we weighted the monthly costs for each patient that was uncensored by the inverse probability, and then summed the weighted costs up to twelve months to estimate one-year average cumulative costs, and up to 60 months to estimate five-year average cumulative costs. This was done separately for thyroid cancer cases and comparison group patients. Multivariate analysis was performed using the approach suggested by Lin. Using this approach, each of the 60 monthly costs were fit to a linear model, where covariates included patient, disease, treatment, and recurrence variables.

Coefficients for months one through twelve were summed to give marginal effects of covariates on one-year costs; coefficients for months one through sixty were summed to give marginal effects on five-year costs. Ninety-five percent confidence intervals were obtained from 1,000 bootstrap replicates.

### *Results*

Manuscript 1: Using data from the SEER database 4,969 patients were identified with either primary papillary or follicular thyroid cancer between 1995 and 2007. Of this group 1,304 patients developed recurrence according to our measure (26.2%). Characteristics of patients stratified by recurrence shows that these groups were similar in demographic characteristics such as age ( $p = 0.51$ ), gender ( $p = 0.09$ ), and race ( $p = 0.23$ ). Recurrence was observed in 1,304 (26.2%) of the 4,969 patients in the cohort. Older patients (hazard ratio [HR]=1.03,  $p<0.0001$ ) with regional (HR=1.52,  $p<0.0001$ ) or distant metastases (HR=2.30,  $p<0.0001$ ) were at greater risk for developing recurrent disease. Follicular histology (HR=0.71,  $p<0.0001$ ) was associated with lower risk for recurrence. Patients with a recurrence were significantly less likely to die from cancer (HR=0.64;  $p<0.0001$ ) than patients with no recurrence. They were also less likely to die from any cause (HR=0.72;  $p<0.0001$ ) (Figure 1).

To our knowledge, this study represents the largest series of recurrent well differentiated thyroid cancer in the elderly Medicare population. The most important departure from the literature in our findings was that patients with recurrence were less likely to die—either from cancer or from any cause—than patients without a recurrence. There are several possible explanations for this finding. First, it may call into question the use of billing data to identify recurrence. However, the specific procedures we used to identify recurrence are rarely used outside the context of a recurrence. Furthermore, the fact that the rates of recurrence both in the aggregate and for specific histologies was so similar to previous studies, lends face validity to our billing code proxy. The most likely explanation is that recurrence and mortality are competing risks that are more important in an older population. Some time is required for micrometastases to grow into full-blown recurrence. In a younger population where thyroid cancer is seen most often, it would be rare for a patient not to outlive the recurrence. However, in a study population whose average age is 73, this may not be the case. We suspect that many elderly patients in our population are not living long enough for recurrence to become a reality. Recurrence, then, in the elderly population becomes an indicator that a patient has survived longer. The longer survival observed among the population who recurred does not suggest that recurrence contributed to survival, but rather it is an indicator of a patient who would or who has survived longer independent of the recurrence. These results have been accepted in abstract form for presentation at the American College of Surgeons 97<sup>th</sup> Annual Clinical Congress in October 2011.

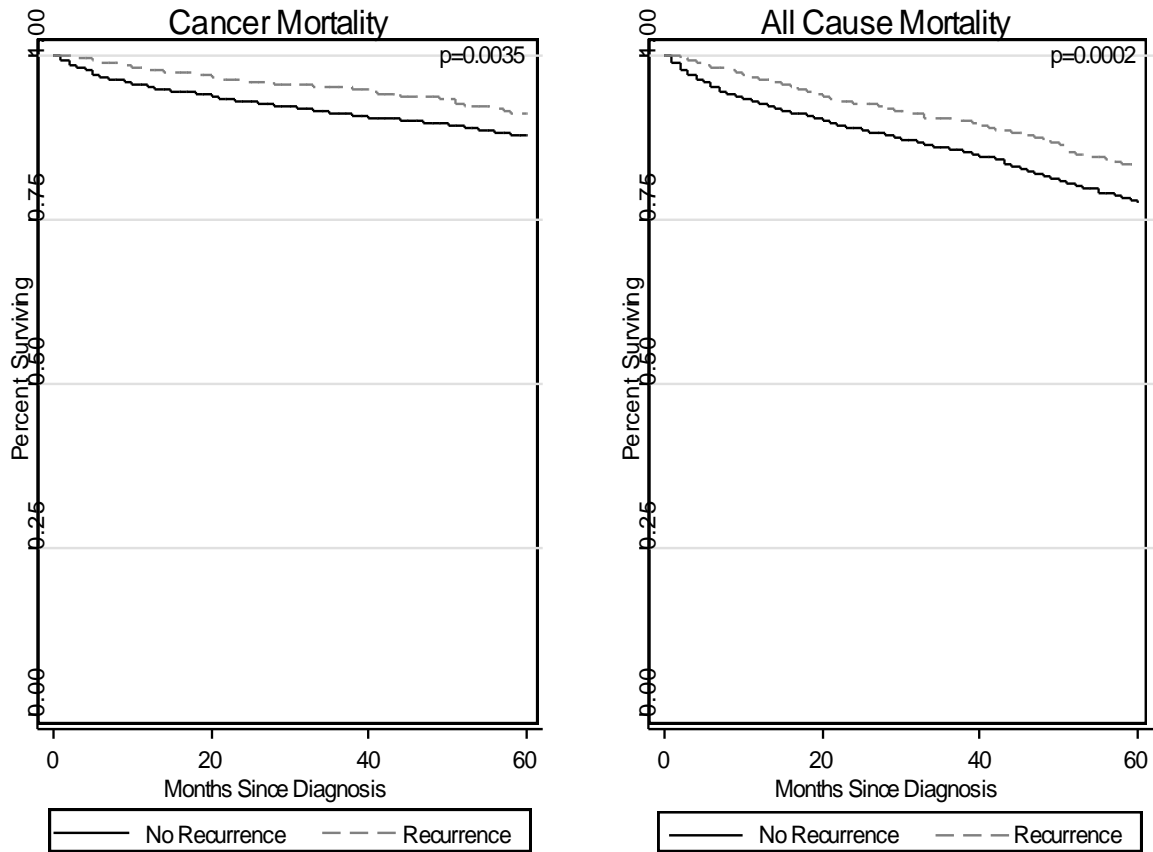
Manuscript 2: A significant portion of the costs attributed to thyroid cancer over five years occurs in the first 7 months of diagnosis. During those first 7 months the average cost attributed to the disease is \$7,000 to \$10,000. At 10 months after diagnosis the costs level out over the remaining 60 month follow-up. The average cumulative costs were calculated under the assumption that the patient survived up to the time period specified on the x-axis. At one year following diagnosis WDTC patients had accumulated approximately \$25,000 while comparison non-cancer group patients had accumulated an average of \$7,000. By five years, accumulated costs were approximately \$100,000 for DTC patients and \$70,000 for comparison patients. In the

multivariable models of one-year costs, several patient, disease, and treatment factors were significantly associated with accumulated costs at one year. At one year, patients age 70-74 had \$4,140 (95% CI: \$321-8,496) higher costs and patients greater than 79 years had \$4,510 (95% CI: \$717-8,656) higher costs than younger patients age 66-70. The higher costs incurred by males and black patients were not statistically significant. Disease stage was a significant determinant of cost. Patients with regional disease incurred \$9,612 (95% CI: \$6,703-12,725) and patients with distant disease incurred \$28,059 (95% CI: \$20,357-36,345) in additional costs. Comorbidities were the most substantial driver of costs where 1-2 comorbidities added \$12,966 (95% CI: \$6,398-20,686) and greater than 3 comorbidities added \$36,011 (95% CI: \$25,289-47,623) in costs. Treatment also significantly affected 1-year costs. Compared to surgery alone, patients undergoing both surgery and radiation incurred \$13,380 (95% CI: \$6,817-20,138) higher cost, and patients undergoing other treatment including chemotherapy incurred \$21,575 (95% CI: \$10,617-34,374) higher costs. Similar effects were observed for costs accumulated at five years following diagnosis (Table 1). Patients aged 70-74 incurred on average \$9,168 (95% CI: \$1,870-16,563) in higher costs, patients age 74-78 incurred on average \$8,045 (95% CI: \$1,459-14,846), and patients age 79 or older incurred on average \$14,038 (95% CI: \$6,512-22,430) compared to younger patients (reference age 66-69). In contrast to 1-year cumulative costs, the higher costs of approximately \$7,342 (95% CI: \$827-13,847) in male patients was statistically significant. Disease stage was also a significant determinant of costs as patients with regional disease accumulated \$9,521 (95% CI: \$3,670-\$15,437) and patients with distant metastases incurred on average \$21,264 (95% CI: \$9,615-32,130) in additional costs, which was similar to 1-year costs. Comorbidities were a substantial driver of costs where patients having 1-2 comorbidities incurred \$26,470 (95% CI: \$16,653-36,381) in additional costs and greater than 3 comorbidities \$51,812 (95% CI: \$37,012-67,599) in additional costs. Treatment choice was significantly associated with 5-year costs. Compared to patients who received surgery alone, patients who received surgery and radiation therapy had \$21,495 (95% CI: \$10,359-33,886) higher costs and patients who underwent other treatments which included chemotherapy had \$21,876 (95% CI: \$2,601-43,950) higher costs. While patients with recurrence incurred \$4,417 in additional costs, it was not statistically significant (95% CI: -\$1,417-10,353). These results will be submitted to the American Society of Health Economists meeting. Both manuscripts will be submitted for publication in the journal *Thyroid*.

**Table 1. Ordinary Least Squares Regression for 5-year Costs**

Variable	Parameter Estimate, \$	95% Confidence	
		<i>Lower</i>	<i>Upper</i>
Intercept	41,373	35,598	47,575
Age 66-69	0		
Age 70-73	9,168	1,870	16,563
Age 74-78	8,045	1,459	14,846
Age 79+	14,038	6,512	22,430
Female	0		
Male	7,342	827	13,847
White	0		
Black	11,543	-4,219	28,566
Asian	-3,128	-13,177	7,156
Race, Other	-7,497	-17,333	2,544
Married	0		
Single	15,854	2,776	29,148
Separated/Divorced	3,420	-6,130	13,525
Widowed	8,988	2,429	16,012
Marital status unknown	2,246	-11,965	17,784
Big Metro	0		
Metro	-9,689	-15,042	-3,954
Urban	-3,637	-14,762	8,584
Less urban/Rural	-14,913	-22,766	-6,734
Localized	0		
Regional	9,521	3,670	15,437
Distant	21,264	9,615	32,130
Unstaged	-10,271	-25,204	4,231
No comorbidities	0		
1-2 comorbidities	26,470	16,653	36,381
3+ comorbidities	51,812	37,012	67,599
Surgery alone	0		
No treatment	7,121	-6,768	22,372
Surgery and radiation	21,495	10,359	33,886
Other treatment	21,876	2,601	43,950
No recurrence	0		
Recurrence	4,417	-1,417	10,353

Figure 1. Time to death from cancer or from any cause, stratified by recurrence



**Research Project 29: Project Title and Purpose**

*Body Weight- and Nutrition-Sensitive Regulation of Skeletal Muscle Composition in Health and Obesity* – The purpose of this project is to extend preliminary findings showing that experimental manipulation of body weight results in precise adjustments to skeletal muscle *Troponin T* (*Tnt*) expression, and that this response is impaired in a genetic model of obesity. This response is mediated by alternative splicing and is sufficiently accurate that a unit of externally attached load has the same effect on the *Tnt* mRNA splice form profile as does a unit of actual body weight. The project will more firmly establish body weight- and nutrition-dependent causes of variation in mammalian skeletal muscle *Tnt* expression, and the generality of a mismatch between body weight, *Tnt* splicing, and skeletal muscle performance and energy expenditure during obesity.

**Anticipated Duration of Project**

9/1/2010 – 8/31/2011

## **Project Overview**

*Tnt* splice form expression affects muscle calcium sensitivity, force output, and ATP consumption rate during activity, and therefore this newly recognized regulatory mechanism may be important for both resisting gravitational forces and maintaining energy homeostasis. We hypothesize that this mechanism is impaired in obesity, causing a mismatch between body weight, muscle performance, and energy expenditure. Consequently, body-weight inappropriate skeletal muscle *Tnt* splicing will result in chronic muscle weakness, reduction in exercise participation, and reduction in the rate of energy consumption. The proposed studies will more firmly establish body weight- and nutrition-dependent causes of variation in mammalian skeletal muscle *Tnt* expression, and the generality of a mismatch between body weight, *Tnt* splicing, and skeletal muscle performance and energy expenditure during obesity. Elucidation of mechanisms controlling body weight- and nutrient sensitivity of *Tnt* expression in skeletal muscle will ultimately allow interventions that may restore *Tnt* homeostasis, overall mobility, and body weight-appropriate energy expenditure in obese humans. The following specific aims are proposed:

*Specific Aim 1. Troponin T homeostasis in a diet-induced model of obesity.* To determine the generality of obesity-associated (i.e., in both genetic and non-genetic disease models) impaired *Tnt* splicing response to body weight, we will induce obesity in otherwise healthy rats by means of a high-fat feeding diet, and examine the time course of *Tnt* splicing responses to changes in body weight. We expect that as body weight increases, *Tnt* splicing responses will be progressively attenuated in diet-induced obesity compared to control rats, resulting in *Tnt* splice form profiles that are poorly matched to body weight.

*Specific Aim 2: The effect of caloric restriction on Troponin T expression in rat skeletal muscle.* How nutrition may affect *Tnt* alternative splicing in mammalian skeletal muscle is presently unknown. Therefore, in a fashion similar to our recent work in insects, we will assess how caloric restriction affects *Tnt* splicing in skeletal muscle from adult rats. We expect that caloric restriction will positively affect body weight-specific skeletal muscle performance and that the *Tnt* splice form profile in muscles from caloric restricted rats therefore will resemble that of control rats of higher body weight.

## **Principal Investigator**

Scot R. Kimball, PhD  
Professor  
Cellular and Molecular Physiology  
Penn State University College of Medicine  
Physiology, H166  
P.O. Box 850  
Hershey, PA 17033

## **Other Participating Researchers**

Rudolf J. Schilder, PhD, Leonard S. Jefferson, PhD, James H. Marden, PhD – employed by

## **Expected Research Outcomes and Benefits**

We expect to more firmly establish the novel insight that impaired homeostasis of body weight and skeletal muscle composition (in the form of *Tnt* mRNA alternative splicing) potentially contributes to obesity development. The proposed analyses of nutritional inputs to this homeostatic mechanism will expand this research in an important way; in addition to its applicability to genetic obesity models, it will link directly to ongoing research in more pervasive, non-genetic, diet-induced obese disease states. Thus, the proposed work would allow us to establish a conceptual framework allowing the design of novel experiments that should yield significant insights into (signaling) pathways linking skeletal muscle composition, and function, with those that sense weight and nutritional status in both health and disease. In the longer term, such funding would enable us to validate the generality of the mechanistic link between *Tnt* splicing, muscle performance and body weight, and impairments thereof in human subjects.

## **Summary of Research Completed**

### Overview

In a recent study (*J. Expt'l. Biol.* 214:1523-32, 2011), we reported that the mRNA encoding fast troponin T (*Tnnt3*) undergoes alternative splicing in gastrocnemius muscle in response to changes in body weight. Importantly, body weight-induced changes in *Tnnt3* mRNA alternative splicing were impaired in a genetic model of obesity (i.e. the obese Zucker rat). In Specific Aim 1 of the original application, the overall goal was to assess the generality of obesity-associated impairment of the *Tnnt3* splicing response to body weight through induction of obesity in otherwise healthy rats by means of feeding a high-fat diet. In these studies, alternatively spliced forms of *Tnnt3* mRNA were quantitated by real-time polymerase chain reaction (RT-PCR) using fluorescently tagged primers followed by capillary electrophoresis. As described in greater detail below, the results support the hypothesis that body weight-induced changes in *Tnnt3* mRNA alternative splicing are impaired in skeletal muscle in obese rats, and that the impaired response may lead to a mismatch between body weight, muscle performance, and energy expenditure.

### Methods

**Animals.** All studies using rats were reviewed and approved by the institutional animal care and use committee (IACUC) of The Pennsylvania State University College of Medicine. Obesity-prone male Sprague-Dawley rats (OP-CD; Charles River) weighing approximately 200 g were randomly divided into two groups. Rats in the first group were fed a control diet containing 10% of total energy (kcal%) from fat (Research Diets, Inc.) and rats in the second group were fed a diet with 30 kcal% from fat (Research Diets, Inc.) for up to 13 weeks. At various times, body composition was measured using a Bruker Minispec LF90 NMR Analyzer (Bruker Optics, Inc., Billerica, MA). Briefly, rats were weighed, immobilized in a Plexiglas cylinder, and placed inside the Minispec for approximately 1min. During this time, measurements of whole body fat and lean (muscle) mass content were obtained using manufacturer-recommended rat-specific acquisition parameters. Prior to removal of the gastrocnemius, rats were deeply anesthetized

using isoflurane.

Quantitation of *Tnnt3* mRNA splice form relative abundance. *Tnnt3* mRNA splice form abundance in gastrocnemius was quantitated as described previously (*J. Expt'l. Biol.* 214:1523-32, 2011). Briefly, total RNA was extracted from muscle using Trizol reagent (Invitrogen, Carlsbad, CA, USA), and precipitated in isopropanol, according to the manufacturer's instructions. Total RNA was reverse transcribed using a High Capacity cDNA Reverse Transcription kit (Applied Biosystems, Foster City, CA, USA) using a fluorescein-labeled forward primer, and two unlabeled reverse primers. Using this amplification strategy, all of the possible alternative *Tnnt3* mRNA splice form amplicons have a unique size, with a minimum length difference of three nucleotides. PCR was performed using HotStart GoTaq polymerase (Promega, Madison, WI, USA). For quantitative analyses of *Tnnt3* splice form relative abundance, fluorescein-labeled PCR products were analyzed by capillary electrophoresis (ABI DNA Analyzer, Applied Biosystems). The relative abundance of each amplicon in the PCR reaction was determined by dividing its peak height by the total of all peak heights. Amplicon fragment size was determined using an internal size standard and Genemapper® (Applied Biosystems) fragment analysis software.

## Results

When outbred Sprague-Dawley rats are placed on a high-fat diet, only about 50% of them overeat and develop diet-induced obesity, while the remainder of the animals gain no more weight than ones fed a control, low-fat diet (*Am. J. Physiol.* 285:R1184-91, 2003). Consequently, in the present study, obesity-prone, male Sprague-Dawley rats (OP-CD; Charles River) were used because we reasoned that it might be difficult to distinguish animals responsive to the high-fat diet from non-responders at the shorter time points. Surprisingly, over the 13-week time course of the present study, rats gained similar amounts of body weight, regardless of the diet consumed (Figure 1A). To determine whether consumption of the high-fat diet led to increased adiposity compared to consumption of the control diet, at various times after the start of high-fat feeding fat and lean body mass were measured by NMR analysis using a Bruker Minispec. As shown in Figure 1, the proportion of fat (Figure 1B) and lean (Figure 1C) body mass was the same in rats consuming the high-fat diet (red bars) as those consuming the control diet (blue bars) up until the 8 week time point.

To identify potential high-fat diet-induced changes in splicing of the *Tnnt3* mRNA, a combination of quantitative RT-PCR and capillary electrophoresis was used to assess the relative distribution of the mRNA in the various splice forms in gastrocnemius muscle. A total of 12 *Tnnt3* splice forms were detected (Figure 2). Based on the criteria described in our recent study (*J. Expt'l. Biol.* 214:1523-32, 2011), we refer to the forms as *Tnnt3*  $\beta$ 1-9 (contains exon 17) and *Tnnt3*  $\alpha$ 1-3 (contain exon 16). Notably, even though feeding a high-fat diet had no detectable effect on total body weight or fat or lean body mass, specific splice forms were differentially expressed in muscle from high-fat fed rats compared to controls at the time points examined. For example, in muscle of rats fed a high-fat diet (red symbols and line), the relative expression of the *Tnnt3* $\alpha$ 1 splice form was significantly less than in rats fed a control diet (blue symbols and line), even after only one week (Figure 3). In contrast, the relative expression of *Tnnt3* $\beta$ 5 and *Tnnt3* $\beta$ 9 splice forms was significantly increased at all time points in rats consuming a high-fat compared to a control diet. However, as shown for the *Tnnt3* $\beta$ 3 splice form (Figure 3), not all

splice forms exhibited diet-induced alterations in expression. Indeed, the relative expression of 7/12 forms was found to be altered in muscle of rats consuming a high-fat compared to a control diet.

### Discussion

In agreement with results presented in our recent study (*J. Expt'l. Biol.* 214:1523-32, 2011), *Tnnt3* mRNA splice form expression changed with alterations in body weight, such that the relative expression of some splice forms was upregulated whereas others were downregulated with increasing body weight. However, in rats fed a diet containing 30%kcal from fat, the pattern of splice form expression was altered compared to animals fed a control diet with 10%kcal from fat, with some splice forms exhibiting increased, and others decreased, relative expression. Interestingly, the high-fat diet-induced changes in expression manifested without a detectable increase in adiposity until 13 weeks of treatment. This finding suggests that the observed changes in *Tnnt3* mRNA alternative splicing were a result of diet *per se* rather than to obesity. It is also interesting that some, but not all, of the *Tnnt3* splice forms found to change in the present study (e.g. *Tnnt3* $\alpha$ 1 and *Tnnt3* $\beta$ 5) were shown to be differentially expressed in muscle from obese compared to lean Zucker rats (*J. Expt'l. Biol.* 214:1523-32, 2011). This finding suggests that the commonalities between the models may represent splice forms that were differentially modulated in response to the hyperphagy that occurs in obese Zucker rats, rather than to a change in fat mass.

Overall, when combined with the results of our previous study (*J. Expt'l. Biol.* 214:1523-32, 2011), the results of the present study suggest that excess calorie consumption, particularly of a diet containing a high proportion of calories from fat, interferes with the normal regulation of alternative splicing engendered by increases in body weight. It is also tempting to speculate that, because Troponin T is involved in modulating muscle force and power output, the mismatch between body weight and *Tnnt3* splice form expression in high fat-fed animals may contribute to pathologies common in human obesity, such as chronic muscle weakness, increased load-induced muscle injury, and unwillingness to participate in exercise.

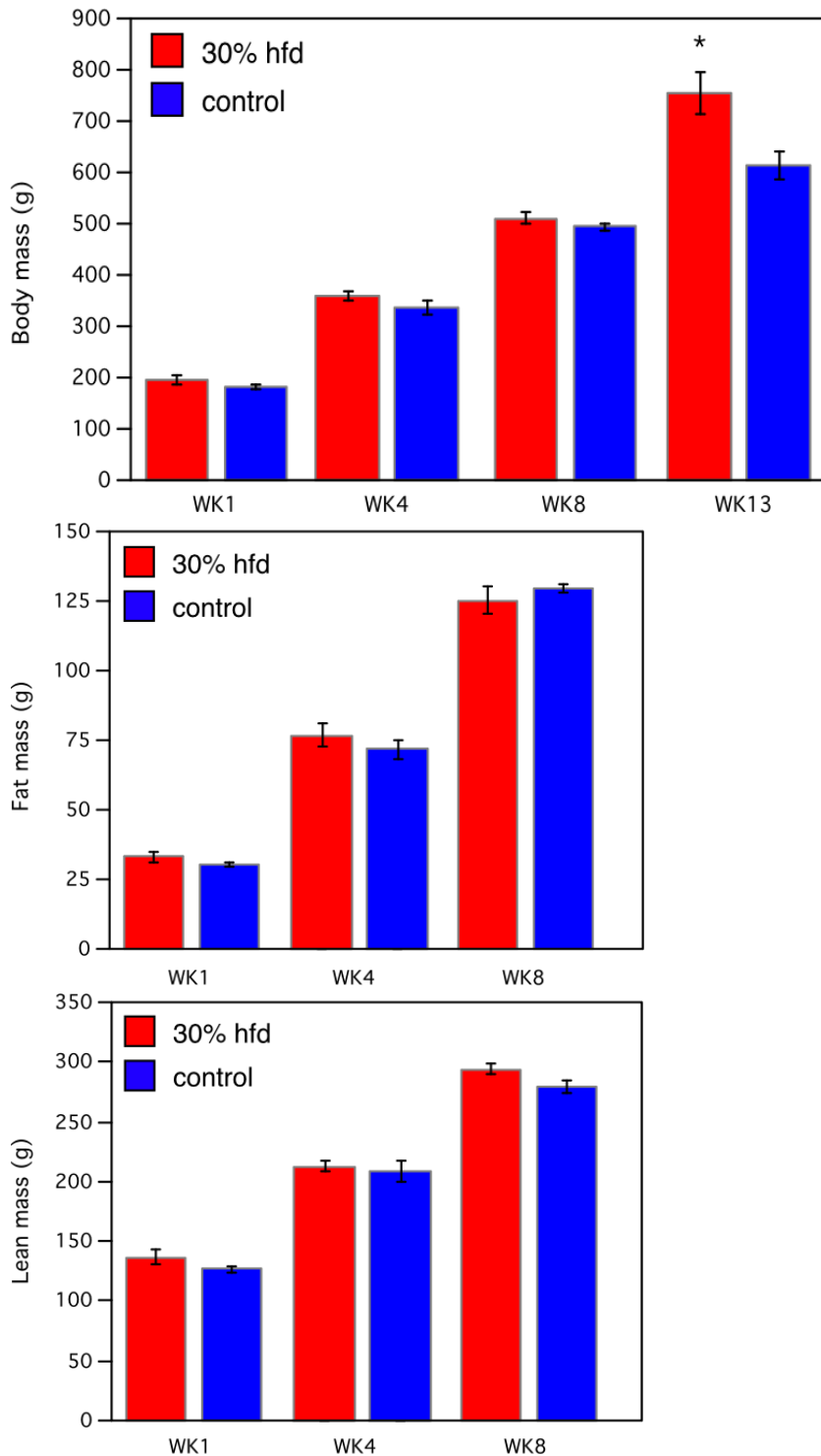


Figure 1 A,B,C. Legend: Body mass and composition in rats fed either a control or 30% high fat diet up to 13 weeks. Presented are mean values (N = 4 per treatment at each time point) and associated standard errors. The dietary treatment did not affect body weight until the 13 week time point, and had no effect on fat and lean mass contributions to total body mass.

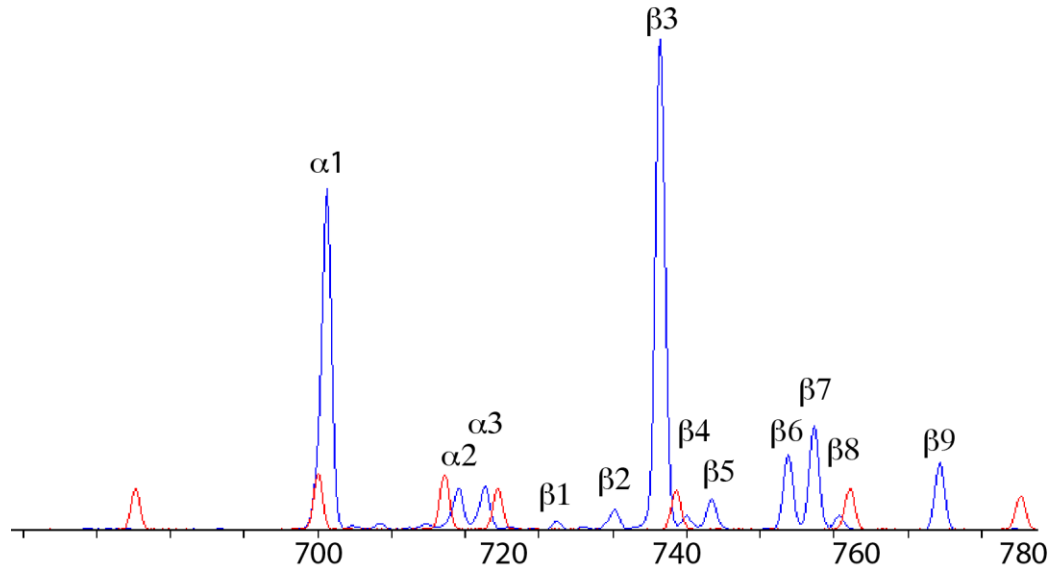


Figure 2. *Tnnt3* DNA fragment analysis. Fluorescently labeled DNA fragment peaks showing *Tnnt3* splice form diversity and abundance (i.e. peak height) of each splice form in rat gastrocnemius muscle. Internal size standards are represented by red traces. Relative abundance of specific troponin T mRNA splice forms is defined as the ratio of its peak height and total peak height of all splice forms.

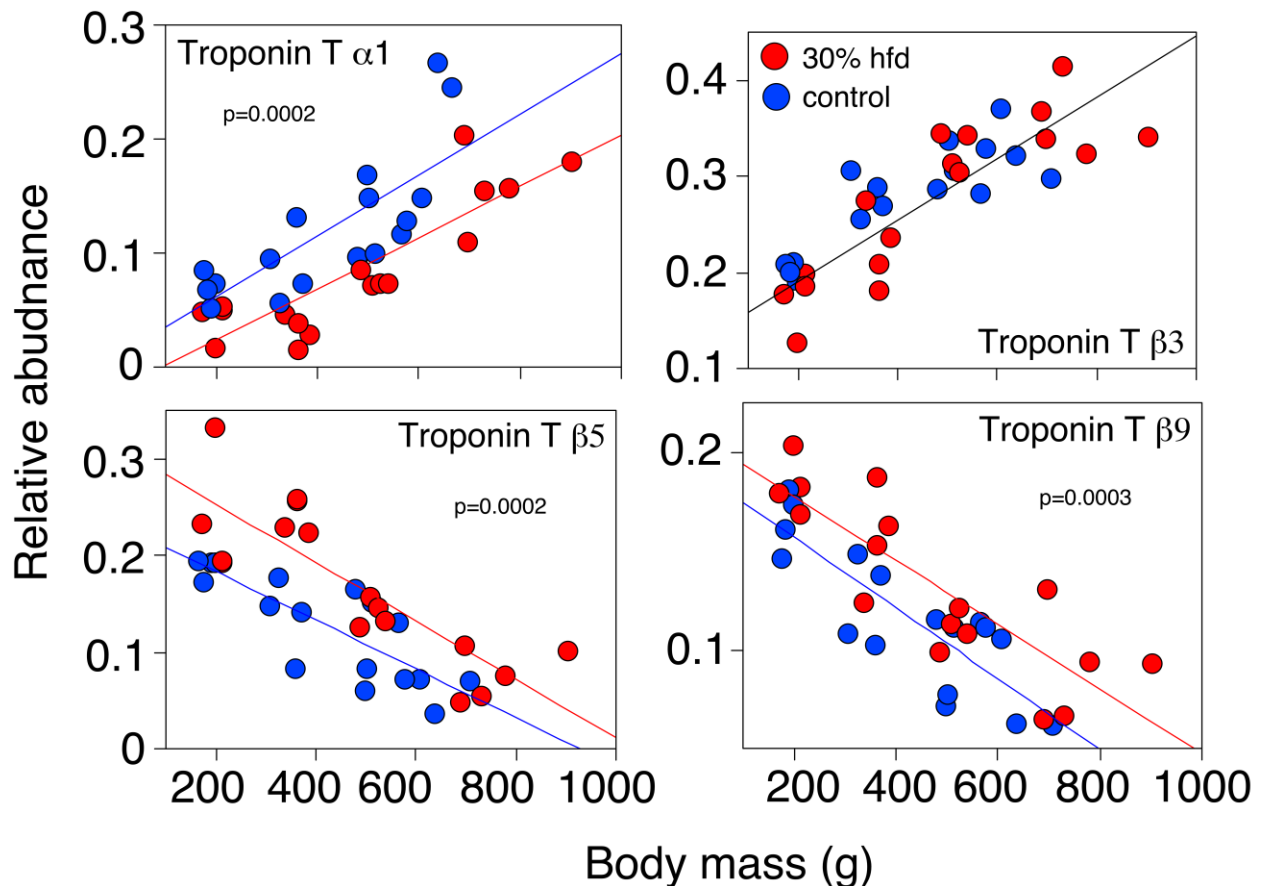


Figure 3. Effect of 30% high fat diet on gastrocnemius muscle alternative Tnnt3 pre-mRNA splicing. Presented are the relative abundances of Tnnt3 splice forms  $\alpha 1$ ,  $\beta 3$ ,  $\beta 5$ , and  $\beta 9$  (the 4 most abundant splice forms in gastrocnemius muscle) as a function of body mass. Solid lines depict linear regression fits to data for control and 30% high fat diet fed animals separately. Data shows significant depression (i.e. Tnnt3  $\alpha 1$ ), and elevation (i.e. Tnnt3  $\beta 5$ ,  $\beta 9$ ) of the slope of fits relating relative splice form abundance to body weight. No effect of the dietary treatment was observed for Tnnt3  $\beta 3$ .

### **Research Project 30: Project Title and Purpose**

*Role of Olfactory Cues in Addictive Behavior* – In this pilot study we will be studying altered brain activity related to the reward value of eating/smoking in smokers, binge-eaters, smokers who binge-eat, and healthy controls. This project will test the following hypotheses concerning the human brain's response to food/smoking cues. We predict that responses will be 1) lowest for pictures, larger for odorants, and maximal for combined congruent pictures with odorants; 2) larger for smokers for smoking cues and larger for binge-eaters for food cues. These responses may have implications for treatments designed to change smoking or eating patterns.

### **Anticipated Duration of Project**

9/1/2010 - 12/31/2011

## **Project Overview**

Studies of the neural pathways active in binge-eating and tobacco smoking indicate that altered reward and control systems contribute to these hedonic consumption patterns. Neuroimaging research that uses food and/or smoking cues to study the brain's reward pathway often lacks the potent component of odor. We propose to leverage the extensive expertise in olfactory fMRI at Penn State to study the reward pathways of binge-eating and smoking using the powerful combination of both sight and smell. The specific aims of this project are to:

- 1) Evaluate the saliency of multisensory cues (visual/odorant) delivered separately or simultaneously
- 2) Examine the construct of binge-eating as an addiction by comparing and contrasting cue-related brain activation in groups who binge-eat, smoke, or do both.

This project will require the use of an MRI-compatible odorant-delivery system (an olfactometer) and functional MRI (fMRI). Brain activation will be examined in four groups: healthy controls (HC), persons who binge-eat (BE), smokers (SM), and smokers who binge-eat (SB). We expect that brain activation will be strongest to cues that combine olfactory and visual stimulation, in comparison to either type of cue alone. We also expect that each group will show the strongest responses to their respective substance, and that the comorbid group will show a superadditive effect, exhibiting activation greater than the sum of responses to each individual cue.

For the first time, the twin 3T Siemens scanners installed in the Social, Life, and Engineering Sciences Imaging Center (SLEIC) at University Park (UP) and the Center for NMR Research (CNMRR) at Penn State Hershey College of Medicine would be used conjointly in a cross-campus collaboration. These technical developments will foster research across the UP/Hershey campuses by equipping both 3T MRI scanners to deliver olfactory stimuli in addition to standard audio/visual stimuli. The long-term objectives include facilitating multi-site collaboration between UP and Hershey campuses and building critical mass in the sensory neuroscience of addiction. In addition, a deeper understanding the neural pathways affecting eating and smoking addictions may help to design effective treatment and prevention programs.

## **Principal Investigator**

Susan K Lemieux, PhD  
Senior Research Associate  
Penn State University  
102 Chandlee Laboratory  
University Park, PA 16802

## **Other Participating Researchers**

Rebecca L. Corwin, PhD, Stephen J. Wilson, PhD, John E. Hayes, PhD, Anna S. Engels, PhD, David R. Pennell, MS, RT(MR), Joe P. Stitt, PhD, Jeffrey J. Vesek, BS, RT(MR), Qing Yang, PhD, Amanda Gearhart, RT(MR) – employed by Pennsylvania State University.

## **Expected Research Outcomes and Benefits**

It is well known that cigarette smoking presents an enormous burden on the health care system. Binge-eating likewise is associated with substantial health problems. Both behaviors are also highly associated with compromised mental health and are often seen in the same individuals. Binge-eating and smoking are both characterized by craving in response to environmental cues.

The long-term objective of this project is to identify the neuronal correlates of exposure to such cues in smokers and bingers using a novel stimuli delivery system that more closely mimics the natural environment. This will be the first neuroimaging study of its kind. The outcomes will inform our understanding of the similarities and differences between healthy and unhealthy responses to environmental stimuli enabling tailored treatment strategies. For example, successful treatment plans for binge-eaters may need to be tailored to take into account whether or not the person smokes. Likewise, smoking cessation programs may need to consider whether or not the person binge-eats. Finally, the knowledge gained from this project may be broadly applicable to the development of targeted treatments for other comorbid unhealthy behaviors.

## **Summary of Research Completed**

*Progress on Specific Aim 1: Install olfactory fMRI at SLEIC and test on healthy controls (HC), (Months 0-6).*

At Penn State Hershey, we are currently able to generate olfactory stimuli for fMRI experiments to:

- 1) Reproduce this capability at the University Park SLEIC laboratory.
- 2) Test/validate the visual-olfactory stimulation paradigm and data acquisition methods on HC at SLEIC.

This aim has been accomplished. Details are provided below.

*Progress on Specific Aim 2: Test hypotheses about visual/olfactory responses, (Months 7-12).*

- 1) Acquire and begin the analysis of fMRI data for the HC, BE, SM and SB groups with the goal of an NIH R01 submission in October 2011.

Work on this aim is ongoing. The report on progress is below.

### Progress Made On Research Design, Methods and Analysis:

Odorant and odorant delivery system. As described in our proposal, Prof. Qing Yang's team built the existing MRI-compatible odor-delivery system at CNMRR and funds from this pilot grant were used to construct an identical system for the Social, Life, and Engineering Sciences Imaging Center (SLEIC). The odorant delivery system consists of a set of Teflon tubing that transports the odorless medical grade compressed air from a canister through a set of six odorant chambers to the subject's nose. The odorant chambers are designed to allow for rapid switching and precise timing between the odor and no-odor states. The clean air with or without odorant is presented through a tubing about 1 cm away from the subject's nose with a constant flow rate. A 20 cm diameter ventilation pipe located superior to the head coil removes air in the magnet bore at a rate of 2.0 L/min.

The olfactometer is installed at the SLEIC 3T laboratory now and has been extensively tested.

Our tests have demonstrated that the olfactometer must be ventilated before use. Using its own pumping and air supply clears any residual odorant traces so that the participant starts fresh with clean odorless air. Six odorants have been tested for intensity and pleasantness: the high-calorie (HC) food odorants, chocolate and cinnamon bun, the low-calorie (LC) odorants, cucumber and melon, and smoking odorants (SM), cigarette tobacco and burning pipe tobacco.

Figure 1. Representative pictures: cinnamon bun (HC), cucumber (LC), cigarette smoking (SM) In this stimulation paradigm, olfactory and visual stimuli are administered simultaneously. To minimize habituation, each odor intensity is presented briefly for 6 sec followed by a 28 sec resting period that includes a Likert scale rating task presented after the HC, LC, or SM stimuli at a random interval between 12-18 seconds after the stimuli.

### MRI Scanning:

Physiological Data Collection: It is well-understood in the fMRI community that physiological noise from the respiratory motion and cardiac pulsation limit the sensitivity in the time course analysis. To improve our sensitivity to the stimuli responses, we have developed a routine to collect image-synchronized respiratory and cardiac wave form data. As described in the data analysis section below, we are using these data for noise reduction during the analysis. Figure 2 shows a sample at the start of a scan. The change in the square wave from the scanner indicates the start of the first image acquisition.

Anatomical scans: The subjects lie supine in a dark environment. The respiratory and cardiac rates and associated motions will be recorded through a chest belt and pulse oximeter incorporated into the MRI scanner system to monitor respiratory and cardiac patterns. T2-weighted two-dimensional fast gradient-echo images will be first acquired for anatomical structure and volume selection for fMRI study. 3D spoiled gradient-echo will be acquired for a high-resolution volume image for image registration during data analysis.

Functional MRI data acquisition: The investigative team has had the benefit of attending a week-long functional MRI workshop sponsored by SLEIC, taught by Dr. Thomas Zeffiro from Harvard Medical School. We have modified our image acquisition and analysis as a result of new information obtained during this workshop. We are now using an imaging protocol designed to maximize the MRI signal from the orbital frontal cortex, an area of the brain that is subject to signal loss from susceptibility artifact in MRI. The SENSE-EPI-BOLD method is used for acquiring fMRI images. The fMRI images consisting of 50 axial slices with 2.5 mm spatial resolution in all direction are called “isovoxels” in the MRI jargon. Tacq per brain volume is 3 sec. The timing and switching of the odorant’s delivery are automatically controlled by TTL signals incorporated in the pulse-timing program. Results from our first pilot scan session using these finalized parameters are shown below in Figure 3.

### Prescan Assessments

Since this award was received, we have worked to streamline our prescan procedures for participant ease, experimental accuracy, efficiency and to economize where possible.

Light Lunch. The light lunches will now be prepared by the General Clinical Research Center Metabolic Kitchen to ensure accurate and precise caloric content across participants.

Smoking Baseline assessment measures. Demographic and smoking history information will be assessed with standard forms: the Brief Substance Use Questionnaire (BSUQ), a smoking history form and the smoking dependency scale (NDSS). Only smokers will complete the smoking history form, the NDSS and take the carbon monoxide level test.

Binge eating status We have included an additional measure for all subjects - the food craving inventory (FCI). The other binge-eating questionnaires will be also be used: the weight patterns-revised (QEWPR) and the binge eating scale (BES).

Psychophysical Olfactory Threshold and Intensity Tests. We have modified this part of the design. All the subjects will be evaluated with smell threshold tests before being included in the fMRI studies. Participants who find that the odorants are aversive or who cannot smell them at the prepared intensities will be excluded from further participation in the study.

#### Data Analysis.

Analysis of the first pilot fMRI data sets have been conducted using the best features of each of several standard image processing packages. Data were corrected for motion using the AFNI package from NIH. Transformations were applied to localize responses using brain atlases. Estimation of the standard parametric maps of experimental effects (t-tests) at the voxel level was determined by means of appropriate instances of the general linear model. Figures 3 and 4 below shows the results that have been corrected for motion but not for physiological noise or field distortions yet. Since both of those corrections will result in higher signal to noise for the functional data we are very pleased to see such high levels of activation in our first data set before the corrections have been applied.



Figure 1. Representative pictures: cinnamon bun (HC), cucumber (LC), cigarette smoking (SM)

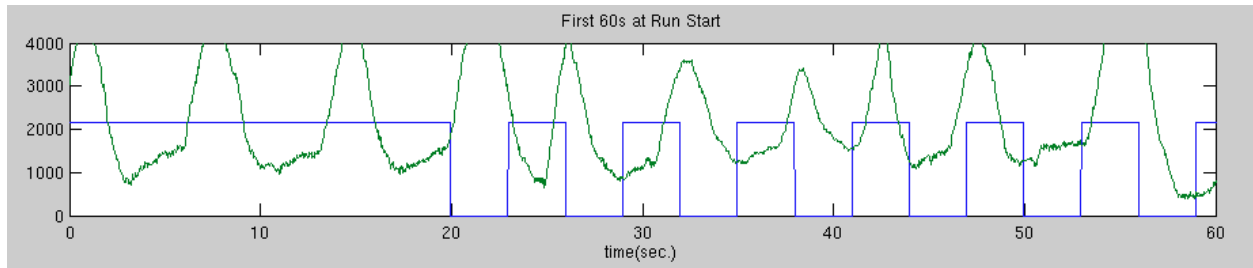


Figure 2. Respiration and scanner trigger signals show that the first image acquisition began 20 seconds after the start of physiological data collection.

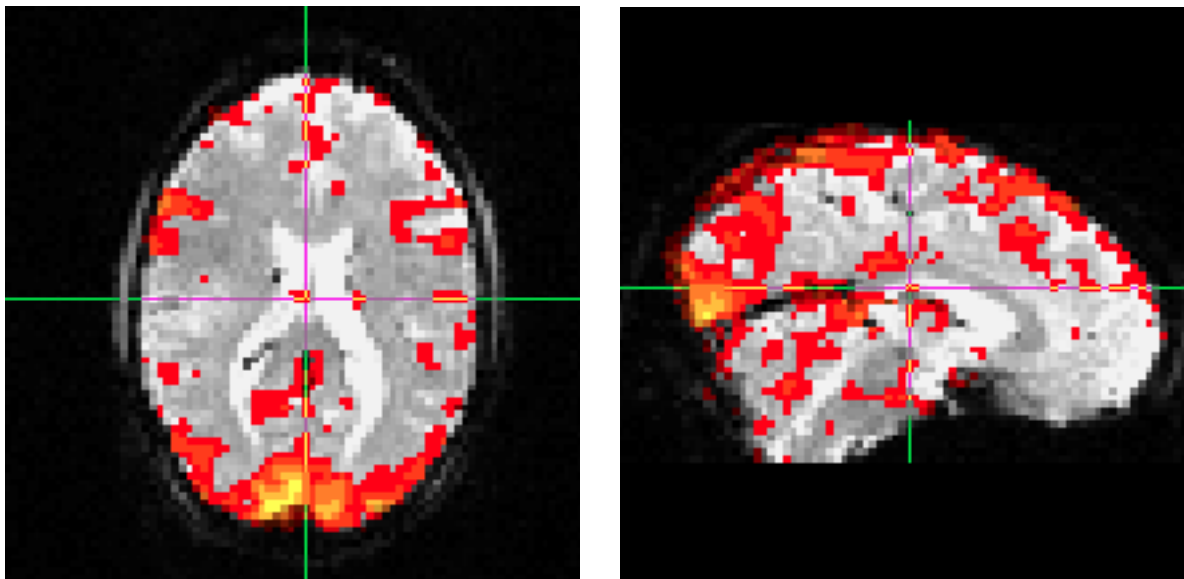


Figure 3. Bright yellow and orange areas show occipital lobe activation to the visual stimuli at the  $p < 0.05$  level in a single subject for a single run 10 minutes long with 18 stimuli, 6 of each type, HC, LC, SM presented with accompanying congruent odorants. Bilateral premotor cortex response is also seen.

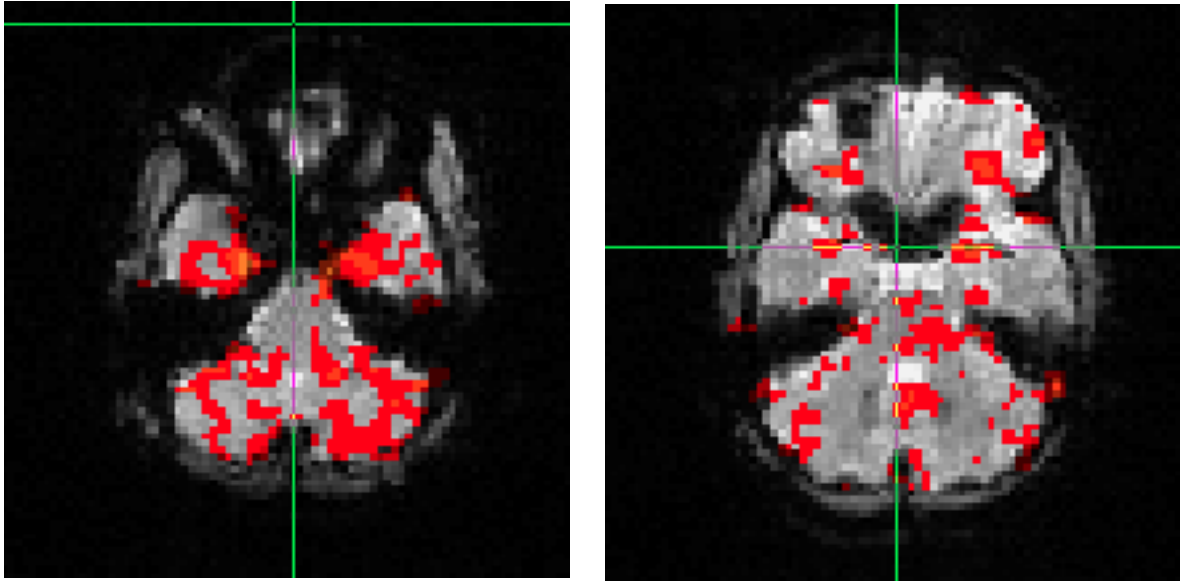


Figure 4. Response to the visual-olfactory stimulus in the predicted areas of orbital frontal cortex and in the cerebellum are seen at the  $p < 0.05$  level.

### **Research Project 31: Project Title and Purpose**

*MRI Marker(s) for Neuropsychological Outcomes in Adolescents with Mild Concussion* – The purpose of this study is to identify MRI markers that correlate with neuropsychological outcomes in adolescents who have suffered a mild concussion. Recent imaging results in adults with concussions have demonstrated alterations in imaging parameters that are associated with outcome measures. The current project will extend these results to adolescents with mild concussions to test the central hypothesis that axonal injuries, microbleeding, and/or functional interruption occurring during concussion may be responsible for the observed neuropsychological dysfunction and predictive of recovery patterns in adolescents.

### **Anticipated Duration of Project**

9/1/2010 - 6/30/2012

### **Project Overview**

Mild traumatic brain injury (concussion) affects >1 million adolescents annually and is a leading cause of disability in this population. As recent news reports have highlighted, there is a dearth of data to guide the response to concussion, particularly in adolescents. Whereas most mild concussion symptoms resolve in adolescents, patients can develop neurocognitive impairments that affect memory, attention, and executive function that interfere with their ability to participate in school and other activities. Outcomes often are variable, and presently difficult to predict. The diverse neuropsychological outcomes in concussed adolescents may relate to specific disruptions of brain function in susceptible regions related to axonal integrity, microbleeding, and functional interruption that can be measured using MR imaging [diffusion

tensor (DTI), susceptibility weighted (SWI), and functional (fMRI) imaging, respectively]. Indeed, recent imaging studies in adults with concussion have demonstrated not only alterations in these imaging parameters but also correlations with outcome measures. The current project will extend these results to adolescents with mild concussion to test the central hypothesis that axonal injuries, microbleeding, and/or functional interruption occurring during concussion may be responsible for the observed neuropsychological dysfunction and predictive of recovery patterns in adolescents. We propose to study 20 mildly concussed and 15 non-concussed adolescents (age 13-18 y) using DTI, SWI, fMRI, and neuropsychological evaluations, with follow-up neuropsychological evaluation of concussed adolescents two months after injury in an effort to determine the predictive value of MRI markers in mild concussion. Our aims are: 1) Demonstrate the axonal disruption, increased microbleeding, and functional interruption in susceptible regions of brain (i.e., deep white matter regions of the corpus callosum, internal capsule, and frontal lobe) in adolescents with mild concussion; 2) Delineate the functional correlation of brain changes in adolescents with mild concussion; and 3) Explore the predictive value of brain MRI changes in the specified regions of interest to neuropsychological outcomes in adolescents with mild concussion.

### **Principal Investigator**

Mechelle M. Lewis, PhD  
Assistant Professor of Neurology and Pharmacology  
Penn State University College of Medicine  
500 University Drive  
PO Box 850, Mail Code H-037  
Hershey, PA 17033

### **Other Participating Researchers**

Matthew L. Silvis, MD, Paul J. Eslinger, PhD, Qing Yang, PhD, Harry Bramley, DO, Michele L. Shaffer, PhD, Suman Sen, MD, Daymond Wagner, BS – employed by Pennsylvania State University

### **Expected Research Outcomes and Benefits**

Although the number of mild concussions in adolescents is significant, the true incidence is likely higher, as many events go unnoticed or may not be reported. Scholastic and intercollegiate sports have tended to mirror the standards of professional sports, and while mild concussion has finally begun to receive the appropriate attention, there remains a dearth of scientific data to guide responses to concussion. This project will apply imaging techniques, along with comprehensive neuropsychological tests, to adolescents with mild concussions. The long term goal of the project is to provide a better understanding of the underlying brain mechanisms of mild concussion in adolescents, and to develop MRI markers of mild concussion that are predictive of neuropsychological outcomes and that may ultimately guide the clinical treatment for this population. Based on numerous previous studies, we expect mildly concussed adolescents to demonstrate axonal disruption, increased microbleeding, and functional interruption in susceptible regions of brain (i.e., deep white matter regions of the corpus

callosum, internal capsule, and frontal lobe) compared to non-concussed adolescents. Moreover, we predict that these imaging parameters in concussed adolescents will be correlated with the neuropsychological scores that we shall collect. Lastly, we expect that concussed adolescents will show improvement in their neuropsychological scores after two months and that the imaging markers that we measure will be able to predict neuropsychological outcome. Although highly explorative, the results of this last aim may have the potential to guide interventional therapies and long-term management of mild concussion.

### **Summary of Research Completed**

The long term goal of the project is to provide a better understanding of the underlying brain mechanisms of mild concussion in adolescents and to develop MRI markers of mild concussion that are predictive of outcome. Although both genders suffer mild concussions, we focused our study on right handed adolescent males in an effort to control for possible confounding factors such as level of physical activity, activity contact, brain laterality, and gender effects. Upon notification of the award, we prepared materials to obtain IRB approval to recruit subjects for the study (consent forms, flyers, phone script, questionnaires, screening forms, etc.), submitted the IRB protocol, made the requested changes, and received IRB approval. Subsequently, we have made two slight modifications to the protocol and consent form with IRB approval granted in each case.

Following IRB approval, Dr. Silvis contacted the high school and middle school trainers via email to inform them of the study and schedule a time to meet with them to hand out the flyers and answer any questions regarding the protocol. Unfortunately, this process was delayed significantly due to the various schools requesting him to present the study to the school board to obtain their approval to engage the trainers in assisting with recruitment for the study. School board meetings are held regularly, though infrequently, and although we moved with as much speed as was possible, we were not able to meet with the trainers until well into the fall season. As a result, we missed a large portion of the season when boys play football and soccer, two sports with considerable rates of concussion in the population we wish to recruit.

Although slightly discouraged by this delay, we have continued efforts to recruit subjects for the study. Drs. Silvis, Bramley, and Lewis have met on a regular basis to discuss the study and strategize ways to improve recruitment. In addition, both Dr. Silvis and Dr. Lewis have maintained contact with area school athletic trainers via email. Dr. Lewis also has been in touch with Mr. Jeff Shields, Director of the Athletic Training Services for Central Pennsylvania Rehabilitation Services regarding the study, and met with and presented to the school athletic trainers at their monthly meeting in March 2011. During that meeting, Dr. Lewis explained the rationale for the study, the target population we are looking to recruit, and what we are asking the trainers to do. In addition, Dr. Lewis answered any questions. Dr. Lewis also attended recently the annual meeting of the Brain Injury Association of Pennsylvania (June 27-28, 2011), where she met with representatives of the Pennsylvania Athletic Trainers' Society (PACT), Inc. They discussed the study, what it entails, and the target population. It was agreed that Dr. Lewis would draft a letter to parents that explains the study and what it involves and, following IRB approval of that letter, that she send the letter and flyers to the PACT representatives. The representatives then will distribute the letter and flyers at up-coming meetings they have

scheduled with parents and athletes participating in fall sports, as well as sending the materials to colleagues for distribution.

We have enrolled four male control subjects into the study. Detailed demographic information is listed in Table 1.

Each subject gave informed consent and completed the compensation form, demographic and sport form, the handedness inventory, and the MRI screening form. In addition, all subjects completed the neuropsychological battery that included an evaluation of overall intelligence [Wechsler Intelligence Scales (WIS)], working memory (the N-Back test and Working Memory Index from the WIS) processing speed (subtests of the WIS), attention (Connor’s Continuous Performance Test II), and executive function (Delis-Kaplan Executive Function, Trailmaking, Stroop, Controlled Oral Word Association, and Tower tests). Collectively, these tests took approximately 1.5-2 hrs to complete for each subject. As the number of subjects enrolled is small at this time, we did not analyze any of the neuropsychological data.

Following completion of the neuropsychological battery, subjects underwent an MRI scan at the Center for NMR Research. Sequences acquired on the 3 T scanner included a T1-weighted scan and diffusion tensor (DTI), susceptibility weighted (SWI), and functional (fMRI) images. For the functional imaging tasks, subjects completed the n-back (0-, 1-, and 2-back) and the face-name recognition task. Total imaging time was approximately 1 hr for each subject.

As no concussion subjects are enrolled in the study as yet, comparison of imaging results is premature. We have provided descriptive statistics of the functional imaging behavioral data in Table 2.

As can be seen in Table 2, accuracy was relatively similar during the 0- and 1-back tasks but dropped dramatically when subjects completed the 2-back task. Preliminary comparisons revealed no significant difference in accuracy between the 0- vs. 1-back or 1- vs. 2-back tasks, although the 0- and 2-back tasks did demonstrate significance on this measure ( $p=0.04$ ). Consistent with previous studies, increased memory load during the n-back test led to increased reaction times across tasks. Comparison of reaction times indicated significant differences among all tasks, with the 0- vs. 1-back and 0- vs. 2-back comparisons highly significant ( $p$  values  $<0.00001$ ) and the 1-vs. 2-back tasks significant ( $p=-.02$ ). For the face-name recognition task, accuracy was significantly better when the faces were female ( $p=0.04$ ) but there was no difference in reaction time for the two tasks. Although these results are preliminary and don’t compare non-concussed to concussed subjects, they provide pilot data suggesting our small control subject pool displays results typical of these measures.

Table 1: Subject demographic information.

<b>Subject ID</b>	<b>Age (yrs)</b>	<b>Grade</b>	<b>Handedness</b>	<b>Sport</b>	<b>Experience (yrs)</b>
Control_001	18.1	12	R	Soccer, baseball	8
Control_002	15.0	9	R	Basketball, lacrosse	6
Control_003	18.6	12	R	Soccer	8
Control_004	18.6	12	R	Football	8

Table 2: Behavioral data from fMRI tasks.

Test name		Accuracy (%, mean±SD)	Reaction time (ms, mean±SD)
N-Back	0 Back	91.1±28.6	598±287
	1 Back	92.9±25.8	751±336
	2 Back	85.9±34.9	850±432
Face-name recognition	Male	34.7±48.3	1853±1241
	Female	59.4±49.9	1740±1184

### **Research Project 32: Project Title and Purpose**

*Epigenetic Changes in Gene Expression Associated with an Anxious Depressive like Phenotype –*  
 The purpose of this study to discover gene expression changes that could serve as diagnostic biomarkers of anxious depressive disorders. Such biomarkers hold the promise of 1) improving the speed and accuracy of diagnosis, thereby reducing the time consuming and often futile guesswork involved in finding an efficacious therapy for anxious depressive disorders, and 2) finding novel therapies for currently drug resistant forms of the syndrome.

### **Anticipated Duration of Project**

9/1/2010 - 6/30/2012

### **Project Overview**

Depressive disorders are severe neuropsychiatric disorders that exhibit rampant comorbidity with anxiety disorders, with depressed patients often showing a history of treatment for anxiety, and vice versa. Depressive disorders exhibit variable contributions of genetic and environmental risk factors and highly unpredictable responsiveness to different types of antidepressant drugs. The drugs currently in use are effective in about 60% of patients only, and among these only one-third enters remission. Even among patients who respond or remit, alleviation of symptoms is typically not seen until after one month of treatment. Thus, some patients are moved from one ineffective drug to another, without relief from suffering for months or forever. The identification of biomarkers for anxiety and depressive disorders holds the promise of 1) improving the speed and accuracy of diagnosis, thereby reducing the time consuming and often futile guesswork involved in finding an efficacious therapy, and 2) finding novel therapies for currently drug resistant forms of the syndrome.

Mice rendered heterozygous for the  $\gamma 2$  subunit of GABA type A receptors have been extensively characterized as a model of anxious depression that includes behavioral, cognitive, neuroanatomical, endocrine and pharmacologic features expected of such a model. Emerging evidence suggests that the pathology of depressive disorders depends at least in part on long-lasting, epigenetic changes in gene expression. We propose a collaborative effort to use the  $\gamma 2^{+/-}$  model as a means to identify, on a genome wide scale, chromatin changes indicative of altered gene expression associated with anxious depressive mood states. We will use

immunoprecipitation of chromatin (ChIP) isolated from relevant brain regions of  $\gamma 2^{+/-}$  and WT mice and corresponding antidepressant drug-treated mice with antibodies specific for histone modifications that are implicated in epigenetic regulation of neural genes, followed by quantitation of chromatin associated genes by high throughput sequencing (ChIPseq). Differential expression of candidate genes identified by their differential association with modified histones will be validated by quantitative PCR (QPCR) of cDNA prepared from the same brain regions of  $\gamma 2^{+/-}$  and WT mice, and corresponding antidepressant drug-treated mice. These experiments will provide the foundation for an NIH grant application that aims to identify 1) biomarkers of anxious depressive mood states and 2) new potential targets for therapeutic intervention in mood disorders.

### **Principal Investigator**

Bernhard Luscher, PhD  
Professor  
Pennsylvania State University  
301 Life Sciences  
University Park, PA 16802

### **Other Participating Researchers**

Franklin B Pugh, PhD, Qiuying Shen, BACC, Yao Guo, MS – employed by Pennsylvania State University

### **Expected Research Outcomes and Benefits**

The increased responsiveness to tricyclic antidepressants vs. fluoxetine and the elevated HPA axis activity of  $\gamma 2^{+/-}$  vs. WT mice are characteristics of severe and relatively drug resistant forms of depression in patients known as melancholic and/or psychotic depression. Thus, we anticipate that the  $\gamma 2^{+/-}$  model of depression will allow the identification of gene expression changes representative of severe forms of depression in humans, especially including forms of the disorder that respond poorly to fluoxetine. Gene expression changes observed in  $\gamma 2^{+/-}$  vs. WT mice that are reversible by chronic treatment of  $\gamma 2^{+/-}$  mice with desipramine but not fluoxetine are of special interest. Moreover, gene expression changes reversed by fluoxetine *and* desipramine are expected to be representative of anxious but not depressive phenotypes.

### **Summary of Research Completed**

#### Production of mice and tissue harvest:

The mice to be used for experiments (6 females each per genotype (WT and  $\gamma 2^{+/-}$ ) and treatment (fluoxetine, desipramine, vehicle) were produced by crossing WT and  $\gamma 2^{+/-}$  mice. The offspring females were genotyped at 3 weeks of age and housed two mice per cage in a regular cage. Starting at eight weeks of age they were treated with fluoxetine or desipramine or vehicle alone (drinking water) for 4 weeks as described (Shen et al. 2010). Mice were decapitated in the room next to the husbandry room to avoid stress at (1:30 PM to 4 PM, mice kept on a standard 7AM:7PM light cycle) and the brains quickly dissected by hand using a Brain Matrix and Blades

(Electron Microscopy Sciences). Four consecutive 2 mm sections from Bregma + 2.4 to 5.6 (Paxinos and Franklin, 2001) were transferred to ice cold phosphate buffered saline (PBS). The cingulate cortex (2-3 punches, Gauge 15, per animal, in total) was punched from the first two sections and included part of the prelimbic cortex. The nucleus accumbens (2 punches) was obtained from the second section. The amygdala (2 punches) was obtained from the third section and the hippocampus (4 punches) from the third and fourth sections. The punches from two animals treated identically were combined and suspended in pre-labeled tubes containing 940  $\mu$ L of 1% formaldehyde in PBS at room temperature for 12 minutes. Crosslinking was stopped by addition of 64  $\mu$ L of 2M glycine. The tissue was washed with PBS and stored at -80degC for use once the protocols are optimized.

#### Adaptation of chromatin immunoprecipitation (ChIP) to brain tissue:

One issue we came across was that it is much harder to fragment brain tissue chromatin than chromatin isolated from cultured cells. Rather than using a cup sonicator used with cultured cells we ended up using a tip sonicator (Branson). A total of 20 cycles of 10 sec sonication at setting 2.5 100% output were needed to yield DNA in the 100 – 200 bp range.

#### Optimizing specificity of Immunoprecipitation:

Initial experiments were done with an H3K9me3 antibody (ab8898, Abcam, Cambridge, MA), which is associated with transcriptionally repressed chromatin. Similar experiments using H3K4me3, which is associated with actively transcribed gene promoters, are under way. To test for efficient and specific ChIP, aliquots of chromatin were immunoprecipitated with ab8898 on IgG coated magnetic beads or IgG coated beads alone. Aliquots of the precipitate were reverse crosslinked and subjected to analyses by PCR using three different primer pairs representative of the MapK13 and Foxe3 genes, which appear to be differentially expressed in  $\gamma 2^{+/-}$  vs. WT mice. These experiments revealed that DNA amplification was strictly dependent on the presence of the H3K9me3 antibody, and thus that immunoprecipitation was specific for the presence of H3K9 as expected.

#### Deep sequencing optimization (ongoing):

Accurate mapping of the chromosomal position associated with specific histone modification sites requires that immunoprecipitated DNA fragments are uniformly small (proximal to the bound histone that led to capturing of the sequence by immunoprecipitation). In addition the amount of DNA fragments isolated must be sufficient to allow detection of most of the genomic fragments associated with a particular histone modification, as well as an adequate dynamic range representative of the different frequencies these associations occur at different loci. Chromatin-derived DNA fragments to be sequenced have to be modified by addition of sample-specific barcode linkers for amplification, sample identification and sequencing. The successful addition of linkers and purification of linker-modified DNA requires two sequential gel purification steps that significantly compromise DNA yield. We are in the process of optimizing these steps to i) ensure linker addition is as efficient as it can be, ii) linker modified genomic DNA is not contaminated with linker dimers, and iii) that the yield of genomic DNA fragments is sufficient to allow detection of even those DNA fragments that are rarely associated with the modified histone species of interest. Test samples are analyzed by deep sequencing to estimate the complexity of the purified and linker modified DNA samples. Identification of each sequence based on its barcode allows that multiple samples are pooled and sequenced in a single flow cell.

The latest edition of our SOLiD sequencer produces 10<sup>8</sup> sequences per flow cells, which is sufficient to produce 50 million sequence reads for each of 20 samples.

### **Research Project 33: Project Title and Purpose**

*Tumor Associated Receptor Targeted Neuroimaging for Effective Diagnosis of HGA* – Our major intention in this project is to develop tumor targeted gadolinium loaded nanovesicles which will allow us to visualize tumor initiation and growth non-invasively in a much more efficient manner compared to free gadolinium. We will also study the ability of the gadolinium loaded IL-13 receptor targeted nanoliposomes to differentiate the radiation induced necrosis and tumor recurrence which is one of the common phenomenon observed among patients undergoing radiation therapy for brain tumors. Diagnosis of radionecrosis is a challenging issue because of the resemblance of radiological pattern with tumor recurrence. In our second aim we will focus more on differentiating the normal and tumor tissues using an IL-13 conjugated nanoconjugate known as quantum dots.

### **Anticipated Duration of Project**

9/1/2010 - 9/30/2011

### **Project Overview**

Glioblastoma Multiforme (GBM), which is classified as a high-grade astrocytoma (HGA), is considered the most devastating type of brain tumor. These tumors grow rapidly and infiltrate normal brain tissue. As a result, high-grade tumors can be difficult to treat surgically and many are resistant to current chemotherapeutic and radiation treatments. We have developed a nanotechnology strategy to target a liposomal delivery system selectively to high grade astrocytomas. Our overall goal is to successfully use the receptor targeted nanoliposomes and nanoparticles to diagnose and treat brain tumors.

*Specific Aim 1:* Determine the efficacy of using gadolinium loaded IL-13 conjugated liposomes to target and retain in the glioma tumors.

The ultimate goal of our project is to effectively image the glioma tumors in the intracranial glioma tumor bearing mouse models in an enhanced way so that the tumor formation can be detected at a much earlier stage and also the tumor boundaries can be marked distinctly to differentiate them from the normal healthy tissues. In order to achieve our goal of enhanced and tumor specific imaging we set forth the following aims to get the preliminary data which can lead to sustainable long term funding for the project.

Objective 1: To demonstrate that IL-13 conjugated nanoliposomes encapsulated with gadolinium can effectively target the intracranial glioma tumors and improve the imaging efficacy

Objective 2: To differentiate radiation induced necrosis and tumor growth using tumor targeted gadolinium enhancement.

*Specific Aim 2:* Investigation of the ability of IL-13 linked semiconductor quantum dots to mark the tumor boundaries in the established glioma tumors

Tracking the glioma tumor cell proliferation in *in vivo* models and demarking the tumor boundaries from normal tissues is one of the major issues in the surgical treatment of

Glioblastoma Multiforme (GBM). Due to the high proliferative capacity and tumor regrowth phenomenon of glioma tumors it is necessary to dissect them completely without leaving even traces of tumor. Quantum dots are demonstrated to be able to visualize by optical microscopic systems like IVIS imaging. As we utilize tumor associated receptor specific quantum dots, it would clearly distinguish tumor boundaries from normal healthy tissues. It will also be significant to diagnose the glioma tumor specimen based on their receptor expression using the targeted quantum dots.

Objective 1: To determine the suitability of IL-13QD for in vitro diagnosis of the glioma tumor from the biopsies and to determine the binding efficacy and intracellular fate in glioma cells.

Objective 2: Feasibility for in vivo optical imaging of receptor targeted quantum dots in glioma tumor bearing mice and to determine their in vivo toxicity.

### **Principal Investigator**

Achuthamangalam B. Madhankumar, PhD  
Assistant Professor  
H110, Department of Neurosurgery  
Penn State University College of Medicine  
Hershey, PA 17033

### **Other Participating Researchers**

Qing X. Yang, PhD, Jonas M. Sheehan, MD, Becky Slagle Webb, BS – employed by Pennsylvania State University

### **Expected Research Outcomes and Benefits**

In our first objective in specific aim 1, we intend to demonstrate that IL-13 conjugated nanoliposomes encapsulated with gadolinium can effectively target the intracranial glioma tumors and improve imaging efficacy. In this study we will evaluate an IL-13 conjugated liposome based gadolinium (Gd) contrast agent for its ability to circulate, to be stable in the blood, to provide tissue contrast and to actively target glioma tumors. Mice with and without intracranial tumors will be subjected to a treatment regimen with targeted liposomes containing gadolinium. We will monitor growth of the tumors with gadolinium by periodic MRI. We anticipate that targeted liposomes carrying gadolinium will improve the T1 weighted MRI imaging and also we expect the formulated nanoliposomes to have prolonged imaging properties. In our second objective we wish to differentiate radiation induced necrosis and tumor growth using tumor targeted gadolinium enhancement using targeted liposome approach. The mouse after radiation induced injury and tumor induction will be subjected to MRI after administration of Gd in free form and in targeted liposomal formulations. We expect the targeted Gd encapsulated liposomes should differentiate the tumor from radiation induced necrosis.

In our second aim we wish to determine the suitability of IL-13QD for in vitro diagnosis of the glioma tumor from the biopsies and to determine the binding efficacy and intracellular fate in glioma cells. We wish to demonstrate the tumor specific binding ability and intracellular fate of the targeted quantum dots in glioma tumors. As a second objective we wish to study the

feasibility for *in vivo* optical imaging of receptor targeted quantum dots in glioma tumor bearing mice and to determine their *in vivo* toxicity where we intend to study the quantum dot localization in the *in vivo* tumor mouse model which can be visualized by intravital microscopy.

## Summary of Research Completed

One of our main goals in this project is to formulate and optimize protein or antibody conjugated liposomes carrying gadolinium an MRI contrast agent, and subsequently to characterize them for imaging the brain tumors effectively with improved tumor contrast properties. Secondly we propose to utilize IL-13 conjugated semiconductor quantum dots for *in vitro* and *in vivo* imaging of glioma tumors. To achieve this goal we performed the preliminary experiments using IL-13 conjugated liposomes carrying gadolinium (IL-13-Lip-Gd) and IL-13 conjugated quantum dots in the cell culture and *in vivo* animal models.

### *Aim 1: Efficacy of IL-13-Lip-Gd for imaging brain tumors*

Here our aim is to demonstrate the ability of these tumor targeted nanoliposomes to show improved MRI contrast property after transporting across the blood-brain barrier and to determine their *in vivo* stability. We formulated IL-13 conjugated liposomes carrying gadolinium and characterized them for particle size and Gd encapsulation. Liposomes were formulated using 1,2-dipalmitoyl-*sn*-glycero-3-phosphocholine (DPPC), cholesterol, 1,2-distearoyl-*sn*-glycero-3-phosphoethanolamine-N-[carboxy(polyethylene glycol)-2000] (ammonium salt) (DSPE-PEG2000), 1,2-distearoyl-*sn*-glycero-3-phosphoethanolamine-N-[maleimide(polyethylene glycol)-2000] (ammonium salt) (DSPE-PEG-Mal) in a mole ratio of 10:5:0.5:0.2.5 which were dissolved in methanol and chloroform in a ratio of 1:1 (v/v). A thin lipid film formed in a round bottom flask using a rotary evaporator (Buchi, Germany). Subsequently, the film was dried under nitrogen and reconstituted in a saturated solution of gadopentetate dimeglumine (Magnevist<sup>R</sup>, Bayer, Inc).

We also optimized the condition for improving the gadolinium encapsulation within the liposomes. For example in our earlier protocol we utilized centriprep concentrator for concentrating the liposomes, which resulted in leakage of liposomes due to high speed centrifugation. This method was modified and we adapted freeze-drying and reconstitution in lower volume of buffer as a method of concentrating the liposomes.

*In vitro relaxivity studies:* One of the potential problems when imaging the tumors or tumor cell line is the quenching effect of the gadolinium as they are encapsulated inside the liposomes. So the water accessibility for the gadolinium is reduced substantially. We devised a method to characterize this ‘quenching effect’ and to determine the duration of quenching of the liposome encapsulated gadolinium compared to free gadolinium. This quenching will have direct effect on the MRI contrast properties in the tumors. We demonstrated this by culturing U251 glioma cells and exposing them to tumor targeted gadolinium liposomes, followed by T1 relaxivity measurement using MRI. We observed that T1 was quenched by liposome encapsulated gadolinium initially (1 h) as evident from T1 relaxation time (Table 1). But later on after incubating the cells for 24 h, the quenching effect was recovered. This indicated that the liposomes once they internalize the glioma cells by endocytosis and release the encapsulated gadolinium in the intracellular region after 24h, thereby the Gd can interact with the water

molecules. This produces an improved T1 MRI contrast image.

#### *In vivo MRI contrast*

As the blood-brain barrier (BBB) of intracranial tumor model with U251 cell line is known to be compromised (leaky vasculature), it is harder to conclude from the liposome accumulation in the tumor that they are capable of getting through the BBB. In order to show the proof of concept that the tumor targeted liposomes carrying the gadolinium get across the BBB, preliminary experiments were performed with Magnevist and IL-13-Lip-Gd injected in mice without tumor (tail vein injection) and measuring the signal and contrast enhancements in the brain and pituitary gland. Since the anterior part of pituitary gland does not have BBB it can be used as an intracranial reference outside BBB. After injection of Magnevist, a large increase (~15%) in signal to noise ratio (SNR) exhibited in the pituitary gland while brain SNR remained unchanged (Figure 1). After injection of IL-13-Lip-Gd, however, the SNRs in *both* pituitary gland and the brain are increased in almost identical fashion. After demonstrating this property in non-tumor bearing mice we are currently in the process of demonstrating the contrast property in the tumor bearing mice.

For radiation necrosis study we used athymic nude mice exposed to various dose of radiation (60Gy, 75Gy and 100 Gy/2 mice per dose) to induce necrosis. The animals could not withstand these doses and they died. From our previous experience we know that 20 Gy radiations were not able to induce necrosis in the mouse model. So no further attempt was made to generate the radiation induced necrosis model.

#### *Aim 2: Tumor targeted quantum dots to detect the glioma tumors*

##### *In vitro studies*

##### *Formulation of IL-13 conjugated quantum dots*

CdSe quantum dots functionalized with carboxylic acid was purchased from Ocean Nanotech Inc. Human IL-13 protein was made in our laboratory using a plasmid encoding the protein and recombinantly expressed in *E.Coli* and purified using Ni column. IL-13 protein was conjugated to the carboxylic acid groups using water soluble carbodiimide (EDC) as conjugating agent. After conjugating IL-13 the particles were confirmed for their conjugation by agarose gel electrophoresis method (Figure 2).

##### *In vitro binding of IL-13QD*

In vitro binding experiments were performed using targeted (IL-13 conjugated quantum dots, IL-13QD) and non-targeted quantum dots on U251 human glioma cells. For binding studies 20,000 cells per well were plated in an 8 well chamber slide which was cultured overnight at 37°C. These cells were exposed to blocking buffer to remove any non-specific binding followed by 100 fold excess of IL-13 protein for 1h. These wells were then exposed to quantum dots at 1mM concentration at 4°C for 10 minutes. The media was aspirated and fixed on coverslides and dried. When observed under fluorescence microscopy binding of IL-13 QD to the glioma cells were evident (Figure 3), whereas the sham control and CD20 conjugated quantum dots were not able to bind to the glioma tumors. When the receptor sites on the tumor cells were blocked with 100 fold excess of IL-13 protein, no binding of IL-13QD was observed. The binding study clearly demonstrated the receptor specific binding of IL-13 conjugated quantum dots to the glioma cells.

*In-vivo imaging studies with IL-13 QD*

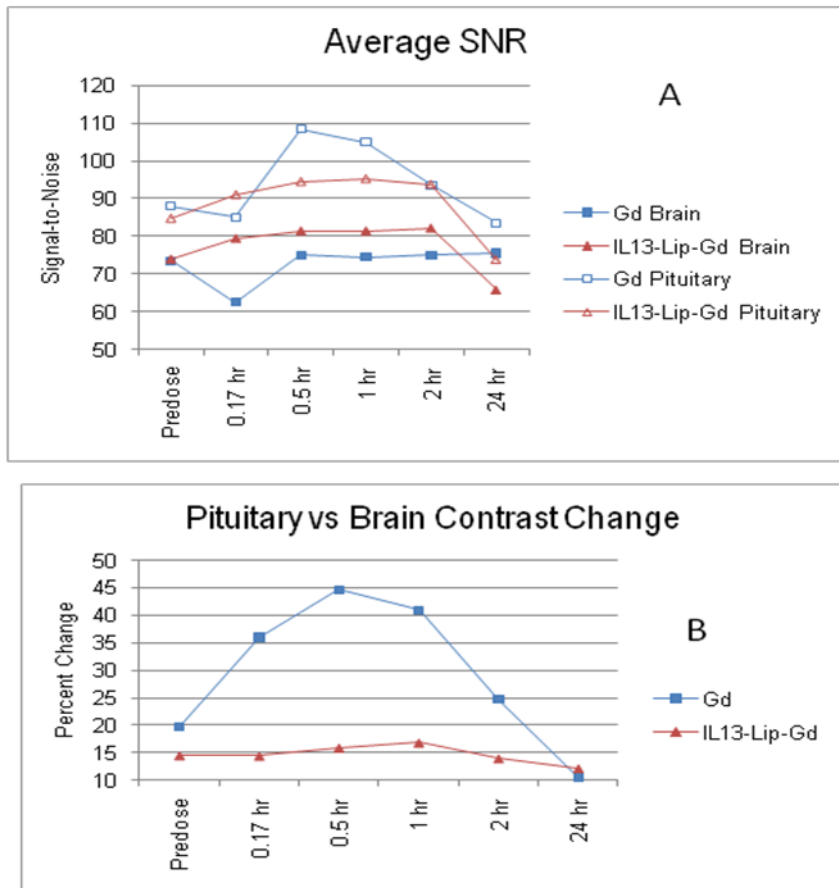
For our studies, a subcutaneous glioma tumor model was established in athymic nude mice by implanting  $15 \times 10^6$  cells subcutaneously. When the tumor volume reaches 15-30 mm<sup>3</sup>, targeted quantum dots were injected through tail vein and imaged using IVIS imager (Caliper Sciences, Inc.) at various time periods in a wavelength region of 600-800 nm. We had 4 animals for our studies (2 animals per group). In one group the animal was injected with IL-13 conjugated non-pegylated quantum dots. In another group they were administered with IL-13 conjugated pegylated quantum dots. From the images it is clear that there is a significant accumulation of quantum dots in the tail vein region (injection site), at least for 24 hours, before distributing to other regions. There was a random distribution of targeted QD particles. However with pegylated quantum dots we observe accumulation in the tumor with some accumulation in other organs also. Intratumoral injection of IL-13 conjugated quantum dots demonstrates the tumor retention property of the IL-13QD for more than 72 hours without substantial loss in the signal intensity.

*Problems encountered/Alternative strategies:*

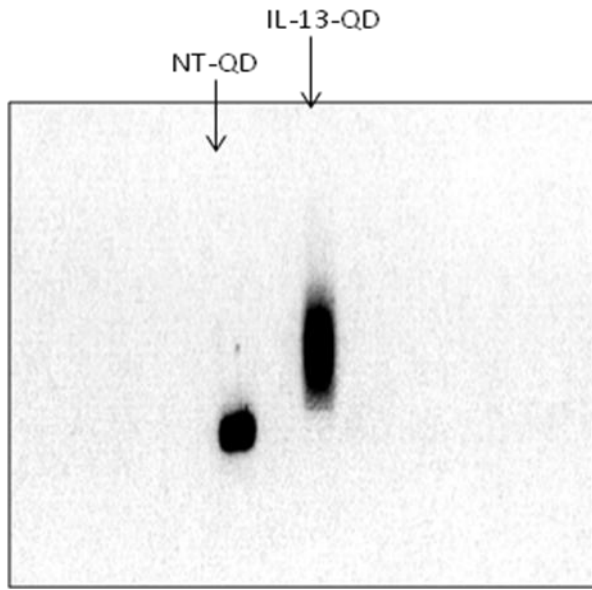
One of the problems we encountered with the tumor targeted quantum dots is their accumulation in the tail vein for prolonged period of time. It is evident from our in vivo experiment that pegylated quantum dots distribute faster than non-pegylated quantum dots. Although there may be several reasons for this behavior we predict that aggregation or immobilization of the QD's at the site of injection seems to be the major reason for such behavior. We are planning to overcome this problem by suspending the quantum dots in FBS before injection, because it has been reported that fetal bovine serum was able to prevent the aggregation of quantum dots. We would also perform other surface modifications to the targeted quantum dots to prevent the aggregation in the serum.

Table 1. T1 of Magnevist and IL-13-Lip-Gd before and after digestion. The T1 “quenched” by encapsulation by the liposome was recovered. The concentration of Gd was normalized for both Magnevist and IL-13-Lip-Gd as 100ug/ml.

Incubation time	Media only	Liposomes+Cell + Media	Magnevist+ Cell +Media
1 h	2592 ms	280 ms	146 ms
22h	2836 ms	198 ms	145 ms



**Figure 1-** The SNR enhancements in pituitary gland and brain followed similar temporal pattern following injection of IL-13-Lip-Gd (A), leading to no contrast change (B). Data for Magnevist injection are also shown (in blue) as a control. The SNR enhancements by IL-13-Lip-Gd are less than Magnevist because the relaxivity of Gd was “quenched” by the encapsulation of liposome. Four mice were used.



**Figure 2-** Agarose Gel Electrophoretogram: Quantum Dots conjugated to protein (right, IL-13 conjugated QD) travel more slowly through the gel than unconjugated dots (left, non-targeted QD), demonstrating successful attachment of protein. Image was acquired on a Fujifilm dark box scanner.

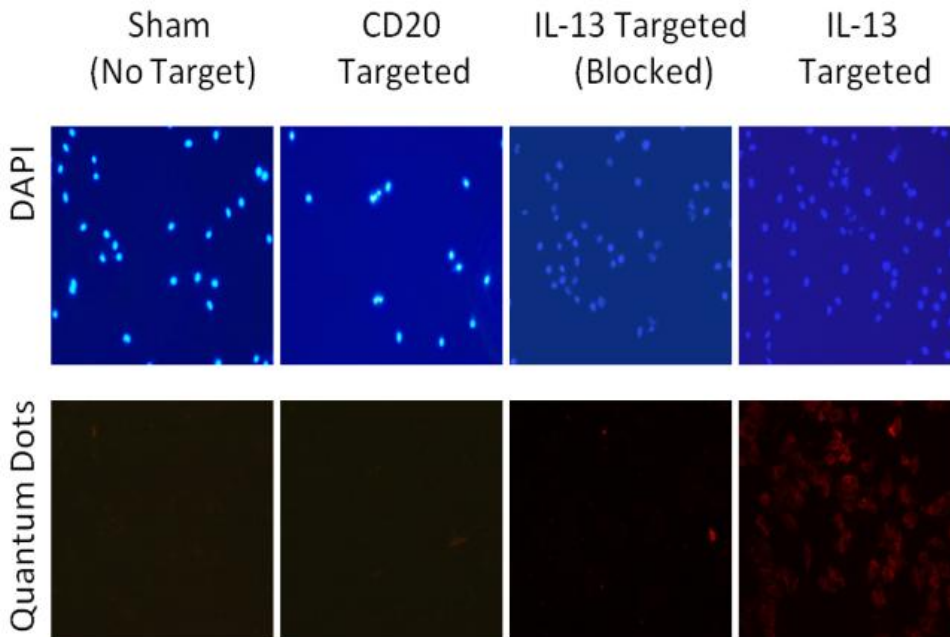


**Figure 3 -** Fluorescence Microscopy: Three control conditions demonstrate specific binding of IL-13 targeted quantum dots to U251 glioma cells. Sham quantum dots with no targeting ligand, CD20-targeted quantum dots, and IL-13-targeted quantum dots with blockade using 100-fold excess IL-13, all showed virtually no binding due to competitive binding by excess IL-13. In contrast, IL-13-targeted quantum dots bind avidly to U251 cells when the receptor was available for binding.

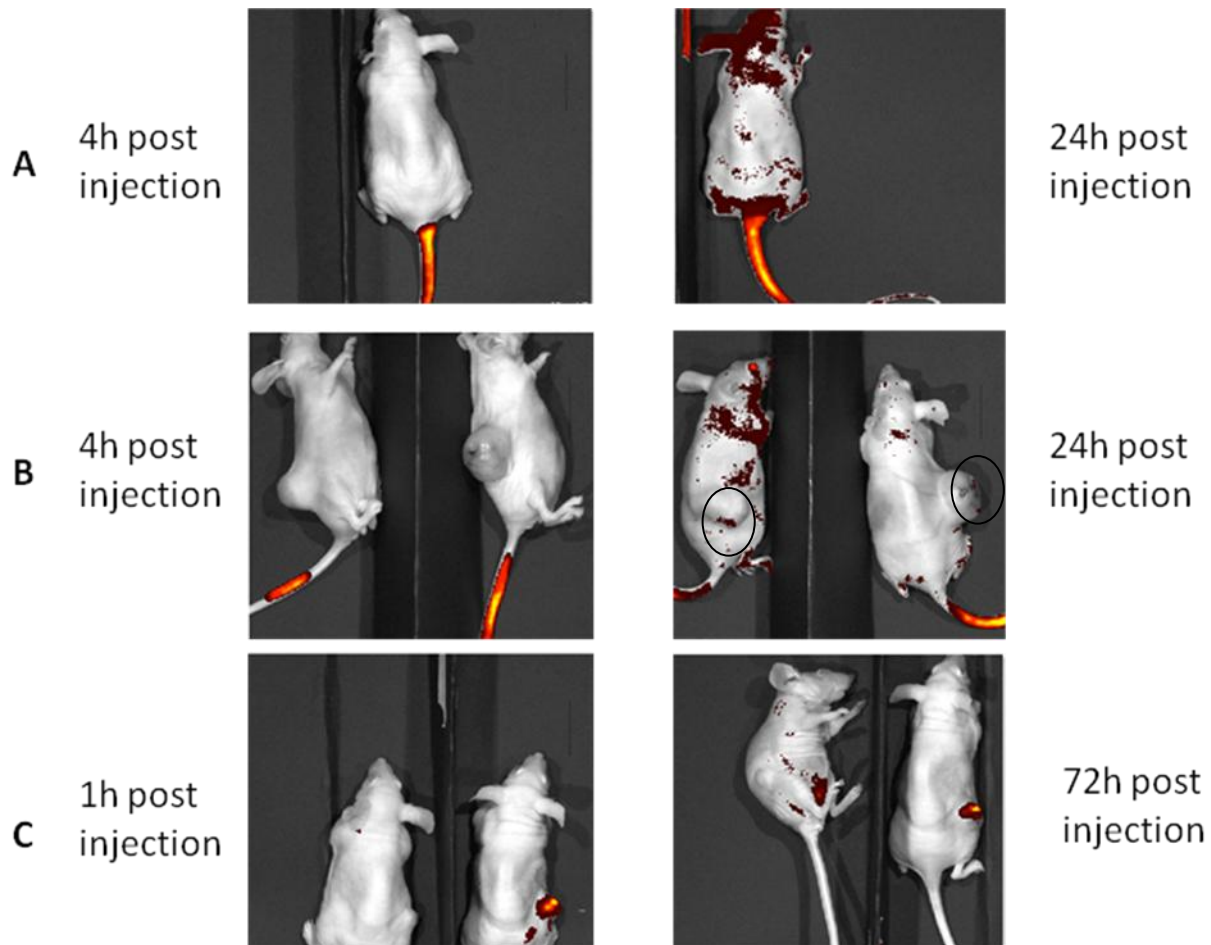


**Figure 4 - In-Vivo Fluorescence:** Nude mice injected with IL-13 conjugated (non-pegylated) quantum dots in the tail vein showed random distribution after 24 Hours (panel A). Mice injected with IL-13 conjugated pegylated quantum dots in the tail vein showed random distribution after 24 hours with some limited accumulation in the tumor (Panel B). Mice injected with IL-13 conjugated (non-pegylated) quantum dots intraperitoneally (left) and intratumorally (right) showed limited distribution of the particles after 3 days in both cases.

### **Research Project 34: Project Title and Purpose**

*Viral RNA Trafficking in Living Cells* – Mouse mammary tumor virus (MMTV) is a retrovirus that causes adenocarcinoma in mice, and MMTV-like elements have been detected in human breast cancers. This project focuses on how MMTV commandeers cellular machinery to facilitate capsid assembly with the ultimate goal of identifying targets for the treatment of retrovirus-induced cancers.

### **Duration of Project**

9/1/2010 - 6/30/2011

## **Project Overview**

This project focuses on the mechanism used by the oncogenic retrovirus MMTV to produce new virus particles in infected mammary cells. We have compelling new evidence that MMTV capsids associate with RNA processing machinery, which is the foundation for our hypothesis: MMTV genomic RNA (gRNA) is targeted to PB/SG/RISCs where it binds to the structural protein Gag to encapsidate the viral genome into assembling capsids. The movement of MMTV Gag and gRNA are dynamic, transient events that can only be revealed using realtime imaging of individual living cells. Therefore, to test our hypothesis, we will develop an innovative method to track MMTV gRNA in live cells using florescence microscopy.

Specific Aim 1: Identify RNA processing factors that mediate MMTV gRNA trafficking in living cells. Following integration of proviral DNA into the host genome, retroviruses produce unspliced viral RNAs that are used for encapsidation into virions (gRNA) or as a template for protein synthesis (mRNA). To initiate capsid assembly, Gag binds the gRNA, then multimerizes to form an immature capsid. Efficient assembly requires that gRNA be separated from viral mRNA and transported to intracellular sites of Gag accumulation. However, the mechanism used to sort gRNA from viral mRNA is unknown. Our preliminary studies suggest that MMTV hijacks the mRNA-silencing pathway to sequester its gRNA into a protected environment, where Gag proteins are localized. Because micro-RNAs (mi-RNAs) bind complementary sequences in mRNAs to suppress their translation, it is feasible that viral or host encoded mi-RNA could serve as a tag to “mark” MMTV gRNA, directing it to PB/RISCs. To test the idea that PBs/SGs/RISCs serve as the staging site for MMTV capsid assembly, we propose this set of experiments:

- 1a. Track MMTV RNA in living cells to visualize sites of gRNA localization.
- 1b. Determine the role of PB/SG/RISCs in MMTV gRNA trafficking.
- 1c. Determine whether the mi-RNA pathway influences MMTV gRNA localization

## **Principal Investigator**

Leslie J. Parent, MD  
Professor  
Penn State University College of Medicine  
Division of Infectious Diseases, MC H036  
500 University Drive  
Hershey, PA 17033

## **Other Participating Researchers**

Darrin Bann, BS – employed by Pennsylvania State University

## **Expected Research Outcomes and Benefits**

Approximately 15–20% of malignancies worldwide are linked to infection. HTLV-I (human T-cell leukemia virus type-I), the cause of T-cell leukemia, was the first human retrovirus discovered. More recent work implicates a murine-derived retrovirus in prostate cancer, and MMTV-related sequences and antibodies were detected in women with breast cancer. The

possibility that an MMTV-like agent may contribute to human breast cancer highlights the need for a more thorough understanding of how MMTV replicates to identify novel therapeutic targets. Through this work, we will identify cellular pathways used by MMTV for virus replication; these pathways may serve as novel targets for the development of new antiviral drugs to treat virus-induced cancers.

An ongoing mystery in retrovirology is how viral mRNA is distinguished from genomic RNA. Because MMTV Gag proteins localize to RNA-induced silencing complexes, as do micro-RNAs (mi-RNA), we propose the innovative hypothesis that a mi-RNA might “mark” MMTV genomic RNA to sequester it in cytoplasmic P bodies or RNA-induced silencing complexes to facilitate virion assembly. While a host-encoded mi-RNA could be a defensive strategy to promote degradation of genomic RNA, we propose that MMTV evolved a counter-offensive measure by protecting genomic RNA prior to its destruction by binding to MMTV Gag in RNA-induced silencing complexes. Alternatively, MMTV might encode its own mi-RNA to separate its genomic RNA from the translation pathway and ensure genome packaging. This project will test these intriguing models of MMTV gRNA encapsidation.

### **Summary of Research Completed**

To initiate the assembly of new virus particles within infected cells, the Gag protein selectively binds to the viral RNA genome (gRNA). Binding of Gag to gRNA initiates oligomerization of Gag and eventually results in the formation of complete virus capsids. For mouse mammary tumor virus (MMTV), immature viral capsids form within the cytoplasm of the cell. The purpose of this proposal was to develop a method to tag viral RNA of MMTV with a fluorescent reporter protein and investigate the role of cellular RNA processing factors in intracellular viral capsid formation.

These are our accomplishments during this funding period:

1. We adapted the  $\lambda_{\text{NeGFP}}$  RNA tracking system to test the effect of stress granule and P body proteins Yb1, Mov10, and Ago2 depletion on MMTV RNA trafficking. Four fused repeats of the bacteriophage lambda coat protein linked to three eGFP ( $\lambda_{\text{NeGFP}}$ ) molecules bound RNA containing 4-16 repeats of a 15 nt stem-loop structure (boxB) (Figure 1A). To avoid technical difficulties with proviral RNA, we created a construct containing MMTV R and U5; 746 nt of the *gag* coding sequence; the Rem response element (RemRE), required for nuclear export of unspliced MMTV RNA; and multiples of four Box-B repeats (CMV-R-U5- $\Delta$ Gag-RemRE-BoxB) (Figure 1A). MMTV R, U5, and 400 nt of *gag* coding sequence was sufficient for RNA encapsidation into virions. Packaging of CMV-R-U5- $\Delta$ Gag-RemRE-BoxB into virus produced by normal mouse mammary epithelial (NMuMG) cells infected with the MMTV C3H strain (NMuMG.C3H) will be confirmed by reverse transcription PCR.

2. In NMuMG.C3H cells, a nuclear localization signal confined  $\lambda_{\text{NeGFP}}$  to the nucleus (Figure 1B top). Expression of a BoxB-containing RNA, Srprb-mRFP-boxB, relocalizes  $\lambda_{\text{NeGFP}}$  to the cytoplasm (Figure 1B bottom). Srprb-mRFP is a marker for Srprb-mRFP-boxB RNA expression. To determine whether  $\lambda_{\text{NeGFP}}$  affected RNA trafficking to SGs, NMuMG.C3H cells expressing  $\lambda_{\text{NeGFP}}$  and Srprb-mRFP-boxB were heat shocked (HS) at 44°C for 15 min. As expected,

$\lambda_{\text{NE}}\text{GFP}$  relocalized to SGs with the SG marker Yb1 (Figure 1C top). Cyclohexamide (CHX) dissolves preformed SGs in stressed cells. Treating heat-shocked cells with CHX for 15 min at 44°C dissolved Yb1-containing SGs, and  $\lambda_{\text{NE}}\text{GFP}$  was diffusely cytoplasmic (Figure 1C bottom). These data demonstrate the feasibility of the  $\lambda_{\text{NE}}\text{GFP}$  system, and that  $\lambda_{\text{NE}}\text{GFP}$  does not affect trafficking of boxB-containing RNA to SGs.

3. We demonstrated that stress granule proteins G3BP-1, TIA-1, HuR, PABC-1, and Yb1 associated with MMTV Gag proteins within infected cells (Figure 2). MMTV Gag co-localized with each of these cellular RNA processing factors at discrete sites within the cytoplasm. We are investigating whether these foci are sites of MMTV capsid assembly.

4. To determine whether the Gag protein itself, in the absence of other viral components, was sufficient for the association with RNA processing factors, we expressed Gag-GFP with stress granule proteins. These experiments (Figure 3) revealed that Gag itself co-localizes with stress granule proteins. We also found that the NC region of Gag, which harbors the RNA interaction domain, is essential for the localization of Gag at cytoplasmic RNA processing sites. Recent studies showed that the interaction of Gag with Yb1 is RNA-mediated. Thus, we conclude that Gag interacts with stress granule components through an RNA intermediate, possibly the viral RNA.

5. We determined that MMTV Gag associated with endogenous Yb1 protein, indicating that ectopic expression of Yb1 was not required for re-localization of Gag to sites of stress granule protein accumulation. We observed that Gag localized with a subset of Yb1 in the cytoplasm that was not involved in the formation of stress granules; rather Gag appeared to interact with a population of Yb1 that was insensitive to cyclohexamide. We propose that Gag and Yb1 associate in the cytoplasm as part of the assembly pathway of MMTV capsids, independently of stress granule formation.

6. We showed that MMTV viral RNA (detected by  $\lambda_{\text{N}}\text{-eGFP}$ ) also associated with stress granule proteins Yb1, PABC-1, and HuR. Thus, it appears that both Gag and viral RNA localize with RNA processing factors. It is not clear whether these trafficking steps are linked or occur independently. Our results support the hypothesis that MMTV viral RNA is shunted away from translation machinery by host RNA processing factor protein to direct it toward the Gag protein at sites of capsid assembly.

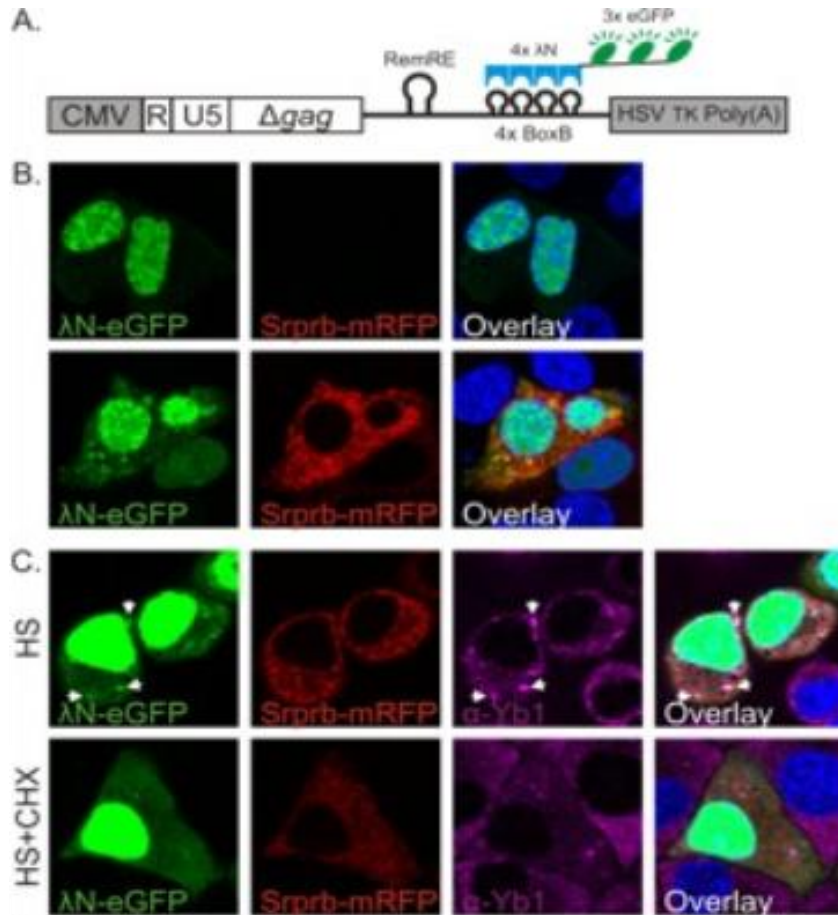


Figure 1.  $\lambda_N$  live cell RNA tracking system.

A) CMV-R-U5- $\Delta$ Gag-RemRE-BoxB contains the MMVT packaging signal, the RemRE, and 4 or 16 boxB loops, which are bound by the  $\lambda_N$ -eGFP reporter. B) Top: In the absence of boxB-containing RNA  $\lambda_N$ -eGFP is confined to the nucleus. Bottom: Expression of Srprb-mRFP-BoxB, which has 4 boxB loops, relocalizes  $\lambda_N$ -eGFP to the cytoplasm. Srprb-mRFP, an ER protein, is a marker for the presence of Srprb-mRFP-BoxB RNA. C) Top: Heat shock (HS) at 44°C causes Srprb-mRFP-BoxB bound by  $\lambda_N$ -eGFP to accumulate in Yb1-containing SGs (arrows). Bottom: Treatment of HS cells with cycloheximide (CHX) dissolves SGs and  $\lambda_N$ -eGFP returns to a diffuse cytoplasmic distribution.

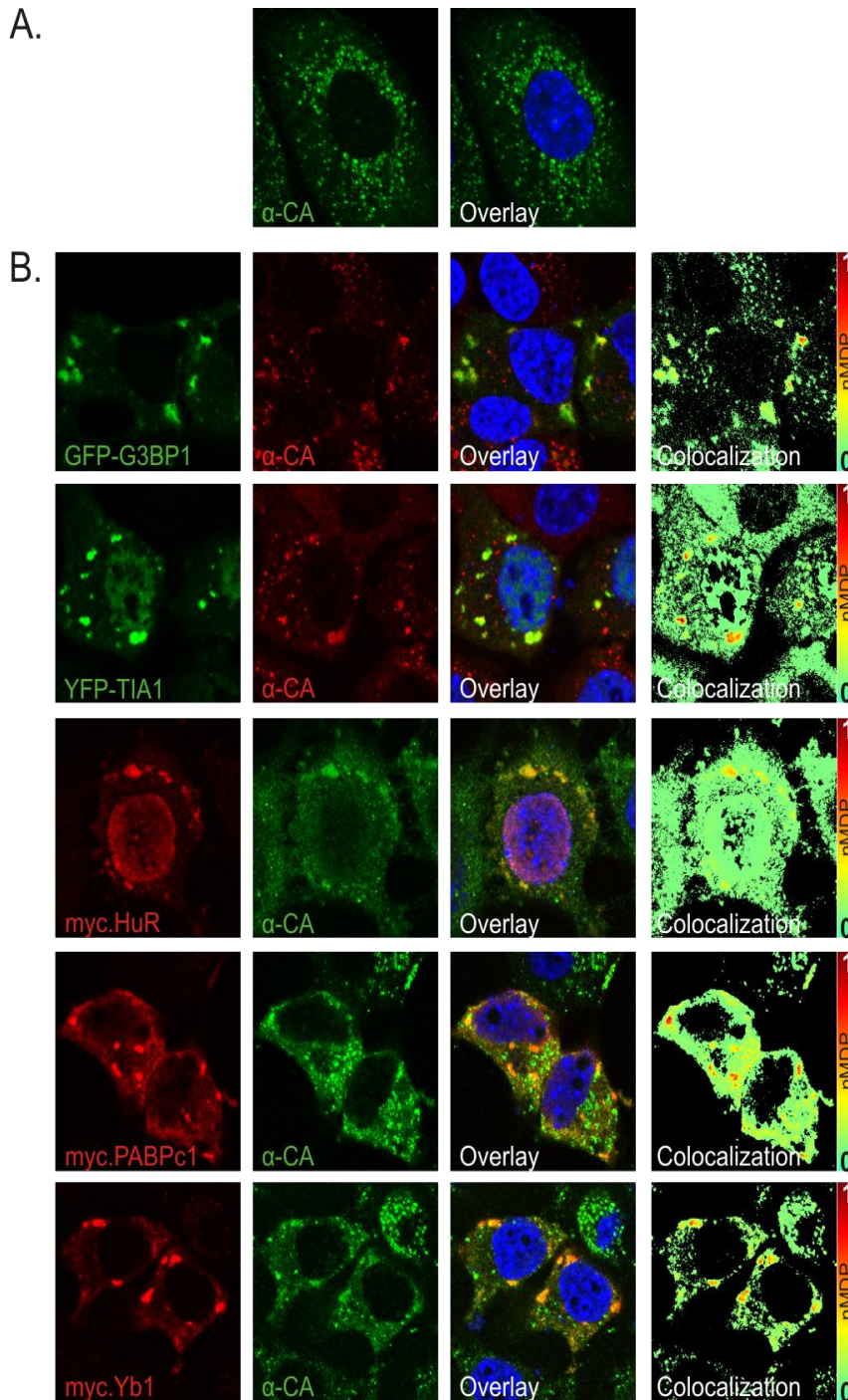


Figure 2. (A) In MMTV-infected normal mouse mammary epithelial (NMuMG) cells immunostained with anti-capsid antibody ( $\alpha$ -CA), assembling MMTV capsids form small cytoplasmic foci. (B) Transient transfection of MMTV-infected NMuMG cells with fluorophore- or myc-tagged SG components results in the formation of cytoplasmic SGs and redistribution of Gag from discrete foci to SGs. Thermal pseudocolored colocalization maps (far right) were generated using the Colocalization Colormap plug-in for Image J. Colocalization is quantified by normalized mean deviation product (nMDP) where 0 indicates no colocalization and 1 indicates a high degree of colocalization.

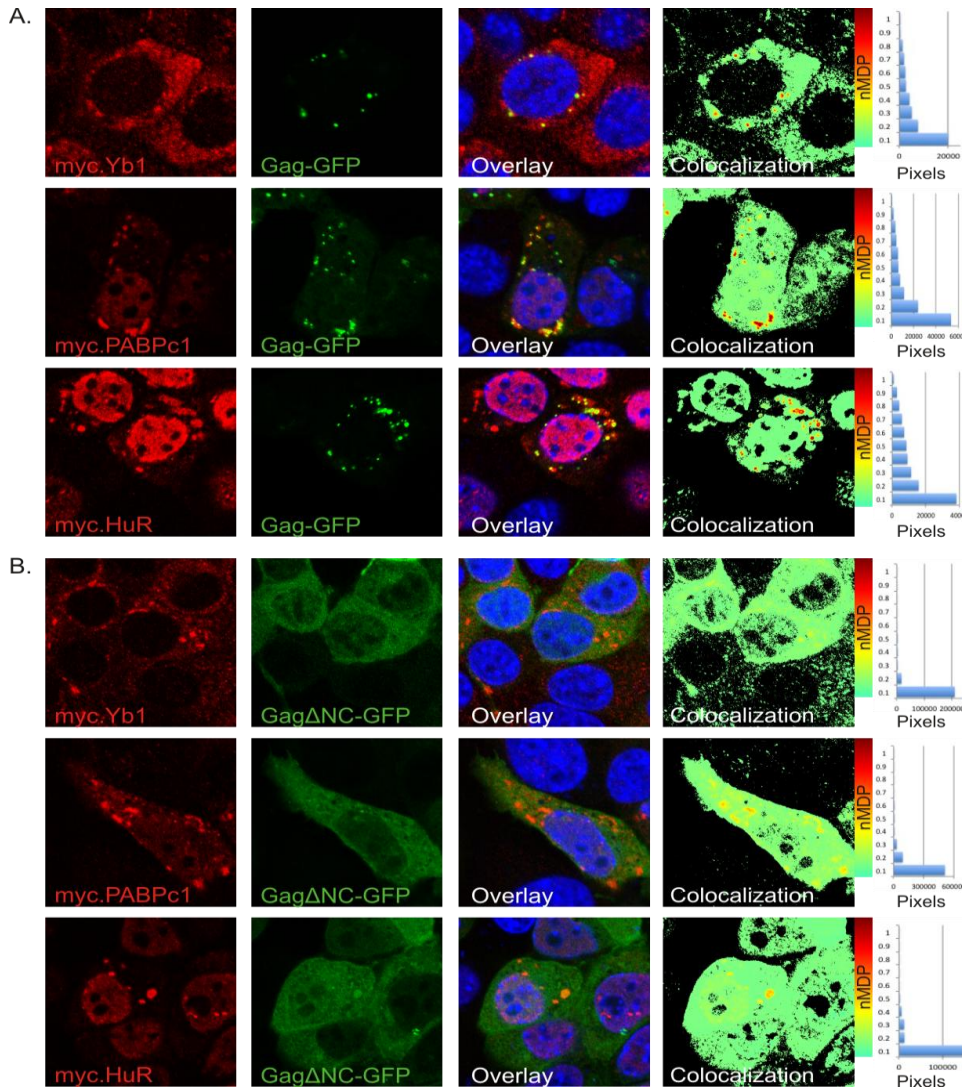


Figure 3. (A) NMuMG cells were co-transfected with myc-tagged SG components and a construct expressing MMTV Gag tagged with GFP (Gag-GFP) in the absence of any other viral factors. MMTV Gag-GFP was sufficient to localize to SGs. Histograms on the right show the number of pixels at each nMDP value. B) The NC domain of Gag mediates both Gag-Gag and Gag-RNA interactions. A Gag truncation mutant in which the NC domain was deleted (Gag $\Delta$ NC-GFP) displayed a reduced ability to colocalize with SG components, as indicated by a reduction in the number of pixels at high nMDP values. This finding suggests that RNA binding is required for Gag to interact with SG components.

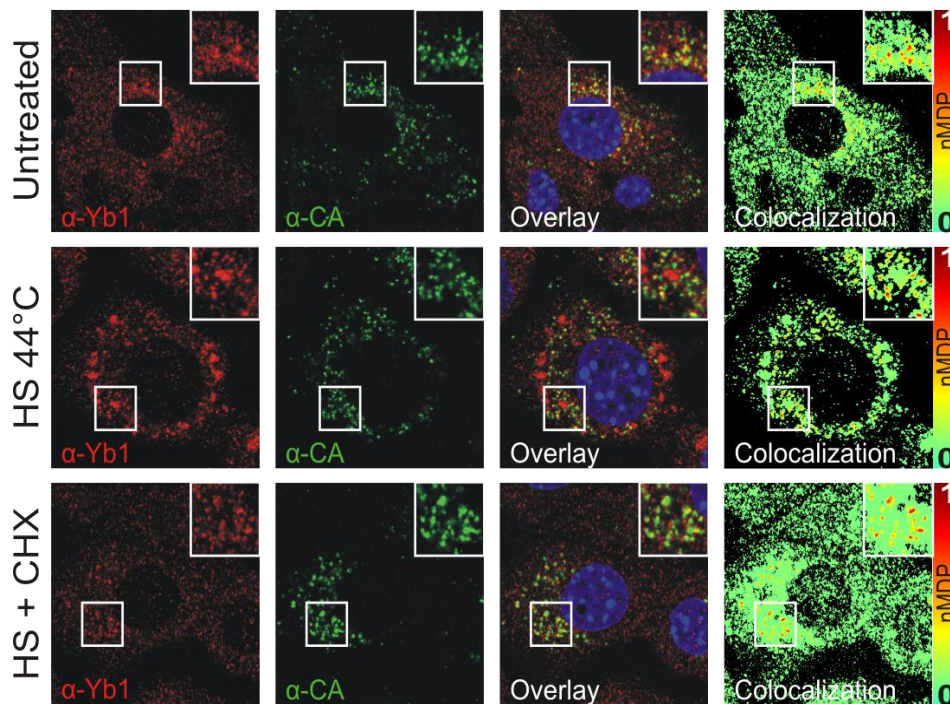


Figure 4. Co-localization of MMTV Gag and endogenous Yb1. MMTV-infected NMuMG cells were immunostained for capsid and the SG component Yb1. The distribution of capsid partially overlapped that of Yb1 (top row, inset). When cells were heat shocked (HS) at 44°C for 30 min., some Yb1 remained associated with Gag while another subset relocated to SGs (middle row). Cyclohexamide (CHX) dissolved SGs but did not disrupt Gag-Yb1 interactions (bottom row).

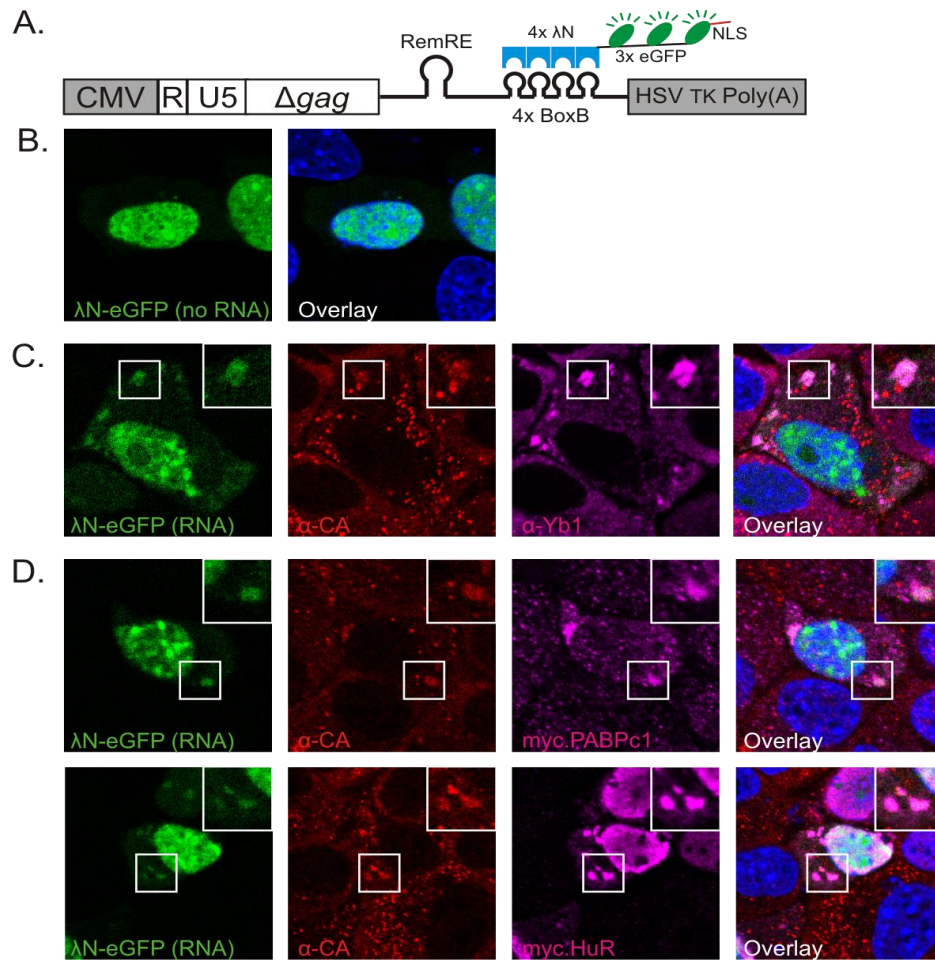


Figure 5. (A) The CMV-R-U5- $\Delta$ gag-RemRE-4BoxB subviral MMTV construct RNA is bound by the  $\lambda$ N-eGFP reporter. B) When expressed alone,  $\lambda$ N-eGFP is confined to the nucleus. C) MMTV-infected NMuMG cells were co-transfected with CMV-R-U5- $\Delta$ gag-RemRE-4BoxB and  $\lambda$ N-eGFP, then immunostained for CA and endogenous Yb1. MMTV RNA, Gag, and Yb1 colocalized in cytoplasmic granules (insets). D) MMTV-infected NMuMG cells were transfected with CMV-R-U5- $\Delta$ gag-RemRE-4BoxB,  $\lambda$ N-eGFP, and myc-tagged SG components then immunostained using  $\alpha$ -CA and  $\alpha$ -myc antibodies. As with endogenous Yb1, the MMTV RNA, Gag, and SG components colocalized in cytoplasmic granules.

### **Research Project 35: Project Title and Purpose**

*Social Networking for Activity Promotion with Cell Phones (SNAP-C)* – Programs designed to help sedentary adults increase their physical activity are often effective in the short-term, but these effects are rarely maintained. Technology-based physical activity programs, such as those using cell phones, may help expand social networks that could support maintenance of physical activity. This project aims to explore the efficacy of using cell phones to engineer social networks that could provide long-term support for active lifestyles. We plan to conduct a randomized controlled trial that compares an intervention group (Social Networking for Activity Promotion with Cell Phones: SNAP-C) to a minimal treatment control group (Usual Care).

## **Anticipated Duration of Project**

9/1/2010 - 6/30/2012

## **Project Overview**

Our project is a randomized controlled trial based on the Behavioral Ecological Model to evaluate the efficacy of using cell phones to build social networks for physical activity (PA). Engineering supportive social networks for PA could increase longer-term maintenance of PA and prevent the decline in PA that typically occurs after interventions end. However, little research has explored how to engineer social networks to increase opportunities for PA.

Cell-phones hold potential to expand social networks for PA because they are widely used and can provide portable interventions with real-time social cues and reinforcement for PA. The use of cell-phones for promoting PA remains underexplored relative to other intervention modalities. We propose to add a cell phone intervention arm to a prior-funded K99/R00 randomized controlled trial that is being conducted to evaluate the effectiveness of an email and web-based intervention to build social networks for PA. The primary specific aims of the cell-phone based intervention arm are to:

1. Compare the effects of a cell phone-based social networking intervention for PA (Social Networking for Activity Promotion with Cell Phones: SNAP-C) to a minimal treatment control group (Usual Care) on change in: aerobic fitness, step counts, blood pressure, body mass index (BMI), and self-reported moderate and vigorous PA from baseline to post-test.
2. Evaluate the moderator effects of selected individual-level self-management skills (goal setting, planning, self-monitoring), ecological variables (number of social networks and activity partners for PA/walking, built environment characteristics, and neighborhood walkability) on treatment group outcomes.
3. Conduct a process evaluation of SNAP-C (recruitment rates, intervention delivery and treatment fidelity, participation rate) to inform the feasibility of future cell-phone interventions and refinements to intervention procedures.

## **Principal Investigator**

Liza S. Rovniak, PhD, MPH  
Assistant Professor of Medicine and Public Health Sciences  
Penn State University College of Medicine  
500 University Drive  
Mail Code H034  
Hershey, PA 17033

## **Other Participating Researchers**

Jennifer L. Kraschnewski, MD, MPH, Stephen A. Matthews, PhD, Chester A. Ray, PhD, Christopher N. Sciamanna, MD, MPH, Michele L. Shaffer, PhD, S. Shyam Sundar, PhD – employed by Pennsylvania State University

## **Expected Research Outcomes and Benefits**

While extensive research supports the importance of social networks for PA promotion, little intervention research has been conducted to explore optimal strategies for implementing social network support systems. This study will contribute new knowledge about how to implement effective social networks, which is urgently needed, given that 70% of U.S. adults are currently inactive.

If participants engage in regular PA, as recommended by both the SNAP-C Intervention and the Usual Care groups, they will likely improve their physical fitness, which is associated with reduced risk of cardiovascular disease, some cancers, diabetes, and high blood pressure. They may also feel as if they have more energy and improved mental well-being as a result of participating in regular PA. On a societal level, the knowledge gained from this program may help researchers to develop more effective PA programs, which could reduce health care costs and morbidity associated with sedentary lifestyles.

## **Summary of Research Completed**

During the initial study period, the research team conducted extensive developmental work to prepare for the launch of the SNAP-C research project. We anticipate starting recruitment of participants in the next month. We have completed the following project developmental activities.

### Staffing:

We hired and trained a project coordinator to help manage this project. The project coordinator has a master's degree in bioengineering and prior experience in health-related research, computer programming, and statistical analyses. We also have interviewed/lined-up other students/job applicants to assist the coordinator during busier study periods (e.g., recruitment, assessments). All existing project staff successfully completed Human Subjects/Institutional Review Board training.

### Recruitment:

We presented the project to local physicians/local physician offices. We have two clinics that have now committed to assisting us with participant recruitment. We designed a tailored letter for physicians to mail to patients, as well as tailored "prescriptions" physicians can distribute to patients to encourage them to participate in this research. We have also worked with the Penn State multimedia department to design study flyers and a newsletter article to assist with recruitment.

### Assessment Protocol:

We designed a comprehensive assessment protocol with selected validated measures, as well as new process measures developed specifically for this study. For example, we developed process measures to measure the types of social networking activities participants engaged in (e.g., contacting others to walk; posting an online walking event; talking with others about places where they like to walk), and participants' use of cell phones during the intervention, as no previous measures existed in this area. We have also developed a secure, online protocol for

survey administration, to enable all questionnaires to be administered online to participants. We researched multiple platforms for online survey administration including the university's WEBUQ system, the RedCap system, SurveyMonkey, and Google Documents. We decided to use SurveyMonkey as it contained similar privacy features to the University's data collection system, while permitting substantially greater flexibility in formatting and survey design. The development of the online survey system will facilitate questionnaire administration, help prevent data entry errors, enable more rapid completion of statistical analyses, and serve as a resource for future studies.

#### Cell Phone Social Networking Protocol:

We researched numerous platforms (e.g., Map My Run, Facebook, Ning, Universal Point of Contact (UPOC), cell-phone applications) to promote cell phone interaction among participants to build their social networks for healthier lifestyles. Our selection criteria were ease of use, compatibility with cell phones, and availability of built-in-features to protect participants' privacy. After pilot-testing multiple platforms, we decided to use the Facebook private groups platform (which has multiple options for protecting privacy, and is highly compatible with cell phones). We will encourage participants to post and join walking events and other healthy lifestyle events using the private Facebook site, and will help participants set up their smartphones so that they can automatically get updates from Facebook each time group members post walking/healthy lifestyle events, contribute to a discussion, etc. This will enable the cell phone to serve as a portable tool connecting participants to their social networks for active living. We have also developed a written set of guidelines for using Facebook to accomplish project activities.

#### Cell Phone Self-Monitoring and Feedback Protocol:

Each week in the program, participants will report their activities from the prior week, and receive tailored feedback. We developed self-monitoring forms that participants can submit via their smartphones through an online link. We also developed a semi-automated feedback protocol using algorithms to give participants feedback on their physical activity and dietary intake, body weight, and Facebook networking activities to build a social community to support a healthy lifestyle. For example, if participants report that they walked 4000 steps with their pedometer, we would give them normative feedback such as "That's great that you walked 4,000 steps. Your level of activity was similar to 33% of the group, and higher than 66% of the group." Participants not meeting recommended activity levels will also be prompted to gradually increase their activity.

#### Other Program Materials:

At the beginning of the program, participants will receive an introductory meeting together with a program manual, and tools such as a pedometer. We have developed a project manual to give to participants, and determined the content for the introductory meeting. We also developed tailored "tips of the weeks" (one page of tips for each week of the program) on how to build a social community to support a healthy lifestyle. The "tips of the week" span diverse topics such as injury prevention, serving as a positive role model for others in the community, planning calorie intake and physical activity to achieve one's targeted body weight, the importance of good sleep hygiene and self-care, and building social networks to help support a healthy lifestyle.

Finally, we developed Facebook discussion topics (these topics overlap with the “tips of the week”) to facilitate social networking among program participants.

#### Interdisciplinary Collaborations:

During the initial study period, we have continued to develop and build new interdisciplinary collaborations to facilitate future grant collaborations based on this work. We are collaborating with faculty members in Exercise Physiology, Medicine, Communications, Public Health Sciences, and Humanities to conduct this research.

### **Research Project 36: Project Title and Purpose**

*Cerebral Malaria as a Cause of Epilepsy* – Malaria is a widespread problem in much of the world. In malaria endemic regions, there is a high rate of childhood epilepsy, approaching a 2-10 fold higher incidence (5-10% prevalence) over developed countries with temperate climates. Clinical studies have clearly linked malarial infection with future chronic seizure disorders in children. There is no animal model for post-malarial epilepsy. The purpose of this project is to develop a mouse model of post-malarial epilepsy that will permit us to explore the feasibility of using modulation of the immune response, in addition to antimalarial medication, to reduce post-malarial epilepsy.

#### **Anticipated Duration of Project**

9/1/2010 - 6/30/2012

#### **Project Overview**

Although cerebral malaria in mice via the virulent strain *Plasmodium berghei* is ordinarily 100% fatal, we have recently shown that 1) rescue of such infected mice with antimalarial medication during cerebral malaria can result in survival, and that 2) mice with knockout genes for proteins in the complement pathway can also survive such infections. In many rodent models of chronic epilepsy, severe seizures induced pharmacologically or electrically can reliably induce chronic seizure disorders.

This is a pilot project between Neurosurgery, Engineering Science and Mechanics, Biology, and Medicine at Penn State. Our objectives are:

- 1) To demonstrate with chronic intracranial EEG recordings whether murine cerebral malaria from *Plasmodium berghei* is linked with subsequent electrographic seizures.
- 2) To investigate the relationship between successful antimalarial therapy and a reduction in lethality and seizures following cerebral malaria.
- 3) To investigate the onset of long-term spontaneous seizures and epilepsy as a consequence of prior cerebral malaria.
- 4) To investigate whether immune modulation through pharmacology or genetic variants protects against the development of subsequent epilepsy.

## **Principal Investigator**

Steven J. Schiff, MD, PhD  
Professor  
Penn State University  
212 EES Building  
University Park, PA 16802

## **Other Participating Researchers**

Bruce J. Gluckman, PhD, Andrew Read, PhD, Jose Stoute, MD, G. Thuku, PhD – employed by Pennsylvania State University

## **Expected Research Outcomes and Benefits**

- 1) We anticipate that animals rescued from cerebral malaria will have epileptic seizures as they recover.
- 2) We anticipate that animals with mild immune deficiency will have less seizure activity as they recover following treatment with antimalarial drugs.
- 3) We anticipate that animals with normal immune systems will have less seizure activity as they recover following treatment with antimalarial drugs.
- 4) The benefits of the above would be:
  - a) We would have established an animal model for childhood epilepsy in malaria prone regions of the world.
  - b) We would have established an animal model to further explore how we can add immune modulation (steroids or non-steroidal anti-inflammatory medication) to improve the outcomes of children being treated for cerebral malaria.

From our beginnings 4 years ago with assistance from 2003 CURE funds, the Penn State Center for Neural Engineering is now on track to become one of the premier centers in the world focusing on the intersection between engineering and diseases of the brain. Our faculty has increased to 8, representing Engineering Science and Mechanics, Mechanical Engineering, Neural and Behavioral Sciences, and Physics. The research being conducted in this laboratory has the potential for significant impact on the health of patients with various degenerative neurological diseases. As a centerpiece for Pennsylvania, this Center will provide significant employment and educational opportunities for people of this state.

## **Summary of Research Completed**

No one has attempted to develop a post-malarial epilepsy model before, so we needed to develop all aspects of this from scratch. We spent the first 6 months working out the surgery, biology, and electrical engineering required to perform this study.

We first developed the surgical techniques to implant a small chronic recording system capable of collecting both electroencephalogram (EEG) and muscle electromyography (EMG) recordings in mice for many weeks and months. An illustration of the recording system, utilizing infrared

LED illumination at night so that the video tracking would work round-the-clock, is shown in Figure 1. This system simultaneously monitors 4 animals at a time, with continuous video, EEG, and EMG recorded with high fidelity to computer.

The next obstacle we needed to overcome was to find a drug regimen capable of rescuing mice infected with the virulent *Plasmodium berghei* strain of mouse malaria. We used artesunate, in daily doses, and monitored parasitemia in the blood until the animal appeared cleared of infection (Figure 2). We noted frequent seizures in our EEG recordings during the height of cerebral malaria (Figure 3), followed by cessation of seizures following clearance of the parasitemia and early recovery.

In numerous other animal models of epilepsy, a period of intense seizures created by a variety of phenomena, including convulsant drugs or intense electrical stimulation, produces chronic epilepsy in the weeks and months following recovery from such events.

We now have a cohort of 5 long-term survivors of cerebral malaria, out of a total of 32 successfully implanted and infected mice, summarized in Table 1. This cohort forms the most valuable animals from this pilot project. If these animals demonstrate seizures in the months subsequent to recovery from cerebral malaria, then we have met our ultimate goal of this project, to determine whether we have an animal model of post-malarial epilepsy. Although the mortality to the mice infected was over 80%, this was due to our learning curve of implantation, and especially in developing a drug regimen with blood monitoring capable of curing these otherwise 100% fatal infections. We of course suspect that the 10 mice that died after previous clearance of parasitemia were likely the result of recurrent parasitemia, since the parasite can harbor in the liver when the blood appears cleared of organisms. If our long-term survivors demonstrate seizures, and thus the model has promise for studying therapy in the human disease, then more extended monitoring of parasitemia following apparent cure, and postmortem examination of the liver in animals that die unexpectedly, will become part of our subsequent studies as we refine this model.

If we find such seizure activity following recovery, then as planned, we will be able to test whether adjunctive treatment such as immune system modulation is protective against the development of post-malarial epilepsy. Since such immune modulation is already a subject of studies in humans seeking to reduce the decrement in IQ in children following cerebral malaria, expanding such trials to include epilepsy as an outcome measure has a straightforward translational path. Furthermore, the availability of an animal model that re-creates cerebral malaria, is treated and cured with the same pharmacology as the human disease, and takes place within a mammalian model where we can study the pathobiology and immune mediated long term sequelae similar to the human disease, will hasten both our understanding of this devastating disease and its consequences.

As of the writing of this report, the long-term survivors of cerebral malaria in Table 1 are being monitored for the next several months. The results of the monitoring of this cohort will determine the final outcome of this study over the coming months.

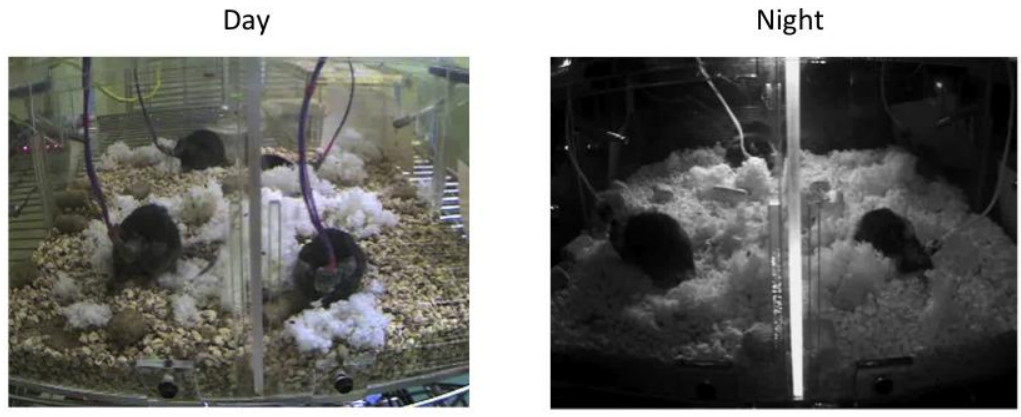


**Figure 1.** Chronic EEG - Accelerometer – Video recording system for 4 mice studied simultaneously. Night time video is performed with infrared LED illumination.

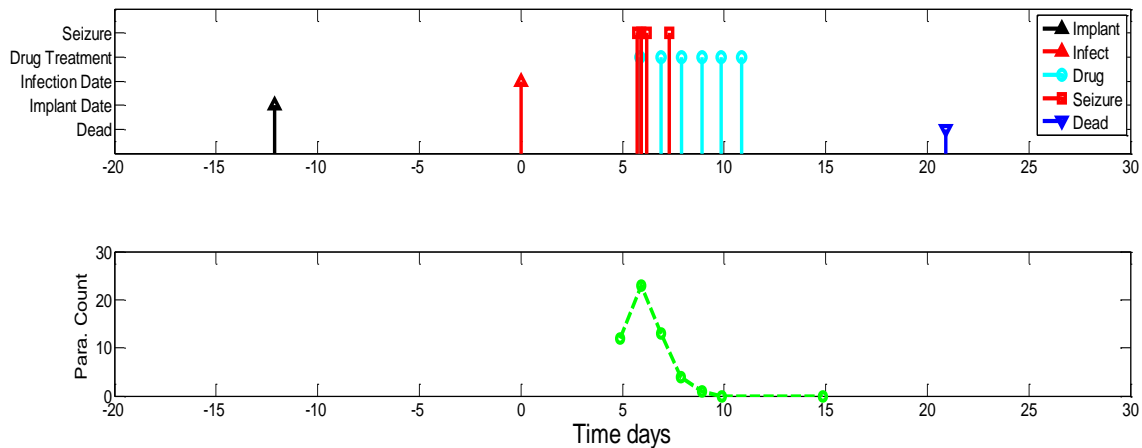


**Figure 2.** Course of electrode implantation, infection with malaria parasite, seizures, drug therapy, and parasite counts in blood showing clearance by treatment. This animal died suddenly on day 22.

**Typical Patterns of EEG and EMG during Seizures in Mice**

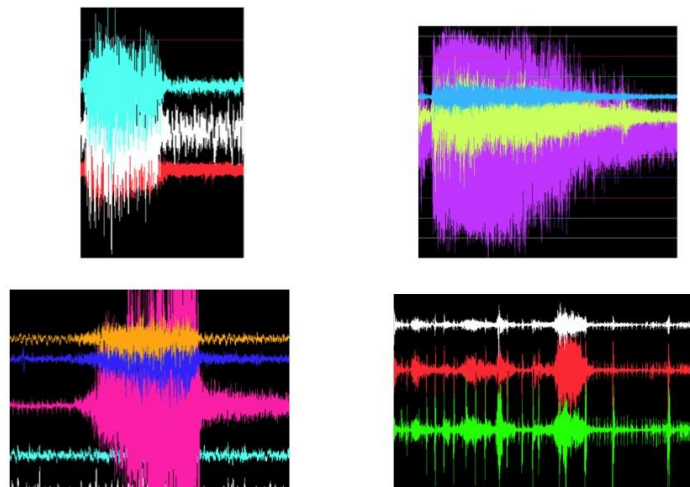


**Figure 3.** Patterns of EEG and EMG activity associated with seizures in mice during cerebral malaria.

CEMA	POI	Seizures		CEMA	POI	Seizures	
9	21days	6	✓	23	15 days		✓
11	11days	Problem w/t infection n EEG		24	15days		✓
12	11days			25	35days		✓
15	12days			27	73days*		✓
16	11days			29	29days*		
17	11days			31	29days*	3+	✓
19	8 days	2	✓	32	29days*	1+	✓
22	101days*	2 +	✓				

\* Animal still alive  
 ✓ Analyzed/ analyzing

**Table 1.** Mice that survived cerebral malaria and clearance of parasitemia. Five of these animals are alive more than 1 month.

**Research Project 37: Project Title and Purpose**

*Mechanisms of Excess Dietary Salt on Sympathetic-Cardiovascular Function* – Both preliminary and recently published data in our laboratory demonstrate the ingestion of excess dietary salt enhances sympathetic-cardiovascular reflexes and increases blood pressure variability in laboratory animals – blood pressure variability is a major risk factor for end-organ damage and cardiovascular disease including hypertension. The purpose of this project is to determine whether excess dietary salt intake alters sympathetic-cardiovascular regulation in humans.

**Anticipated Duration of Project**

9/1/2010 - 12/31/2011

**Project Overview**

Despite compelling evidence that the ingestion of excess dietary salt enhances sympathetic-cardiovascular reflexes and increases blood pressure variability in laboratory animals, there is currently no data available in humans to indicate whether dietary salt intake, by itself, alters sympathetic-cardiovascular regulation. Therefore, the purpose of this project is to examine whether dietary salt intake alters sympathetic-cardiovascular function in humans. Our working hypothesis is that excess dietary salt intake sensitizes central sympathetic circuits to produce greater changes in sympathetic nerve activity (SNA) and more pronounced fluctuations in arterial blood pressure (ABP). Over time, these greater changes in SNA and ABP increase the

probability to develop hypertension. Our rationale for this project is 2-fold: 1) preliminary data in healthy humans to indicate that dietary salt intake alters sympathetic-cardiovascular reflexes and blood pressure variability would provide new evidence of role that excess dietary salt intake plays in increasing the risk of CVD, and 2) such preliminary data would form the foundation for experimental and translational applications for a National Institutes of Health R01, American Heart Association Established Investigator Award, and a Program Project Grant focused on dietary factors and cardiovascular regulation.

Specific Aim #1 will determine whether excess dietary salt intake alters sympathetic-cardiovascular reflexes and blood pressure variability in humans. Normotensive, healthy humans will be placed on a low NaCl (2.5 g per day) or high NaCl (12.5 g per day) for 2 weeks. Then, sympathetic and blood pressure responses to the baroreflex, hypoxia, and isometric handgrip exercise will be determined. In addition, blood pressure variability will be measured through an ambulatory monitor for 24-h. After the experimental session, the subject will be placed on the opposite diet for 2 weeks, and the experimental session will be performed again.

### **Principal Investigator**

Sean D. Stocker, PhD  
Associate Professor  
Department of Cellular & Molecular Physiology  
Penn State University College of Medicine  
500 University Drive H166  
Room C4723  
Hershey, PA 17033

### **Other Participating Researchers**

Lawrence Sinoway, MD, Kevin Monahan, PhD, Jian Cui, PhD – employed by Pennsylvania State University

### **Expected Research Outcomes and Benefits**

The overall hypothesis is that excess dietary salt intake will enhance sympathetic-cardiovascular reflexes and increase arterial blood pressure (ABP) variability in humans. Therefore, the changes in sympathetic nerve activity (SNA) and ABP during baroreflex testing (or gain), handgrip exercise, and hypoxia should be significantly greater when subjects are fed a high versus low salt diet. This would be consistent with previous studies in laboratory animals. More importantly, this would indicate that dietary salt intake has an additional negative impact or risk factor for cardiovascular disease independent of any change in baseline ABP.

One additional consideration in this project is the presence of salt-sensitive versus salt-resistant subjects. Previous studies have indicated salt-sensitive subjects have exaggerated cardiovascular reflexes independent of salt intake. These different populations will be identified by the change in baseline ABP during a low versus high NaCl diet and then analyzed separately. Therefore, it is possible that dietary salt intake may differentially affect sympathetic-cardiovascular responses

between these two groups.

Arterial Blood Pressure (ABP) Variability. ABP variability will be assessed by 24-h ABP measurements. Mean and standard deviation of ABP will be compared within subjects across dietary NaCl conditions. This method has been used extensively in the cardiovascular field, and our preliminary data indicate that dietary salt loading increases ABP variability. However, there are several potential variables to consider: 1) day-time versus night-time measurements – due to differences in activity, mean and standard deviation of ABP which may vary within an individual and across experiments groups. Data collected at different times (day vs. night) could be analyzed separately to limit this variability. The within subjects design should reduce this variability, 2) it is likely that every subject may not use the device for the entire 24-h period – this will be reflected in the data file.

### **Summary of Research Completed**

Recent guidelines published by the American Heart Association emphasize important adverse consequences of excess dietary salt intake. This report suggest that dietary salt can exert negative effects on the cardiovascular system dependent or independent of salt's effects on arterial blood pressure. In the past year, we have established a protocol to examine the effects of excess dietary salt intake on sympathetic-cardiovascular function in humans. In a double-blind, cross-over design, 5 healthy subjects (23-27 years old) ingested both a low (~2.5g/day) and high (~6.5g/day) sodium diet for 2 weeks each. The diets were identical except subjects received sodium (high, 1 g NaCl per capsule, 9 capsules per day) or cellulose (low) capsules to ingest with meals (healthy choice entrees, cheerios, fruits, and vegetables). 1 subject left the study due to the flu. A 2<sup>nd</sup> subject did not complete both low and high salt diets due to last-minute family obligations. Therefore, the data presented to date have been collected from 3 subjects who completed the entire study.

After 2 weeks of a low or high salt diet, subjects were fitted with an ambulatory blood pressure monitor and urine collection container to analyze blood pressure, blood pressure variability, and urine sodium excretion. As illustrated in Figure 1, blood pressure measurements indicate that 1 of 3 subjects were salt-sensitive defined as a difference in blood pressure > 5 mmHg between the low and high salt diet conditions. Consequently, 2 subjects were salt-resistant. When blood pressure variability was analyzed, all 3 subjects had significantly higher blood pressure variability (as reflected by the standard deviation of systolic blood pressure) on a high versus low sodium diet. These findings are important as increased blood pressure variability has been reported as a major risk factor for the development of cardiovascular disease. As expected, a high sodium diet significantly reduced plasma renin activity but increased urine sodium excretion. Plasma sodium concentration tended to increase on a high sodium diet.

To test whether a high sodium diet enhanced sympathetic and cardiovascular reflexes, we measured blood pressure, sympathetic nerve activity via microneurography, and renal blood flow via ultrasound during handgrip exercise after low or high sodium diets. The subject grips a holder at 30% of his/her maximum strength until fatigue. As illustrated in Figure 2, all 3 subjects displayed an increase in blood pressure during handgrip; however, the increase in blood pressure tended to be higher when subjects ingested a high sodium diet. Muscle sympathetic

nerve activity expressed as total activity per min was significantly greater during handgrip after ingestion of a high sodium diet. Finally, handgrip produced a greater increase in renal vascular resistance when subjects ingested a high sodium diet. Collectively, these findings suggest that a high sodium diet produces greater sympathetic and cardiovascular responses to handgrip. We are currently analyzing results from baroreflex testing and hypoxia.

